Department of Civil and Environmental Engineering

Imperial College London

A thesis submitted to Imperial College London for the degree of Doctor of Philosophy

The Impact of Nitrate Dosing and Semi-Conductive Media on Anaerobic Fluidised-Bed Treatment of Low-Strength Wastewater

Emma Beirns

CID: 01819706
Section: Environmental and Water Resources Engineering
Supervisors: Dr. Po-Heng (Henry) Lee and Prof. Stephen Smith
Start date: 29th September 2019
Submission date: 16th December 2024

Declaration of Originality

I declare that this thesis, titled 'The Impact of Nitrate Dosing and Semi-Conductive Media on Anaerobic Fluidised-Bed Treatment of Low-Strength Wastewater' represents my own original work, except where due acknowledgement is made, and that it has not been previously included in a thesis, dissertation, or report submitted to this University or to any other institution for a degree, diploma, or other qualifications.

Copyright Declaration

The copyright of this thesis rests with the author. Unless otherwise indicated, its contents are licensed under a Creative Commons Attribution-Non Commercial 4.0 International Licence (CC BY-NC).

Under this licence, you may copy and redistribute the material in any medium or format. You may also create and distribute modified versions of the work. This is on the condition that: you credit the author and do not use it, or any derivative works, for a commercial purpose.

When reusing or sharing this work, ensure you make the licence terms clear to others by naming the licence and linking to the licence text. Where a work has been adapted, you should indicate that the work has been changed and describe those changes.

Please seek permission from the copyright holder for uses of this work that are not included in this licence or permitted under UK Copyright Law.

Publications

No parts of this thesis have yet been published in any peer-reviewed journals at time of submission. Manuscripts are currently being drafted.

Abstract

This thesis describes the performance of two anaerobic fluidised-bed bioreactors (AFBRs) operated over 290 days and the microbial communities within. Both reactors utilised 7-channel plastic beads as the fluidised media, however, in one reactor, the media had a semi-conductive polyaniline coating to stimulate direct interspecies electron transfer (DIET). The synthetic low-strength wastewater fed into the reactors also contained a low dose of nitrate, stimulating denitrification, as well as both nitric oxide dismutation and dissimilatory nitrate reduction to ammonia (DNRA).

Although the performance data showed no significant difference to the methane production or yield between the two AFBRs, metagenomics analysis showed that the polyaniline coating did favour electroactive microbes. Furthermore, by the late stages of operation, a constant low presence of oxygen stimulated a high relative abundance of oxygen-tolerant methanogens. This demonstrates that polyaniline is successful at stimulating DIET, however, the performance of methanogenesis may have been impacted by the presence of nitrate.

The presence of oxygen in the biogases and the increased concentration of ammonia in the effluents confirmed the activation of nitric oxide dismutation and DNRA. Furthermore, genes for DNRA were detected and sequence similarity searches found genes that had some similarity to nitric oxide dismutase genes. Mass balances calculations showed that the polyaniline-containing AFBR had a higher rates of nitrous oxide production. This implies that DIET favoured conventional denitrification, albeit incomplete, over nitric oxide dismutation or DNRA.

This experiment is the first to explore any relationship between DIET and nitric oxide dismutation, ultimately finding no evidence of linkage between the two. This is likely due to nitric oxide dismutation being an electron neutral reaction, and therefore DIET does not confer any advantage. The establishment of nitric oxide dismutation in an anaerobic wastewater treatment reactor shows great potential for reducing nitrous oxide emissions if the process can be scaled.

Acknowledgements

Thank you to my fellow PhD students, who were so incredibly generous with their time and skills: Henrique de Souza Dornelles, Theo Lam, Maryam Dewiandratika, and Tri Yulianti. I hope I will one day be as much help to you as you were to me. To the Roger Perry lab community and the 307A dwellers, as well: Alex, Ben, Maria, Celia, Jiaodi, Liying, Ziting, Mengru, Anas, Amy, Palm, CJ, Lily. And Adam!

To my supervisors, Dr. Henry Lee and Prof. Stephen Smith, and to Prof. Amy Tan of the City University of Hong Kong, thank you for lending me your expertise and support. To Dr. Ángel Nievas-Pino of the Roger Perry lab, thank you for your invaluable technical assistance and training. And to Paul Crudge of the Structures Department, thank you for your collaboration and design skills.

To my family and friends, who visited me and gave me reasons to take breaks. And thank you to Jem. Without you, there is no way on Earth I would have finished this. I promise I'll never do anything like this again.

Contents

1 Introduction **21**

1.1 Background . . . 21

1.1.1 Biological Wastewater Treatment . . . 21

1.1.2 The Green House Gases of Biological Wastewater Treatment . . . 22

1.1.3 Biological Nitrogen Removal in Wastewater Treatment . . . 23

1.2 Research Statements . . . 25

1.2.1 Problem Statement and Hypothesis . . . 25

1.2.2 Aims and Objectives . . . 25

2 Literature Review **27**

2.1 Anaerobic Wastewater Treatment Design . . . 27

2.1.1 Overview of Anaerobic Technologies . . . 27

2.1.2 A Brief History of Anaerobic, Attached-Growth Technologies . . . 28

2.1.3 The Future of Anaerobic Fluidised-bed BioReactors . . . 29

2.2 Direct Interspecies Electron Transfer . . . 32

2.2.1 Defining the Different Types of Interspecies Electron Transfer . . . 32

2.2.2 Electroactive Microorganisms . . . 32

2.2.3 Microbe-Microbe Electron Sharing . . . 36

2.2.4 Microbe-Electrode Electron Sharing . . . 39

2.2.5 Direct Interspecies Electron Transfer in Anaerobic Wastewater Treatment . . . 40

2.3 Carbon Cycling in Anaerobic Wastewater Treatment . . . 42

2.3.1 Hydrolysis, Acidogenesis, and Acetogenesis . . . 42

2.3.2 Methanogenesis . . . 43

2.3.3 Inhibition of Methanogenesis and Methanotrophy . . . 46

2.3.4 Methane Release from Anaerobic Reactors . . . 48

2.3.5 Direct Interspecies Electron Transfer in Methanogenesis . . . 49

2.4 Conventional Nitrogen Cycling in Wastewater Treatment . . . 52

2.4.1 The Processes of Biological Nitrogen Removal . . . 52

2.4.2 Nitrification . . . 53

2.4.3 Denitrification . . . 55

2.4.4 Anaerobic Ammonia Oxidation . . . 58

2.4.5 Knowledge Gaps in the Nitrogen Cycle . . . 59

2.5 Unconventional Nitrogen Cycling in Wastewater Treatment . . . 62

2.5.1 Nitric Oxide Dismutation . . . 62

2.5.2 Dissimilatory Nitrate Reduction to Ammonia . . . 65

2.5.3 Direct Interspecies Electron Transfer in the Nitrogen Cycle . . . 68

3 Materials and Methods 73

3.1 Experimental Design . . . 73

3.2 Bench-Scale Anaerobic Fluidised-bed Bio-Reactors . . . 74

3.2.1 Reactor Design and Materials . . . 74

3.2.2 System Priming, Inoculation, and Continuous Operation . . . 76

3.2.3 Maintenance Routine . . . 77

3.3 Carbon and Nitrogen Monitoring . . . 78

3.3.1 Sample Collection and Preparation . . . 78

3.3.2 Chemical Oxygen Demand Analysis . . . 78

3.3.3 Dissolved Inorganic Nitrogen Analysis . . . 79

3.3.4 Biogas Composition Analysis . . . 79

3.4 Mass Balance Calculation . . . 80

3.4.1 Balancing Approach . . . 80

3.4.2 Chemical Oxygen Demand to Carbon Mass Equivalent . . . 80

3.4.3 Biogas Volume and Composition to Mass Equivalents . . . 80

3.4.4 Dissolved Gases . . . 81

3.5 Meta-Omics . . . 81

3.5.1 Sampling and Handling . . . 81

3.5.2 Library Prep . . . 82

3.5.3 Assembly-Free Taxonomic Profiling . . . 83

3.5.4 Diversity Analysis . . . 83

3.5.5 *De novo* Assembly of Genome Bins . . . 84

3.5.6 Interrogation of Bins . . . 85

3.5.7 16S rRNA Gene Analysis . . . 86

3.6 Statistical Methods and Quality Assurance . . . 86

4 Performance Review and Substrate Cycling Analysis 88

4.1 Summary of Performance . . . 88

4.1.1 Operation . . . 88

4.1.2 Chemical Oxygen Demand Removal . . . 88

4.1.3 Biogas Production and Composition . . . 92

4.1.4 Total Nitrogen Removal . . . 94

4.2 Mass Balance . . . 94

4.3 Nitrogen Transformations . . . 96

4.3.1 Production of Ammonia . . . 96

4.3.2 Production of Di-Nitrogen Gas . . . 97
4.3.3 Stoichiometry of Denitrifying Nitrate Transformations . . . 98
4.4 Carbon Transformations . . . 99
4.4.1 Methane Yield . . . 99
4.4.2 Carbon Dioxide Yield and Sources . . . 101
4.5 Oxygen Transformations . . . 102
4.6 Discussion . . . 102
4.6.1 Review of Overall Performance . . . 102
4.6.2 Impact of Semi-Conductive Coating on Performance . . . 103
4.6.3 Nitrogen Cycling . . . 104

5 Microbial Community Profiling 106
5.1 Community Overview . . . 106
5.2 Bacterial Taxonomic Profile . . . 109
5.2.1 Dominant Genera . . . 109
5.2.2 Syntrophs . . . 110
5.2.3 Exoelectrogens . . . 110
5.2.4 Methanotrophs . . . 112
5.2.5 Nitrogen Cycling Community . . . 112
5.3 Archaeal Taxonomic Profile . . . 114
5.3.1 Electrotrophs . . . 114
5.3.2 Oxygen Tolerant Methanogens . . . 114
5.4 Diversity Analysis . . . 115
5.4.1 Alpha Diversity . . . 115
5.4.2 Beta Diversity . . . 117
5.5 Community Comparison to Other Anaerobic Wastewater Treatment Reactors . . . 118
5.5.1 Anaerobic Fluidised-bed Membrane BioReactors . . . 118
5.5.2 Staged Anaerobic Fluidised-bed Membrane BioReactors . . . 120
5.5.3 Anaerobic Digesters . . . 122
5.6 Discussion . . . 125
5.6.1 Changing Communities . . . 125
5.6.2 Direct Interspecies Electron Transfer Community . . . 125
5.6.3 Nitrogen Cycling Community . . . 126

6 Genome Bin Interrogation 128
6.1 Metagenome Assembled Genomes . . . 128
6.1.1 Results of Resolution . . . 128

6.1.2 Selection of Bins for Interrogation . . . 128
6.2 Metabolic Pathway Reconstruction . . . 130
6.2.1 Genome Annotation . . . 130
6.2.2 Carbon Metabolism Pathways . . . 131
6.2.3 Nitrate Reduction Pathways . . . 131
6.3 Sequence Similarity Scoring . . . 133
6.4 Discussion . . . 137
6.4.1 Cooperative Glucose Metabolism . . . 137
6.4.2 Conventional Denitrification . . . 138
6.4.3 Unconventional Nitrate Metabolism . . . 138

7 General Discussion 140
7.1 Performance Summary . . . 140
7.1.1 Effective High-Rate Treatment of Low-Strength Wastewater . . . 140
7.1.2 Acclimatisation Time . . . 140
7.2 Methanogenesis . . . 141
7.2.1 Review of Performance . . . 141
7.2.2 Stimulation . . . 141
7.2.3 Inhibition . . . 142
7.3 Nitrogen Cycling Pathways . . . 142
7.3.1 Review of Performance . . . 142
7.3.2 Conventional Denitrification . . . 143
7.3.3 Oxygenic Denitrification . . . 144
7.3.4 Dissimilatory Nitrate Reduction to Ammonia . . . 145
7.4 Novel Microbial Interactions . . . 145
7.5 Potential Applications . . . 147
7.5.1 Auto-Aeration . . . 147
7.5.2 Combination with Partial-Nitrification/Anammox . . . 147
7.5.3 Methanotrophic Denitrification . . . 147
7.5.4 Scalability . . . 148

8 Conclusions and Recommendations 150
8.1 Conclusions . . . 150
8.2 Recommendations for Future Research . . . 151
8.2.1 Improvements to Experimental Design . . . 151
8.2.2 Continued Experiments . . . 152

9 References **153**

A1 AFBR Performance Data **171**

A1.1 Operation . . . 171

A1.1.1 Influent Flow Rate and Hydraulic Retention Times . . . 171

A1.1.2 pH . . . 173

A1.2 Chemical Oxygen Demand Data . . . 175

A1.3 Biogas Production Data . . . 179

A1.4 Biogas Composition Data . . . 181

A1.5 Dissolved Inorganic Nitrogen Data . . . 184

A2 Stoichiometry of Denitrification and Nitric Oxide Dismutation **187**

A2.1 Cell Synthesis Reaction . . . 187

A2.2 Electron Donor Reactions . . . 187

A2.3 Electron Acceptor Reactions . . . 187

A2.3.1 Denitrification . . . 187

A2.3.2 Nitric Oxide Dismutation . . . 187

A2.4 Half Reactions . . . 188

A2.4.1 Synthesis Half Reactions . . . 188

A2.4.2 Energy Half Reactions . . . 188

A2.5 Reaction Energetics . . . 189

A2.5.1 Free Energy Change of Cell Synthesis . . . 189

A2.5.2 Energetic Balance Between Energy and Synthesis Reactions . . . 190

A2.6 Completed Equations . . . 190

A3 Meta-Genomics Scripts and Output Details **192**

A3.1 Library Prep . . . 192

A3.2 Assembly-Free Taxonomic Classification . . . 192

A3.3 Diversity Analysis . . . 193

A3.3.1 Alpha . . . 193

A3.3.2 Beta . . . 194

A3.4 Assembly . . . 194

A3.4.1 MEGAHIT . . . 194

A3.4.2 QUAST . . . 195

A3.5 Alignment . . . 195

A3.5.1 Bowtie2 . . . 195

A3.5.2 SAMtools + HTSlib . . . 195

A3.6 Binning . . . 197
A3.7 Metagenome Assembled Genome Taxonomic Classification . . . 197
A3.7.1 PhyloPhlAn 3.0 . . . 197
A3.7.2 CheckM . . . 197
A3.8 16S rRNA Analysis . . . 197

A4 Pathway Annotation **199**
A4.1 Carbon Metabolism . . . 199
A4.1.1 Aeromonas media . . . 199
A4.1.2 Pseudomonas putida . . . 202
A4.1.3 Sulfurospirillum arsenophilum . . . 205
A4.1.4 Sulfurospirillum cavolei . . . 208
A4.1.5 Sulfurospirillum sp. JPD-1 . . . 213
A4.1.6 Sulfurospirillum sp. UCH001 . . . 216
A4.2 Nitrogen Metabolism . . . 219
A4.2.1 Aeromonas media . . . 219
A4.2.2 Pseudomonas putida . . . 222
A4.2.3 Sulfurospirillum arsenophilum . . . 225
A4.2.4 Sulfurospirillum cavolei . . . 228
A4.2.5 Sulfurospirillum sp. JPD-1 . . . 233
A4.2.6 Sulfurospirillum sp. UCH001 . . . 236

A5 Reproduction Permissions **239**

List of Figures

1 Resource recovery options from wastewater treatment . . . 21
2 Major pathways in the nitrogen cycle . . . 24
3 Putative nitric oxide dismutation pathway . . . 24
4 Early attached-growth anaerobic wastewater treatment reactor designs . . . 29
5 Interspecies electron transfer mechanisms . . . 33
6 Phylogenetic analysis of electroactive microorganisms found in bioelectrochemical systems 34
7 Mechanisms for *c*-type cytochrome electron transport across the outer surface . . . 37
8 Alternative models for direct interspecies electron transfer . . . 39
9 Key anaerobic digestion pathways and genera associated with major intermediates . . . 42
10 Phylogeny of methanogenic archaea . . . 44
11 Methanogenesis pathways and associated enzymes . . . 45
12 Hydrogenotrophic methanogenesis in *Methanosaeta* . . . 50
13 Oxidation states of key intermediates in the nitrogen cycle . . . 52
14 Microbial metabolic pathways in the nitrogen cycle . . . 53
15 Pathways of nitrifying bacteria . . . 53
16 Phylogeny of nitrifying bacterial genera . . . 55
17 Maximum likelihood phylogeny of nitrite reductase gene clusters . . . 57
18 Schematic representation of anammox bacteria cell . . . 59
19 A timeline of discoveries in the nitrogen cycle and biotechnology applications . . . 60
20 Denitrification and methanotrophic genes present in *Methylomirabilis oxyfera* . . . 62
21 Phylogeny of putative nitric oxide dismutase and selected nitric oxide reductase gene sequences 64
22 Proposed alternative nitric oxide dismutation pathway in *Nitrosopumilus maritimus* . . . 64
23 Pathways and enzymes of dissimilatory nitrate reduction to ammonia . . . 67
24 Nitrate removal rates in denitrifying communities with and without *Geobacter* . . . 69
25 Concentration changes of ammonium, nitrite, and nitrate in microbial electrolysis cells and biotic controls in two cycles . . . 71
26 Possible mechanism of biochar-mediated DNRA pathway of anammox bacteria . . . 72
27 Aims and objectives flow chart . . . 73
28 Bench-scale anaerobic fluidised-bed bioreactor schematic and design details . . . 74
29 Photo of bench-scale anaerobic fluidised-bed bioreactors in Roger Perry Lab . . . 75
30 Graphical summary of carbon, nitrogen, and oxygen concentrations in influent and effluents 91
31 Biogas composition results . . . 92
32 Methane yields from anaerobic fluidised-bed membrane bioreactors using coated and uncoated PVDF beads . . . 100

33 Assembly-free taxonomic profiles - dominant bacterial genera . . . 107
34 Assembly-free taxonomic profiles - archaeal genera . . . 108
35 Assembly-free taxonomic profiles - syntrophic bacterial genera . . . 111
36 Assembly-free taxonomic profiles - electroactive bacterial genera . . . 111
37 Assembly-free taxonomic profiles - nitrogen cycling bacterial genera . . . 113
38 Shannon diversity index . . . 116
39 Principal coordinates analysis of Bray-Curtis dissimilarity . . . 118
40 Taxonomic profiles from anaerobic fluidised-bed membrane bioreactors with uncoated and polyaniline coated media . . . 119
41 Taxonomic profiles from Inha staged anaerobic fluidised-bed membrane bioreactor . . . 121
42 Taxonomic profiles from UK anaerobic digesters . . . 124
43 Proposed syntrophic relationship between *Aeromonas media* and *Sulfurospirillum* spp. for glucose metabolism . . . 137
44 Proposed syntrophic relationships in AFBRs . . . 146
45 Proposed schematic for anaerobic treatment followed by partial-nitrification/anammox . . . 148
46 Proposed schematics for anaerobic treatment followed by methanotrophic denitrification . . . 149
47 Hydraulic retention times . . . 172
48 Steady-state hydraulic retention time standardised normal distributions . . . 172
49 pH results . . . 174
50 pH standardised normal distributions . . . 174
51 Chemical oxygen demand results . . . 177
52 Steady-state chemical oxygen demand standardised normal distributions . . . 178
53 Biogas production results . . . 180
54 Gas bag biogas production standardised normal distributions . . . 180
55 R1 steady-state biogas composition standardised normal distributions . . . 182
56 R2 steady-state biogas composition standardised normal distributions . . . 183
57 Dissolved inorganic nitrogen results . . . 186
58 Carbon metabolism pathway annotation - GR1P1biofilm.135 . . . 199
59 Carbon metabolism pathway annotation - GR1P2biofilm.127 . . . 200
60 Carbon metabolism pathway annotation - *A. media* . . . 201
61 Carbon metabolism pathway annotation - GR1P2bulk.29 . . . 202
62 Carbon metabolism pathway annotation - GR2P2bulk.93 . . . 203
63 Carbon metabolism pathway annotation - *P. putida* . . . 204
64 Carbon metabolism pathway annotation - GR1P2biofilm.115 . . . 205
65 Carbon metabolism pathway annotation - GR1P2bulk.131 . . . 206
66 Carbon metabolism pathway annotation - *S. arsenophilum* . . . 207

67 Carbon metabolism pathway annotation - GR1P2biofilm.177 . . . 208
68 Carbon metabolism pathway annotation - GR2P1biofilm.32 . . . 209
69 Carbon metabolism pathway annotation - GR2P1bulk.144 . . . 210
70 Carbon metabolism pathway annotation - GR2P2biofilm.179 . . . 211
71 Carbon metabolism pathway annotation - *S. cavolei* . . . 212
72 Carbon metabolism pathway annotation - GR2P1biofilm.36 . . . 213
73 Carbon metabolism pathway annotation - GR2P2biofilm.71 . . . 214
74 Carbon metabolism pathway annotation - *S. sp. JPD-1* . . . 215
75 Carbon metabolism pathway annotation - GR2P1biofilm.14 . . . 216
76 Carbon metabolism pathway annotation - GR2P1biofilm.42 . . . 217
77 Carbon metabolism pathway annotation - *S. sp. UCH001* . . . 218
78 Nitrogen metabolism pathway annotation - GR1P1biofilm.135 . . . 219
79 Nitrogen metabolism pathway annotation - GR1P2biofilm.127 . . . 220
80 Nitrogen metabolism pathway annotation - *A. media* . . . 221
81 Nitrogen metabolism pathway annotation - GR1P2bulk.29 . . . 222
82 Nitrogen metabolism pathway annotation - GR2P2bulk.93 . . . 223
83 Nitrogen metabolism pathway annotation - *P. putida* . . . 224
84 Nitrogen metabolism pathway annotation - GR1P2biofilm.115 . . . 225
85 Nitrogen metabolism pathway annotation - GR1P2bulk.131 . . . 226
86 Nitrogen metabolism pathway annotation - *S. arsenophilum* . . . 227
87 Nitrogen metabolism pathway annotation - GR1P2biofilm.177 . . . 228
88 Nitrogen metabolism pathway annotation - GR2P1biofilm.32 . . . 229
89 Nitrogen metabolism pathway annotation - GR2P1bulk.144 . . . 230
90 Nitrogen metabolism pathway annotation - GR2P2biofilm.179 . . . 231
91 Nitrogen metabolism pathway annotation - *S. cavolei* . . . 232
92 Nitrogen metabolism pathway annotation - GR2P1biofilm.36 . . . 233
93 Nitrogen metabolism pathway annotation - GR2P2biofilm.71 . . . 234
94 Nitrogen metabolism pathway annotation - *S. sp. JPD-1* . . . 235
95 Nitrogen metabolism pathway annotation - GR2P1biofilm.14 . . . 236
96 Nitrogen metabolism pathway annotation - GR2P1biofilm.42 . . . 237
97 Nitrogen metabolism pathway annotation - *S. sp. UCH001* . . . 238

List of Tables

1 Performance of early attached-growth anaerobic wastewater treatment reactor designs, adapted from Young and McCarty (1969) and Switzenbaum and Jewell (1980) 30
2 Approximate conductivities of e-pili of *Geobacter* species 38
3 Free energy from NADH oxidation coupled to electron acceptors 47
4 Estimates of methane losses in anaerobic effluents 49
5 Dissimilatory nitrate reduction to ammonia bacteria, their habits and physiology 68
6 Composition of synthetic feed solution 76
7 Meta-omics sampling protocol 82
8 Summary of AFBR operation and performance monitoring 89
9 Biogas composition from an anaerobic fluidised-bed bioreactor 93
10 Summary of nitrogen, oxygen, and carbon mass balances 95
11 Summary of performance - nitrogen 97
12 Substrate consumption and production from nitrate transformation stoichiometry 99
13 Summary of performance - methane 100
14 Summary of performance - carbon dioxide 101
15 Clean read counts and classifications of bacteria and archaea from assembly-free taxonomic profiling 106
16 Alpha diversity analysis of bacteria and archaea 115
17 Bray-Curtis dissimilarity analysis of bacteria and archaea 117
18 Clean read counts from anaerobic digester 16S rRNA sequencing 123
19 Summary of metagenome resolution into reconstructed genome bins 128
20 Genome bins for interrogation 129
21 Summary of KEGG genome annotation 130
22 Dissimilatory nitrate reducing genes from selected bins and reference sequences 132
23 Putative nitric oxide dismutase enzyme sequence similarity scoring 134
24 Influent flow rate and hydraulic retention times 171
25 pH results 173
26 Chemical oxygen demand results 175
27 Biogas production results 179
28 Biogas composition results 181
29 Dissolved inorganic nitrogen results 184
30 Energetics of Nitric Oxide Dismutation Reaction Steps 187
31 Nitric Oxide Dismutation Reaction Steps 188
32 Synthesis half reactions (anabolic) 188

33 Energy half reactions (catabolic) . . . 189
34 Energetics with various energy transfer efficiencies . . . 190
35 Completed stoichiometry . . . 191
36 Sequence file read counts from KneadData library prep . . . 192
37 Read classifications from Kaiju assembly-free taxonomic profiling . . . 193
38 Principal coordinates analysis of Bray-Curtis dissimilarity . . . 194
39 Summary of QUAST reports from MEGAHIT assembly . . . 196
40 List of permissions for reproduction of figures . . . 239

List of Equations

1 General form of dismutation reactions . . . 25
2 Methanogenesis via direct interspecies electron transfer . . . 50
3 Ammonia oxidation to hydroxylamine via ammonia monoxygenase . . . 54
4 Hydroxylamine oxidation to nitrite via hydroxylamine oxidoreductase . . . 54
5 Nitric oxide oxidation to nitrite via unknown nitric oxide oxidoreductase . . . 54
6 Oxidation-reduction between nitrite and nitrate via nitrite oxidoreductase . . . 54
7 Nitrate reduction to nitrite via nitrate reductase . . . 56
8 Nitrite reduction to nitric oxide via nitrite reductase . . . 56
9 Nitrite reduction to nitric oxide via nitric oxide reductase . . . 56
10 Nitrous oxide reduction to di-nitrogen via nitrous oxide reductase . . . 56
11 Formation of hydrazine via hydrazine synthase . . . 58
12 Hydrazine oxidation to di-nitrogen via hydrazine dehydrogenase . . . 58
13 Dissimilatory nitrate reduction to ammonia . . . 65
14 Stoichiometry of oxidation of carbonaceous organic compounds . . . 80
15 Gaseous molar volume . . . 81
16 Unitless Henry's law . . . 81
17 Shannon diversity index . . . 83
18 Simpson's diversity index . . . 83
19 Bray-Curtis dissimilarity index . . . 84
20 Z-Score . . . 86
21 Stoichiometry of glycolytic denitrification from nitrate to di-nitrogen . . . 98
22 Stoichiometry of acetotrophic denitrification from nitrate to di-nitrogen . . . 98
23 Stoichiometry of glycolytic nitric oxide dismutation from nitrate to di-nitrogen and oxygen 98
24 Stoichiometry of acetotrophic nitric oxide dismutation from nitrate to di-nitrogen and oxygen 98
25 Simplified stoichiometry of glucose to methane and carbon dioxide . . . 101
26 Cell synthesis reaction (ammonium as nitrogen source) . . . 187
27 Glycolytic electron donor reaction . . . 187
28 Acetotrophic electron donor reaction . . . 187
29 Denitrification electron acceptor reaction . . . 187
30 Nitric oxide dismutation electron acceptor reaction . . . 188
31 Synthesis half reaction . . . 188
32 Energy half reaction . . . 189
33 Acetate activation . . . 189
34 Conversion of activated acetate to cellular carbon . . . 189

35 Energy balance 190
36 Conversion of activated acetate to cellular carbon 190
37 Division of electron equivalents between energy and synthesis 190
38 Stoichiometric reaction 191

Glossary of Terms

***c*-cyt** *c*-type cytochromes

16S rRNA gene sequencing amplicon sequencing technique for taxonomic classification

ammonification mineralisation of organic nitrogenous compounds to ammonia

anammox anaerobic ammonium oxidation

comammox complete ammonia oxidiation

denitratation reduction of nitrate to nitrite

denitrification reduction of nitrate to di-nitrogen

denitritation reduction of nitrite to di-nitrogen

E value expect value

e-pili electrically conductive pili

electroactive capable of direct electron sharing

electrotroph electron accepting species

exoelectrogen electron donating species

feammox iron-based ammonium oxidation

genomic analysis of DNA molecules

meta-omic analysis of biomolecules from an environmental sample

nitratation oxidiation of nitrite to nitrate

nitrification oxidiation of ammonia to nitrate

nitritation oxidiation of ammonia to nitrite

omic the investigation of the entire complement of a specific type of biomolecule

proteomic analysis of protein molecules

redox reduction-oxidation

RuBisCo ribulose-1,5-bisphosphate carboxylase/oxygenase

transcriptomic analysis of RNA molecules

ø diameter

Glossary of Acronyms

AAFEBR Anaerobic Attached-Film Expanded-Bed Reactor

ACP Anaerobic Contact Process

AD Anaerobic Digestion

ADM1 Anaerobic Digestion Model No. 1

AF Anaerobic Filter

AFBR Anaerobic Fluidised-bed BioReactor

AFMBR Anaerobic Fluidised-bed Membrane BioReactor

ANME Anaerobic Methanotrophic

AOA Ammonia Oxidising Archaea

AOB Ammonia Oxidising Bacteria

ATP Adenosine TriPhosphate

BES BioElectrochemical Systems

BLAST Basic Local Alignment Search Tool

BNR Biological Nitrogen Removal

BOD Biochemical Oxygen Demand

bp base pairs

CANON Completely Autotrophic Nitrogen removal Over Nitrite

CAS Conventional Activated Sludge

COD Chemical Oxygen Demand

DEET Direct Extracellular Electron Transfer

DIET Direct Interspecies Electron Transfer

DNRA Dissimilatory Nitrate Reduction to Ammonium

DO Dissolved Oxygen

EGSB Expanded Granular Sludge Blanket

GAC Granular Activated Carbon

GC-MS Gas Chromatography tandem Mass Spectrometry

GHG Green House Gas

HDB Heterotrophic Denitrifying Bacteria

HPC High Performance Computing

HRT Hydraulic Retention Time

IET Interspecies Electron Transfer

KEGG Kyoto Encyclopedia of Genes and Genomes

MAG Metagenome Assembled Genome

MBR Membrane BioReactor

n-DAMO nitrite-Dependent Anaerobic Methane Oxidation

N/DN Nitrification / Denitrification

NADH Nicotinamide Adenine Dinucleotide

NCBI National Center for Biotechnology Information

NOB Nitrite Oxidising Bacteria

NOD Nitric Oxide Dismutation

OLAND Oxygen Limited Autotrophic Nitrification-Denitrification

OLR Organic Loading Rate

PANI Polyaniline

PCoA Principal Coordinates Analysis

PCR Polymerase Chain Reaction

PET PolyEthylene Terephthalate

PN/A Partial Nitrification / Anammox

PVDF PolyVinylidene DiFluoride

RHP Reductive Hexulose Phosphate

SAF-MBR Staged Anaerobic Fluidised-bed Membrane BioReactor

SGB Species-level Genome Bin

SHARON Single-reactor High-activity Ammonium Removal Over Nitrite

SNAD Simultaneous Partial Nitrification, Anammox, and Denitrification

SND Simultaneous Nitrification-Denitrification

SRT Solids Retention Time

SS Suspended Solids

TCD Thermal Conductivity Detector

TOC Total Organic Carbon

TRF Tandem Repeats Finder

UASB Upflow Anaerobic Sludge Blanket

VFA Volatile Fatty Acid

WWTP WasteWater Treatment Plant

Glossary of Chemical Compounds

C carbon species

CH_4 methane

CO_2 carbon dioxide

e^- electron

Fe^{2+} ferrous iron

Fe^{3+} ferric iron

H hydrogen

H_2 dihydrogen

N nitrogen species

N_2 di-nitrogen

N_2H_4 hydrazine

N_2O nitrous oxide

NH_2OH hydroxylamine

NH_3 ammonia

NH_4^+ ammonium

NO nitric oxide

NO_2^- nitrite

NO_3^- nitrate

O_2 oxygen

SO_4^{2-} sulphate

Glossary of *genes* and Enzymes

nod nitric oxide dismutase gene

norZ nitric oxide reductase gene

nrfA nitrite reductase subunit A gene

Amo ammonia monooxygenase

cNor cytochrome-dependent nitric oxide reductase

Hao hydroxylamine oxidoreductase

Hdh hydrazine dehydrogenase

Hzs hydrazine synthase

methyl-com methyl coenzyme M

Mmo methane monooxygenase

Nap periplasmic nitrate reductase

Nar cytoplasmic nitrate reductase

Nir nitrite reductase

NirBD cytoplasmic DNRA nitrite reductase complex

NirK copper-containing denitrification nitrite reductase

NirS cytochrome cd_1-containing denitrification nitrite reductase

Nod nitric oxide dismutase

Noo nitric oxide oxidoreductase

Nor nitric oxide reductase

Nos nitrous oxide reductase

Nrf periplasmic DNRA nitrite reductase

Nxr nitrite oxidoreductase

qNor quinol-dependent nitric oxide reductase

1 Introduction

1.1 Background

1.1.1 Biological Wastewater Treatment

When designing a WasteWater Treatment Plant (WWTP), there are, of course, many factors to consider. In the context of domestic wastewater, the most important functions are the removal of Chemical Oxygen Demand (COD), organic nutrients (namely carbon, nitrogen, and phosphorus), and solids to prevent severe ecological harm to the receiving water bodies and the spread of pathogens. Dating back to the late 19th century (Lofrano and Brown 2010), biological treatment technologies remain popular in the wastewater treatment industry today due to their resilience, low resource demands, and affordability.

Inevitably, over the last 100 years, the expectations for the global wastewater treatment industry have evolved. Engineering advances have lead to performance improvements for the basic requirements, with plenty of novel treatment technologies and plant layouts being designed to meet those needs. However, there is also a need for more than expanded capacity due to population increases. Nowadays, treatment technologies are increasingly expected to factor in climate change consciousness, resource recovery (examples shown in Figure 1), and, most recently, the removal of emerging contaminants and micro-pollutants.

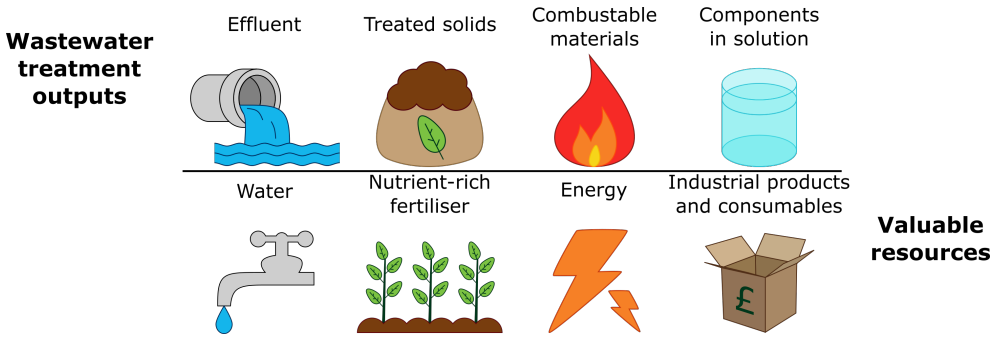


Figure 1: Resource recovery options from wastewater treatment

These changing demands are creating pressure on process engineers to change their design strategies and to think as creatively as possible. Chemical and physical treatment technologies are certainly attractive when it comes to meeting these modified demands, but their resource- and energy-intensity makes them unappealing. On the other hand, biological treatment technologies rely on ineffable microbial communities in an engineered environment to produce the desired outcomes. Hitherto, the design of biological WWTPs has relied on empirical formulae based on experimental evidence to inform engineers of the approximate requirements for treatment. However, multi-meta-omic technologies have allowed the fundamental metabolic mechanisms behind the observed results to become more clearly understood. This term is broken down as follows:

multi - multiple molecular types; **meta** - mixed cultures treated as one genome;
omic - the investigation of the entire complement of a specific type of biomolecule,
i.e., genomic (DNA), transcriptomic (RNA), proteomic (proteins)

As these analyses are becoming ever easier to use, more reliable, and cheaper to perform, environmental engineers are gaining a deeper understanding of the processes that they are trying to harness. This will ultimately lead to more advanced designs to meet the changing demands on WWTPs, as well as offering engineers an expanding repertoire of innovative solutions as novel microbial metabolic processes are discovered. One such discovery that has already garnered a lot of interested for WWTP design is Direct Interspecies Electron Transfer (DIET).

Since the first proposal of this new form of microbial metabolism by Summers et al. (2010), it has been recognised in anaerobic environments with methanogenic and methanotrophic microbial communities (Lovley 2017a), even in the mammalian gut (Wang et al. 2019a). Research into the phenomenon itself indicates that it provides energetic advantages to enabled communities and therefore could pave the way to superior treatment designs (Jin et al. 2022). This demonstrates the potential that environmental engineers can unlock when complex metabolic processes are understood, rather than relying on chemical measurements of the outcomes. One aspect that could certainly benefit from an overhaul in design approach towards the metabolically fundamental is Green House Gas (GHG) emission reduction.

1.1.2 The Green House Gases of Biological Wastewater Treatment

As part of the ambition to increase the environmental friendliness of wastewater treatment, there have been many efforts to reduce both the energy demand of treatment and the GHGs emitted. Unfortunately, the release of some GHGs in the course of wastewater treatment is inevitable, the most important of which are carbon dioxide (CO_2), methane (CH_4), and nitrous oxide (N_2O). With estimates that the global wastewater treatment industry is responsible for up to 7 % and 10 % of anthropogenic CH_4 and N_2O emissions, respectively, this seems a reasonable goal (Maktabifard et al. 2023).

In order to make a complete assessment of the GHG emissions of wastewater treatment, it is important to take a plant-wide approach, which includes both the direct and indirect emissions (Mannina et al. 2016). Direct emissions are those associated with the treatment process itself, which for biological treatment are the metabolic outputs from the microbes employed. Indirect emissions are those associated with the consumption of imported electrical or thermal energy (indirect internal) and those associated with commissioned activities by third parties, such as chemical production and logistics (indirect external).

To undertake plant-wide assessments, the industry relies on sophisticated mathematical models to estimate their gross and net emissions, models that are frequently updated to reflect the latest research and climate science (Water UK 2021). Naturally, factors such as the potency of GHGs are an important modelling component, given that CH_4 has a global warming potential that is 27.9 times that of CO_2, while N_2O is 273 times as impactful (Ritchie et al. 2023). With this in mind, it should be particularly concerning that current models are markedly flawed for N_2O emissions, due to incomplete understanding of the mechanisms by which it is generated (de Haas and Andrews 2022).

With mounting pressure on governments and the private sector to do all in their power to protect our changing climate, it should come as no surprise that the body of research surrounding the reduction of emissions from WWTPs is rapidly growing. While modelling improvements could, and no doubt will, be made to ensure plant designers and operators have a clearer idea of the environmental risks they are undertaking, there is a definite need to develop engineering solutions that will actually curb direct and indirect emissions. Tactics such as changes to operational conditions to minimise emissions, treatment of biogases, and novel configurations to prevent emissions have been experimented with for a number of years. From these experiences, the presiding ideas for emission **prevention** can be summarised as: reduction of energy consumption; minimisation of sludge production; and optimisation of the amount and quality of combustible biogas (Campos et al. 2016).

All of the aforementioned emission prevention tactics can be achieved using anaerobic treatment technologies. Consequently, there has been increased interest in anaerobic technologies for domestic wastewater treatment. The inherent benefits are certainly appealing: lower energy demand, reduced sludge production, and CH_4-rich biogas. What's more, design evolutions such as the inclusion of DIET are making anaerobic technologies ever more appealing to industry. However, Biological Nitrogen Removal (BNR) from wastewater cannot be completed by anaerobic treatment alone. Furthermore, given the potency of N_2O as a GHG, it cannot be ignored when proposing novel configurations or processes.

1.1.3 Biological Nitrogen Removal in Wastewater Treatment

Previous BNR designs focused on nitrogen assimilation to biomass as a means of resource recovery, generating high value fertiliser that can be sold for agricultural land-application. However, there are points of contention with this approach. Firstly, it relies on the production and stabilisation of a substantial amount of biomass, which is not always energy or cost effective. Secondly, there are growing concerns over micro-pollutants in wastewater and its end-products that are discouraging the use of treated sludge for food production (Pozzebon and Seifert 2023).

The microbially-mediated processes for nitrogen cycling that are currently widely recognised are shown in Figure 2. As applied by engineers for BNR, the conventional process is aerobic nitrification followed by anaerobic denitrification, and the relatively recent introduction of anaerobic ammonium oxidation (anammox) has offered attractive alternative configurations. However, in all three of these processes, there is a risk of N_2O release (Zhang et al. 2018). Fortunately, a fascinating microbial capability that has the potential to resolve, or at the very least de-escalate, this particular problem was recently discovered.

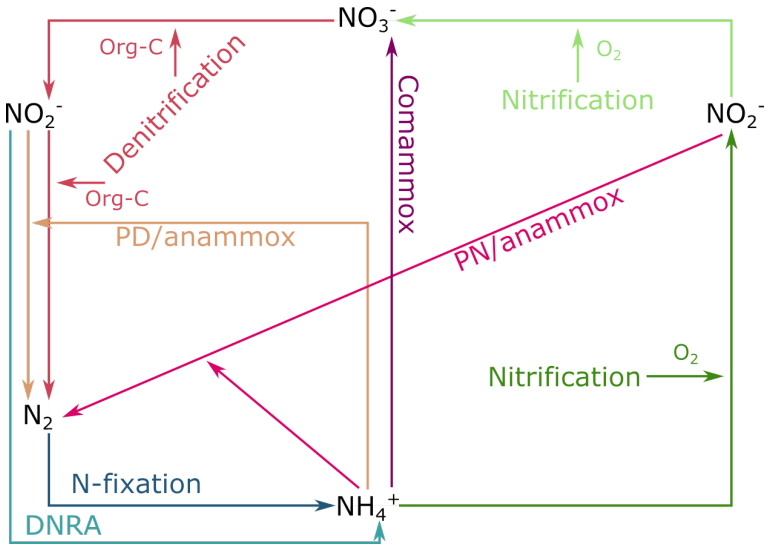


Figure 2: Major pathways in the nitrogen cycle, adapted from Venturin et al. (2022)

First proposed by Ettwig et al. (2010), Nitric Oxide Dismutation (NOD) intercepts the release of N_2O in anaerobic environments by instead transforming nitric oxide (NO) into harmless di-nitrogen (N_2) and oxygen (O_2), as shown in Figure 3. Similarly to DIET, this phenomenon appears to have developed as a coping strategy in harsh anaerobic environments, where energetically favourable reactions are hard to come by. This process is also referred to as "oxygenic denitrification", and as such, it has significant implications for metabolic substrate cycling in otherwise anaerobic environments.

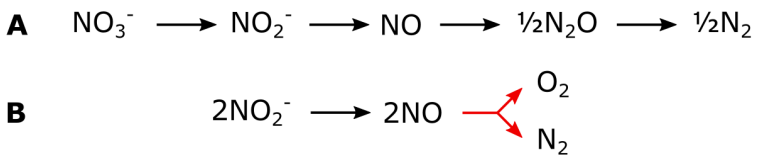


Figure 3: Putative nitric oxide dismutation pathway, adapted from Ettwig et al. (2012): (a) conventional denitrification pathway; (b) nitric oxide dismutation pathway

Dismutation (a.k.a. disproportionation) is a type of reaction in which a molecule of intermediate oxidation state is converted into two products of asymmetrical oxidation states (IUPAC 2019). In these reactions, the general formula of which is shown in Equation 1, a molecule is simultaneously oxidised and reduced. This can occur spontaneously, as is the case for the decomposition of hydrogen peroxide, or it can

be facilitated by dismutase enzymes. If successfully applied to wastewater treatment as a complement to conventional denitrification, the NOD pathway has the potential to not only resolve a significant design challenge in BNR technologies, but also further the appeal of anaerobic technologies for domestic wastewater treatment.

$$A + A \rightarrow A' + A'' \tag{1}$$

1.2 Research Statements

1.2.1 Problem Statement and Hypothesis

Beyond effective removal of COD and nitrogen species (N) from domestic wastewaters, WWTPs must contribute to the global effort to mitigate climate change by reducing their direct and indirect GHG emissions. The advantages of anaerobic treatment technologies for doing so are apparent, however, despite the interest, a suitable technology that can treat large volumes of low-strength wastewater has yet to be integrated into industry. Hence, there is a need to investigate effective anaerobic technologies that can effectively and quickly treat wastewaters while generating a CH_4-rich biogas coupled with N_2O free/limited BNR.

Given that both DIET and NOD are found in environments that select for genes to cope with a lack of O_2, it is hypothesised that these phenomena can act cooperatively, leading to simultaneous CH_4 generation and complete BNR to N_2. This will be beneficial for future wastewater treatment plant design, as the primary treatment technology can be anaerobic.

1.2.2 Aims and Objectives

The aim of this research project is to investigate the impact of a low nitrate (NO_3^-) dose on an anaerobic system that has previously been shown to accommodate DIET for successful high-rate treatment of low strength wastewater. As such, this project is an enrichment study for a microbial community in an engineered environment and a feasibility study for the coupling of DIET and NOD. It is also an application of meta-omics to further the literature and understanding of how NOD functions in complex environments. The aims will be achieved and the hypothesis tested by taking a holistic approach to assess the coupling of DIET and NOD, undertaken by adhering to the following objectives:

1. Develop two bench-scale anaerobic reactors - one with conductive material, one without to explore electron (e^-) sharing pathways - to treat a synthetic wastewater containing NO_3^- under identical operational conditions.

2. Monitor the performance of the reactors using chemical analyses to confirm successful operation and assess substrate transformations. Achieved by implementing routine testing on influent and effluent streams.

3. Complete a mass balance for carbon, nitrogen, and oxygen from the performance data.

4. Extract samples for meta-omic analysis to provide insight into the microbial communities and metabolic pathways.

   (a) Assess the microbial community structure and the functional profile, and compare to other relevant Anaerobic Digestion (AD) meta-omic datasets to look for significant differences.

   (b) Resolve meta-genome data into Metagenome Assembled Genomes (MAGs) and interrogate relevant, high-quality genome bins for metabolic pathway reconstruction.

5. Assess the impact of conductive material and NO_3^- dosage by reviewing DIET and inorganic-N metabolism, and the commercialisation potential.

2 Literature Review

2.1 Anaerobic Wastewater Treatment Design

2.1.1 Overview of Anaerobic Technologies

With the wide variety of wastewater treatment technologies available today, it is perhaps more complex than ever for engineers to select the appropriate technology for any given circumstances. This is especially true when considering anaerobic technologies as the primary biological treatment step. Their appeal is in the promise of lower operational expenditure, energy recovery potential from CH_4-rich biogas, and substantially reduced biomass production (Stazi and Tomei 2018). However, inevitably, they present their own operational challenges, such as the need for extended retention times due to the slow-metabolising nature of anaerobic microbes, acidification, and temperature sensitivity.

Despite their slow-growing nature, high-rate, suspended-growth anaerobic processes have had many successes. One of the most successful is the Upflow Anaerobic Sludge Blanket (UASB), which is very popular in Latin America and India, where ambient temperatures are higher (Daverey et al. 2019). Or, a variation on the UASB, the Expanded Granular Sludge Blanket (EGSB), which has shown remarkable performance capability and has been rising in popularity for some time (Lier et al. 2015). In addition, to attempt to mitigate temperature sensitivity, influent heating to create either a mesophilic (35-40 °C) or thermophilic (55-60 °C) environment has become a popular compliment to enhance microbial activity, achieved with the excess heat from burning biogas and/or with grid electricity (Labatut et al. 2014).

On the other hand, Membrane BioReactors (MBRs) have seen a surge in popularity in recent years (Deng et al. 2022). The combination of microbial activity to remove COD and the membrane filtration of Suspended Solids (SS) has accrued a lot of interest in these reactors for both anaerobic and aerobic technologies. The primary drawback of MBRs is the fouling, which incurs the greatest operational challenge to manage (Chang et al. 2019). Despite this, the ability to completely decouple Hydraulic Retention Time (HRT) and Solids Retention Time (SRT), and produce almost unbeatably high effluent quality maintains their appeal.

Alternatively, attached-growth anaerobic technologies - such as the Anaerobic Fluidised-bed BioReactor (AFBR) - are entering the market, presenting an exciting opportunity to further shift the paradigm. The AFBR technology specifically has drawn much engineering interest owing to its consistent success, most notably achieving high quality effluent at short HRTs (Yeshanew et al. 2018). These can largely be attributed to the good mass transfer of substrate to the biofilm, the extended SRTs, and low clogging potential (Shin et al. 2011).

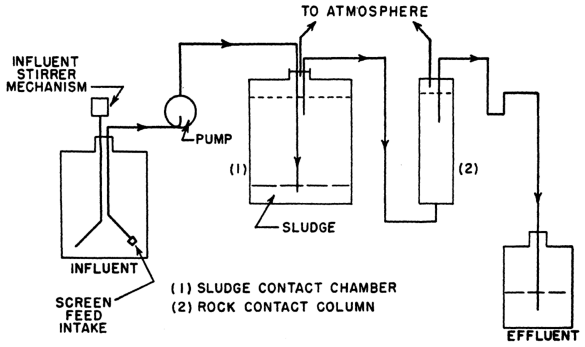
Furthermore, when combined with submerged membranes, the fluidised media provides a scouring effect, reducing operational problems associated with membrane fouling (Aslam et al. 2017). These reactor formations are known as the Anaerobic Fluidised-bed Membrane BioReactors (AFMBRs) or the Staged Anaerobic Fluidised-bed Membrane BioReactors (SAF-MBRs). By combining the benefits of high-rate anaerobic treatment, attached growth, and MBR, these reactors can achieve high COD removal at low retention times, and even micro-pollutant removal (Dutta et al. 2014).

2.1.2 A Brief History of Anaerobic, Attached-Growth Technologies

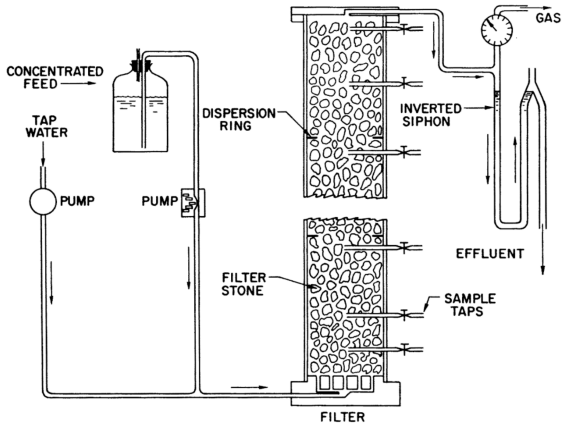
In the course of this literature review, the earliest report found of an anaerobic attached-growth design for low-strength wastewater treatment was the Anaerobic Contact Process (ACP) by Coulter et al. (1957), shown in Subfigure 4a. A two-stage design that featured an anaerobic sludge contact tank that fed into a column packed with gravel. In both stages, wastewater was fed directly to the bottom of the tanks, creating an upflow schematic. Although an average Biochemical Oxygen Demand (BOD) removal rate of 82 % was achieved at room temperature, issues with sulfides lead to the determination that the overall performance of the process was dissatisfactory.

12 years later came the Anaerobic Filter (AF) by Young and McCarty (1969), shown in Subfigure 4b. This design skipped the preceding stage of the ACP, and wastewater was fed upflow directly into a tall column packed with larger stones. In this way, the biomass within the AF itself provided the biological treatment, as opposed to the ACP, in which the column served mostly to prevent high SS in the final effluents following treatment in the contact tank. The advantages of this design were noted as: ideal for the treatment of soluble wastes; no effluent or solids recycling requirement; no heating requirement; and effluents were "essentially free" of SS. With that being said, extended HRTs were required, with COD removal rates falling below 90 % at anything less than 18 hours. Further results are summarised in Table 1. Moreover, issues with plugging were acknowledged, as well as high effluent SS at high Organic Loading Rates (OLRs). The design was ultimately recommended for waste strengths above 1,000 mg COD/l.

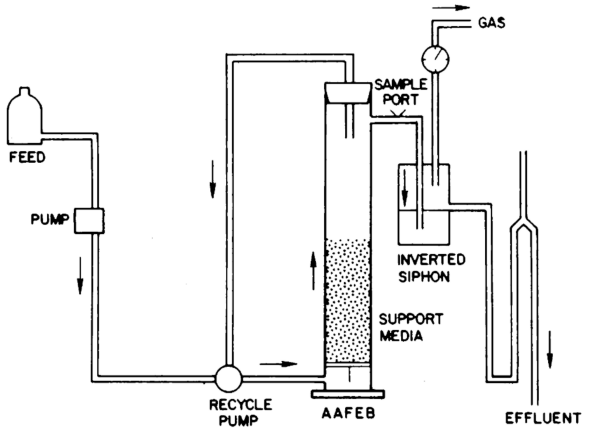
The next significant design evolution came 9 years later with the Anaerobic Attached-Film Expanded-Bed Reactor (AAFEBR) by Switzenbaum and Jewell (1978), shown in Subfigure 4c. This design, like its predecessors, was comprised of a tall column that was fed upflow through small metallic granules. However, unlike its predecessors, the media occupied only 40 % of the reactor height, which was then fluidised up to 50 % by an upflow effluent recycling line. As an improvement on the AF, the AAFEBR was able to treat wastes as dilute at 200 mg COD/l at reduced HRTs and temperatures. The performance metrics shown in Table 1 highlight the best and the worst COD removals at each temperature point tested. The primary issue highlighted with this design was the energy demand for recirculation pumping, which the previous



(a) Anaerobic contact process (Coulter et al. 1957)



(b) Anaerobic filter (Young and McCarty 1969)



(c) Anaerobic attached-film expanded-bed reactor (Switzenbaum and Jewell 1980)

Figure 4: Early attached-growth anaerobic wastewater treatment reactor designs. *Images reproduced with permission from the copyright holder (see Table 40 in Appendix A5).*

designs did not incur.

The attached-growth technique has undoubtedly facilitated the success of the AAFEBR, hereafter referred to as AFBR, by extending the SRT. Meanwhile, the fluidisation of the media provides improved mass transfer between the liquid, biofilms, and headspace. Nevertheless, continuing over 65 years of design evolution, there are still ongoing experiments to optimise the technology. One avenue being explored is the choice of media itself.

2.1.3 The Future of Anaerobic Fluidised-bed BioReactors

There have been experiments with many types of media, including activated carbons (Kim et al. 2011; Park et al. 1999), sand, glass beads, and expanded clay (Oliveira et al. 2010), and plastics (Kim et al. 2020; Kwon et al. 2022). Beyond the surface area provided for microbial growth, engineers are increasingly aware that the choice of media can serve a variety of desirable functions. Indeed, one of the most intriguing

Table 1: Performance of early attached-growth anaerobic wastewater treatment reactor designs, adapted from Young and McCarty (1969) and Switzenbaum and Jewell (1980)

Technology	HRT (h)	OLR (kg COD/m^3/d)	Temp. (°C)	COD removal (%)	SS (mg/l)
AF	72.00	0.42	25	93.4	24.0
	36.00	0.42	25	92.1	9.0
	18.00	0.85	25	91.5	6.0
	9.00	1.70	25	79.3	5.0
	4.50	3.39	25	36.7	250.0
AAFEBR	4.00	3.6	30	85.3	37.3
	0.33	14.4	30	25.5	10.0
	6.00	1.6	20	87.8	17.3
	0.33	14.4	20	38.0	10.0
	6.00	1.6	10	83.2	48.0
	0.33	14.4	10	35.2	32.0

properties is the electrical conductivity of the media, which plays an important role in facilitating DIET between the microbes that grow there.

Conductive and highly porous, activated carbon seems an ideal media for DIET-enabled biofilm formation. However, its use as a fluidised media instead of a packing media proved to be operationally challenging due to its brittle nature. During early lab work using Granular Activated Carbon (GAC), it was found that the constant movement caused the particles to break into ever smaller sizes, leading to wash out and destructive abrasion of the recirculation pumps. Washout has also been reported as an inhibitor elsewhere in the literature (Baek et al. 2023). Hence, exploration of alternative conductive media was required.

Plastic medias such as PolyVinylidene DiFluoride (PVDF) and PolyEthylene Terephthalate (PET) proved to be much more durable, albeit non-conductive. Hence, the study by Kwon et al. (2022), in which a semi-conductive Polyaniline (PANI) coating was applied to the plastics makes an interesting proposal. During operation of bench-scale AFMBRs, it was observed that the PANI coated media had much shorter acclimatisation times, but ultimately COD removal was not strongly impacted by the presence of the PANI coating, with all reactors reaching ~90 % removal. However, the coating did impact the CH_4 yields and the microbial community structure. Over the course of the experiment and the various operational conditions examined, it was found that CH_4 yields were up to 190% higher for the coated medias. Upon examination of the microbial community structure, significant differences were observed that provided fascinating insights into the potential source of these performance results. This will be discussed in detail in subsubsection 2.2.5.

The opportunity presented by the AFBR technology is clear. A low-energy, high-rate, small footprint solution that can optimise CH_4 yields via advection and media selection, and can be combined with membranes to produce high quality effluent while reducing membrane fouling. Given the impressive performance already being achieved by the AFBR technology, efforts to further understand the active pathways within could lead to discoveries with far reaching impacts on how WWTP design is approached.

2.2 Direct Interspecies Electron Transfer

2.2.1 Defining the Different Types of Interspecies Electron Transfer

Interspecies Electron Transfer (IET) is the umbrella term for the sharing of electrons between microbes to facilitate metabolism. Under the umbrella term, there are several distinct variations that appear in the literature, a graphical representation of which is shown in Figure 5. Conventional IET is the transfer of electrons via diffusion of shuttle molecules such as hydrogen (H) and formate, represented in Figure 5a. Direct Extracellular Electron Transfer (DEET) is the microbial capacity to exchange electrons with insoluble materials without first absorbing them (Lovley 2011), represented in Figure 5d-e. With this definition in mind, the distinction between DEET and DIET is the recruitment of another microbe for e^- exchange, represented in Figure 5b-c. Despite this distinction, the term DIET is commonly used for both biological and mineral mediated e^- exchange in the literature. As such, Sravan et al. (2021) defined DIET as:

> *"a syntrophic metabolism where free electrons flow from one cell to another through shared physical (microbe-microbe/microbe-electrode) and electrical connections (via conductive pili) without the requirement of reduced electron carriers (redox mediators) like molecular hydrogen or formate."*

The following subsections will summarise what is currently known about DIET, as well as establish conventions that will be used throughout the remainder of this thesis. Firstly, the term DIET will be predominantly used to refer to e^- exchange with both materials and other microbes. However, the term DEET may be used to emphasise e^- exchange with media rather than other cells.

2.2.2 Electroactive Microorganisms

In the first study of DIET, Summers et al. (2010) showed that *Geobacter sulfurreducens* and *Geobacter metallireducens* were able to share electrons without using redox mediators. 14 years later, the vast diversity of electroactive microorganisms - including bacteria, archaea, and eukaryotes - is still only beginning to be understood. However, the basic premise is clear, that two parties are required for the formation of a DIET community: exoelectrogens (electron donating species) and electrotrophs (electron accepting species). To attempt to list all of the species that have been described as electroactive would be reductive, as this field of research continues to rapidly expand, largely due to improved access to multi-meta-omic analysis tools. To emphasise this point, Figure 6 shows the phylogenetic diversity results from a review paper on electroactive microorganisms found in BioElectrochemical Systems (BES).

Fortunately, in methanogenic communities, as found in anaerobic bioreactors and soils, it is primarily archaeal methanogens that accept the electrons donated by fermentative bacterial neighbours (Dubé and

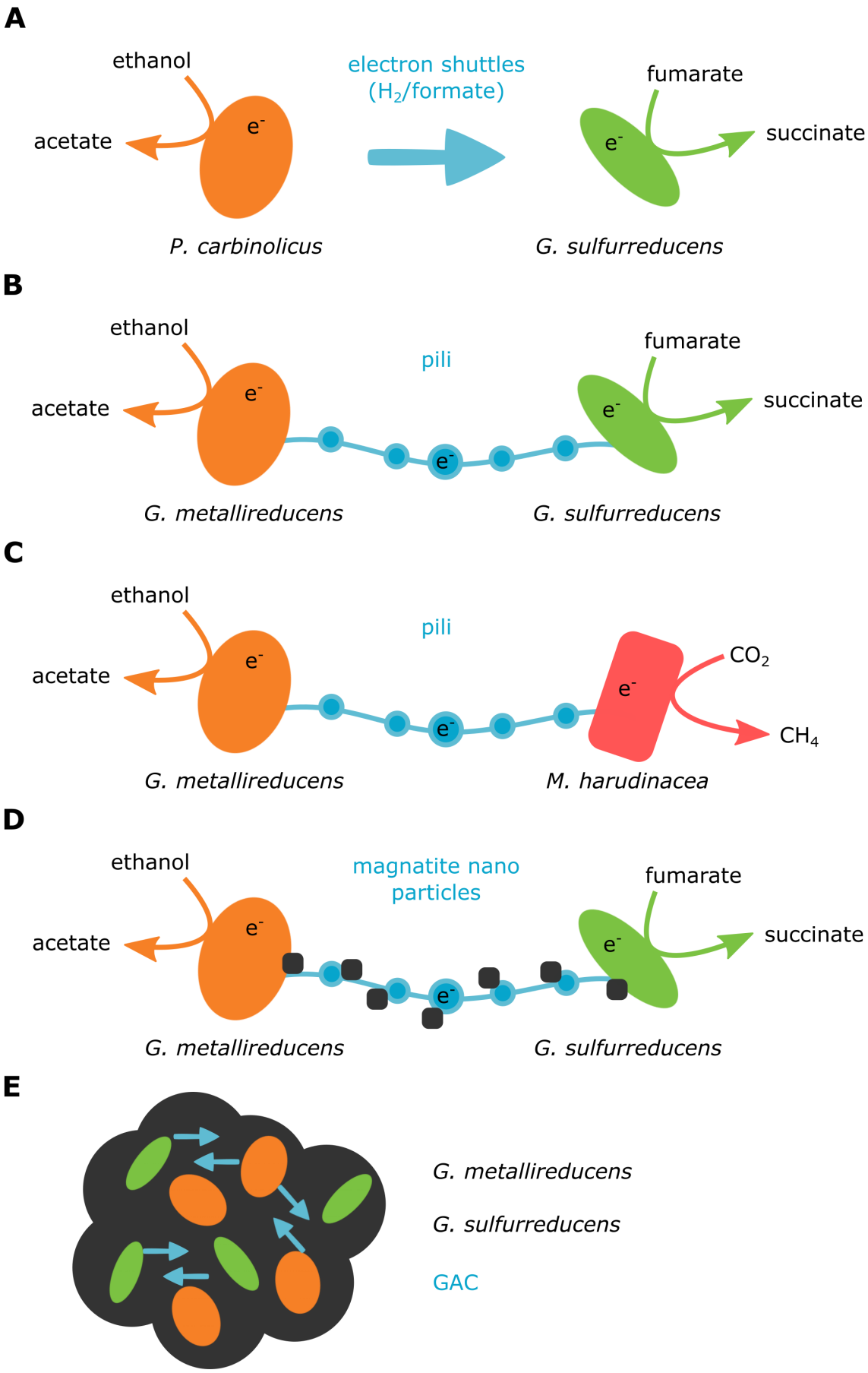


Figure 5: Interspecies electron transfer mechanisms, adapted from Shrestha and Rotaru (2014): (a) conventional IET via electron shuttle molecules; (b) DIET via pili; (c) methanogenic DIET via pili; (d) DEET via magnetite nano particles; and (e) DEET via GAC.

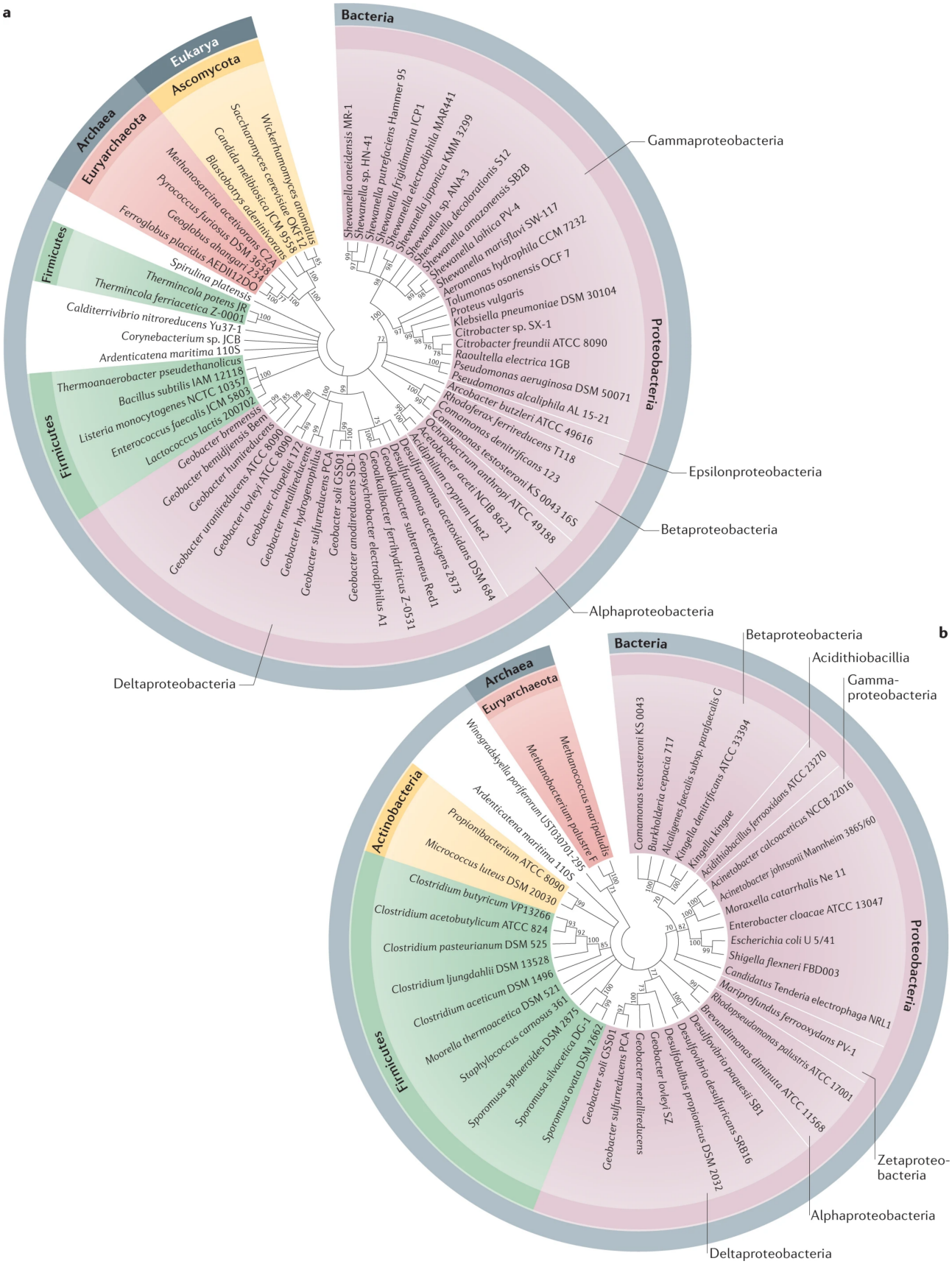


Figure 6: Phylogenetic analysis of electroactive microorganisms found in bioelectrochemical systems: (a) exoelectrogenic species; (b) electrotrophic species. Note that some species, such as *G. sulfurreducens*, appear in both circles, being able to both give and take electrons. *Image reproduced with permission from the copyright holder (see Table 40 in Appendix A5).*

Guiot 2015). Hence, for the purposes of this research programme, with an emphasis on methanogenesis, the focus will be on archaeal electrotrophic methanogens and their bacterial exoelectrogenic partners.

In the literature on BES, there are two bacterial species that have been given the moniker of "model exoelectrogens": *G. sulfurreducens*[1] and *Shewanella oneidensis* (Yang et al. 2012). This is largely due to their dissimilatory metal reduction capabilities and the fact that both species have multiple completely annotated genomes, making them simpler to assess. Including *G. metallireducens* and *G. sulfurreducens*, there are 4 confirmed DIET-capable *Geobacter* species, the most recent additions being *Geobacter hydrogenophilus* (Rotaru et al. 2015) and *Geobacter grbiciae* (Deng et al. 2023).

Despite studies that indicate plenty of others, there are precious few that make the cut as confirmed DIET-capable exoelectrogens - these are *Desulfovibrio* strain JY, *Rhodoferrax ferrireducens*, and *Syntrophus aciditrophicus* (Akram et al. 2024). Nevertheless, other implicated exoelectrogenic genera that have appeared frequently in the literature, or are particularly interesting in the context of anaerobic wastewater treatment, include, but are far from limited to: *Thauera*, *Pseudomonas*, *Syntrophomonas*, and the sulphate reducing bacteria *Desulfotomaculum* and *Desulfobulbus* (Lovley 2017b; Lovley and Holmes 2022; Valero et al. 2018).

The register of electrotrophic methanogens is more conservative, mostly in the genera *Methanosaeta*[2] and *Methanosarcina*. The confirmed DIET-capable species are *Methanosaeta harudinacea*, *Methanosaeta soehngenii*, *Methanosaeta thermoacetophila*, *Methanosarcina barkeri*, *Methanosarcina acetivorans*, *Methanosarcina horonobensis*, *Methanosarcina subterranean*, *Methanosarcina mazei*, and one *Methanobacterium electrotrophus* (Akram et al. 2024). Others that have been implicated include *Methanosaeta concilii* (Yang et al. 2019) and species in the *Methanolinea*, *Methanoregula*, and *Methanospirillum* genera (Valero et al. 2018).

The distinction between "confirmed" and "implicated" DIET-capable microbes is attributable to the state of the field. Being a relatively young field of research, there are few agreed upon methodologies for the confirmation of novel electroactive species, despite the veritable boom in interest and high quality research. This is compounded by two factors: the difference between DEET-capable species in BES and DIET-capable species in methanogenic environments; and the differences in certainty between defined co-cultures and uncontrolled mixed cultures.

In BES studies, such as microbial fuel cells, there are clear distinctions between the exoelectrogens

[1] *G. sulfurreducens* is also electrotrophic, and appears more frequently as such in the literature
[2] The *Methanosaeta* genera is also sometimes referred to as *Methanothrix*

on the anode and the electrotrophs on the cathode (Ajunwa et al. 2021). As such, species with strong preferences for those facilities are implicated as electroactive, hypothesised to harness the e^- source/sink provided externally to the cell. However, while those species may be DEET-capable, this does not guarantee a translation to DIET-capable. For example, while *S. oneidensis* is a model exoelectrogen, it has been shown to be incapable of DIET syntrophy with either *M. barkeri*, *M. acetivorans*, *M. horonobensis*, or *M. subterranean* (Holmes et al. 2022).

Meanwhile, defined co-culture studies use extremely controlled conditions and gene mutants to provide very strong evidence that a particular microbial partnership is DIET-syntrophic. Hence, it is only once a defined co-culture is observed to form a successful DIET-syntrophic relationship that those species are bestowed their official title of DIET-capable. However, in uncontrolled mixed cultures, be that BES or methanogenic environments, where complex metabolic processes and flexible syntrophic partnerships are relied upon for survival, it is much more difficult to provide certainty.

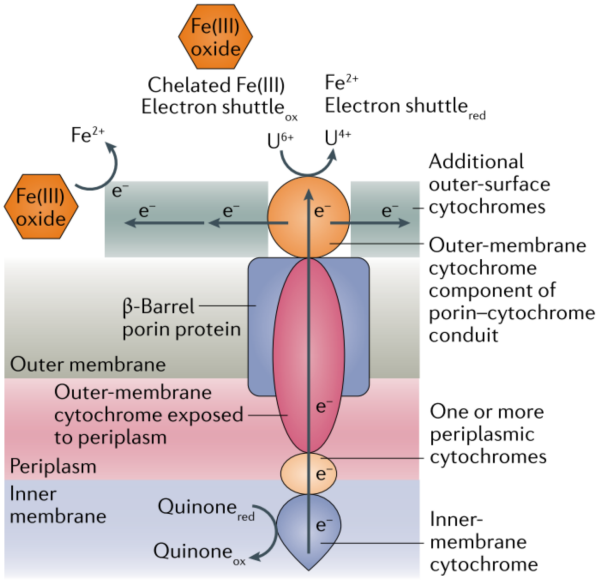
Across the field-wide literature, this blended approach between mixed culture and pure culture, BES and methanogenic studies, works to propose and confirm novel electroactive and DIET-capable species. Further evidence to support such claims is usually the observation of particular growth behaviours, which will now be discussed.

2.2.3 Microbe-Microbe Electron Sharing

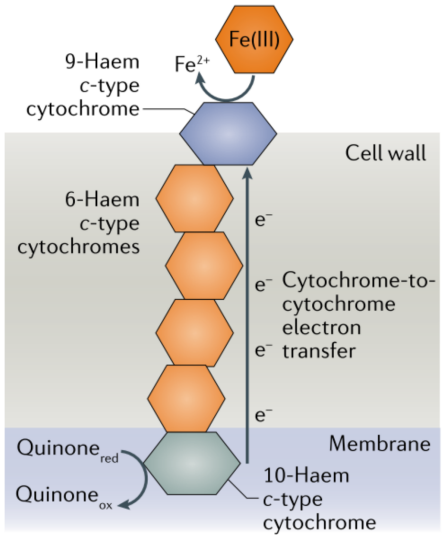
In the original DIET study by Summers et al. (2010), *G. metallireducens* was co-cultured with a gene deletion mutant of *G. sulfurreducens* that was unable to consume H – thereby preventing interspecies H or formate transfer. It was observed that this modified co-culture was able to form large aggregates within 21 days, compared to 7 months for the same achievement with the wild type of *G. sulfurreducens*. The clear syntrophy between these two species that had no means of sharing electrons through diffusion lead to the proposal that another mechanism for e^- transfer must be at play. Since then, further studies and developments in analytical technologies have progressed the understanding of the various DIET mechanisms. However, it is acknowledged that a full understanding remains elusive, particularly for Gram positive bacteria and archaea (Lovley and Holmes 2022). The microbe-microbe e^- sharing mechanisms that are most commonly examined are *c*-type cytochromes (*c*-cyts) and electrically conductive pili (e-pili).

Cytochromes are a diverse collection of proteins with multiple classes and subclasses, however, they all share one common trait: embedded iron-containing heme rings that can undergo reversible redox reactions (Bendall 2016). This specialised ability has placed cytochromes at the centre of biological e^- transfer studies for decades. In particular, *c*-cyts have been studied extensively for their role in DIET due to their

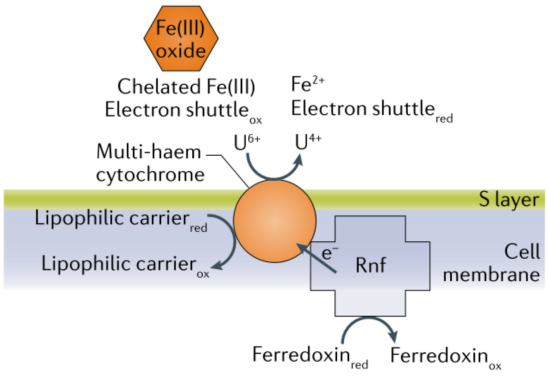
capacity to hold multiple heme moieties and their presence at every sub-cellular level from the inner to the outer membrane and in the extracellular matrix (Edwards et al. 2020; Ueki 2021). Current models for *c*-cyt-based e^- transfer in Gram negative, Gram positive, and archaea are shown in Subfigure 7a, Subfigure 7b, and Subfigure 7c, respectively.



(a) the porin–cytochrome system found in Gram negative bacteria



(b) the cytochrome-based system in Gram positive bacteria



(c) the cytochrome-based system in archaea

Figure 7: Mechanisms for *c*-type cytochrome electron transport across the outer surface. *Images reproduced with permission from the copyright holder (see Table 40 in Appendix A5).*

Despite these properties, the linkage between *c*-cyts and DIET is not as strong as originally anticipated. Association with porin-like structures or pili has lead to an increasing awareness that the presence of *c*-cyts alone is a poor indicator for DIET activity (Leang et al. 2010; Liu et al. 2014a). Furthermore, some methanogenic co-cultures have been shown to be capable of *c*-cyt independent DIET-syntrophy (Yee and Rotaru 2020). Nevertheless, while *c*-cyts may be weak indicators of DIET, they should not be dismissed out of hand.

Pili, on the other hand, are long non-flagellar appendages protruding from the cell surface, present in

a diversity of Gram negative and Gram positive bacteria and archaea (Hospenthal et al. 2017). There are several types of pili, serving a variety of purposes, including horizontal gene transfer, biofilm formation, and virulence factors. Their association with e^- transfer was first reported in 2005, wherein they were described as "microbial nanowires" capable of electrical conductance (Reguera et al. 2005). To date, type IV pili (and associated homologs) are the only ones shown to have conductive properties, extending the e^- sharing network over micrometer distance (Lovley and Holmes 2020).

The linkage between DIET and e-pili is much stronger, although their actual mechanism for e^- transfer is not fully elucidated (Boesen et al. 2021). Moreover, not all e-pili are created equal - some are more conductive than others. Table 2 shows the measured e-pili conductivities for various *Geobacter* species, including *Geobacter uraniireducens*, which has poorly conductive e-pili and is not DIET-capable. Hence, when associated with known electroactive microbes, expression of e-pili can be taken as a good indicator of DIET in mixed cultures.

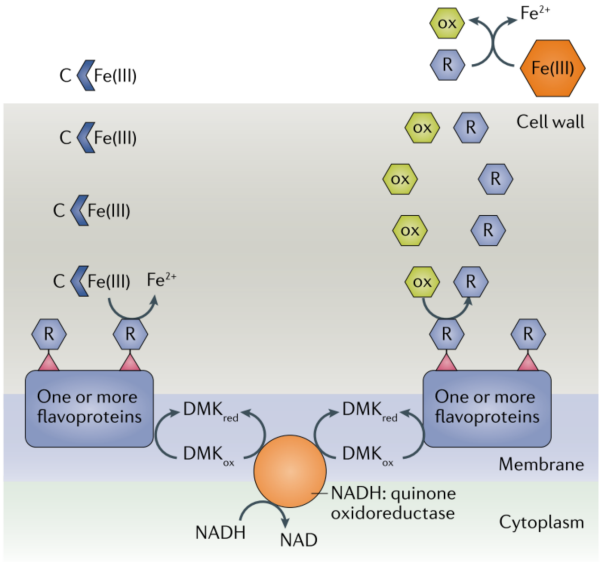
Table 2: Approximate conductivities of e-pili of *Geobacter* species, adapted from Akram et al. (2024)

Microorganism	Conductivity (mS/cm)
G. metallireducens	2.77e5
G. sulfurreducens	51
G. uraniireducens	0.3

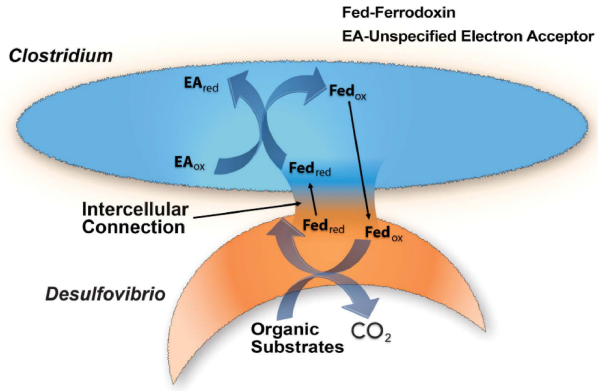
While the research into *c*-cyts and e-pili continues, including species dependency (Holmes et al. 2022), alternatives cannot be ignored. Not least because *D.* strain JY - a confirmed exoelectrogen - is capable of participating in DIET with *M. harudinacea* without genes for either outer-membrane *c*-cyts or e-pili (Zheng et al. 2021). While their absence can be mitigated by the presence of conductive materials (discussed in the next subsection), there are a handful of proposed alternative microbe-microbe DIET pathways. For example, flavoproteins and biological nanotubes.

Like cytochromes, flavoproteins are a class of oxidizing enzymes featuring flavin moieties, known to be involved in e^- transport (Costas et al. 2017). As observed thus far, their engagement in DIET is unique to Gram-positive bacteria that lack *c*-cyts (Lovley and Holmes 2022). However, unlike cytochromes, they are embedded in the cell membrane, contained behind the cell wall, shown in Subfigure 8a. Unable to reach the extracellular environment themselves, flavoproteins transfer electrons to chelated iron or flavins that can permeate through. Hence, the role of flavoproteins is akin to an essential middle man in the execution of DEET, if not strictly DIET.

Lastly, biological nanotubes are cell membrane connections that pave a direct road for the transfer of



(a) Model for electron exchange by Gram positive bacteria proposed by Light et al. (2018)



(b) Model for electron exchange between *Desulfovibrio vulgaris* and *Clostridium acetobutylicum* proposed by Benomar et al. (2015)

Figure 8: Alternative models for direct interspecies electron transfer: (a) flavoproteins for redox of permeable electron carriers; (b) biological nanotubes for direct transfer of electron carriers. *Images reproduced with permission from the copyright holders (see Table 40 in Appendix A5).*

resources, a concept that has been acknowledged in microbiology for some time (Dubey and Ben-Yehuda 2011). As a DIET mechanism, this refers specifically to the transfer of e^- carriers, such as flavins or ferrodoxins, shown in Subfigure 8b. Nanotubes are distinguished from conventional diffusion by the direct delivery mechanism and the requirement for direct cell-cell contact. However, the continued reliance on shuttle molecules may mean that it may not be as efficient as other methods.

2.2.4 Microbe-Electrode Electron Sharing

The phenomenon of microbial e^- transfer via an electrode was first demonstrated by Liu et al. (2012) using co-cultures of *G. metallireducens* and *G. sulfurreducens* with GAC. The use of gene deletion mutants and the observation that 80 % of the cells were associated with the GAC, but not closely aggregated, indicated that cells were unlikely to be utilising biologically mediated e^- transfer. Simultaneously, syntrophic metabolism rapidly increased and, in cocultures of *G. metallireducens* and *M. barkeri*, CH_4 production was increased. It was ultimately concluded that the conductive properties of GAC were foundational to the performance enhancements observed.

In the interest of clarity, the term "electrode" refers to any conductive material provided to cells, whether connected to an external electrical circuit or not. Outside of BES, the conductive materials that can be utilised by electroactive microbes are typically iron (hematite, magnetite, ferrihydrite, ferricoxyhydroxide) or carbon based (activated carbon, carbon cloth, carbon nanotubes, biochar, hydrochar, graphene). Interestingly, just as microbe-microbe DIET has shown species dependency, microbe-electrode DIET has also

shown electrode dependency, with syntrophic partnerships altering their connection mechanisms depending on the presence and type of electrodes (Liu et al. 2014c; Zhou et al. 2023b). Review papers by Park et al. (2018) and Akram et al. (2024) provide detailed summaries of experiments with these materials, as well as others. Doubtlessly, experiments will continue, especially as industries look towards creating a more circular economy.

The benefits of microbe-electrode DIET, as compared to microbe-microbe, have been summarised as follows: accelerated innoculation times for new communities; enhanced long-term metabolism and, in the case of methanogenesis, enhanced CH_4 production; longer distance e^- sharing (which, by estimation, is what enables the former two); and compensation for the lack of *c*-cyts and e-pili (Akram et al. 2024). It must be noted that this latter advantage is perhaps the strongest indication that important DIET mechanisms remain unknown. Regardless of electrode type, it is hypothesised that these benefits are derived from two factors: the higher conductivity of the materials provided compared to biologically produced electrical connections; and the reduced need for cells to expend energy producing those connections (Liu et al. 2012).

As with much of this burgeoning field, a full understanding of the mechanisms remains elusive. However, engineering applications designed to take advantage of the benefits provided have already become popular. As is relevant to this research programme, the applications to anaerobic wastewater treatment will now be discussed.

2.2.5 Direct Interspecies Electron Transfer in Anaerobic Wastewater Treatment

Establishment of DIET in anaerobic wastewater treatment reactors has been associated with shortening of the lag phase at start up, accelerating CH_4 production, and improving CH_4 yields. It has also been associated with buffering against various inhibitors, as stronger syntrophic relationships are formed (Jin et al. 2022). It is unsurprising, therefore, that there have been numerous experiments looking to stimulate the effect. In reactors that don't contain conductive materials, cells require direct contact with each other to establish biological DIET. Hence, the stimulating effect is to simply encourage flocculation, as in UASBs, or biofilm formation, as in AFBRs. Supplementation of ethanol has also been shown to stimulate DIET (Feng et al. 2021). On the other hand, stimulation by supplementing with conductive materials has been widely attempted, with much success (Kang et al. 2021).

Activated carbon materials have received a lot of interest due to their high conductivity and absorptive properties that can also be beneficial for micro-pollutant removal (Allahkarami and Monfared 2024). Moreover, activated carbons such as biochar can be generated from waste streams of other industries, garnering a lot of interest for circular economic applications. However, as previously mentioned, their

brittle nature has been associated with operational problems. On the other hand, iron-based materials are subjected to corrosion by the very process engineers are trying to foster. Hence, there is appetite for alternative conductive materials that can be applied.

PANI was first experimented with by Hu et al. (2017), using nano rods in 1 l bottles inoculated with UASB sludge. Microbes were shown to have an affinity for the rods and CH_4 production was doubled compared to a control without PANI. Moreover, 16S rRNA gene sequencing revealed a significant increase in the relative abundance of *Methanosaeta* genera and a tremendous increase in *Clostridium sensu stricto* in the cultures that contained PANI. The combination of these factors led to the conclusions that PANI is a suitable material for stimulating DIET in anaerobic wastewater treatment and that *C. sensu stricto* may have DIET capabilities.

5 years later, Kwon and Kim (2022) applied a PANI coating to PET beads and PVDF pellets to conduct a feasibility test. The results showed increases in conductivity of the surfaces of the media, indicating the application was successful. Notably, adherence to the PVDF pellets was greater. Subsequently, in batch tests conducted with AD sludge, CH_4 yields were 9 % and 25 % higher for the coated PET and PVDF, respectively. Following this success, those media were deployed in a series of bench-scale AFMBRs to further determine their efficacy as DIET stimulants and as fluidised media (Kwon et al. 2022). As described in the previous section, the coated media provided accelerated acclimation and enhanced CH_4 yields, which in and of themselves is suggestive of DIET activity.

Concurrently, the taxonomic profiles from 16S rRNA gene sequencing analysis corroborated this observation, although unfortunately the biofilm samples from both coated and uncoated PET beads failed. From the archaeal profile, elevated relative abundance of *Methanosaeta* was found on samples from PANI-coated medias, especially in the biofilms. A confirmed electrotroph having a strong preference for the semi-conductive coating demonstrates that the PANI was functioning as intended. Meanwhile, the bacterial profile revealed high relative abundance of the *Cryptoanaerobacter* genus on the coated PVDF media. This lead to the proposal that this genus potentially has DIET capacity.

Ultimately, the successful application of PANI as a DIET-stimulant on a durable media in AFBRs presents an exciting step forward in the development of anaerobic wastewater treatment. It represents a high-rate, high-advection system that can benefit from accelerated start-up, enhanced CH_4 yields, and improved resistance to inhibitors using an operationally sustainable media. With an understanding of the mechanisms of DIET in hand, how it can be stimulated, and an idea of the benefits it can provide, the following sections will discuss the chemical and metabolic processes that take place during wastewater treatment that lead to the removal of COD and N and the role that DIET has within those processes.

2.3 Carbon Cycling in Anaerobic Wastewater Treatment

2.3.1 Hydrolysis, Acidogenesis, and Acetogenesis

The organic macromolecules that make up the COD of domestic wastewater are polysaccharides, proteins, and lipids, which are broken down via hydrolysis into simple sugars, amino acids, and fatty acids, respectively. This preliminary stage of catabolism follows the same path under both aerobic and anaerobic conditions, as they are decomposition reactions dependent on water, not redox reactions dependent on oxidising or reducing reagents. Although this process is expedited by extracellular enzymes secreted by hydrolytic bacteria (Meegoda et al. 2018). Beyond the hydrolytic stage, including glycolysis and the production of pyruvate, aerobic and anaerobic catabolism diverges, as the presence of O_2 does become a determining factor in how the process proceeds. In anaerobic environments, following Anaerobic Digestion Model No. 1 (ADM1), the stages following hydrolysis are acidogenesis, acetogenesis, and methanogenesis (Batstone et al. 2002). These stages are represented as the blue, orange, and green lines in Figure 9, respectively.

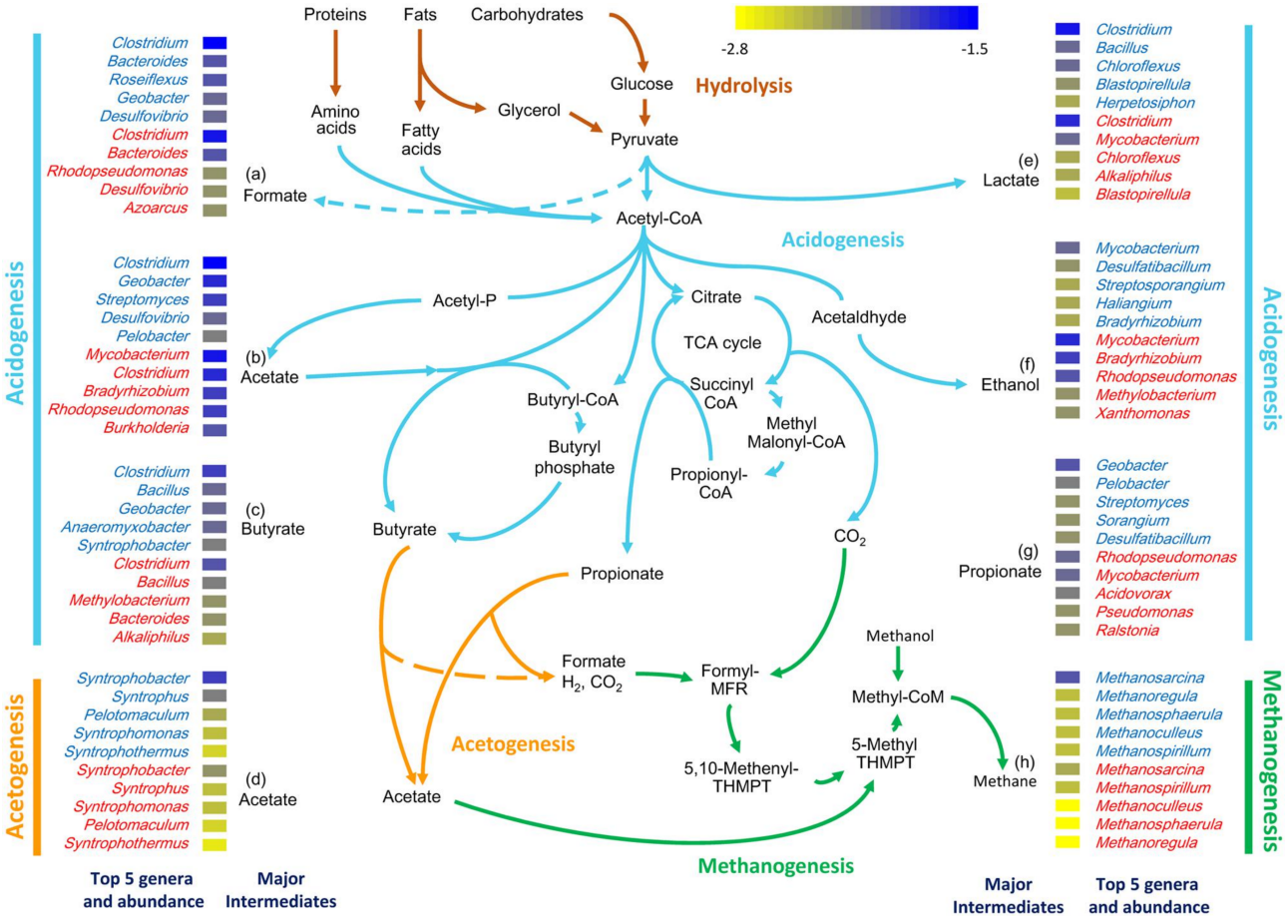


Figure 9: Key anaerobic digestion pathways and genera associated with major intermediates. Top 5 most abundant genera from each sample listed. Genomic samples taken from two different wastewater treatment plants: genera in blue text from Guangzhou; genera in red text from Shek Wu Hui. *Image reproduced with permission from the copyright holder (see Table 40 in Appendix A5).*

Acidogenic fermentation produces various Volatile Fatty Acids (VFAs), ethanol, dihydrogen (H_2), and

CO_2 through a diverse array of metabolic processes (Zhou et al. 2018). In recent years, there has been interest in arresting the process here, as longer-chain VFAs and H_2 can be extracted and sold for various high-value industrial applications (Dahiya et al. 2023). However, scalability and sustainability analyses remain as challenges to this type of bioindustry. In uninterrupted AD, acetogenesis then creates an abundance of acetate, achieved through either proton-reducing pathways (the version shown in Figure 9) or homoacetogenesis via the Wood-Ljungdahl pathway (Zhou et al. 2018). The former is the continued fermentation of longer-chain VFAs down to the smallest 2-carbon iteration, undertaken by secondary fermentative species. The latter is a H_2-consuming CO_2 fixation pathway, undertaken by autotrophic species (Ragsdale and Pierce 2008).

Of course, in reality, these processes are all happening simultaneously, especially in continuously stirred reactors. Nevertheless, all three of the preceding steps have an impact on methanogenesis. Hydrolysis, as it produces the substrates for the entire microbial community below it (Meegoda et al. 2018). Acidogenesis, as the accumulation of VFAs leads to inhibitory acidification and reactor failure (Zhang et al. 2023). Acetogenesis, as a final opportunity to moderate the partial pressure of H_2, either by producing more (fermentation) or consuming it (homoacetogenesis) at the penultimate stage.

This complex system is largely what has caused the operational challenges associated with AD. Thus, engineering solutions to better manage have been researched and implemented for years. For example, thermal hydrolysis has been used since 1995 and has proved to be highly successful at improving anaerobic biodegradation of substrates (Barber 2016). Additionally, multiple tactics have been developed to manage acidification, which can be largely grouped into: the use of additives, optimisation of process parameters, modification of process configuration, and co-digestion (Alavi-Borazjani et al. 2020).

With all of that said, viewing this process as a linear degradation of long organic carbon chains down to simpler chains, and eventually single carbon molecules, belies other important microbial metabolic processes. While the removal of organic substrates is important for meeting COD discharge requirements, WWTPs must also consider the removal of inorganic nutrients, carbon based or otherwise. Herein lies the importance of the metabolic cooperation between heterotrophs and autotrophs.

2.3.2 Methanogenesis

Differentiated from CH_4 generation as a by-product, methanogens are reliant on CH_4 synthesis for energy conservation, achieved by creating an ion motive force across the cytoplasmic membrane (Rother 2010). It is an exclusively anaerobic archaeal capability that, with expanding multi-meta-omic research, is being found in an ever greater diversity of microbes (Wu et al. 2024). However, most currently recognised species

belong to the *Euryarchaeota* phylum. The phylogeny of a selection of important methanogens is shown in Figure 10. Across the various methanogenic genera currently known, there are three core metabolic pathways, shown in detail with the associated enzymes in Figure 11: hydrogenotrophic, acetotrophic[3], and methylotrophic. Each of these pathways can be obligate or facultative, and, despite the nomenclature, can use an overlapping array of substrates. Nevertheless, their unifying feature is the actual methanogenic step, which is the reduction of methyl-com to CH_4 by the enzyme methyl-com reductase (Buan 2018).

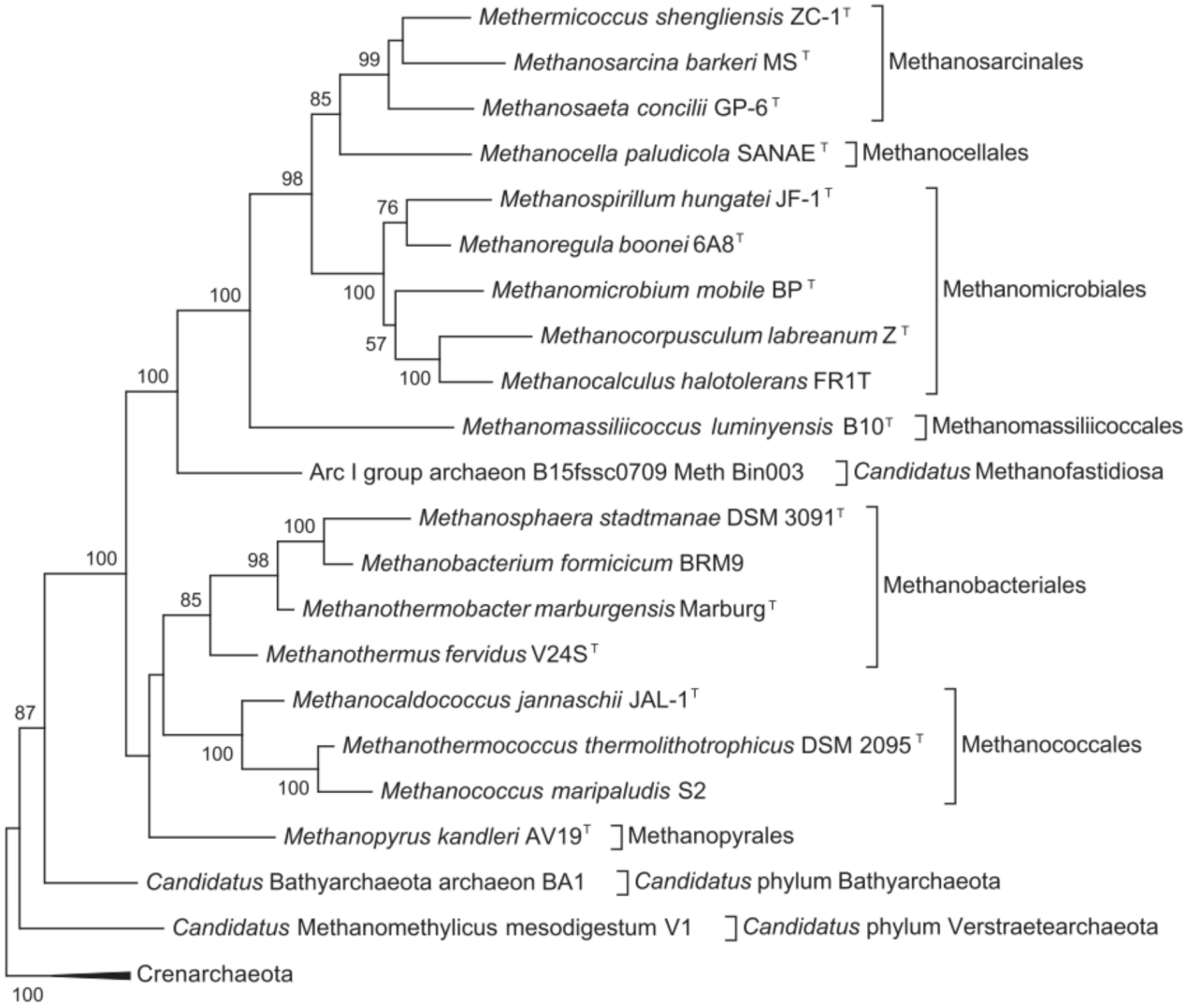


Figure 10: Phylogeny of methanogenic archaea. *Image reproduced with permission from the copyright holder (see Table 40 in Appendix A5).*

The hydrogenotrophic pathway is the most common, found in all of the Euryarchaeota orders. The standard application of this pathway is the reduction of CO_2 to CH_4 using H_2 as the e^- donor, with alternate substrates including formate (as either the carbon source or e^- donor) and methanol (as the carbon source) (Wagner et al. 2018). Hydrogenotrophic methanogenesis can be further divided by the presence or absence of cytochromes, with a lack thereof condemning a species to obligate hydrogenotrophy, with one exception

[3]Also referred to as acetoclastic

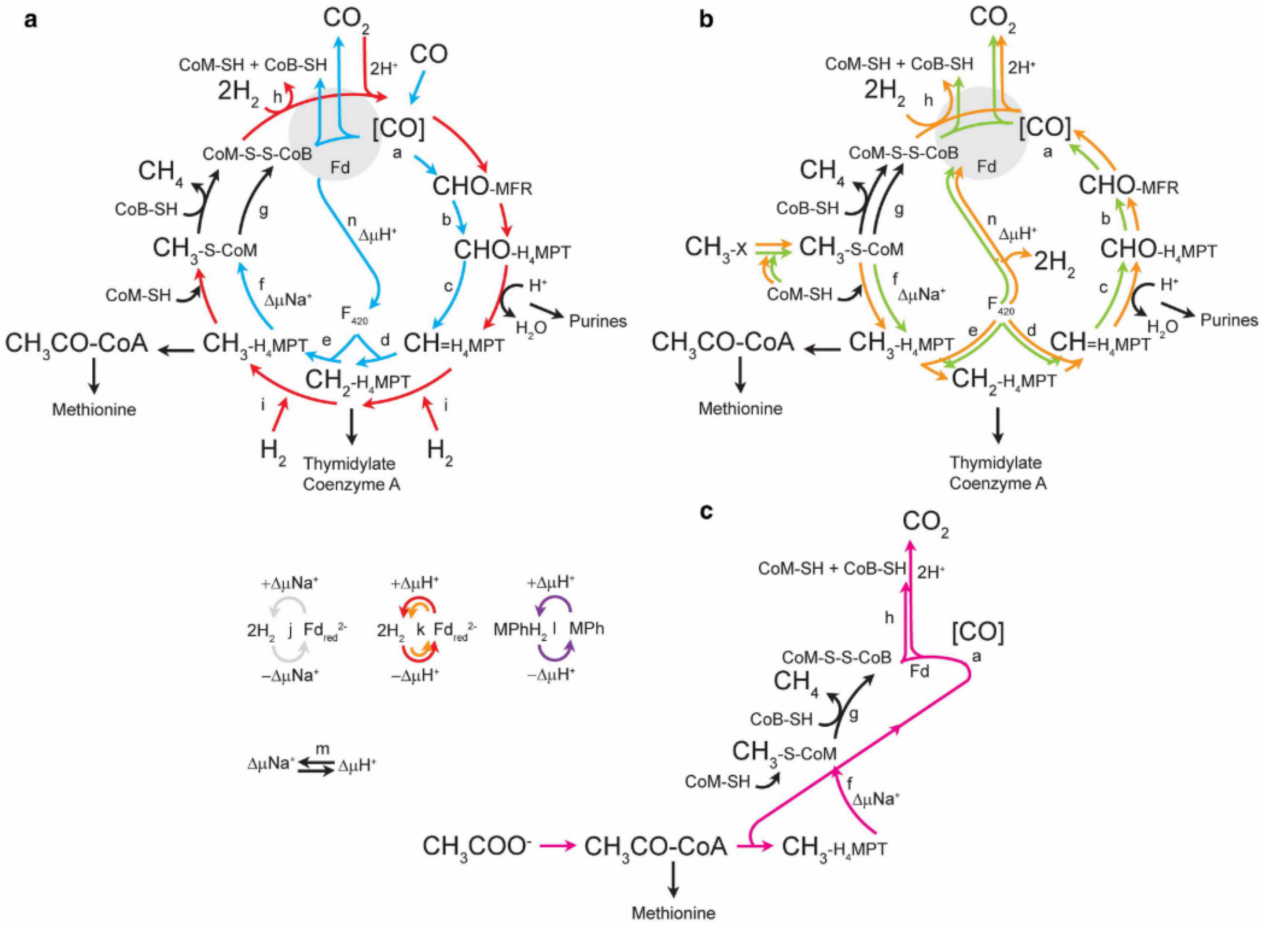


Figure 11: Methanogenesis pathways and associated enzymes: (a) hydrogenotrophic (red) and carboxydotrophic (blue) pathways; (b) methyl-respiration pathway (orange) and methylotrophic pathway (green); (c) acetotrophic pathway (fuchsia). Arrows represent direction of biochemical reactions. Black, reaction steps and directions common to all methanogenesis pathways. Purple, reactions found only in Methanosarcina species. Gray, proposed reactions. Shaded, electron bifurcation/confurcation reaction steps. *Image reproduced with permission from the copyright holder (see Table 40 in Appendix A5).*

- *Methanosphaera stadtmaniae*, which is obligate methylotrophic (Thauer et al. 2008).

Possession of cytochromes among methanogens is exclusive to the Methanosarcinales order (Mand and Metcalf 2019). As the last to diverge off of the Euryarchaeal evolutionary line (Boone et al. 1993), this relative modernity seems to impart some significant benefits, as well as unusual limitations. Beyond facultative hydrogenotrophy, species that contain cytochromes have the most metabolic diversity, exhibit higher growth yields, and can tolerate higher concentrations of H_2. On the other hand, they also have longer doubling times, an intolerance for high temperatures, and an inability to use formate as the e^- donor (Mand and Metcalf 2019; Thauer et al. 2008).

Also unique to the Methanosarcinales order are the two acetotrophic genera: *Methanosarcina* and *Methanosaeta*. Of these, *Methanosaeta* is the only obligate acetotroph, as it lacks the vital hydrogenases (Stams et al. 2019). This exclusivity may be due to the relative novelty of process, but more likely it

is associated with the low energetic favourability of the process, the lowest of the methanogenic routes (Schöne and Rother 2019). The acetotrophic pathway can be summarised as the dismutation of the acetate molecule, resulting in its transformation to a carboxyl group and a methyl group, eventually transformed into CO_2 and CH_4, respectively (Ferry 2010).

The term "methylotrophic" refers to any species that is capable of oxidising single carbon compounds that are more reduced than CO_2 or multi-carbon compounds lacking carbon-carbon bonds (i.e., dimethyl ether, dimethylamine, etc.). When discussing methylotrophic methanogenesis, there is an important distinction to be made: "true" methylotrophs dismutate methylated substrates without an additional e^- donor, a pathway found only in the Methanosarcinales order; whereas methyl-respiring hydrogenotrophs require H_2 or formate as a reductant (Conrad 2020; Schöne and Rother 2019).

Beyond these three "core" methanogenic routes, ongoing research is continually expanding this field. For example, finding novel substrates, such as carbon monoxide (carboxydotrophic, Schöne and Rother (2019)) and methoxylated aromatic compounds (methoxydotrophy, important components of lignin and coal, Kurth et al. (2021)). As well as alternate pathways, such as obligate mixotrophy (hydrogenotrophic CH_4 production which is only achieved in the presence of acetate for cell growth (Nagoya et al. 2020)) and alkylotrophy (combining the degradation of long-chain alkanes with methanogenesis without the need for syntrophs (Zhou et al. 2022)).

It is clear that there is still much for scientists to learn about this key microbial process, including gaining a full understanding of the critical methyl-com reductase (Wagner et al. 2018). While the process fundamentals are under constant review, for anaerobic wastewater treatment, the next step is understanding the factors that may prevent optimal CH_4 yields.

2.3.3 Inhibition of Methanogenesis and Methanotrophy

There are many factors that may produce dissatisfactory CH_4 yields from a fully established anaerobic wastewater treatment reactor. Environmental conditions such as pH, Dissolved Oxygen (DO) levels, temperature, salinity, and pressure can all impact methanogenic metabolism (Hoehler et al. 2019), all of which are factors that, with awareness, engineers can take steps to control. However, at the metabolic, biochemical level, there are important factors to be aware of that cannot easily be controlled through engineering systems. Namely: the H_2 partial pressure; the presence of thermodynamically preferable terminal e^- acceptors; and the activity of methanotrophic species.

The presence of H in methanogenic environments is paramount, as it is an important e^- donor. However,

high H_2 partial pressure is associated with inhibition of methanogenesis. Regulation of the concentration of H_2 is managed by the syntrophic partnership between secondary fermenters and methanogens to maintain mutually favourable conditions. H_2-producing syntrophs require low H_2 partial pressures for their metabolism to be energetically feasible. Hence, the role of hydrogenotrophic methanogens is to consume H_2 at an accordant rate in order to secure their own supply and prevent the accumulation of VFAs (Sieber et al. 2018). Alternatively, at high H_2 partial pressure, homoacetogens preferentially channel H_2 and CO_2 into additional acetate. This may go some way to explaining the high tolerance for H_2 partial pressure amongst methanogens with cytochromes, i.e., acetotrophs (Thauer et al. 2008).

As for the presence of alternative e^- acceptors, due to the low energy yields and consequent slow growth rates from methanogenesis, when other organisms that reduce more energetically favourable substrates are able to flourish, methanogens can be outcompeted for H_2 and/or acetate (Hoehler et al. 2019). Of the reductants shown in Table 3, NO_3^- and sulphate (SO_4^{2-}) are the most readily bioavailable, hence their presence can be the most detrimental to CH_4 yields. Furthermore, as well as depriving methanogens of substrate, these same alternative e^- acceptors can be utilised as substrates in Anaerobic Methanotrophic (ANME) processes.

Table 3: Free energy from NADH oxidation coupled to electron acceptors, adapted from Kim and Gadd (2008)

Reduction half reaction	Gibb's free energy released (kJ/2e$^-$)
$\frac{1}{2}O_2 \rightarrow 2H_2O$	-219.07
$Fe^{3+} \rightarrow Fe^{2+}$	-209.46
$2NO_3 \rightarrow N_2$	-206.12
$MnO_2 \rightarrow Mn^{2+}$	-134.52
$SO_4^{2-} \rightarrow HS^-$	-20.24
$CO_2 \rightarrow CH_4$	-14.58

During anaerobic treatment, the oxidation of CH_4 requires the presence of alternative e^- acceptors and takes place via the reversal of the final reaction of methanogenesis (Guerrero-Cruz et al. 2021). As it pertains to NO_3^- specifically, nitrite-Dependent Anaerobic Methane Oxidation (n-DAMO) is relevant, of which there are two confirmed variations: one that takes place via NOD in *Candidatus* Methylomirabilis oxyfera, which will be discussed in detail in subsubsection 2.5.1; and one that requires a syntrophic relationship between ANME archaea and denitrifying species (Lee et al. 2018). While it may negatively impact CH_4 yields, the potential of methanotrophic denitrification for reducing dissolved CH_4 emissions is undergoing current research (Costa et al. 2022). Although these factors may be difficult to control under reasonable operational management of a WWTP, stimulation of DIET can mitigate and bolster CH_4 generation in spite of them.

2.3.4 Methane Release from Anaerobic Reactors

At first glance, it appears that anaerobic technologies align almost perfectly with the GHG emission prevention strategies. The aforementioned reduced energy demand, lower biomass production rate, and CH_4-rich combustible biogas that can be easily captured tick all the right boxes. Of course, by burning the biogas, the exhaust CO_2 is ultimately released to the atmosphere. However, this technique amounts to a renewable energy source that reduces the need for imported electrical energy (Maktabifard et al. 2018). Despite the known operational challenges of anaerobic technologies, it is becoming evermore evident that carbon neutrality is far more attainable by using them than Conventional Activated Sludge (CAS) (Zhang et al. 2024).

Nevertheless, the atmospheric isolation required to create the O_2-free environment introduces contradictory consequences. The CH_4-rich atmosphere inside the reactor results in partial pressures that keep a portion of the CH_4 dissolved in solution until the effluent eventually leaves. At which point, those partial pressures drop, and the dissolved portion is released untreated to the atmosphere. Moreover, the solubility of CH_4 is strongly impacted by temperature, becoming more soluble at lower temperatures. Hence, the CH_4 losses in temperate climates has historically been prohibitive (Liu et al. 2014b). Theoretical values of dissolved CH_4 (and indeed any gas) can be calculated using Henry's law, which incorporates temperature and pressure to produce solubility constants. However, in advection limited (low movement) systems, supersaturation can occur, owing to the reduced mass transfer to the headspace (Crone et al. 2016).

Defined as the ratio of the actual value to the value calculated using Henry's law, supersaturation can range from 1.3 to 6.9, as shown in Table 4. Fortunately, there are mitigation strategies to reduce CH_4 losses, which are largely broken down into removal, recovery, and reuse. Table 4 also shows that anaerobic MBRs are highly successful at reducing CH_4 supersaturation, owing to the higher fluid velocities enabled by complete decoupling of HRT and SRT, even at lower temperatures. Although the benefit seems to be best realised using submerged membranes, rather than side stream. Indeed, many of the CH_4 management strategies centre on the application of various membrane technologies, while alternatives include gas stripping, biological oxidation, and vacuum degassing (Li et al. 2021).

With that being said, it is beyond the scope of this research project to determine which of these strategies is the "best" or to comment on this growing field of research. This is included simply to bring to the reader's attention that these technologies exist and to return to the context of an entire WWTP. When anaerobic technologies are applied as the final treatment step, it is those final effluents that pose the greatest risk of elevated CH_4 emissions. Hence, by applying them first, there are greater opportunities to address the issue without having to employ separate tertiary treatments. Fortunately, ongoing research into

Table 4: Estimates of methane losses in anaerobic effluents, adapted from Crone et al. (2016).

Reactor type	Degree of supersaturation	Average CH_4 lost in effluent (%)	Temp. (°C)
Sidestream anaerobic MBR	1	88	25
Submerged anaerobic MBR	1.007	46	21
Submerged anaerobic MBR	1.009	43	33
SAF-MBR	1.05	63	25
UASB	1.3	45	25
Submerged anaerobic MBR	1.5	40–50	15
EGSB	1.57	45	16
Fixed Film	4.3	81	29
UASB	6.9	85	28

anaerobic technologies as the first-line biological treatment stage has shown steady promise for decades. In particular, again, the AFBR technology.

2.3.5 Direct Interspecies Electron Transfer in Methanogenesis

The mechanisms by which DIET produces the consistently observed elevated CH_4 yields have been speculated on in many studies. One of the most important factors being the thermodynamic advantage of not having to form and consume diffused e^- shuttles. When oxidising propionate, for example, it has been estimated that up to 85 kJ/mol can be saved when 50 % of the electrons are transferred via DIET as opposed to traditional H transfer (Wang and Lee 2021). As well as providing a means for enhanced energy efficiency, DIET can also assist methanogenic communities in resisting inhibition. Of the factors mentioned previously, the one that DIET can help with the most is overcoming the limitation imposed by H_2 partial pressure. By promoting DIET, the reliance on diffused e^- shuttles can be reduced, hence the barrier formed by H partial pressures can be bypassed, resulting in superior CH_4 yields (Jin et al. 2022).

DIET-enhanced methanogenesis functions mostly through the hydrogenotrophic pathway, utilising directly shared electrons to reduce CO_2, as shown in Equation 2. Nevertheless, even obligate acetotrophic *Methanosaeta* has been proven to reduce CO_2 to CH_4 in DIET co-cultures (Rotaru et al. 2014). Further study revealed two thermodynamically feasible pathways for *Methanosaeta* to achieve this. Firstly, upon dismutating acetate into the methyl and carboxyl groups, the methyl group proceeds through the acetotrophic pathway as normal. Meanwhile, the carboxyl group enters the hydrogenotrophic pathway, reduced by electrons derived from DIET, without the need to consume extracellular H_2.

$$CO_2 + 8H^+ + 8e^- \rightarrow CH_4 + 2H_2O \quad (2)$$

Secondly, *Methanosaeta* genera utilise the ribulose-1,5-bisphosphate carboxylase/oxygenase (RuBisCo)-mediated CO_2 fixation pathway. This pathway, known as the Reductive Hexulose Phosphate (RHP) pathway, reduces CO_2 and produces formaldehyde as an intermediate. Incidently, when condensed with tetrahydromethanopterin, formaldehyde forms a key intermediate in hydrogenotrophic methanogenesis, thereby, acting as an additional substrate for CH_4 generation (Yang et al. 2019). These pathways are shown in Figure 12

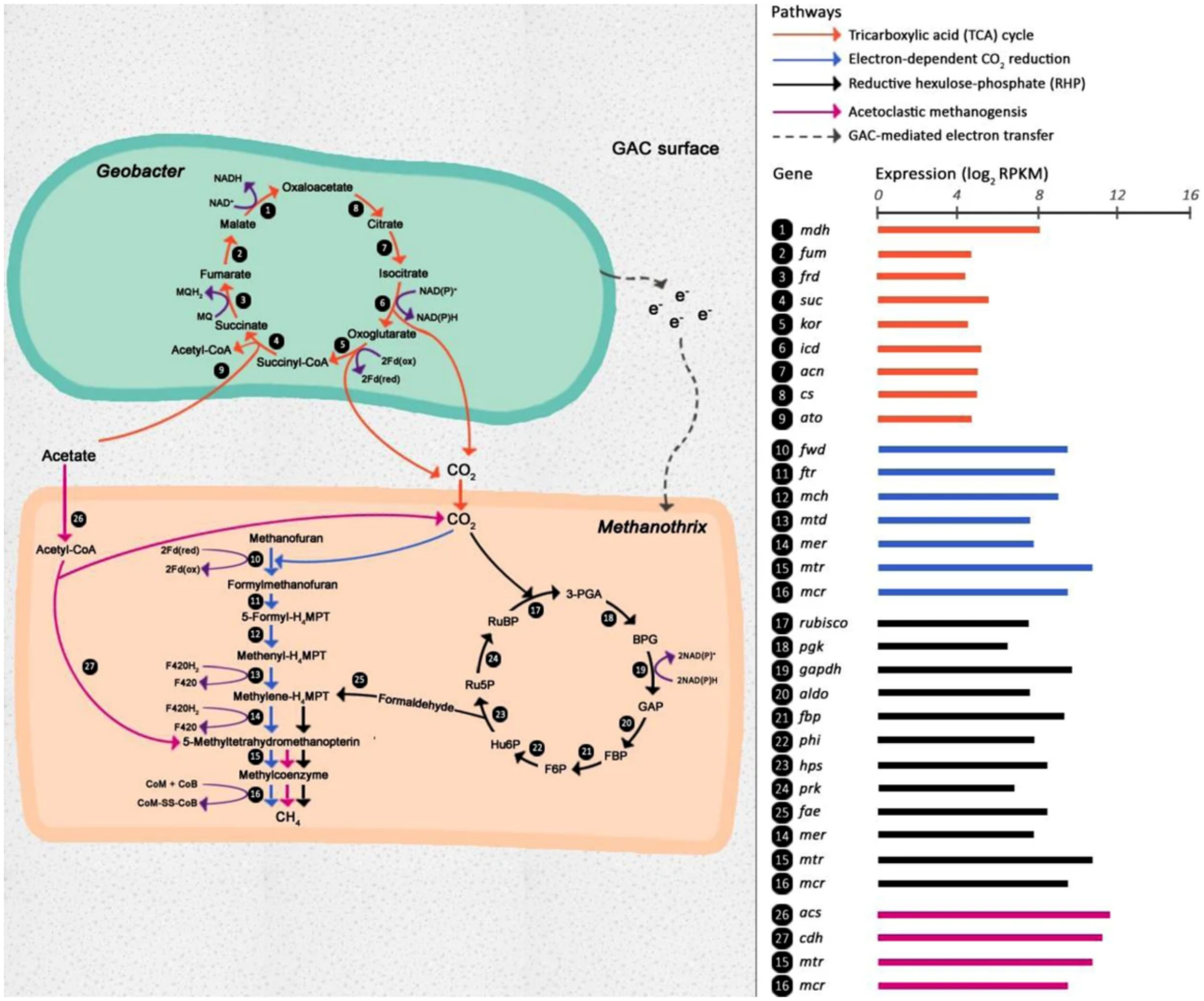


Figure 12: Hydrogenotrophic methanogenesis in *Methanosaeta*. *Image reproduced with permission from the copyright holder (see Table 40 in Appendix A5).*

Alternative studies have also recently provided evidence to suggest that the acetotrophic pathway can also benefit directly from DIET (Xiao et al. 2020). Moreover, the relationship between electrotrophic methanogens and exoelectrogenic syntrophs, such as *S. aciditrophicus* and other H/formate producing syntrophs with related e-pili genes, are yet to be explored (Walker et al. 2020). Since its discovery, the vast

majority of the research into DIET has focused on its role in carbon species (C)-cycling. The knowledge base has rapidly expanded and the novel technologies that are already being implemented are largely successful, despite the fact that the role of DIET in methanogenesis is still not fully understood. Hence, a substantial area of opportunity lies in investigating the role of DIET in N-cycling.

2.4 Conventional Nitrogen Cycling in Wastewater Treatment

2.4.1 The Processes of Biological Nitrogen Removal

The removal of nitrogen is one of the core functions of a WWTP. If inappropriately designed, the consequences can include the release of harmful amounts of N to the receiving water body (Zhou et al. 2023a) and/or the emission of the potent GHG N_2O (McCarty 2018). As mentioned, there is a considerable amount of pressure for a design evolution away from BNR via assimilation, which relies on the generation of marketable biomass, towards complete transformation to N_2. Nitrogenous organic compounds are those that contain amine groups, such as amino acids, nucleic acids, and urea. However, whilst trapped inside these macromolecules, the N atoms are not available to enter the nitrogen cycle or assimilatory processes. Hence, they must first be mineralised to ammonium (NH_4^+)/ammonia (NH_3), i.e., ammonification. The vital importance of N in cellular life means that this process is ubiquitous in both the aerobic and anaerobic microbiomes (Reineke and Schlömann 2023). Strock (2008) provides a concise summary:

> *"Bacteria and related microorganisms derive metabolically useful energy from the oxidation of organic nitrogen to ammonium. Ammonium is then available to be assimilated and incorporated into amino acids or used for other metabolic purposes. If microorganisms produce ammonium in excess of their own metabolic requirements, the surplus is excreted into the ambient environment, such as soil or water, and is available for use as a nutrient by plants, or as a substrate for other microbial processes"*

Once the inorganic NH_3/NH_4^+ has been isolated, it is available to the nitrogen cycle. As shown in Figure 13, starting from this point, the N atom must be sequentially oxidised and reduced via a series of intermediates before it can reach the final neutral N_2 state, hence the common practice of employing both aerobic and anaerobic treatment on WWTPs. Research in this field has expanded rapidly over the last few decades, with longstanding models being challenged and remarkable novel processes being found and implemented for various biotechnology applications. The following subsections will describe current understanding of relevant microbes and the pathways they employ to achieve the various transformations. An overview of the processes that will be discussed is shown in Figure 14, highlighting the complex relationship between the substrates and processes.

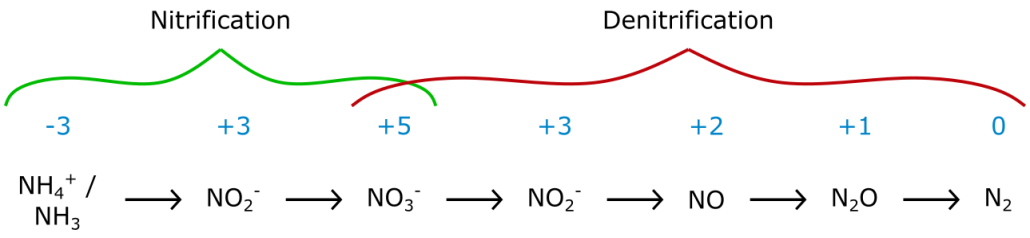


Figure 13: Oxidation states of key intermediates in the nitrogen cycle

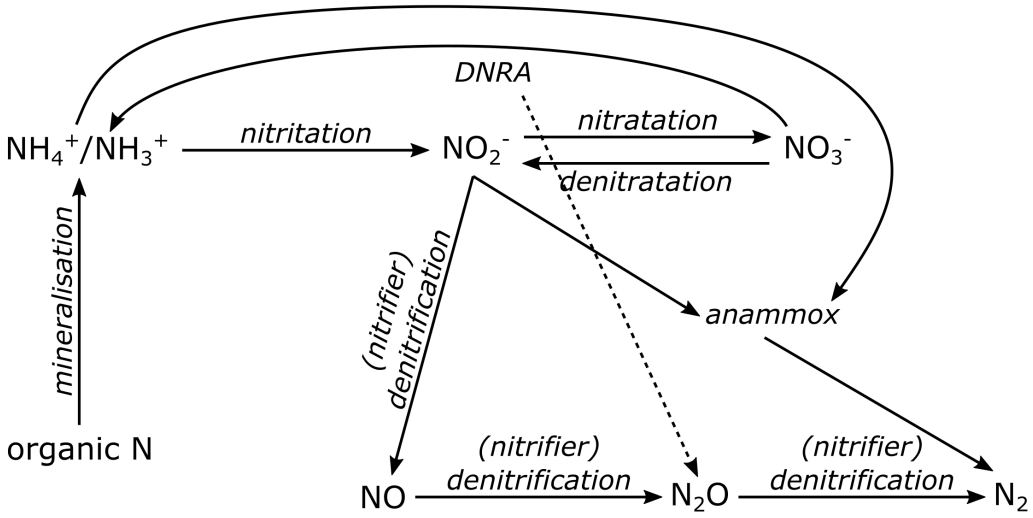


Figure 14: Microbial metabolic pathways in the nitrogen cycle, adapted from Wrage-Mönnig et al. (2018)

2.4.2 Nitrification

In environments with abundant O_2 to accept electrons, reduced forms of inorganic N are used as an e^- donors by autotrophic microbes, resulting in the transformation from the most reduced form (NH_3) to the most oxidised (NO_3^-). Following the key intermediates, the complete nitrification process proceeds through two stages: nitritation - the oxidation of NH_3 to nitrite (NO_2^-); then nitratation - the oxidation of NO_2^- to NO_3^-. Until recently, it was thought that these two stages were divided between Ammonia Oxidising Bacteria (AOB) and Ammonia Oxidising Archaea (AOA) for nitritation, followed by Nitrite Oxidising Bacteria (NOB) for nitratation. However, the discovery of *Nitrospira* species that are capable of complete ammonia oxidiation to NO_3^- within a single cell - now known as comammox - shifted the model (Daims et al. 2015). On that note, an overview of the pathways used by the aforementioned bacterial nitrifiers is shown in Figure 15.

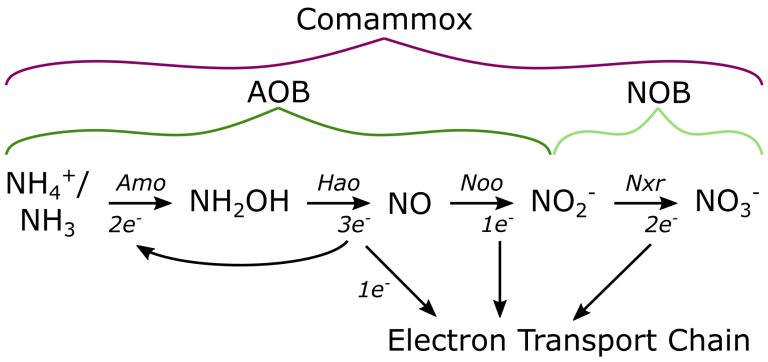


Figure 15: Pathways of nitrifying bacteria, adapted from Stein (2019)

Despite their differences, the NH_3-oxidisers share a common first step of oxidising NH_3 to hydroxylamine (NH_2OH). This reaction, catalysed by ammonia monooxygenase (Amo), is shown in Equation 3.

$$NH_3 + O_2 + 2H^+ + 2e^- \xrightarrow{Amo} NH_2OH + H_2O \quad (3)$$

In the original model for nitritation proposed by Whittaker et al. (2000) based on studies of *Nitrosomonas europaea*, it was thought that the subsequent oxidation of NH_2OH to NO_2^- was a single step catalysed by hydroxylamine oxidoreductase (Hao)[4]. However, this was challenged by Caranto and Lancaster (2017), who showed that NO was the obligate product of Hao in bacterial NH_3 oxidisers. This updated function is shown in Equation 4.

$$NH_2OH \xrightarrow{Hao} NO + 3H^+ + 3e^- \quad (4)$$

To date, the final mechanism to complete the bacterial nitritation process remains unresolved. The model pathway is shown in Equation 5, catalysed by an unknown nitric oxide oxidoreductase (Noo) (Stein 2019). Genes for Noo have yet to be determined, although proposals have been made. As for NH_2OH oxidation in AOA, understanding of the mechanism is even more elusive, with multiple models and enzyme combinations having been proposed.

$$NO + H_2O \xrightarrow{Noo} NO_2^- + 2H^+ + e^- \quad (5)$$

When completing the nitrification process, further oxidation of NO_2^- to NO_3^- proceeds through nitrite oxidoreductase (Nxr) as shown in Equation 6, carried out by NOB and comammox bacteria (Stein 2019). Importantly, while this reaction is currently undisputed, Nxr is bidirectional, and factors that determine the direction of e^- flow remain to be fully understood (Chicano et al. 2021).

$$NO_2^- + H_2O \xleftrightarrow{Nxr} NO_3^- + 2H^+ + 2e^- \quad (6)$$

The phylogeny of the most commonly recognised nitrifying bacterial genera is shown in Figure 16. Most AOB are contained within three main genera: *Nitrosomonas*, *Nitrosospira*, and *Nitrosococcus* (Clark et al. 2021). Known NOB genera include: *Nitrobacter*, *Nitrococcus*, *Nitrotoga*, *Nitrospira* (the only genus to contain comammox species), *Nitrolancea*, and *Nitrospina* (Daims et al. 2016). There are a greater number of AOA genera, which are exclusive to the Thaumarchaeota phylum. However, they tend not to dominate in WWTPs, hence their phylogeny is not included (Lehtovirta-Morley 2018).

All of the aforementioned genera are autotrophic, as the majority of studies have focused on them as the primary enactors of nitrification. This is despite knowledge of heterotrophic nitrifiers since at least 1894 (Martikainen 2022). Recently, studies of heterotrophic nitrifying bacteria have started to increase in

[4]Sometimes referred to as hydroxylamine dehydrogenase, still with the Hao acronym

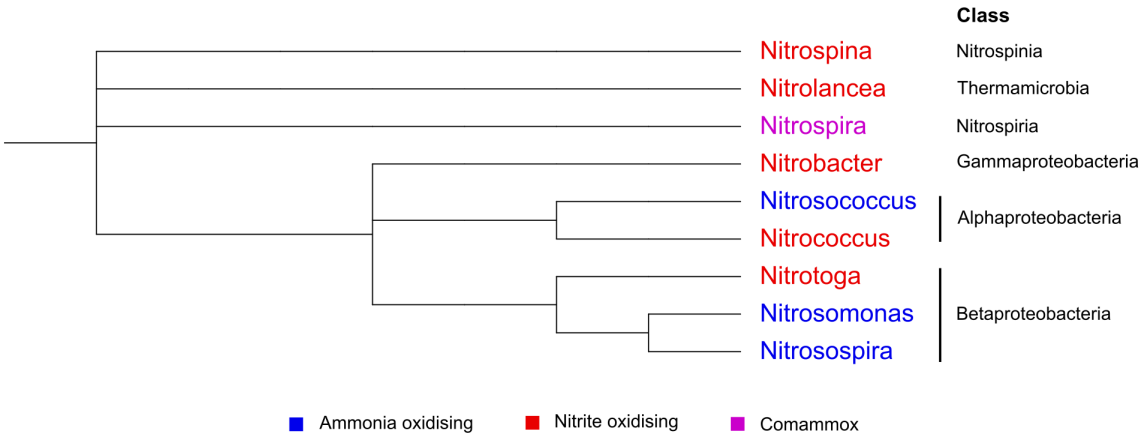


Figure 16: Phylogeny of nitrifying bacterial genera

popularity due to indications of improved N and COD removals (Duan et al. 2022b) and their potential application in simultanous heterotrophic nitrification aerobic denitrification systems (Hu et al. 2023). However, much is still unknown about this phenomenon, and most of the potential pathways for NH_3 oxidation by heterotrophs can be considered as secondary metabolism. Furthermore, distinguishing the activity of autotrophic and heterotrophic nitrifiers in wastewater BNR systems remains a challenge (Duan et al. 2022b; Martikainen 2022).

Of course, as the scientific knowledge develops, engineers are able to design improved systems. One of the most influential examples to date is the ability to undertake partial nitrification via the Single-reactor High-activity Ammonium Removal Over Nitrite (SHARON) process. By understanding the differing DO and SRT requirements of AOBs and NOBs, plant designers can implement a "NO_2^- shunt" by suppressing NOB. When successful, nitritation processes consume 25 % less energy for aeration as well as reducing the COD supplementation for an associated denitritation process by 40 % (Duan et al. 2022a). No matter how it is achieved, or how far the process is permitted to go, once in an oxidised state, inorganic N must be reduced back down to 0 in order to complete the transformation to the neutral N_2 form.

2.4.3 Denitrification

The enzymatic pathway of denitrification follows 4 well-studied steps. For dissimilatory NO_3^- reduction, the first step is either the reversal of Equation 6 or reduction via the cytoplasmic or periplasmic NO_3^- reductases, Nar and Nap, respectively. From there, NO_2^- reduction to NO is catalysed by one of two nitrite reductases (Nir), copper-containing NirK or cytochrome cd_1 containing NirS. Subsequently, NO reduction to N_2O is catalysed by nitric oxide reductase (Nor). Lastly, N_2O reduction to N_2 is catalysed by nitrous oxide reductase (Nos). These are represented in Equations 7, 8, 9, and 10, respectively.

$$NO_3^- + 2H^+ + 2e^- \xrightarrow[Nap]{Nar} NO_2^- + H_2O \quad (7)$$

$$NO_2^- + 2H^+ + e^- \xrightarrow[NirS]{NirK} NO + H_2O \quad (8)$$

$$2NO + 2H^+ + 2e^- \xrightarrow{Nor} N_2O + H_2O \quad (9)$$

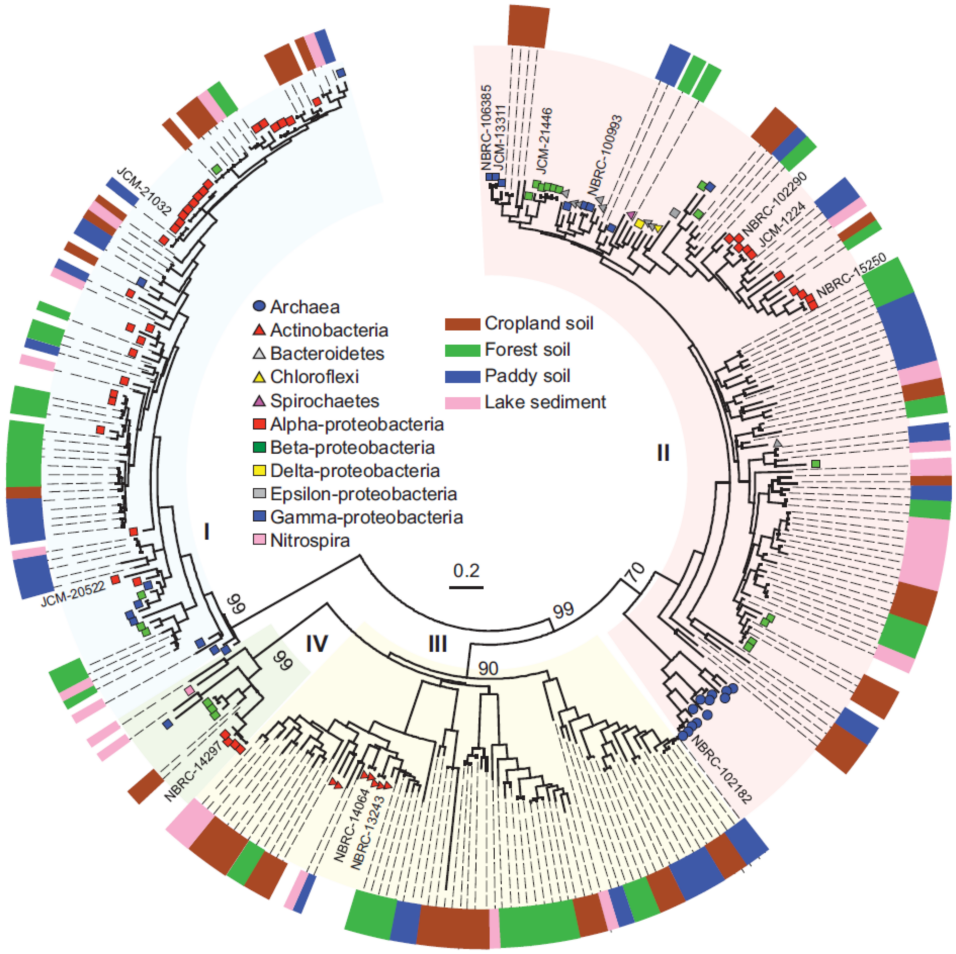
$$N_2O + 2H^+ + 2e^- \xrightarrow{Nos} N_2 + H_2O \quad (10)$$

Denitrification was previously believed to be a uniquely anaerobic process in order to stimulate the use of NO_2^-/NO_3^- as e^- acceptors. Indeed, this version remains the design foundation of BNR on WWTPs (McCarty 2018), as many denitrifying microbes are heterotrophic, facultative anaerobes, capable of utilising either O_2 or oxidised inorganic-N as the terminal e^- acceptor. Important representatives of typical Heterotrophic Denitrifying Bacteria (HDB) are noted as *Bacillus*, *Paracoccus*, and *Pseudomonas* (Reineke and Schlömann 2023). While the pathway itself may be largely consistent, research into denitrification over the decades has shown that this process is incredibly ubiquitous, capable of functioning in a range of environments and present in phylogenetically diverse microbes. To illustrate this point, Figure 17 shows the maximum likelihood phylogeny of NirK and NirS, including archaea and bacteria from multiple phyla, found in multiple environments.

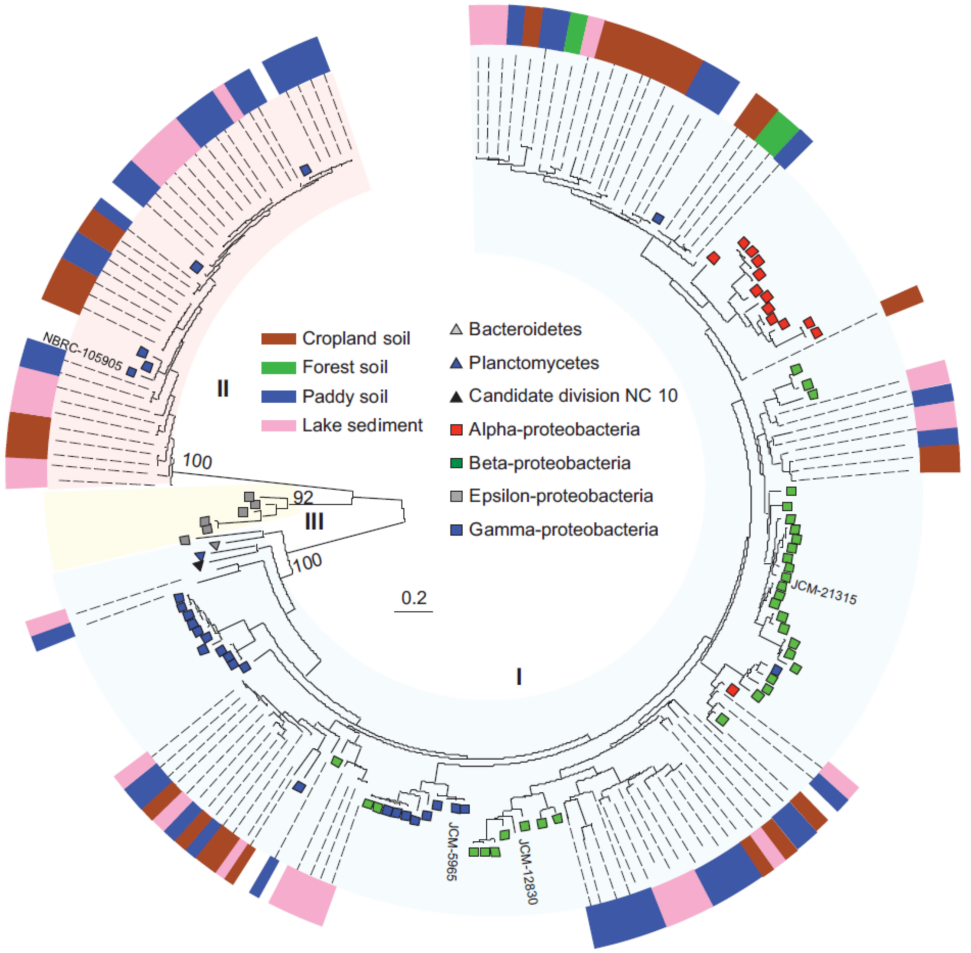
Despite initial assumptions, denitrification can proceed under aerobic conditions, also mostly carried out by heterotrophs (Hao et al. 2022). In such environments, O_2 and NO_3^- are simultaneously used as terminal e^- acceptors for respiration and denitrification, respectively, established by Robertson and Kuenen (1984). Research into the intracellular e^- transfer mechanisms that support this process are ongoing (Yang et al. 2020a) and its association with heterotrophic nitrification is a popular subject among those looking to promote aerobic treatment technologies (Hu et al. 2023).

Meanwhile, under anaerobic conditions, autotrophic (or mixotrophic) denitrifiers can use inorganic compounds as the e^- donors to also undertake denitrification. The most common reducing agents are H_2 and reduced inorganic sulphur compounds, while others including ferrous iron (Fe^{2+}), thiocyanate, arsenite, and manganese have been explored (Di Capua et al. 2019). Although they may compete with their heterotrophic counterparts for NO_3^-, studies have suggested that they can cooperate via cross-feeding under low C/N ratios (Xing et al. 2024).

Conventional Nitrification / Denitrification (N/DN) processes (direct line or recycle) rely on the



(a) NirK amino-acid sequences (from four clusters)



(b) NirS amino-acid sequences (from three clusters)

Figure 17: Maximum likelihood phylogeny of nitrite reductase gene clusters. *Images reproduced with permission from the copyright holder (see Table 40 in Appendix A5).*

conversion of all NH_3 present to either NO_3^- or NO_2^- in the nitrification stage before the wastewater is passed to the denitrification stage. This increases the demand on the nitrification stage, which, as the aerated process, increases the energy demand (Mishra et al. 2022). Hence, the alternative anammox technology has drawn a lot of engineering interest since its discovery.

2.4.4 Anaerobic Ammonia Oxidation

Long thought to be impossible, microbial oxidation of NH_3 under anaerobic conditions was first demonstrated by van de Graaf et al. (1995), and Strous et al. (1999) were the first to isolate an anammox species. In proving that NH_3 could be anaerobically oxidised by bacteria, not only was the understanding of biogeochemical nitrogen cycling changed, but biotechnology applications of the N cycle had an entirely novel option. In the anammox process, NH_3 is oxidised with NO_2^- via the intermediate hydrazine (N_2H_4) to produce N_2 (~90 %) and NO_3^- (~10 %). In the first stage, NO_2^- is partially reduced to NO via Nir as in Equation 8, while also partially oxidised to NO_3^- via Nxr as in Equation 6, which is released as a waste product. The NO then combines with NH_4^+ to form N_2H_4 via hydrazine synthase (Hzs) as shown in Equation 11, a process that is unique to anammox bacteria. From this intermediate, N_2 is finally formed via hydrazine dehydrogenase (Hdh), as shown in Equation 12 (Venturin et al. 2022).

$$NO + NH_4^+ + 2H^+ + 3e^- \xrightarrow{Hzs} N_2H_4 + H_2O \tag{11}$$

$$N_2H_4 \xrightarrow{Hdh} N_2 + 4H^+ + 4e^- \tag{12}$$

Anammox bacteria are autotrophs found uniquely within the Planctomycetes phylum across six genera: *Brocadia*, *Kuenenia*, *Scalindua*, *Anammoxoglobus*, *Jettenia*, and *Anammoximicrobium*. The specialised structure of these microbes that allows them to carry out anammox is known as the anammoxosome, shown in Figure 18. Accounting for ~60 % of the cell volume, this organelle is the forge of anammox (Venturin et al. 2022). As autotrophs, anammox bacteria are slow growing, making the process notoriously operationally challenging to maintain. This is largely due to competition with HDB for NO_2^- in environments with sufficient organic C for HDB to flourish. With that being said, there is evidence to suggest that some anammox bacteria may be capable of mixotrophic growth, with genes for VFA metabolism found in *Kuenenia* and *Brocadia* (Zhang et al. 2020).

As the process requires NO_2^-, it is most commonly applied as Partial Nitrification / Anammox (PN/A). Applied over two reactors, the process is referred to as the SHARON-anammox process. Applied as a simultaneous process, it can be referred to as the Completely Autotrophic Nitrogen removal Over Nitrite (CANON) or Oxygen Limited Autotrophic Nitrification-Denitrification (OLAND) system. Compared to

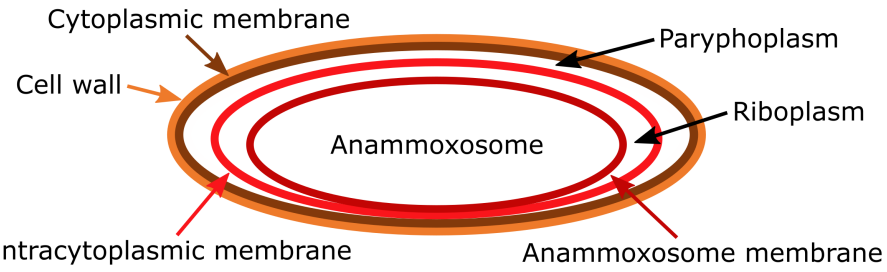


Figure 18: Schematic representation of anammox bacteria cell, adapted from Venturin et al. (2022)

N/DN, the PN/A system offers up to 100 % reduction in COD supplementation and reduced sludge production (Mishra et al. 2022). However, the application of PN/A in main stream treatment is still limited, as it is not efficient at removing COD, and its effluents contain NO_3^-. As such, anammox-based systems often require a subsequent treatment stage (Mishra et al. 2022). However, being sensitive to the presence of organics and requiring the presence of NO_2^-, the PN/A process became particularly popular for treatment of AD supernatant, which has a low C/N ratio to support anammox bacteria.

2.4.5 Knowledge Gaps in the Nitrogen Cycle

As demonstrated, scientific research into how N is moved through ecological cycles is highly active, with more constantly being learned about metabolism, stimulation, inhibition, and interdependency. Concurrently, engineering applications of biological N cycling for wastewater treatment are robust, and engineers have developed multiple techniques and designs to successfully and reliably accomplish BNR using both legacy and novel understandings (Liu et al. 2024). Both of these points are highlighted in Figure 19, which also shows that many discoveries and innovations have been made in just the last 20 years. However, several scientific knowledge gaps remain that impact understanding and management of inorganic N in engineered environments. These knowledge gaps relate primarily to unknown microbial pathways and organisms, environmental factors influencing N transformations, interactions between processes, N_2O emissions, and modelling and measurement limitations.

Paradigm-shifting N transformations, like anammox or comammox, were only recently discovered, in 1995 and 2015, respectively (Daims et al. 2015; van de Graaf et al. 1995). In addition, changes to the fundamental understanding of existing transformations, such as the vital nitrifying Hao enzyme, only occured in 2017 (Caranto and Lancaster 2017). Separately, many microbes responsible for N cycling are still unidentified or poorly understood, such as AOA (Stein 2019). This is highly suggestive that other unknown pathways and N cycling species could very well exist (Kuypers et al. 2018).

As with most microbially-mediated processes, environmental conditions have strong impacts on the N cycle. Factors such as temperature, pH, carbon sources (organic, inorganic, substrate specificity, and ratio

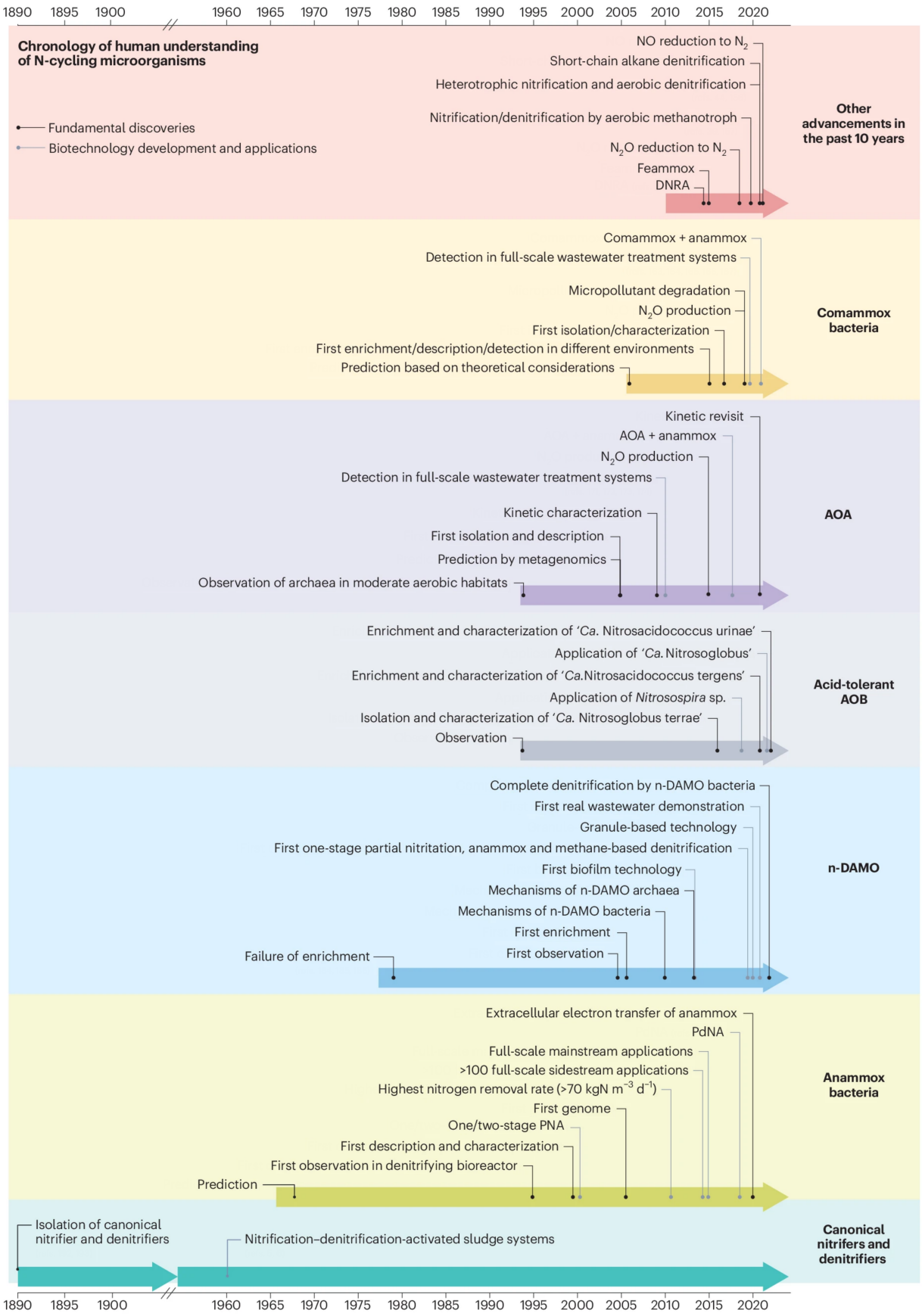


Figure 19: A timeline of discoveries in the nitrogen cycle and biotechnology applications. *Image reproduced with permission from the copyright holder (see Table 40 in Appendix A5).*

to N), O_2 levels, and presence of alternative e^- acceptors have all been shown to have impacts at various stages (Di Capua et al. 2019; Duan et al. 2022a; Hao et al. 2022; Mishra et al. 2022; Pan et al. 2023). Indeed, further research into these factors is recommended in order to develop control strategies for BNR (Mishra et al. 2022).

While engineering applications of BNR can lead to thinking of the N cycle as a sequential process, the more knowledge is gained of the metabolic versatility of the microbes involved, the more it becomes clear that this is a fallacy. The processes of the N cycle are interconnected, but the interactions between these processes, under varying environmental conditions, are not fully understood (Kuypers et al. 2018). For example, the interactions and competition between anammox and denitrification, especially to understand which process dominates in different environments and why (Cao et al. 2021; Al-Hazmi et al. 2023). In addition, furthering the understanding of simultaneous processes, such as Simultaneous Nitrification-Denitrification (SND) (Di Capua et al. 2022; Hu et al. 2023) and Simultaneous Partial Nitrification, Anammox, and Denitrification (SNAD) (Preetham et al. 2024; Su et al. 2022).

The final two knowledge gaps mentioned - N_2O emissions and modelling and measurement limitations - are both products of the aforementioned factors, as well as being particularly inter-related. As mentioned in the Introduction, N_2O is produced by several N cycle processes, recognised as being primarily nitrifier denitrification, incomplete heterotrophic denitrification, and incomplete NH_2OH oxidation. However, the precise conditions and mechanisms that control its release are not fully understood (Guo et al. 2021).

With the abundant complexity of the N cycle, involving multiple chemical forms and microbial processes, both known and unknown, it is somewhat unsurprising then that models that can accurately simulate these processes across scales (from microbial to ecosystem levels) are still in development and require refinement. Moreover, development of more accurate, cost-effective methods for measuring N transformations and fluxes, particularly in situ, is essential for advancing our understanding of process dynamics (Chen et al. 2020a; de Haas and Andrews 2022).

Although considerable, these knowledge gaps provide plentiful opportunities for advancement, and the application of emerging processes to BNR. Given the ecological importance of N, and the potency of N_2O as a GHG (273 times that of CO_2 (Ritchie et al. 2023)), it has never been more important for scientific and engineering advancements to take place in tandem. Hence the aim of this research programme to investigate the potential linkage between the novel NOD process and DIET in an effective and energy efficient anaerobic wastewater treatment reactor.

2.5 Unconventional Nitrogen Cycling in Wastewater Treatment

2.5.1 Nitric Oxide Dismutation

In what is regarded as the original study of NOD, Ettwig et al. (2010) were investigating n-DAMO enrichment cultures from freshwater sediment samples. In those cultures, which successfully performed CH_4 oxidation coupled to denitrification under anoxic conditions, it was noted that the novel bacterium *Ca.* M. oxyfera (of phylum NC10) was dominant, representing 70 - 80 % of the communities. Following genome reconstruction, the complete pathway for aerobic CH_4 oxidation was found, but the pathway for denitrification was incomplete, missing the final step to convert N_2O to N_2.

Following meta-transcriptomic and proteomic analysis, as well as multiple stable isotope experiments to confirm substrate cycling pathways, they were able to conclude that this species was undertaking n-DAMO following the pathways shown in Figure 20. Denitrification proceeds according to the canonical process up to NO, at which point, the process deviates, resulting in the production of N_2 and O_2. The O_2 is then utilised in the aerobic CH_4 oxidation pathway, enabled despite the anoxic environment. Furthermore, high transcription levels of two putative quinol-dependent nitric oxide reductase (qNor) genes (*norZ* in Figure 20) were found, despite very small amounts of N_2O accumulation. Hence, it was concluded that the function of these genes could be the dismutation of NO, rather than its reduction. These potential NOD genes (*nod*) are therefore hypothesised to encode the novel enzyme, nitric oxide dismutase (Nod).

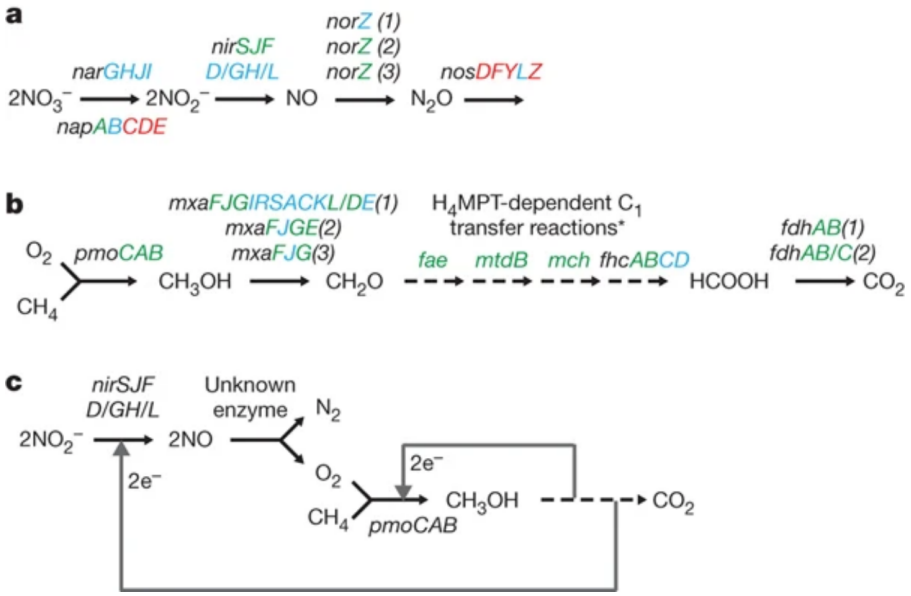


Figure 20: Denitrification and methanotrophic genes present in *Ca.* M. oxyfera: (a) canonical pathways of denitrification; (b) aerobic methane oxidation; (c) proposed pathway of methane oxidation with nitrite. Genes in red were absent from the genome, those in blue were present in the genome, and those genes in green were present in both the proteome and the genome. *Image reproduced with permission from the copyright holder (see Table 40 in Appendix A5).*

Although Nod may be a member of the qNor family, proteomic analysis revealed critical differences between them. It was found that these enzymes exhibit substitutions at positions that are essential for the quinol-binding site, the proton supply channel, and the catalytic centre in canonical qNor. These distinctive features, which would impede typical NO reduction, suggest an electron-neutral reaction that works to bind and rearrange two NO molecules into N_2 and O_2 (Ettwig et al. 2012; Zhu et al. 2017). In addition to being a novel mechanism for N cycling, this pathway is also the third known non-photosynthetic oxygenic pathway after detoxification of reactive oxygen species and chlorite dismutation (Ettwig et al. 2010).

Shortly after the study by Ettwig, NOD was also proposed in the denitrifying alkane-oxidizing γ-proteobacteria strain HdN1. Similarly to *Ca.* M. oxyfera, this microbe was able to utilise an aerobic pathway in the absence of molecular O_2, leading to the conclusion that an oxygenic denitrification pathway was active (Zedelius et al. 2011). This demonstrated that NOD is not strictly associated with n-DAMO. 14 years later, *Ca.* M. oxyfera and strain HdN1 remain the primary case studies for NOD, and the majority of *nod* sequences available in public databases are homologs of these first sequences.

This is due to Polymerase Chain Reaction (PCR) primers created to amplify Nod genes being designed around those putative *nod* sequences (Bai et al. 2024). Potentially, this leaves open the possibility that there are alternative versions of Nod that have yet to be identified. Nevertheless, with these primers in hand, there is mounting evidence to suggest that this process may be far more wide-spread than currently appreciated, as *nod* sequences have been found in a diversity of engineered, natural, and contaminated environments, including WWTPs (Lv et al. 2024). Moreover, their distinction from canonical qNor and cytochrome-dependent nitric oxide reductase (cNor) is apparent, as distinct phylogenetic clusters were found in samples taken from 2 contaminated aquifers, 2 wastewater treatment plants, and 6 lab-scale reactors, shown in Figure 21.

Elsewhere, NOD-like pathways have also been demonstrated in the AOA *Nitrosopumilus maritimus* and denitrifying *Pseudomonas aeruginosa* (Kraft et al. 2022; Lichtenberg et al. 2021). In *N. maritimus*, O_2 accumulation in excess of N_2 production led to the conclusion that a modified dismutation reaction may be taking place, converting 4 NO molecules to O_2 and N_2O, shown in Figure 22. The capacity to auto-aerate would explain the abundance of obligate aerobic AOA in marine oxygen minimum zones and further expand the relevance of oxygenic denitrification (Kraft et al. 2022). During the culture studies of *P. aeruginosa* by Lichtenberg et al. (2021), it was indeed shown that NO was involved in the production of O_2 peaks at the onset of anoxia, provided that the culture was initiated with some amount of O_2. Not only was this suggestive of NOD, but an NO sensing mechanism that is active at low DO. However, no recognised *nod* sequences were found in the *P. aeruginosa* genome from pseudomonas.com, utilised as *de novo* omics sequencing was not conducted in this study.

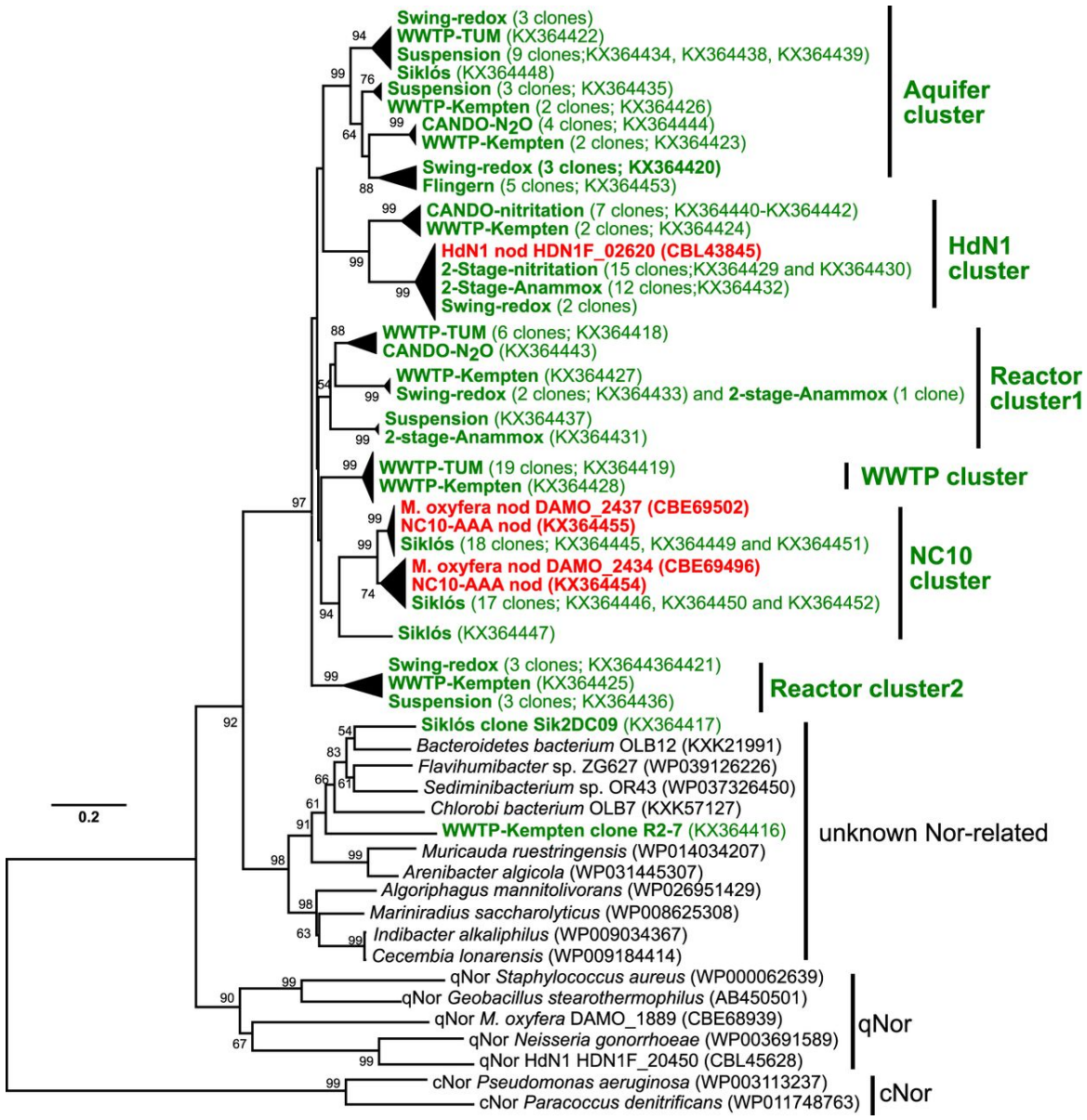


Figure 21: Phylogeny of putative Nod and selected Nor gene sequences. Gene clones generated in study in green, reference sequences in red. The 6 subclusters of *nod* identified are indicated. The accession numbers of reference sequences used and of selected *nod* clone sequences are shown in brackets. *Image reproduced with permission from the copyright holder (see Table 40 in Appendix A5).*

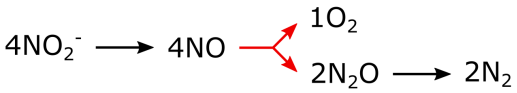


Figure 22: Proposed alternative nitric oxide dismutation pathway in *Nitrosopumilus maritimus*, adapted from Kraft et al. (2022)

Although much remains to be understood about NOD, including how it interacts with conventional denitrification and anammox, there is great potential for its application in biotechnologies. In terms of wastewater treatment specifically, its application as n-DAMO could have significant implications for reducing the release of GHGs. Multiple studies have confirmed that N_2O emissions during n-DAMO are

extremely low, owing simply to the interception of the conventional denitrification process before N_2O is produce (An et al. 2024). Furthermore, the application of an n-DAMO reactor as a subsequent treatment stage to anaerobic treatment offers an opportunity to mitigate the release of dissolved CH_4. Moreover, it would also reduce the requirement for additional e^- donors for denitrification, as CH_4 would serve this purpose (Costa et al. 2022).

2.5.2 Dissimilatory Nitrate Reduction to Ammonia

Another lesser known N cycling process that is beginning to gain attention for biotechnology applications is Dissimilatory Nitrate Reduction to Ammonium (DNRA). Unlike NOD, reports of DNRA date as far back as 1905 (Woods 1938). As knowledge developed over the 20th century, it was initially thought that this process only took place under highly-reducing conditions, and hence wasn't considered ecologically relevant (Stanford et al. 1975; Tiedje et al. 1982). However, almost a century later, a pivotal study showed that the process was indeed active in tropical forest soils, from which point interest escalated (Pandey et al. 2020; Silver et al. 2001). As compared to other NO_3^- transformations, there is an important difference to DNRA, summarised by Chen et al. (2021):

> *"Both denitrification and anammox permanently remove reactive N from a system... Dissimilatory Nitrate Reduction to Ammonium (DNRA) also plays a key role in N cycling but unlike denitrification and anammox where N is eliminated as N_2, DNRA favors N retention within the system as it recycles NO_3^- to NH_4^+... Therefore, competition between denitrification, anammox, and DNRA for NO_3^-/NO_2^- strongly influences N elimination/retention dynamics."*

This process is executed using one of two NO_3^-/NO_2^- reducing enzyme pairs: cytoplasmic Nar/Nir or periplasmic Nap/Nrf[5]. This is shown in Equation 13, with the cytoplasmic pair beneath the arrows, and the periplasmic pair above. Studies have shown that Nrf can also reduce NO and NH_2OH to NH_4^+ (Burlat et al. 2005), and alternative enzymes have been proposed for detoxification of NH_2OH via DNRA, however these are still under review (Soler-Jofra et al. 2021). The initial NO_3^- reduction step is a respiratory pathway shared with denitrification, proceeding as shown in Equation 7 in subsubsection 2.4.3. The distinction, therefore, is in the reduction of the resultant NO_2^-, which can proceed through either fermentation or respiration (Pandey et al. 2020).

$$NO_3^- \xrightarrow[Nar]{Nap} NO_2^- \xrightarrow[Nir]{Nrf} NH_4^+ \tag{13}$$

[5] nitrite reduction with formate (Besson et al. 2022)

The Nicotinamide Adenine Dinucleotide (NADH)-dependent NirBD enzyme complex enacts the fermentative pathway, in which cells produce energy, not through the reduction of NO_2^-, but through substrate level phosphorylation with the reoxidised NADH generated (Wang et al. 2019b). As such, this pathway is unique to heterotrophs. On the other hand, the respiratory NO_2^- to NH_4^+ pathway, enacted by Nrf, is directly linked to energy production (Wang et al. 2019b). Using either non-fermentable organics (formate, H_2, acetate) or inorganic substrates (sulphur, CH_4) as e^- donors, this version of the process can be undertaken by both heterotrophs and autotrophs (Pandey et al. 2020; Wang et al. 2024).

The physiological "choice" between these two pathways comes down to the environmental conditions, most impactfully, NO_3^- concentration and presence of O_2. Nap/Nrf are associated with low NO_3^- concentrations, typically below 3 mM and 1 mM, respectively (Wang et al. 2019b). Whereas Nar/Nir are more tolerant of higher concentrations. As for DO, Nap is insensitive to O_2 (hence its association with aerobic denitrification), whereas Nar is only expressed under anaerobic conditions (Yang et al. 2020b). Figure 23 shows a summary of these processes, including enzyme localisation.

The nitrite reductase subunit A gene (*nrfA*) specifically is considered the marker for DNRA, because high abundance is positively correlated with DNRA activity (Pandey et al. 2020). It has also not been found to catalyse assimilatory processes, while NirBD can perform both assimilatory and dissimilatory NO_2^- ammonification (Huang et al. 2023). However, there are some microbes that can perform DNRA without Nrf (Slobodkina et al. 2017). Hence, the use of *nrfA* as a marker gene for DNRA is statistically backed, but not a golden rule.

There are many different types of bacteria that are able to carry out DNRA, some of which have just one pair of the necessary enzymes, while others have both. Table 5 shows a list of bacterial species that have been shown to have DNRA capacity, where they were found, and their physiology. Not shown in the table is the small list of mixotrophic anammox bacteria that have also shown DNRA metabolism: *Ca. Anammoxoglobus propionicus*, *Ca. Kuenenia stuttgartiensis*, *Ca. Brocadia fuldiga*, and *Ca. Jettenia caeni* (Wang et al. 2022a).

Of course, DNRA competes with denitrification for NO_3^-. One of the most commonly found deciding factors between these two is the ratio of e^- donors (organic C or CH_4) to e^- acceptor (NO_3^-). In NO_3^- limiting conditions, DNRA (which transfers 8 electrons) is able to dominate, whereas denitrification (which transfers 5 electrons) is more competitive during C limitation (Pandey et al. 2020; Wang et al. 2024). However, they are able to coexist over a range of ratios, owing to different substrate affinities (van den Berg et al. 2016).

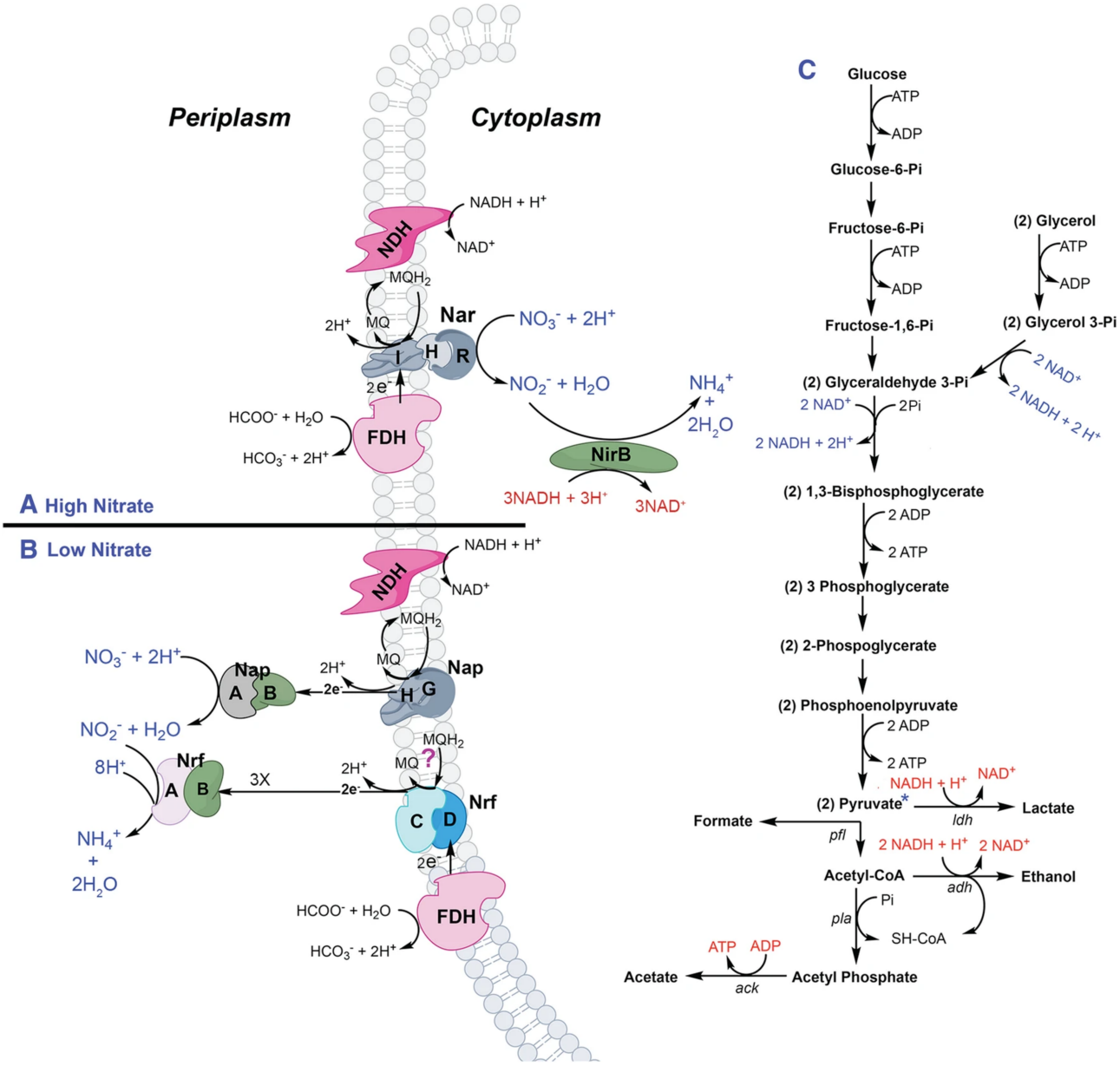


Figure 23: Pathways and enzymes of dissimilatory nitrate reduction to ammonia: (a) cytoplasmic Nar/Nir, fermentative pathway expressed under high NO_3^- concentrations; (b) periplasmic Nap/Nrf, respiratory pathway expressed under low NO_3^- concentrations; (c) anaerobic glucose and glycerol metabolism in the cytoplasm. *Image reproduced with permission from the copyright holder (see Table 40 in Appendix A5).*

In systems that require N retention - such as terrestrial, marine, and wetland ecosystems - DNRA has accrued much interest over the last 20 years. On the other hand, for BNR, its greatest potential is in association with anammox. When combined with anammox, either within anammox bacteria themselves or as a separate community, co-activity of DNRA can boost system performance through a combination of NO_3^- reduction to NO_2^-, provision of NH_4^+ in an otherwise limited system, and prevention NO_3^- accumulation in effluents (Castro-Barros et al. 2017; Wang et al. 2022b).

Table 5: Dissimilatory nitrate reduction to ammonia bacteria, their habits and physiology, adapted from Pandey et al. (2020). (AT) = chemolithoautotrophs

Species	Habitat	Physiology
Facultative anaerobic		
Wolinella succinogenes	Soil	Respiratory
Shewanella loihica strain PV-4	Deep sea hydrothermal vent	Respiratory
Photobacterium profundum SS9	Soil, deep sea	Fermentative
Caldilinea aerophila DSM 14535	Soil, hot spring	Respiratory
Aerobacter aerogenes	Soil, waste water	Fermentative
Escherichia coli	Soil	Respiratory
Marivirga tractuosa DSM 4126	Soil, beach sand	Fermentative
Anaeromyxobacter sp. Fw109-5	Soil	Respiratory
Citrobacter sp.	Soil, waste water	Fermentative
Erwinia carotovora	Soil	Fermentative
Klebsiella pneumoniae	Soil, waste water	Fermentative
Vibrio (Several spp.)	Sediment	Fermentative
Obligate anaerobic		
Opitutus terrae PB90-1	Rice fields	Fermentative
Desulfomonile tiedjei DCB-1	Soil, waste	Fermentative
Ignavibacterium album JCM 16511	Soil, Hot spring	Fermentative
Sulfurospirillum deleyianum	Soil	Respiratory (AT)
Clostridium spp.	Soil	Fermentative
Thiobacillus denitrificans	Rice fields	Respiratory (AT)
Desulfovibrio desulfuricans	Rice fields, marine sediment	Respiratory (AT)
Desulfobulbus propionicus	Rice fields, marine sediment	Respiratory (AT)
Desulfobacterium spp.	Rice fields, marine sediment	Respiratory(AT)
Thioploca spp.	Sediment	Respiratory (AT)
Desulfovibrio gigas	Rice fields	Respiratory (AT)
Aerobic		
Pseudomonas (Several spp.)	Soil, water	Respiratory (AT)
Bacillus (Several spp.)	Soil, food	Respiratory

2.5.3 Direct Interspecies Electron Transfer in the Nitrogen Cycle

Since the discovery of DIET in 2010, much of the research has been focused on its role in methanogenesis. Indeed, it has been shown that, when stimulated using conductive materials, DIET can help alleviate NH_3 inhibition of AD, increasing CH_4 yields by up to 50 % under NH_3-stress conditions (Akram et al.

2024). Beyond this feature, as more is understood about the fundamentals of DIET, a growing body of research is investigating its role in N cycling. In one of the earliest investigations into DIET associated with N cycling, anaerobic cocultures of *Thiobacillus denitrificans* and *G. sulfurreducens* performed acetate oxidation coupled to NO_3^- oxidation, mediated by magnetite nanoparticles. Interestingly, the NO_3^- was oxidised to NH_3 in this study (Kato et al. 2012).

Since then, *G. sulfurreducens* has been shown to collaborate with denitrifiers *Diaphorobacter* and *Shinella*, forming aggregates in which they were the predominant genera. In those cultures, ~38 % of the NO_3^- was reduced to NH_3, while the majority was denitrified (Wan et al. 2018). The improved NO_3^- removal rates achieved when *G. sulfurreducens* was added are shown in Figure 24. *S. oneidensis* has also been shown to form DIET syntrophic relationships with denitrifiers, resulting in significant performance improvements. In co-culture with *Paracoccus denitrificans*, electron exchange via conductive nanotubes promoted denitrification with minimal accumulation of NO_2^- or N_2O (Jiang et al. 2020). In a mixed culture with various denitrifiers, *S. oneidensis* formed an electroactive relationship with *Pseudomonas* to efficiently remove NO_3^- without NH_3 production (He et al. 2023).

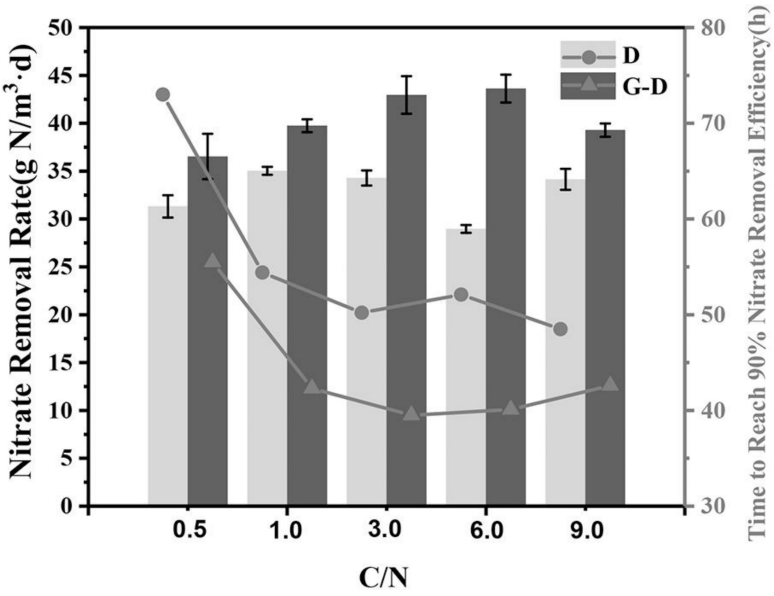


Figure 24: Nitrate removal rates in denitrifying communities with and without *Geobacter*. Group D = denitrifying microbial community, group G-D = *G. sulfurreducens* added denitrifying microbial community. *Image reproduced with permission from the copyright holder (see Table 40 in Appendix A5).*

In a recent BES study, *Geobacter* was hypothesised to transfer electrons from the cathode to a diverse denitrifying community, including autotrophs *Petrimonas*, *Synergistaceae*, *Azoarcus*, and *Thiorhodospira* and heterotrophic *Alicycliphilus*. Unlike the previous culture studies, this experiment resulted in only small amounts of NH_3 accumulation, as well as trace N_2O, indicating that the dominant pathway was complete denitrification to N_2 (Guo et al. 2023). The potential reason for the dominance of denitrification over DNRA was not discussed in the paper.

Besides NO_3^- reduction, DIET has also been demonstrated in cultures that undertake NH_3 oxidation, termed electroanammox. Referring back to the oxidation states of inorganic-N, NH_3 is the most reduced form (-3), and NO_3^- is the most oxidised (+5). Accordingly, BES studies have established the preferences of exoelectrogenic nitrifiers for anodes and electrotrophic denitrifiers for cathodes (Song et al. 2019). An early indicator that anaerobic nitrifiers could execute extracellular e^- transfer was the discovery of feammox (iron-based ammonium oxidation), first described in 2005 upon observing concomitant oxidation of NH_3 to NO_2^- with dissimilatory reduction of ferric iron (Fe^{3+}) to Fe^{2+} (Clément et al. 2005).

Although much remains unknown about feammox microbes, with few having been isoloated, there is interest in their potential for electroanammox (Liu et al. 2024). For example, *Acidimicrobium* sp. strain A6, as one of the few feammox isolates, was found to colonise an electrode while undertaking NH_3 oxidation (Ruiz-Urigüen et al. 2018). The first demonstration that NH_3 could be anaerobically oxidised using an electrode as the terminal e^- acceptor was in 2014. In this BES study, the anodic chamber was provided with a feed containing NH_3, producing NO_3^- as the main product, despite an absence of known NOB. Instead, *N. europaea*, an AOB which lacks Nxr, was highly enriched (Qu et al. 2014). This suggests that, when provided with an external e^- sink, some AOB may be able to take advantage of novel N-cycling mechanisms.

A later BES study using a single chamber experimented on the impact of C/N ratio on electroanammox. It was demonstrated that NH_4^+ oxidation was electrode-dependent, as there was no change in the concentration in the biotic control, as shown in Figure 25. NH_3 was also sensitive to high C/N ratios, presumed to be associated with a switch to methanogenesis. On the electrodes, mixed communities of nitrifying bacteria (*Nitrosomonas* and *Comamonas*) and denitrifying bacteria (*Truepera*, *Arenimonas*, and *Cryobacterium*) were abundant. NO_3^- reduction, however, was most strongly impacted by the C/N ratio, increasing as the ratio increased (Zhou et al. 2021).

Studies of conventional anammox bacteria themselves have also shown that they are capable of electroactive metabolism. The anammox bacteria *Brocadia* and *Scalindua* were shown to perform NH_4^+ oxidation using graphene oxide or electrodes as the e^- acceptors, confirming their DEET capability. Moreover, complete NH_3 oxidation was achieved without accumulation of NO_3^-. This was attributed to the use of the external e^- source as opposed to NO_2^-, as is conventional for anammox metabolism (Shaw et al. 2020).

As the study of DIET is in its infancy, the same is even more true for the study of electroactive N cycling. Much remains to be discovered about species that may partake in the phenomenon and how it impacts their internal metabolism as well as their syntrophic relationships with the microbes around them.

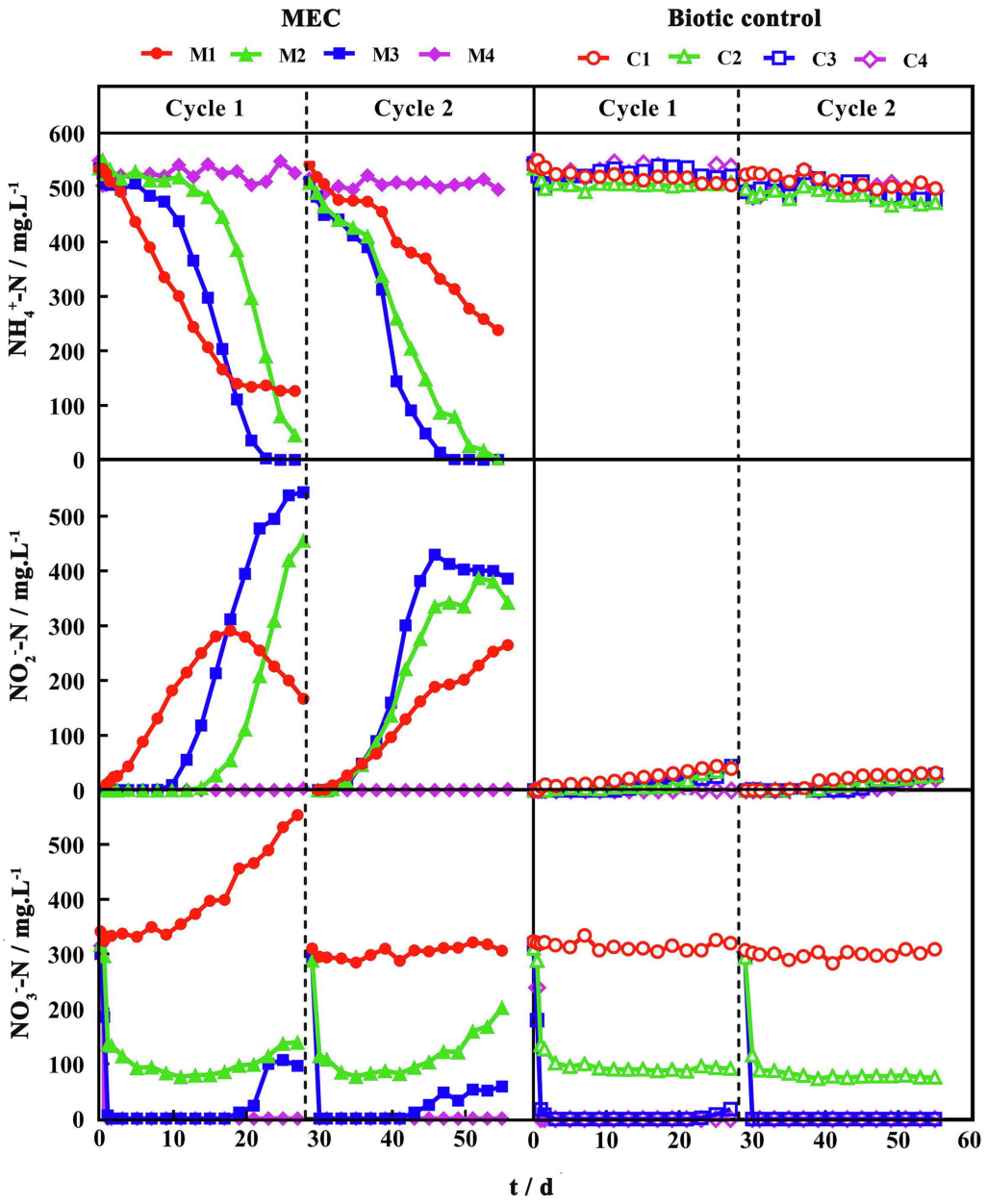


Figure 25: Concentration changes of ammonium, nitrite, and nitrate in microbial electrolysis cells (MECs) and biotic controls in two cycles. The red (M1/C1), green (M2/C2), blue (M3/C3), and purple (M4/C4) lines represent the C/N ratios of 0, 1, 1.5, and 3, respectively. *Image reproduced with permission from the copyright holder (see Table 40 in Appendix A5).*

Combined with the unconventional N cycling processes described herein, it is apparent that there exists a substantial gap in the current knowledge. To provide concluding examples of recent research, there is evidence to suggest that the anaerobic methanotroph *Candidatus* Methanoperedens nitroreducens may directly transfer electrons from CH_4 oxidation to denitrifiers, potentially forming a type of DIET mediated n-DAMO (McIlroy et al. 2023). Meanwhile, the anammox bacteria *Jettenia* was shown to take advantage of biochar-mediated DIET to undertake anammox coupled to DNRA, the proposed pathway of which is shown in Figure 26 (Wang et al. 2022a).

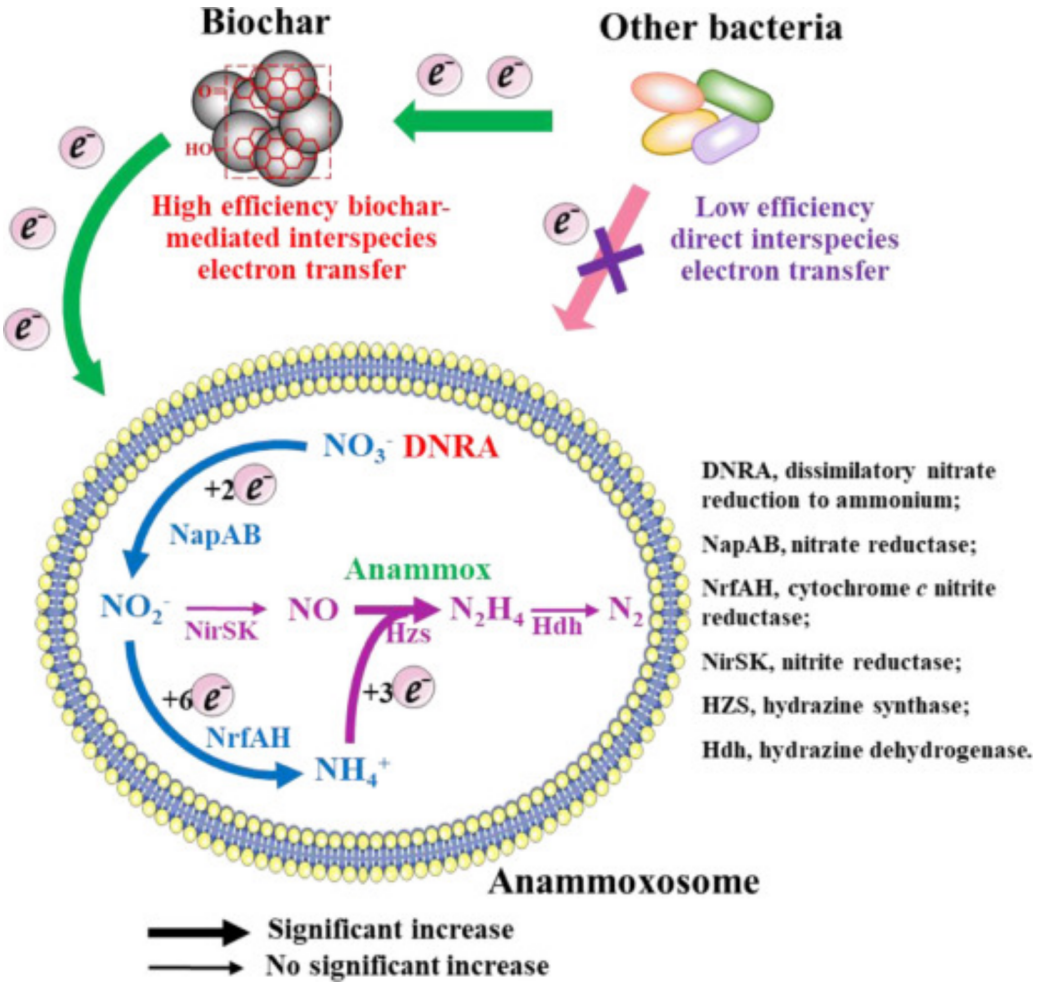


Figure 26: Possible mechanism of biochar-mediated DNRA pathway of anammox bacteria. *Image reproduced with permission from the copyright holder (see Table 40 in Appendix A5).*

3 Materials and Methods

3.1 Experimental Design

The core of this experiment is the tangential operation of two bench-scale AFBRs. The independent variable whose impact is being assessed is the conductivity of the fluidised media. This will assessed by operating one reactor with semi-conductive PANI coated PVDF beads - denoted Reactor 1 (R1) - and the other with non-conductive uncoated PVDF beads - denoted Reactor 2 (R2). The dependent variables to be measured are: COD removal; inorganic-N removal; biogas production rate and composition; and microbial community structure and function. The control variables of this experiment are the seed sludge used to inoculate the reactors and the control of reactor operation, i.e., influent composition; OLR; and HRT. Figure 27 shows the work packages to be executed to achieve the objectives as stated in subsubsection 1.2.2. The methodologies for each of those work packages are described in the following subsections.

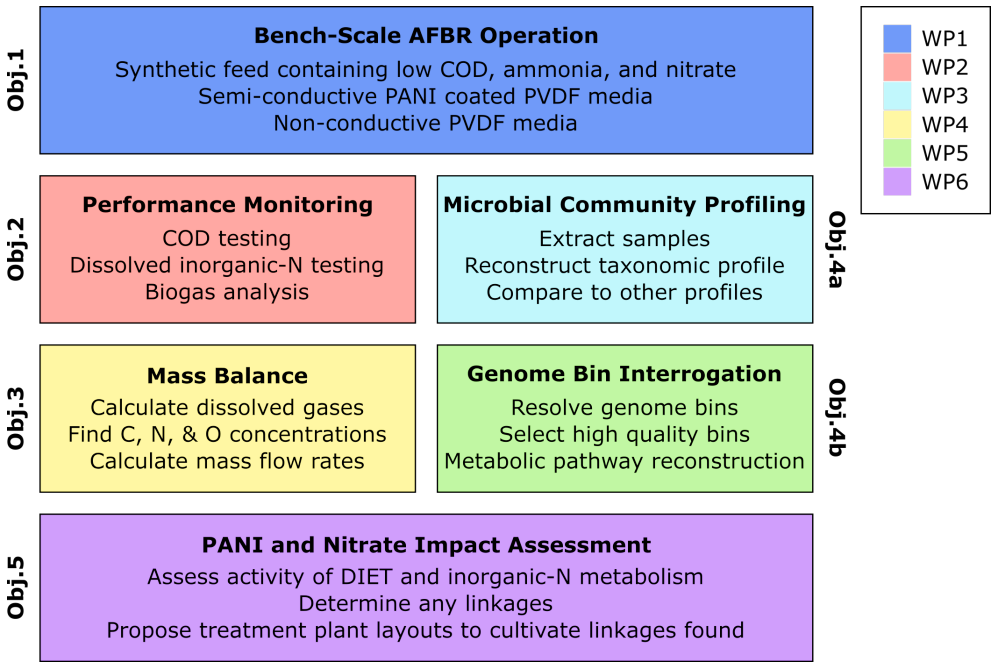


Figure 27: Aims and objectives flow chart

Although both reactors will receive equal volumes from a single source of seed sludge, controlling the inoculation microbial community is not possible. Additionally, although every attempt will be made to ensure that the reactors are operated in the same manner at all times, it will occasionally be necessary for their treatment to deviate, depending on conditions and observed problems. Hence, this experiment is a quasi-experiment, meaning that any results observed are casual.

3.2 Bench-Scale Anaerobic Fluidised-bed Bio-Reactors

3.2.1 Reactor Design and Materials

The detailed schematic of the AFBR layout is shown in Figure 28. The structural design of the AFBRs is centred on the clear acrylic columns measuring 1000 h x 52 mm Inø (2.12 l volume) with five 3/8 inch ø access ports spaced evenly along the height. The heads are made from opaque grey PVC measuring 180 h x 160 mm Inø with 2 rows of 4 access ports around the sides and 5 access ports on the top. The base plates are also made from opaque grey PVC and feature a single front-facing port and a base port. All of these structural plastics were ordered from The Plastic Shop and the components were manufactured to specification by the Structures Laboratory in Skempton Building.

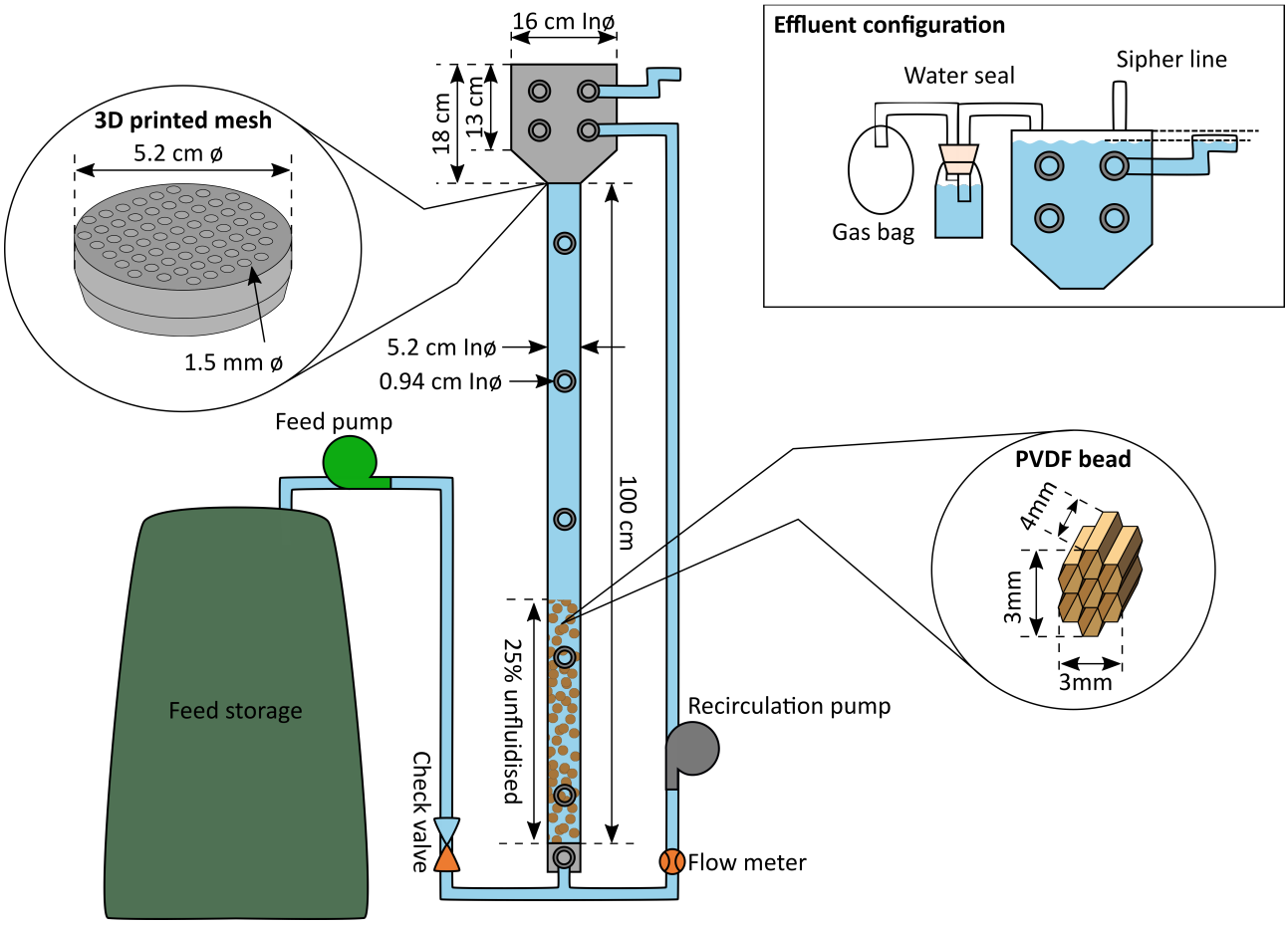


Figure 28: Bench-scale anaerobic fluidised-bed bioreactor schematic and design details

The feed pumps were 520S peristaltic pumps (Watson-Marlow) and the recirculation pumps were M510S-V centrifugal brushless micropumps (TCS Micropumps). All of the ports were managed using non-conductive materials: glass fibre reinforced plastic blanking plugs (Elesa-Clayton) and acetal copolymer push-in pneumatic fittings (John Guest). Acetal single check valves (RS Components) were installed on the feed lines just before they joined the base plate inlets to facilitate line cleaning and prevent backwashing. A siphon line was attached at the top to allow head space purging and flow control when extracting samples

for meta-omic sequencing. Tubing used for both liquid and gas flow was a combination of clear silicone and opaque Fisherbrand Neoprene tubing to balance the need for visibility with the need to prevent light infiltration. Finally, further to the need to control light infiltration, the columns were wrapped with foam sheets. A photo of the practical layout with both AFBRs are shown in Figure 29

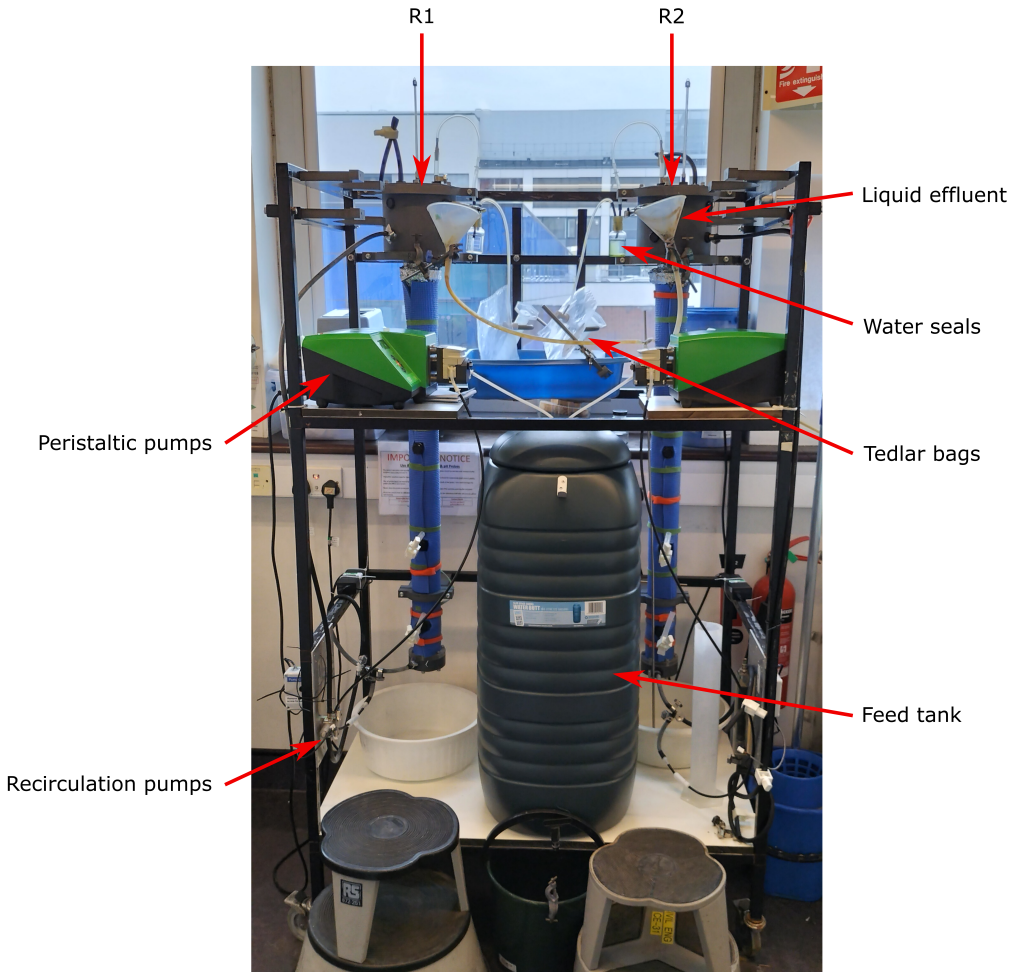


Figure 29: Photo of bench-scale anaerobic fluidised-bed bioreactors in Roger Perry Lab

To ensure a liquid and gas tight seal between the structural components, 3 mm ø nitrile rubber O-ring cord (RS Components) was used. On the liquid and gaseous effluent lines, water seals prevented atmospheric air ingress and ensured that the system was kept under positive pressure, so that any leaks would flow out and not in. The initial seal design on the gaseous effluent line featured an inverted calibrated 500 ml plastic bottle. This was upgraded on day 159 of operation to a much smaller inverted siphon attached to 0.6 l gas bags (Tedlar) to remove the additional pressure that the former system created.

The 7-channel PVDF beads used for fluidised media were supplied by the Inha University, who also applied the PANI coating as previously described (Kwon and Kim 2022). Once prepared (described in subsubsection 3.2.2), beads were added into the columns up to 25 % of the height while flow was static. Additionally, 3D printed plastic meshes, manufactured by the Structures Laboratory, were placed at the top

of the acrylic columns after beads were found to travel around the system, ending up inside the recirculation pumps and flow meters.

3.2.2 System Priming, Inoculation, and Continuous Operation

The small size of the channels in the PVDF beads meant that it was necessary to prewet them to remove air bubbles and ensure they settled in solution. The dry beads were placed in beakers and submerged in ethanol, sonicated for 5 minutes and drained. They were then resubmerged in distilled water, sonicated again for 5 minutes and drained, repeated 3 times. After the final sonication and drainage, the beads were resurmerged in the inoculation feed solution described in Table 6. At all stages, the synthetic feed was made using tap water instead of distilled water, and this was treated as the sole source of NO_3^- and NO_2^- throughout this experiment. While it does mean that the concentration was not controlled in the influent, subsection 3.3 will describe the means by which it was monitored.

Table 6: Composition of synthetic feed solution

Substrate (mg/l)	Inoculation Feed	Operational Feed	
COD (from glucose)	1500.00	300.00	
Glucose	1406.25	281.25	
Ammonium chloride	480.00	96.00	
Nitrate/nitrite	~30.00	~30.00	
Monopotassium phosphate	40.00	8.00	
Supernatant (ml/l)	100.00	0.00	
Yeast extract	0.00	40.00	
Sodium bicarbonate	0.00	40 - 400	
HRT (h)	20	30	6
OLR (kg COD/m^3·d)	1.50	0.24	1.20
OLR (mg COD/l·h)	62.50	10.00	50.00

The seed sludge was collected from an industrial AD in Basingstoke, UK on Thursday 18th August 2022 and transported on ice directly to the Roger Perry Lab, whereupon it was stored at 5 °C until Monday 22nd August 2022 - day 1 of reactor operation. The columns were partially filled with inoculation feed solution before the PANI-PVDF beads and the uncoated PVDF beads were added up to 25 % of the column height into R1 and R2, respectively. Following this, 500 ml of sludge was added to each reactor, the remaining volume was filled with inoculation feed solution, and all lines were primed. At this point, the heads were sealed and an anaerobic environment was created by purging with N_2 gas through the siphon line. Finally, the recirculation flow rate was set so that the beads were gently fluidised, up to no more than 35 % of

the column height. The recirculation flow rate was not measured, however the degree of fluidisation was monitored by eye.

An inoculation period was enacted over the following 8 days, during which the reactors were operated in batch mode to prevent wash-out and encourage biofilm formation on the beads. During this period, 2.12 l of inoculation feed solution was supplied over 4 hours each day and AD supernatant from the same WWTP that provided the seed sludge was included to provide micronutrients. In the subsequent continuous operation phase, this was switched to yeast extract to prevent excessive feed degradation by the microbes present. Continuous feeding began on day 9 of operation using the operational feed solution described in Table 6. A high HRT was initially maintained to extend the acclimatisation period, and was slowly decreased from 30 hours to 6 hours over the following 7 weeks. Continuous steady-state operation was reached on day 52 of operation. The sodium bicarbonate was included as a pH buffer, and its concentration was varied depending on the observed pH readings during acclimatisation.

3.2.3 Maintenance Routine

To maintain appropriate fluidisation throughout continuous operation, the media were checked by eye on an ad-hoc basis, and the recirculation pumps were adjusted as deemed necessary. During sample collection, the effluent volumes over 10 minute periods were recorded and used to adjust the RMP settings of the influent pumps accordingly. As the system was operated under atmospheric pressure, it was assumed that the influent and effluent flow rates were equal. Fresh feed was prepared 3 times a week - Mondays, Wednesdays, and Fridays - to maintain the quality of the feed. During feedings, a cleaning routine was also implemented to remove any biofilm that had formed inside the feed tank and in/on the influent tubing to prevent excessive feed degradation and blockages.

The cleaning solution used was dilute sodium hypochlorite mixed with tap water (~100 ml/l). Firstly, the feed lines were disconnected from the reactors at the check valves and the old feed was discarded. The portions of the tubing that had been submerged in the old feed were submerged in the cleaning solution, while it was also pumped through. The dirty feed tank was placed aside with a small volume of the cleaning solution spread over the internal walls to the same end, left to soak until the next feeding/cleaning day. A separate clean tank was rinsed three times with clean tap water to remove the old cleaning solution before being used to store the incoming fresh feed. The outsides of the feed tubes were rinsed by pouring over clean tap water and the insides were flushed by pumping through a minimum of 500 ml of clean tap water. The lines were then primed with a minimum of 500 ml of fresh feed (which was then discarded) before being reconnected to the AFBRs to resume feeding.

3.3 Carbon and Nitrogen Monitoring

3.3.1 Sample Collection and Preparation

Liquid influent and effluent samples were used for COD, dissolved inorganic-N, and pH analysis. These samples were taken according to the following weekly schedule: influent samples were taken on Mondays and Wednesdays from the fresh feed prepared on those days. The associated effluent samples were taken on Tuesdays and Thursdays respectively. This was to ensure that the effluent samples were reflective of the reactor performance from the fresh feed. Once collected, pH readings were taken using an electrode (Hanna Instruments) connected to a Hydrus 500 benchtop pH meter (Fisherbrand). Samples were then immediately frozen to -20 °C to be stored. Prior to further analysis, samples were defrosted overnight at 5 °C and filtered through 0.45 µm hydrophilic filters to remove SS that may interfere with analysis or cause blockages in machinery.

Biogas was continuously captured by the inverted bottles and gas bags. Following the switch to the gas bags on day 159, biogas volume was measured by emptying the bag using a graduated syringe. As both of these systems were passive, and therefore could be implemented continuously, volume data was simply recorded when deemed necessary.

The method for the biogas composition assessment was also changed during the operational period, conducted on an ad-hoc basis in both cases. Initially, a Geotech GA2000 Infrared Gas Analyser (Keison) was used to both analyse biogas composition and to re-zero the gas collection bottles. Prior to sampling, the volume measurement was taken from the collection bottle, the gaseous effluent tube at the top of the reactor was clamped shut, and the collected gas was drawn out by the analyser. From day 74 of operation, the samples were taken by piercing a Gastight #1710 100 µl syringe (Hamilton, USA) into the silicone tubing at the top of the reactors and analysed using Gas Chromatography tandem Mass Spectrometry (GC-MS). Once inserted, the syringe was filled and evacuated three times to ensure that no atmospheric contaminants were included in the sample and the needle was plugged during the walk to the machinery.

3.3.2 Chemical Oxygen Demand Analysis

Samples were analysed in triplicate using method 5220C - closed reflux, titrimetric method from Standard Methods (Baird and Bridgewater 2017). All of the required reagents were prepared according to the method in the Roger Perry lab. Mercuric sulphate was included in the digestion solution to reduce the interference of chlorides from the ammonium chloride or the tap water. Feed samples were diluted to 50 % with distilled water as the concentration was found to be too high. Distilled water was used as the blank and the potassium hydrogen phthalate standard was prepared monthly - this solution was also diluted to

50 % when conducting the test.

3.3.3 Dissolved Inorganic Nitrogen Analysis

To measure dissolved inorganic-N, samples were analysed using a Skalar San^{++} Classic continuous flow colorimetric analyser fitted with a 1050 autosampler. The pathways for NH_3/total nitrogen, NO_3^- + NO_2^-, and NO_2^- were used to get a full picture of all the inorganic-N present in the samples. All of the required reagents and standards were prepared fresh for each run according to the manufacturer's documentation in the Roger Perry lab. Stock solutions for the standards were prepared monthly and stored in amber bottles at 5 °C. For the NH_3/total nitrogen pathway, all samples were diluted by a factor of 20 by the autosampler and corrections were applied to the results by the software.

3.3.4 Biogas Composition Analysis

The Geotech GA2000 Infrared Gas Analyser provides percentage composition readings for CH_4, CO_2, O_2, and N_2, while other gases are attributed to the "balance" fraction. This was deemed suitable as no other major gases were anticipated. However, this method was abandoned from day 74 of operation for two key reasons: firstly, when only small volumes of biogas were collected in the inverted bottles, it made sample extraction difficult; secondly, it was found that the measurements obtained by GC-MS were significantly different, and deemed more reliable.

A Clarus 600 Gas Chromatograph (Perkin Elmer, USA) system equipped with a fused silica capillary column (Carboxen-1010 PLOT) and a Thermal Conductivity Detector (TCD) was used. The method, developed by Maryam Dewiandratika (a fellow PhD student in the department), is as follows: the injector and detector temperatures were maintained at 200 °C and 230 °C, respectively. The oven temperature was programmed to ramp from 35 °C (held for 8 minutes) to 120 °C (held for 3 minutes) and finally to 220 °C (held for 1 minute). Helium served as the carrier gas at a flow rate of 3 ml/min. The injection volume was 100 µl. Following initial calibration, the percentage composition readings provided by the software were used for further analysis, rather than the precise volumetric measurements of each constituent gas. This was deemed suitable as, just like for the Geotech Gas Analyser, no other major gases were anticipated that would dilute the composition and it meant that ongoing standardisations were not required.

3.4 Mass Balance Calculation

3.4.1 Balancing Approach

Both the C and the N overall balances can be calculated based on the assumption that their totals can be largely accounted for from four components: (1) the dissolved quantities of COD and inorganic-N remaining in the effluent; (2) the gaseous quantities of CH_4, CO_2, and N_2; (3) the corresponding dissolved portions of those gases; and (4) CO_2 consumed by alkalinity consumption and biomass growth. Regarding the latter component, although pH was measured, early measurements of SS proved to be negligible, hence it was not measured on an ongoing basis. In addition to not measuring VFAs to distinguish their contribution to acidification from CO_2, it becomes difficult to accurately calculate this contribution. However, as this is expected to be the smallest component, it is considered to be negligible.

3.4.2 Chemical Oxygen Demand to Carbon Mass Equivalent

The dissolved influent and effluent C will be calculated using stoichiometric conversions from the COD readings. Given that all the other major feed components are inorganic, the sole source of COD in the influent is glucose. The yeast extract and uncontrolled composition of tap water may provide small amounts, but these are considered to be negligible. For the effluent, it is not possible to discern which chemical species are contributing to the readings, hence, these results from the COD test were treated as untransformed glucose for the purpose of calculation. Using the stoichiometric balancing formula for oxidation of organic compounds as shown in Equation 14, it was calculated that $1.0\dot{6}$ g O_2 are required to fully oxidise 1 g glucose. Hence, once the COD readings are converted into glucose concentrations, it is a simple conversion of 6 moles of C per mole of glucose.

$$C_aH_bO_cN_d + \left(a + \frac{b}{4} - \frac{c}{2} - \frac{3d}{4}\right) O_2 \rightarrow aCO_2 + \left(\frac{b}{2} - \frac{3d}{2}\right) H_2O + dNH_3 \tag{14}$$

3.4.3 Biogas Volume and Composition to Mass Equivalents

Using the gas composition data, the partial pressure of each constituent gas can be calculated, as the percentage by volume (derived from the GC-MS) is equal to the percentage by pressure. From there, using the average gas volume produced per day, the number of moles of each constituent gas can be calculated, assuming ideal conditions. With the gas bag collection method, pressure within the reactor is atmospheric (101325 Pa) and the temperature in the Roger Perry lab is maintained at 21 °C. Therefore, the ideal gas law equation can be applied as described in Equation 15. Once the number of moles of each component gas has been calculated, the number of moles of each element (carbon, nitrogen, oxygen) can be used to calculate the generated mass of each element per day.

$$n = p\left(\frac{V}{RT}\right) \tag{15}$$

where: n = number of moles of the constituent gas
p = the partial pressure of the constituent gas (Pa)
V = volume of total gas sample (l)
R = the gas constant = 8314.46 (l·Pa/K·M)
T = absolute temperature = 294.15 (K)

3.4.4 Dissolved Gases

The saturation concentration of gases dissolved in the influent and the effluents will be calculated using the unitless form of Henry's law, as described in Equation 16. The constants used for CH_4, CO_2, N_2, and O_2 were calculated using the constants and temperature modification equations given by Tchobanoglous et al. (2014), determined as: 28.53, 1.09, 60.79, and 31.11, respectively. Mathematical formulae to predict rates of CH_4 supersaturation in an AFBR-type reactor were not found in the course of the literature review. However, reported values of CH_4 supersaturation in a SAF-MBR were 1.05 and 1.44, corresponding to total HRTs of 2.3 and 3.4 hours Yoo et al. (2012). Hence, although the membrane inclusion means that these supersaturation degrees are likely to be lower than those that will be present in this experiment, they will be used in dissolved CH_4 calculations.

$$C_g = C_s \cdot H_u \tag{16}$$

where: C_g = concentration of constituent in gas phase (mg/l)
C_s = saturation concentration of constituent in liquid phase (mg/l)
H_u = unitless Henry's law constant

3.5 Meta-Omics

3.5.1 Sampling and Handling

Throughout the operational period, meta-omic samples were taken twice. The first round of samples - denoted Point 1 (P1) - was extracted on day 193 of operation and the second round - denoted Point 2 (P2) - was extracted on day 290 of operation. In each round, 4 samples were taken: biofilm and bulk samples from both R1 and R2. The sample extraction and preservation protocol is described in Table 7. Preserved samples were sent to Novogene UK for DNA extraction and pair-ended sequencing using the Illumina Novaseq6000 platform, targetting 20 GB per sample. At the P1 sampling point, the biofilm samples were

sent for sequencing still attached to the beads. At the P2 sampling point, samples were delivered on the day of extraction, hence freezing was not necessary.

Table 7: Meta-omics sampling protocol

Process step	P1	P2
Initial bulk solution collected from ports along column sent to waste	X	X
Bulk solution and beads collected in containers	X	X
Beads separated from bulk by sieving and beads resuspended in distilled water	X	X
Biofilm removed from beads by shaking, beads removed by sieving		X
Centrifuging using Sarstedt 50 ml sterile tubes	X	X
Supernatant removed and additional sample added to tube in between each round	X	X
3500 RPM for 5 minutes, 4500 RPM for 5 minutes twice, 5000 RPM for 10 minutes	X	
5000 RPM for 10 minutes repeated 3 times		X
100% ethanol applied to fix samples	X	X
Samples frozen to -80 °C for temporary storage	X	

All samples were successfully extracted and sequenced, and are denoted as: GR1P1biofilm, GR1P1bulk, GR2P1biofilm, GR2P1bulk, GR1P2biofilm, GR1P2bulk, GR2P2biofilm, and GR2P2bulk. G denoting genomic. The raw reads from Novogene were uploaded to the National Center for Biotechnology Information (NCBI) Sequence Read Archive, accession number PRJNA1083991. The pipeline developed for analysis of the raw sequence data, described in the following sub-sections, was based off of recommendations and support available from colleagues in Dr. Lee's group, primarily Theo Lam. The scripts used to perform the various process steps were executed using the Imperial College High Performance Computing (HPC) service, and can be found in Appendix A3.

3.5.2 Library Prep

For a streamlined sequence denoising procedure, the KneadData (v0.12.0) pipeline was applied (The Huttenhower Lab 2023). This pipeline incorporates three commonly used raw data clean-up packages, namely: Trimmomatic (v0.39-2) which removes low quality bases and adpaters (Bolger et al. 2014); Tandem Repeats Finder (TRF) (v4.09) which removes overrepresented sequences (Benson 1999); and FastQC (v0.12.1) which produces the sequence quality reports (Babraham Bioinformatics 2023). Default settings were applied, which entailed a minimum read length of 75 base pairs (bp) and a quality score of phred 33.

Prior to library prep, the pair-ended raw read files were synchronised (there were the same number

of reads in the forward and reverse files). However, they became desynced following the final TRF stage, meaning they could not be processed by downstream software packages that require pair-ended read files to be synced. Fortunately, the post-Trimmomatic reads were synced and the FastQC quality reports confirmed that there were no overrepresented sequences in those files. Moreover, TRF removed less than 1 % of reads from each file. Hence, it was decided to carry forward the post-Trimmomatic reads through the rest of the pipeline.

3.5.3 Assembly-Free Taxonomic Profiling

Although not as practical for functional analysis, assembly-free taxonomic profiling offers a wider look at the taxonomic profile of a microbial community. By including all of the (clean) reads, assembly-free profiling can capture low abundance microbes that would be unlikely to be represented in the MAGs, as they lack the necessary depth and coverage (Quince et al. 2017). Thus, a genera-level taxonomic profile of each sample was produced using Kaiju (v1.9.2) (Menzel et al. 2016) against the 2023-05-10 nr protein database (available from Kaiju here). Minimum abundance was set to 0.01 % for classification. Otherwise, default settings were applied, which entailed running in greedy mode with a minimum E-value of 0.01, a minimum match length of 11, a minimum match score of 65, and a maximum number of mismatches of 3.

3.5.4 Diversity Analysis

In order to gain a fuller picture of the microbiome, it is useful to have quantitative measures of diversity. This can be applied two ways: alpha diversity, which measures the diversity within a single sample; and beta diversity, which assesses the differences in community composition between samples. In order to achieve these analyses, the R packages Tidyverse (v2.0.0) and Vegan (v2.7-0) (Oksanen et al. 2024) will be used, applied to the relative abundances obtained from the assembly-free taxonomic profile.

Alpha diversity metrics give insight into the richness (number of species) and evenness (distribution of individuals among species) within a given community. The most commonly used metrics are the Shannon diversity index, Simpson's index, and the inverted Simpson's index, calculated using the formulae given in Equations 17 and 18, respectively. Inverted Simpson's index is calculated simply as $1/D$.

$$H = -\sum_{i=1}^{S} p_i \cdot ln(p_i) \tag{17}$$

$$D = \frac{\sum_{i=1}^{S} n_i(n_i - 1)}{N(N-1)} \tag{18}$$

where: H = the Shannon diversity index
D = Simpson's diversity index
S = the number of genera (i.e., richness)
n_i = the number of reads assigned to genera *i*
p_i = the relative abundance of genera *i*
N = the total number of reads

Beta diversity analysis facilitates the comparison of diversity across different environments, conditions, or time points, providing insights into the factors that shape biodiversity and community structure. Typically, these analyses are performed over tens of samples, in order to get a strong idea of influential factors. Since there are only 8 samples in this study, only Bray-Curtis Dissimilarity will be performed, as it is the most widely used and reliable (Xia and Sun 2023). The formula is described in Equation 19.

$$BC = \frac{\sum_{i=1}^{n} |A_i - B_i|}{\sum_{i=1}^{n} (A_i + B_i)} \tag{19}$$

where: A_i = the abundance of genera *i* in sample A
B_i = the abundance of genera *i* in sample B
n = the number of genera across both samples

This measure is a non-Euclidean metric, meaning that it doesn't measure "straight-line" distances and may not satisfy all metric space properties. Thus, Bray-Curtis dissimilarities are often analysed with non-metric ordination methods in order to reduce complex, high-dimensional dissimilarity data to a 2D or 3D space, with each axis representing a dimension that captures variation in the data. The method used in this programme will be Principal Coordinates Analysis (PCoA).

3.5.5 *De novo* Assembly of Genome Bins

In order to undertake functional analysis, the next step of the process is the resolution of the millions of clean short reads into MAGs. The process to achieve this followed three high-level stages: assembly of short-reads into contigs and scaffolds; alignment of the short-reads back on to the contigs (crucial for downstream abundance, coverage, and depth analysis); and finally binning of contigs into distinct genome-bins.

For contig assembly, the multi k-mer succinct *de Bruijn* graph assembler, MEGAHIT (v1.2.9), was used (Li et al. 2015, 2016). Applying the default settings to MEGAHIT, the k values used were 21, 29, 39, 59, 79, 99, 119, and 141. The assembly quality was evaluated using QUAST (v5.2.0) (Gurevich et al. 2013). Bowtie 2 (v2.5.2) was used to generate a custom index from the assembled contigs and to map the short reads back to contigs in order to establish sequence depth (Langmead and Salzberg 2012). The default end-to-end alignment setting was used. Once completed, in order to proceed and to save computational power, it is necessary to reformat the output files from Bowtie 2, and this was accomplished using SAMtools

(v1.18) (Danecek et al. 2021), including the integrated HTSlib (v1.18) (Bonfield et al. 2021).

The production of contig depth files and the resolution into MAGs was achieved using MetaBAT 2 (v2:2.15) (Kang et al. 2019). A minimum contig length of 2500 bp was used to do so. In order to assess the completeness and contamination levels of each bin, CheckM (v.1.2.2) was used (Parks et al. 2015). As well as producing MAG quality reports, CheckM functions were also used for community structure analysis, and translation of nucleotide files to amino acid format. Finally, PhyloPhlAn 3.0 (v3.0.67) was used for species-level taxonomic classification of the generated MAGs (Asnicar et al. 2020) against the July 2020 Species-level Genome Bin (SGB) database (available from Zenodo here).

3.5.6 Interrogation of Bins

Once the MAG bins have been assembled and taxonomically profiled, functional analysis can be undertaken. This entails analysis of the specific genes present in individual genomes, discovered by submitting the protein sequence files to online Basic Local Alignment Search Tool (BLAST) services (Altschul et al. 1990, 1997). These tools enable the investigation of the content of a bin against enormous existing databases that are considered as industry standards.

Since multiple MAGs can be classified as the same species, interrogation was performed on those multiples to check for blind spots - genes that may be missing from one bin may be included in another. This will provide a clearer idea of the functional profile of a particular species within the AFBR environment. While this tactic goes some way to remediate potential sequencing errors, analysis of pure culture genomes can also provide insight into the capabilities of a species and thereby the microbial community. Hence, reference genomes for each of the species investigated were downloaded from NCBI and subjected to the same interrogation.

For pathway reconstruction, selected bins were submitted to Kyoto Encyclopedia of Genes and Genomes (KEGG) BlastKOALA (Kanehisa et al. 2016). This service enables visualisation of complete and incomplete metabolic pathways present within a genome, provided those pathways are accepted as "canonical" within the microbiological field. For sequence similarity scoring and potential homolog identification, the NCBI protein-protein BLAST service (blastp) was used (Sayers et al. 2022). For this project, the option to align two or more sequences was selected, using the selected genome as the subject sequence and genes of interest as the query sequences. Hence, genomes can be interrogated for enzymes that may be close matches to processes that are not yet confirmed in the KEGG database.

3.5.7 16S rRNA Gene Analysis

16S rRNA amplicon sequencing was performed on samples from 3 ADs operated on real WWTPs in the UK, the objective being to provide a baseline for comparison of typical anaerobic microbial community structure. Samples were collected on 5th February 2020 and stored at -80 °C. Once defrosted, DNA was extracted using a DNeasy PowerSoil kit (QIAGEN) on 3rd December 2020, these extractions were temporarily stored at -20 °C until they were sent to Novogene Hong Kong on 8th December 2020.

The Illumina HiSeq platform (Illumina, San Diego, CA, USA) was used for pair-ended sequencing using the following primers: 341F (CCTAYGGGRBGCASCAG) to 806R (GGACTACNNGGGTATCTAAT) targeting the variable region V3-V4 of bacteria; and SSU1ArF (TCCGGTTGATCCYGCBRG) to SSU520R (GCTACGRRYGYTTTARRC) targetting the variable region V1-V2 of archaea (custom, based on newly designed primers (Bahram et al. 2019)). Raw sequences were processed using Qiime2 v2021.8 (Bolyen et al. 2019). Denoising was achieved using DADA2 set at a trim length of 220 and reads had a median quality score of 37 (Callahan et al. 2016). Taxonomic classification was performed using a pre-trained classifier (available here (Bokulich et al. 2018; Robeson et al. 2020)) trained on the SILVA 138 database (Quast et al. 2013).

3.6 Statistical Methods and Quality Assurance

All COD tests were performed in triplicate, with blanks and controls utilised as recommended in the 5220C method from Standard Methods (Baird and Bridgewater 2017). For dissolved inorganic N measurements, standards were produced and run with every batch of samples to ensure accurate calibration of the Skalar. Following the GC-MS method development, ongoing calibration was not required as the biogas composition was recorded as percentage composition rather than accurate volumes of each gas. The pH meter was calibrated before each use, using standards that were prepared fresh no more than fortnightly. Following data collection, all performance data was reviewed for performance stabilsation. Once stable, averages (means) and standard divations were calculated and standardised normal distribution calculations were used to remove outliers. Z-scores were calculated using the formula shown in Equation 20.

$$Z = \frac{x - \mu}{\sigma} \tag{20}$$

where: x = reading

μ = mean

σ = standard deviation

Quality control for meta-omic sequencing was undertaken by Novogene, according to their internal

processes. Once sequenced, quality analysis steps were integrated into the sequence analysis pipeline as described in the previous subsections. Statistical analysis beyond diversity analysis is not required, as replicates weren't used.

4 Performance Review and Substrate Cycling Analysis

4.1 Summary of Performance

4.1.1 Operation

The summary of the AFBRs' performances - flow rates, pH, COD, dissolved inorganic-N, biogas production and composition, and dissolved gases - is described in Table 8, calculated from the steady-state averages, which will be described in the following subsections. From this, a graphical representation of the liquid and gaseous effluent flow rates and the carbon, nitrogen, and oxygen concentrations in the influent and effluents is shown in Figure 30. Full detailed results, including standardised normal distributions of readings, can be found in Appendix A1.

Following the commencement of the continuous operation phase on day 52, as described in the methodology subsubsection 3.2.2, the AFBRs were operated for 238 days. The average values for HRT were 6.00 and 6.05 h from R1 and R2, respectively. Although there is a minor difference in the HRTs between R1 and R2, it was considered to be minor enough to not warrant further investigation or mitigation strategies. Values followed normal distribution patterns, shown in Figure 48 in subsubsection A1.1.1. The average pH readings were 7.80, 7.13, and 7.24 from the influent, R1, and R2, respectively. All values followed normal distribution patterns, shown in Figure 50 in subsubsection A1.1.2. Some slight acidification in the effluent was observed, attributable to accumulated VFAs or carbonic acid from dissolved CO_2, but pH remained within an acceptable range.

4.1.2 Chemical Oxygen Demand Removal

Effluent COD readings stabilised on day 88 for both reactors, indicating that they were successfully inoculated by this time. The average concentrations, removals, and removal efficiencies shown in Table 8 include all readings from that point that followed a normal distribution pattern, with anomalous readings removed, shown in Table 26 and Figure 52 in subsection A1.2. Not shown in Table 8 are the average COD removal rates, calculated as the average COD removed x the average effluent flow rate, which were 2467.85 and 2529.46 mg $COD_{removed}$/d from R1 and R2, respectively.

In the AFMBR study that also used coated and uncoated PVDF beads, the reactors were fed an acetate and propionate based synthetic wastewater with a COD of 300 mg/l. When operated at 8 h HRT, those AFMBRs achieved ~90 % COD removal, even with the benefit of submerged membranes (Kwon et al. 2022). This highlights the successful operation of the AFBRs in this experiment and the comparable performance to those AFMBRs.

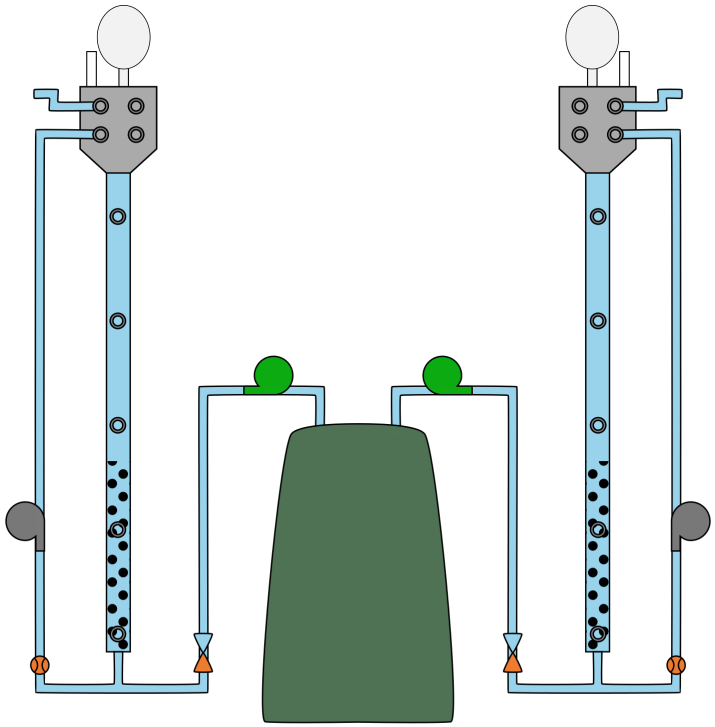
Table 8: Summary of AFBR operation and performance monitoring. Days = operational dates of first and last readings. n = number of readings included in average calculations. Average = mean with anomalous readings removed.

		Influent			R1 effluent			R2 effluent		
Measurement	Unit	Days	*n*	Average	Days	*n*	Average	Days	*n*	Average
Operation										
Effluent flow	l/d				52-286	58	8.51±0.42	52-282	57	8.43±0.41
HRT	h					58	6.00±0.30		57	6.05±0.31
pH		85-274	27	7.80±0.03	52-282	58	7.13±0.07	52-282	58	7.24±0.09
Chemical oxygen demand										
COD concentration	mg O_2/l	88-289	51	339.13±56.56	88-289	47	48.59±20.84	88-289	44	41.74±19.87
COD removed	mg O_2/l						290.16±46.82			300.14±56.10
COD removal efficiency	%						85.65±5.93			87.66±5.60
Biogas										
Biogas flow	l/d				159-284	55	0.19±0.07	159-284	56	0.23±0.08
Biogas total composition	%				228-290	16	96.73±5.64	228-290	16	99.41±0.39
Biogas CH_4	%				228-290	16	53.50±4.33	228-290	16	55.97±5.32
Biogas CO_2	%				228-290	16	8.86±1.14	228-290	16	8.22±1.71
Biogas N_2	%				228-290	16	33.03±3.89	228-290	16	32.99±5.02
Biogas O_2	%				228-290	16	1.34±0.51	228-290	16	2.23±1.86
Dissolved gases										
Dissolved CH_4*	mg CH_4/l			0.00			17.90±1.45			18.73±1.78
Dissolved CO_2	mg CO_2/l			0.00			148.34±19.10			137.59±28.65

Continued...

Table 8 Continued.

		Influent			R1 effluent			R2 effluent		
Measurement	Unit	Days	*n*	Average	Days	*n*	Average	Days	*n*	Average
Dissolved N_2	mg N_2/l			14.90			6.30±0.74			6.30±0.96
Dissolved O_2	mg O_2/l			8.92			0.57±0.22			0.95±0.79
Dissolved inorganic nitrogen										
Total N concentration	mg N/l	235-289	15	31.21±1.30	235-289	12	25.76±3.40	235-289	9	26.29±2.37
Total N removed	mg N/l						5.60±3.14			5.20±2.49
Total N removal efficiency	%						17.89±10.28			16.40±7.83
NH_3-N concentration	mg N/l	179-289	29	23.23±1.97	165-289	31	24.45±3.06	165-289	31	25.35±2.19
NH_3-N removed	mg N/l						-1.19±2.35			-2.11±1.87
NH_3-N removal efficiency	%						-5.08±10.31			-9.36±8.63
NO_3^--N concentration	mg N/l	235-289	15	6.76±0.32	235-289	12	0.20±0.17	235-284	9	0.27±0.15
NO_3^--N removed	mg N/l						6.62±0.28			6.67±0.22
NO_3^--N removal efficiency	%						97.05±2.39			96.09±2.09
NO_2^--N concentration	mg N/l	235-289	15	0.06±0.02	235-289	14	0.00±0.00	235-289	14	0.01±0.00
NO_2^--N removed	mg N/l						0.05±0.02			0.05±0.02
NO_2^--N removal efficiency	%						91.70±4.12			89.36±4.80



R1 Biogas

Flow rate (l/d)

Biogas: 0.19 ±0.07

Carbon (mg C/l)

CH_4: 265.98 ±21.53
CO_2: 44.03 ±5.67

Nitrogen (mg N/l)

N_2: 383.16 ±22.57

Oxygen (mg O/l)

O_2: 17.80 ±6.71
CO_2: 117.42 ±15.12

R2 Biogas

Flow rate (l/d)

Biogas: 0.23 ±0.08

Carbon (mg C/l)

CH_4: 278.26 ±26.44
CO_2: 40.84 ±8.50

Nitrogen (mg N/l)

N_2: 382.71 ±29.11

Oxygen (mg O/l)

O_2: 29.61 ±24.60
CO_2: 108.91 ±22.68

R1 Effluent

Flow rate (l/d)

Effluent: 8.51 ±0.42

Carbon (mg C/l)

COD: 18.22 ±7.82
Dissolved CH_4: 13.42 ±1.09
Dissolved CO_2: 40.46 ±5.21

Nitrogen (mg N/l)

Inorganic N: 25.76 ±3.40
Dissolved N_2: 6.30 ±0.37

Oxygen (mg O/l)

COD: 24.30 ±10.42
NO_3+NO_2: 0.71 ±0.58
Dissolved O_2: 0.57 ±0.22
Dissolved CO_2: 107.88 ±13.89

Influent

Carbon (mg C/l)

COD: 127.17 ±21.21

Nitrogen (mg N/l)

Inorganic-N: 31.21 ±1.30
Dissolved N_2: 14.90

Oxygen (mg O/l)

COD: 169.57 ±28.28
NO_3+NO_2: 23.30 ±1.13
Dissolved O_2: 8.92

R2 Effluent

Flow rate (l/d)

Effluent: 8.43 ±0.41

Carbon (mg C/l)

COD: 15.65 ±7.45
Dissolved CH_4: 14.04 ±1.33
Dissolved CO_2: 37.53 ±7.81

Nitrogen (mg N/l)

Inorganic N: 26.29 ±2.37
Dissolved N_2: 6.30 ±0.48

Oxygen (mg O/l)

COD: 20.87 ±9.94
NO_3+NO_2: 0.95 ±0.51
Dissolved O_2: 0.95 ±0.79
Dissolved CO_2: 100.07 ±20.84

Figure 30: Graphical summary of carbon, nitrogen, and oxygen concentrations in influent and effluents

4.1.3 Biogas Production and Composition

Following the switch to the gas bag collection method on day 159, there was a drastic change in the biogas volume being collected, shown in Figure 53 in subsection A1.3. Although measured values remained highly variable, they followed normal distribution patterns, shown in Figure 54 in subsection A1.3, and they are considered to be a more accurate representation. Hence, they are the only readings included in the average values shown in Table 8, giving 0.19 l/d and 0.23 l/d for R1 and R2, respectively.

Despite switching to the GC-MS method on day 74, the biogas composition readings also remained volatile until day 228 for both reactors. Prior to stabilisation, the composition showed a distinct alternating pattern, shown in Figure 31: when CH_4 increased, so did CO_2; then when N_2 increased, so did O_2. This immediately raised concerns that atmospheric air was leaking in. However, repeated checks of connection points and the water seals on both the liquid and gaseous effluent points confirmed this was not the case.

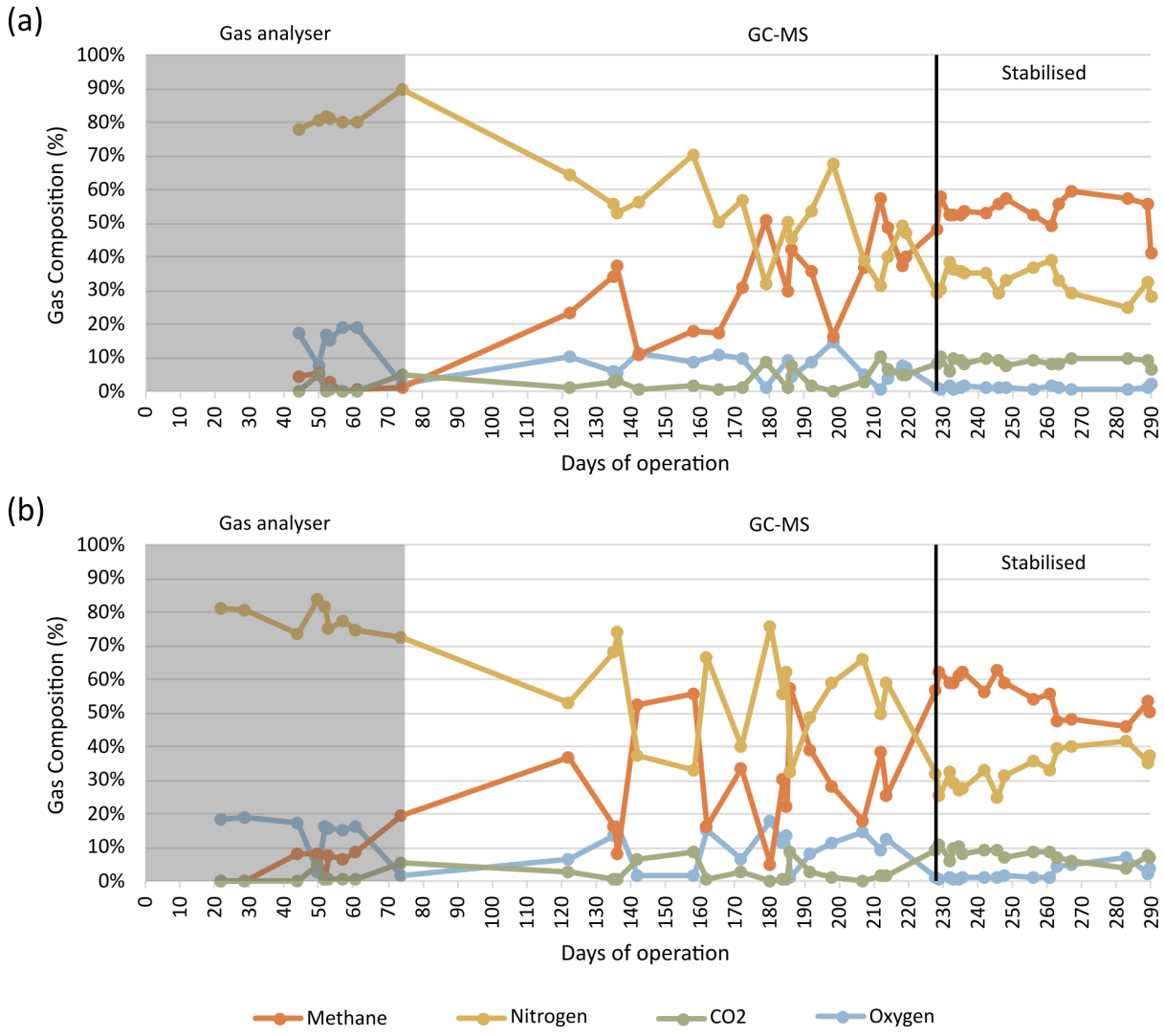


Figure 31: Biogas composition results: (a) R1; (b) R2

Once the biogas composition did stabilise, the four measured components (CH_4, N_2, CO_2, and O_2) made up 96.73±5.64 % and 99.41±0.39 % of the biogases in R1 and R2, respectively (shown in Table 8). The distribution patterns were largely normal with some skew, shown in Figures 55 and 56 in subsection A1.4. A more lenient approach was taken for this data due to the fluctuations until the late stages of operation. It is likely that the absent portions are mostly unmeasured N_2O and other trace gases. Unitless Henry's Law (Equation 16) was applied to the stabilised composition readings to calculate the dissolved portions of the gases, including the supersaturation constant of 1.44 applied to dissolved CH_4.

With the exception of the dominance of the CH_4 component by ~20 %, the portions of the remaining 3 components were unusual. Typical AD biogases are composed of ~60 % CH_4 and ~40 % CO_2. However, neither of the AFBRs in this experiment produced more than 9 % CO_2 on average. Furthermore, there was a constant presence of O_2, and N_2 was the second most abundant component, representing $\sim\frac{1}{3}$ of the biogases from both R1 and R2. Upon reviewing these results, it became clear that there was an opportunity to explore novel microbial processes that could provide these unusual biogas compositions. Hence, the focus of this entire research programme was changed to conduct further detailed analysis.

The closest similar example comes from the same SAF-MBR study referenced for the CH_4 supersaturation degree. In that study, N_2 outweighed CH_4, and there was a similarly small portion of CO_2, shown in Table 9. These reactors used GAC as the carrier and were fed primary effluent from a local WWTP. Operated at very low HRTs and with low influent COD, it was determined that N_2 had been stripped from the influent and the high solubility of CO_2 contributed to its relative absence from the biogas. However, O_2, NO_2^-, and NO_3^- were not measured (Yoo et al. 2012).

Table 9: Biogas composition from an anaerobic fluidised-bed bioreactor, adapted from Yoo et al. (2012)

	Mode II	Mode III
HRT (h)	1.5	1.0
Influent soluble COD	94 ±12	95 ±26
COD removal (%)	63 ±10	61 ±13
Biogas composition (%)		
CH_4	32	40
CO_2	10	8
N_2	58	52

4.1.4 Total Nitrogen Removal

At the outset of this project, there was no intention to monitor nitrogen specifically, however, following the aforementioned unusual biogas readings, it was decided to include dissolved inorganic-N measurements as part of routine testing. It is for this reason that NH_3 readings didn't commence until day 165, while NO_3^- and NO_2^- readings were successfully taken from day 235 due to over dilution of the first batch of samples causing pathway failure. Following that instance, the method was corrected and full results were obtained, except where concentrations fell below the detection limit of the Skalar. See Table 29 and Figure 57 in subsection A1.5.

As shown in Table 8, there was almost complete removal of NO_3^- and NO_2^- from both reactors, ultimately producing total N removal rates of 17.89 % and 16.40 % in R1 and R2, respectively. This is in line with expectations of an anaerobic treatment process, as well as previous applications of the AFBR technology for NO_3^- removal (Ersever et al. 2014; Omena et al. 2013). However, there was a small increase in the concentration of NH_3 in the effluents, 5.08 % and 9.36 % in R1 and R2, respectively.

4.2 Mass Balance

Using the stabilised values for each measured component as shown in Table 8, the nitrogen, oxygen, and carbon mass balances were calculated on a mg per day basis, to account for the differing flow rates between the liquid and gaseous effluents. The summary of the mass balances is described in Table 10. For use in the mass balance calculations, it was assumed that the remaining COD in the effluents was in the form of untransformed glucose, which is the basis of the COD-C and COD-O shown in the table.

The nitrogen balance is almost completely closed, with 88.34 % and 94.72 % accounted for in R1 and R2, respectively. The remaining portion can likely be attributed to assimilation to biomass or unmeasured N_2O or NO, particularly for R1 which had 3.27 % of the biogas composition unaccounted for. This indicates that the measured and theoretical values are accurate.

The mass balance for oxygen is less complete, with 67.67 % and 62.78 % accounted for in R1 and R2, respectively. The vast majority of the oxygen in the effluents is associated with dissolved CO_2, representing ~79 % in both reactors. The second largest portion is associated with the remaining COD, making up 17.8 % and 16.5 % of the effluent balances. In the absence of effluent composition monitoring, including DO, the assumption that the remaining COD was in the form of untransformed glucose potentially leaves significant oxygen-containing compounds undetected.

Table 10: Summary of nitrogen, oxygen, and carbon mass balances

		R1						R2					
		Influent			Effluent			Influent			Effluent		
Nitrogen (mg N/d)	NH_3	197.55	±	0.82	207.91	±	1.27	195.75	±	0.81	213.63	±	0.89
	$NO_3^- + NO_2^-$	57.98	±	0.14	1.77	±	0.07	57.45	±	0.14	2.35	±	0.06
	Dissolved N_2	126.72			53.60	±	0.15	125.56			53.05	±	0.20
	Gaseous N_2	0.00			74.39	±	3.30	0.00			89.74	±	4.83
	Total	382.25			337.68	±	4.80	378.76			358.77	±	5.98
	Balance (%)				88.34	±	1.26				94.72	±	1.58
Oxygen (mg O/d)	COD	1442.17	±	11.75	206.63	±	4.33	1429.03	±	11.53	175.88	±	4.05
	$NO_3^- + NO_2^-$	198.20	±	0.47	6.03	±	0.24	196.39	±	0.46	8.00	±	0.21
	Dissolved O_2	75.90			4.87	±	0.09	75.21			8.02	±	0.32
	Dissolved CO_2	0.00			917.55	±	5.77	0.00			843.32	±	8.50
	Gaseous O_2	0.00			3.46	±	0.49	0.00			6.94	±	2.04
	Gaseous CO_2	0.00			22.80	±	1.11	0.00			25.54	±	1.88
	Total	1716.27	±	12.22	1161.33	±	12.03	1700.63	±	11.99	1067.71	±	17.00
	Balance (%)				67.67	±	0.70				62.78	±	1.00
Carbon (mg C/d)	COD	1081.63	±	8.81	154.97	±	3.25	1071.77	±	8.65	131.91	±	3.04
	Dissolved CH_4	0.00			114.18	±	0.45	0.00			118.36	±	0.54
	Dissolved CO_2	0.00			344.08	±	2.16	0.00			316.25	±	3.19
	Gaseous CH_4	0.00			51.64	±	1.58	0.00			65.25	±	2.20
	Gaseous CO_2	0.00			8.55	±	0.41	0.00			9.58	±	0.71
	Total	1081.63			673.42	±	7.85	1071.77			641.35	±	9.67
	Balance (%)				62.26	±	0.73				59.84	±	0.90

Lastly, the balance for carbon is the least complete, with 62.26 % and 59.84 % accounted for in R1 and R2, respectively. Importantly, the dissolved portion of CO_2 alone contributes 32 % and 30 % of the balances. The unitless Henry's Law constant for CO_2 at 21 °C is 1.09, making it the most soluble gas. As such, the low biogas production rate combined with the comparatively high effluent rate may explain why ~97 % of the CO_2 was washed out, instead of appearing in the biogas. Yoo et al. (2012) came to the same conclusion in their SAF-MBR that reported a similarly small CO_2 fraction of the biogas.

There are four possible causes for this gap in the carbon balance. Firstly, some loss in translation from not taking accurate measurements of Total Organic Carbon (TOC) or VFAs in the effluents. Secondly, alkalinity consumption, as slight acidification was observed despite the inclusion of sodium bicarbonate as a pH buffer. Thirdly, biomass production, although early measurements of SS were negligible. Finally, the possibility that the degree of CH_4 supersaturation is higher than the 1.44 used in the calculations, as that value was calculated from final SAF-MBR effluents that had been passed through a membrane (Yoo et al. 2012).

Although the mass balances for carbon and oxygen are incomplete, these results can still be used to calculate probable substrate cycling pathways by analysing the available data and applying stoichiometric formulae. Especially by assessing the nitrogen cycling pathways, as that balance was almost complete.

4.3 Nitrogen Transformations

4.3.1 Production of Ammonia

Calculated as the average NH_3 removed x the average effluent flow rate, the average production rates of NH_3 were 10.13 and 17.77 mg NH_3-N/d in R1 and R2, respectively. Given that all samples were filtered through 0.45 µm hydrophilic filters, the observed increase is unlikely to be due to erroneous inclusion of cellular biomass, and therefore must be a result of either N_2 fixation or DNRA. The former requires the nitrogenase enzyme complex, expression of which is suppressed in the presence of NH_3 due to the exorbitant energetic cost of the process - a total of 16 Adenosine TriPhosphate (ATP) (Reineke and Schlömann 2023). Hence, it is more likely that this increase can be attributed to DNRA.

In general, DNRA dominates over denitrification under NO_3^- limiting conditions (Pandey et al. 2020). Moreover, in a continuous chemostat study, it was shown that DNRA dominated over denitrification at a COD/NO_3^--N ratio of 7.7, using acetate as the COD source (van den Berg et al. 2015). The COD/NO_3^--N ratio in this experiment was 50.19, owing to the very low NO_3^- concentration. This strongly indicates that DNRA is indeed active.

4.3.2 Production of Di-Nitrogen Gas

Calcualted as the sum of the average NO_3^--N and NO_2^--N removed x the average effluent flow rate, the oxidised inorganic-N removal rates were 56.78 and 56.65 mg N/d from R1 and R2, respectively. Removing the NH_3 production rates from these figures, 46.65 and 38.88 mg N/d was left available to, ostensibly, be transformed into N_2 gas. This is summarised in Table 11.

Table 11: Summary of performance - nitrogen

	mg N/d		% NO_3^-+NO_2^- removal	
	R1	R2	R1	R2
NO_3^- + NO_2^- removal rate	56.78	56.65		
NH_3 production rate	10.13	17.77	17.84	31.37
N removal from effluent	46.65	38.88		
N_2 influent (dissolved atmospheric)	126.72	125.56		
N_2 effluent (gaseous + dissolved)	128.00	142.79		
N_2 production rate	1.28	17.23	2.26	30.41
Unaccounted	44.57	19.99	78.49	35.29

Unlike CO_2 and CH_4, atmospheric properties meant that the influent contained dissolved atmospheric N_2. As described by Yoo et al. (2012), some of this atmospheric N_2 was likely stripped from the aqueous phase into the gaseous phase due to the significant decrease in the partial pressure in the headspace. Moreover, the unitless Henry's law constant for N_2 at 21 °C is 60.79, making it the least soluble gas. This might partially explain the observed oscillations in the biogas composition prior to stabilisation, as the partial pressure of N_2 (and O_2) fluctuated trying to reach equilibrium. Accounting for the slight difference in influent flow rates, it was calculated that 126.72 and 125.56 mg atmospheric N_2-N/d was introduced into R1 and R2, respectively. From both the dissolved and gaseous effluents during steady-state, the amount of N_2 leaving the AFBRs was 128.00 and 142.79 mg N_2-N/d. Therefore, the total increases were 1.28 and 17.23 mg N_2-N/d, as summarised in Table 11.

Subtracting the NH_3 and N_2 production rates from the NO_3^- + NO_2^- removal rates, it can be shown that, in total, 44.57 and 19.99 mg N/d was unaccounted for from R1 and R2, respectively. Presumably, these quantities can be attributed to a small amount of assimilation to biomass, NO and/or N_2O production, or errors in the calculations of dissolved N_2. While some N_2 was successfully produced, the production of NO and/or N_2O indicate that the conventional denitrification pathway was active but incomplete.

4.3.3 Stoichiometry of Denitrifying Nitrate Transformations

While the production of NH_3 quantifiably establishes the amount of N channelled through DNRA, the division of substrate between conventional denitrification and NOD is not clear. The greatest indicators are the gaps in the mass balance, a reasonable portion of which can be assumed to be N_2O from incomplete conventional denitrification, and the production of O_2, which indicates NOD. In order to gain further insight as to which N-cycling pathways are active, stoichiometric formulae developed in collaboration with Tri Yulianti (a fellow PhD student in Dr. Lee's group who is continuing to work on the AFBRs from this experiment) were applied. On the assumption that the majority of denitrifying bacteria in the AFBRs were heterotrophs, stoichiometry was calculated using both glucose and acetate as the primary carbon and e^- sources. Full details of these stoichiometric formula are provided in Appendix A2.

Equation 21 describes the overall transformation of NO_3^- to N_2 via conventional denitrification using glucose as the organic C source and Equation 22 describes the same transformation using acetate. Equation 23 describes the overall transformation of NO_3^- to N_2 and O_2 via NOD using glucose and Equation 24 describes the same transformation using acetate. Formulae are derived from those in Table 35 in subsection A2.6, adjusted to per mole NO_3^-. From the formulae themselves, it can be deduced that the conventional denitrification pathways have around double the demand for organic-C, as well as producing greater quantities of biomass ($C_5H_7O_2N$) per mole of NO_3^-. Of course, the NH_4^+ consumption implies that rates of DNRA are higher than assessed from the mass balance. However, since SS was not measured, this unfortunately cannot be further quantified.

$$NO_3^- + 0.570C_6H_{12}O_6 + 0.434HCO_3^- + 0.434NH_4^+ + 1.000H^+ \rightarrow$$
$$0.434C_5H_7O_2N + 1.684CO_2 + 0.500N_2 + 3.487H_2O \quad (21)$$

$$NO_3^- + 1.323CH_3COO^- + 0.419CO_2 + 0.279NH_4^+ + 1.000H^+ \rightarrow$$
$$0.279C_5H_7O_2N + 0.625CO_2 + 1.044HCO_3^- + 0.500N_2 + 1.544H_2O \quad (22)$$

$$NO_3^- + 0.337C_6H_{12}O_6 + 0.254HCO_3^- + 0.254NH_4^+ + 1.000H^+ \rightarrow$$
$$0.254C_5H_7O_2N + 1.004CO_2 + 0.500N_2 + 2.267H_2O + 0.500O_2 \quad (23)$$

$$NO_3^- + 0.782CH_3COO^- + 0.244CO_2 + 0.163NH_4^+ + 1.000H^+ \rightarrow$$
$$0.163C_5H_7O_2N + 0.375CO_2 + 0.619HCO_3^- + 0.500N_2 + 1.119H_2O + 0.500O_2 \quad (24)$$

Applying the complete NO_3^- and NO_2^- quantities that should have been transformed to N_2 (46.65 and 38.88 mg N/d from Table 11, equivalent to 3.33 and 2.78 mM N/d from R1 and R2, respectively), the stoichiometric results are shown in Table 12. A value of 1.07 g COD/g org-C, calculated using Equation 14 in the methodology subsubsection 3.4.2, was used to calculate the COD equivalents. By applying the maximum potential NO_3^- that could be transformed via these pathways, these results provide a guideline for the analysis of carbon and oxygen cycling, discussed in the subsequent subsections.

Table 12: Substrate consumption and production from nitrate transformation stoichiometry

		Denitrification		NOD	
	mg/d	R1	R2	R1	R2
Glycolytic	Glucose consumption	341.98	285.00	202.03	168.36
	COD equivalent	364.78	304.00	215.49	179.59
	NH_4^+-N consumption	20.26	16.88	11.86	9.88
	CO_2 production	246.93	205.79	147.23	122.70
	O_2 production			53.32	44.43
Acetotrophic	Acetate consumption	260.08	216.74	153.77	128.15
	COD equivalent	277.42	231.19	164.03	136.69
	NH_4^+-N consumption	13.02	10.85	7.60	6.33
	CO_2 production	91.64	76.37	54.98	45.82
	O_2 production			53.32	44.43

4.4 Carbon Transformations

4.4.1 Methane Yield

Calculated as the sum of the average gaseous CH_4 x the average biogas flow rate and the dissolved concentration of CH_4 x the average effluent flow rate, the total CH_4 production rates were 221.09 and 244.82 mg CH_4/d (equivalent to 13.82 and 15.30 mM CH_4/d) from R1 and R2, respectively. This equates to CH_4 yields of 0.13 and 0.15 l CH_4/g $COD_{removed}$, respectively. However, 68.86 % and 64.46 % of this was lost in the effluents. These results are summarised in Table 13. Using the standard conversion of 1 mol CH_4 = 64 g COD (Heidrich et al. 2011), it was calculated that 884.38 and 979.26 mg COD/d was directed to methanogenesis in R1 and R2, respectively, equivalent to 35.84 % and 38.71 % of the average COD removed from each reactor. This indicates that the majority of the COD was directed towards other microbial processes besides methanogenesis.

Comparing again to the study by Kwon et al. (2022), the CH_4 yields during 16 h and 8 h HRT operation

Table 13: Summary of performance - methane

	unit	R1	R2
Gaseous CH_4	mg/d	68.86	87.00
Dissolved CH_4	mg/d	152.24	157.82
Total CH_4	mg/d	221.09	244.82
	mM/d	13.82	15.30
Dissolved	%	68.86	64.46
Yield	l CH_4/g $COD_{removed}$	0.13	0.15

are shown in Figure 32. During the initial 16 h HRT phase, the reactor with coated PVDF beads produced significantly greater methane yields than its uncoated media counterpart, reaching 0.3 and 0.15 l CH_4/g $COD_{removed}$, respectively. Nevertheless, the biogas composition for both was ~50 % CH_4. As the HRT was decreased, the performed from the uncoated media improved, up to 0.23 l CH_4/g $COD_{removed}$. In both cases, the yields were greater than in the AFBRs operated in this experiment.

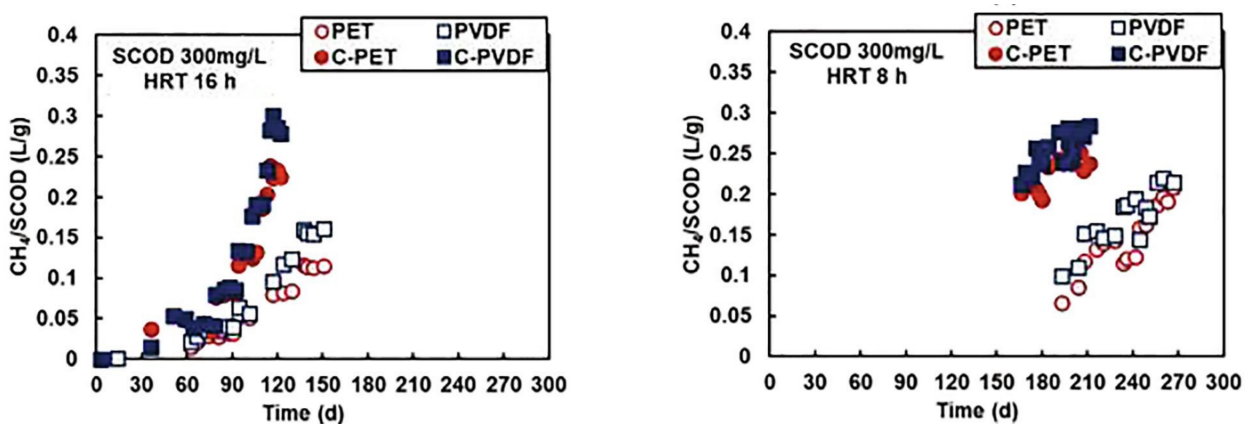


Figure 32: Methane yields from anaerobic fluidised-bed membrane bioreactors using coated and uncoated PVDF beads. Yields when operated at hydraulic retention times of: (a) 16 hours; (b) 8 hours. *Images reproduced with permission from the copyright holder (see Table 40 in Appendix A5).*

There are a handfull of potential causes for the decreased CH_4 yield in this experiment. It is likely that the submerged membranes provided additional protection from dissolved CH_4 loss as well as enabling greater advection, and thereby transference to the headspace. In addition, the use of simpler organic carbon (acetate) to supply COD may have provided greater stimulation/less competition to syntrophs supporting the methanogenic community. Finally, since e^- competitors, such as NO_3^-, NO_2^-, and sulphate, were not included in the synthetic feed, there was less opportunity for inhibition of methanogenesis.

On the other hand, compared to the SAF-MBR operated by Yoo et al. (2012), the CH_4 portion of the

biogas was significantly greater in this experiment. The very low HRTs employed, reduced COD removal, and presence of sulphates in the primary effluent used as feed are likely the primary causes for the reduced presence of CH_4 in their biogas. However, even with the membranes in the second stage, 63 % of the CH_4 generated was lost in the effluent. This suggests that the results in this experiment may be more representative of larger scale application.

4.4.2 Carbon Dioxide Yield and Sources

Calculated as the sum of the average gaseous CO_2 x the average biogas flow rate and the dissolved concentration of CO_2 x the average effluent flow rate, the total CO_2 production rates were 1292.98 and 1194.69 mg CO_2/d (equivalent to 29.39 and 27.15 mM CO_2/d) from R1 and R2, respectively. These results are summarised in Table 14.

Table 14: Summary of performance - carbon dioxide

	unit	R1	R2
Gaseous CO_2	mg/d	31.35	35.11
Dissolved CO_2	mg/d	1261.63	1159.57
Total CO_2	mg/d	1292.98	1194.69
	mM/d	29.39	27.15
Dissolved	%	97.58	97.06

As stated, the average COD removal rates were 2467.85 and 2529.46 mg $COD_{removed}$/d from R1 and R2, respectively, 35.84 % and 38.71 % of which was directed towards methanogenesis. During methanogenesis, it is conventionally assumed that each mole of glucose can be transformed into 3 moles each of CH_4 and CO_2 as described in Equation 25. However, in this experiment, for every mole of CH_4 produced per day, there were 2.13 and 1.77 M CO_2/d produced in R1 and R2, respectively. Ergo, at least 684.97 and 521.44 mg CO_2/d was produced by non-methanogenic processes.

$$C_6H_{12}O_6 \rightarrow 3CH_4 + 3CO_2 \tag{25}$$

This result is not unusual, as there are many more microbial metabolic processes that produce CO_2 than there are for CH_4. Referring to the results from the stoichiometry of NO_3^- denitrification shown in Table 12, the glycolytic conventional denitrification pathway initially seems the most likely, as it produces the most CO_2 and consumes the most COD. However, it isn't enough to close the gap between the CO_2 balance and the stoichiometry, meaning that there would still need to be alternative sources of CO_2. Furthermore, it does not produce O_2. Hence, the glycolytic NOD pathway stands out as the next best contender, as it

produces more CO_2 per mole of NO_3^- by a substantial margin.

4.5 Oxygen Transformations

Just as for N_2, dissolved atmospheric O_2 is introduced to the AFBRs via the influent, calculated as 75.90 and 75.21 mg atmospheric O_2-O/d into R1 and R2, respectively. However, unlike N_2, O_2 is highly reactive and far more soluble (unitless Henry's law constant of 32.67 at 21 °C), meaning it has fewer opportunities to escape out into the headspace, despite the drop in partial pressure. Between the gaseous and dissolved portions, the effluent O_2 masses were 8.32 and 14.96 mg O/d, equivalent to 10.96 % and 19.89 % of the influent atmospheric O_2 into R1 and R2, respectively.

Referring to the results in Table 12, these values are less than the amount produced via the NOD pathways according to the stoichiometry. However, the fact that O_2 was detectable in the biogas at all is remarkable, as conventional wisdom would anticipate that it would have been entirely consumed by suffocating aerobic species or fast-acting facultative species. As previously described, the two largest contributors to the effluent oxygen balances were dissolved CO_2 and extant COD. In an aerobic environment, the terminal output from many microbes is CO_2, hence the abundance of CO_2 relative to CH_4 (despite losing the majority in the effluents) suggests that aerobic metabolism may have been sustainable within the AFBRs.

4.6 Discussion

4.6.1 Review of Overall Performance

At their relatively low HRTs and operated at ambient temperature, both of the AFBRs operated in this experiment produced excellent results as treatment options for low-strength wastewater. The high COD removal efficiency and CH_4 rich biogas reaffirm the high-rate performance of the AFBR technology. Simultaneously, the observation of a distinct alternating pattern in the biogas composition between N_2-O_2 and CH_4-CO_2 until the late stage of operation led to remarkable findings. Analysis of these chemical results alone does not provide a clear and certain reason for the alternating pattern in the biogas composition prior to stabilisation, especially since the pH and COD removals were consistent throughout. Moreover, even once all readings had stabilised, the incomplete mass balances are an unfortunate hindrance to establishing the possible and/or probable substrate cycling pathways.

Nevertheless, from the available data, one of the most intriguing factors is that the presence of small amounts of O_2 did not appear to severly inhibit methanogenesis in either of the AFBRs. Indeed, despite a

higher proportion of O_2 in the biogas from R2, the CH_4 production and yield were slightly higher. Studies of micro-aeration for AD have been ongoing for some time, demonstrating that small amounts of O_2 can stimulate methanogenesis by accelerating hydrolysis, scavenging hydrogen sulphide, and affecting microbial diversity (Chen et al. 2020b). In the same vein, it has been shown that some methanogenic archaea in the orders of Methanocellales, Methanomicrobiales, and Methanosarcinales are oxygen tolerant (Fu et al. 2023).

Ultimately, even if more holistic measurements - such as SS, TOC, and dissolved gases - had been taken, there are significant pathways for nutrient cycling that cannot be captured simply by measuring the compounds in and out. The meta-omic analysis, discussed over the subsequent chapters, will provide a clearer picture of the unmeasurable microbial activity that produced the observed performance results, as the presence of relevant microbes and genes will be revealed.

4.6.2 Impact of Semi-Conductive Coating on Performance

Based on previous studies that established the performance improvements in a range of anaerobic wastewater treatment technologies when conductive media was introduced, it was expected that the same trend would be observed in this experiment. That the performance of R1, with the PANI-coated PVDF beads, would reap the benefits of microbe-electrode DIET to produce superior results, particularly for methanogenesis. Even though PANI is a semi-conductor, previous studies demonstrated that it can stimulate accelerated start-up times and sustained higher CH_4 yields (Kwon and Kim 2022; Kwon et al. 2022). However, against key metrics during both acclimatisation and long-term operation, the performances of these AFBRs were highly similar. They achieved stabilisation for COD removal and biogas composition at the same time, and with marginal differences between their ultimate averages. Furthermore, total CH_4 production and CH_4 yield were slightly higher in R2.

Hence, from the results of this part of the experiment, there is no evidence to suggest that the PANI coating imparted a substantial advantage to C-cycling performance of R1, as would be expected based on prior studies. While this could be associated with the slight increase in HRT in R2, it could also indicate that electroactive microbes in the biofilm - particularly methanogens - were not able to form microbe-electrode connections with the PANI in R1, although the reasons for this are unclear. With that being said, microbe-microbe DIET could still be active in the R1 and R2 biofilms.

Nevertheless, there were some significant differences in other measurements associated with N cycling: the biogas production rate, which was 20.77 % higher in R2; the portion of O_2 in the biogas, which was 66.34 % higher in R2; and the NH_3 production rate, which was 75.46 % higher in R2. The sole metric in which R1 exceeded R2 was total inorganic-N removal, which was 8.08 % higher, owing mostly to the fact

that the NH_3 increase was smaller. Even so, once atmospheric N_2 had been taken into account, the N_2 production rate was 12.45 times greater in R2 (see Table 11). This result shows that the PANI coating did have an impact on the metabolism of inorganic-N substrates.

4.6.3 Nitrogen Cycling

Assessment of inorganic-N unveiled almost complete removal of NO_3^- and NO_2^- in both R1 and R2, as would be expected in an anaerobic denitrifying environment. The contribution of N_2 to almost a third of the biogas initially drew attention, however, upon reviewing the sources in and out, it became clear that atmospheric N_2 was in large part responsible, although there was some increase. Beyond that, two key factors indicate that conventional denitrification is not the only active N-cycling process: the increase in the concentration of NH_3 in the effluents, associated with DNRA; and the production of O_2, associated with oxygenic denitrification.

In R2, it appears that the fate of oxidised inorganic-N was evenly split between DNRA, complete and incomplete denitrification (see % NO_3^-+NO_2^- removal in Table 11). Whereas in R1, incomplete denitrification was more dominant that either DNRA or complete denitrification. In both reactors, DNRA was stimulated by the high COD/NO_3^--N ratio, as per previous studies (van den Berg et al. 2015). The greater NH_3 production rate in R2 implies that the PANI coating didn't provide an advantage to DNRA. Indeed, the only mentions of DNRA in relation to DIET were in combination with anammox (Wang et al. 2022a). Given the abundance of organic-C and the successful removal of NO_3^-, this seems unlikely. On the other hand, denitrification was able to outcompete DNRA for substrate in R1, indicating that DIET-mediated denitrification was stimulated.

Regarding denitrification, determining the split between the conventional and oxygenic pathways is challenging, given the incomplete mass balances. The greater unaccounted N from R1 combined with the smaller O_2 production indicates that, while NOD was active, incomplete denitrification dominated, resulting in higher quantities of unmeasured N_2O. Meanwhile, the more complete N mass balance in R2 and the greater production of O_2 indicates that NOD was more able to compete in the non-conductive environment. While the PANI coating wasn't overly beneficial or detrimental to C cycling, the absence of PANI improved the N-cycling performance in R2, determined on the basis of reduced losses as N_2O. A potential reason for this is the fact that NOD is an e^- neutral reaction (Zhu et al. 2017), and therefore wouldn't derive benefit from an external e^- sink. On the other hand, research has established that conventional denitrification does benefit from DIET metabolism.

Hence, in this experiment, exoelectrogenic denitrifiers may have utilised the e^- sink of the PANI coating

in R1, giving them a competitive advantage for substrate over both NOD and DNRA. However, because PANI only a semi-conductor, the metabolic advantage wasn't enough to complete the process, resulting in accumulation of N_2O and NO.

5 Microbial Community Profiling

5.1 Community Overview

Following library preparation, there were 65.3 to 98.4 million paired-end clean reads per sample, all between 75-150 bp with average quality per read scores of 36 (minimum score of 30). The total number of reads from each stage of the library prep can be seen in Table 36 in subsection A3.1. As stated in subsubsection 3.5.1, the first round of meta-omic samples, denoted P1, was taken on day 193 of operation, roughly a month before the biogas composition stabilised on day 228. The second round, denoted P2, was taken on day 290, the same day as all final samples from this experiment.

The final clean read counts are summarised in Table 15, along with the assembly-free bacterial and archaeal community proportions from assembly-free taxonomic profiling. A full breakdown of the Kaiju read classifications - including those below 0.01 % relative abundance, unclassified reads, and others - is summarised in Table 37 in subsection A3.2. From the kingdom-level classifications, the taxonomic profiles of dominant (above 1 % relative abundance) bacterial and archaeal genera are shown in Figures 33 and 34, respectively. Unlike amplicon sequencing techniques - such as 16S rRNA gene sequencing - full meta-genomic datasets include an overwhelming amount of non-marker genes, hence the majority of the material is not included in assembly-free taxonomic profiling. However, this technique provides a vital overview of the community, including low abundance species and reads that may not make it into the MAGs downstream (Quince et al. 2017).

Table 15: Clean read counts and classifications of bacteria and archaea from assembly-free taxonomic profiling

Point	Sample name	Clean read counts	Archaea	Bacteria
P1	GR1P1biofilm	65,368,820	0.72%	31.46%
	GR1P1bulk	67,109,668	1.58%	49.05%
	GR2P1biofilm	84,745,329	0.69%	37.84%
	GR2P1bulk	85,283,850	1.23%	35.05%
P2	GR1P2biofilm	73,565,305	0.40%	16.51%
	GR1P2bulk	54,644,278	0.23%	33.07%
	GR2P2biofilm	98,448,451	1.21%	20.79%
	GR2P2bulk	70,332,632	0.32%	35.29%

At the P1 sampling stage, the read counts between the biofilms and bulks were reasonably even within each reactor, suggesting that biofilm adherence to the media was not especially strong yet. However, by the P2 stage, the biofilms had considerably higher total read counts and higher proportions of archaea than

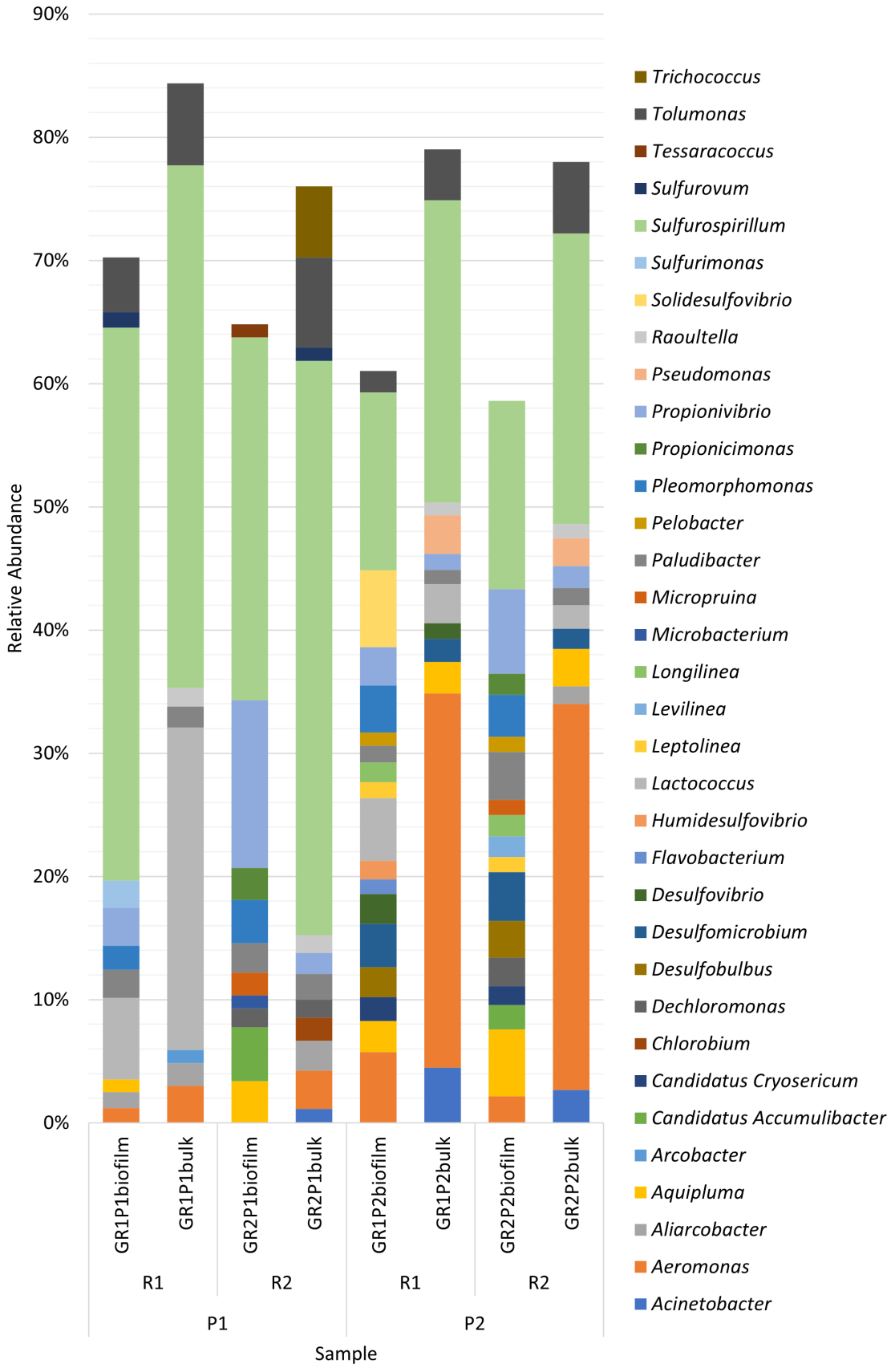


Figure 33: Assembly-free taxonomic profiles - dominant bacterial genera

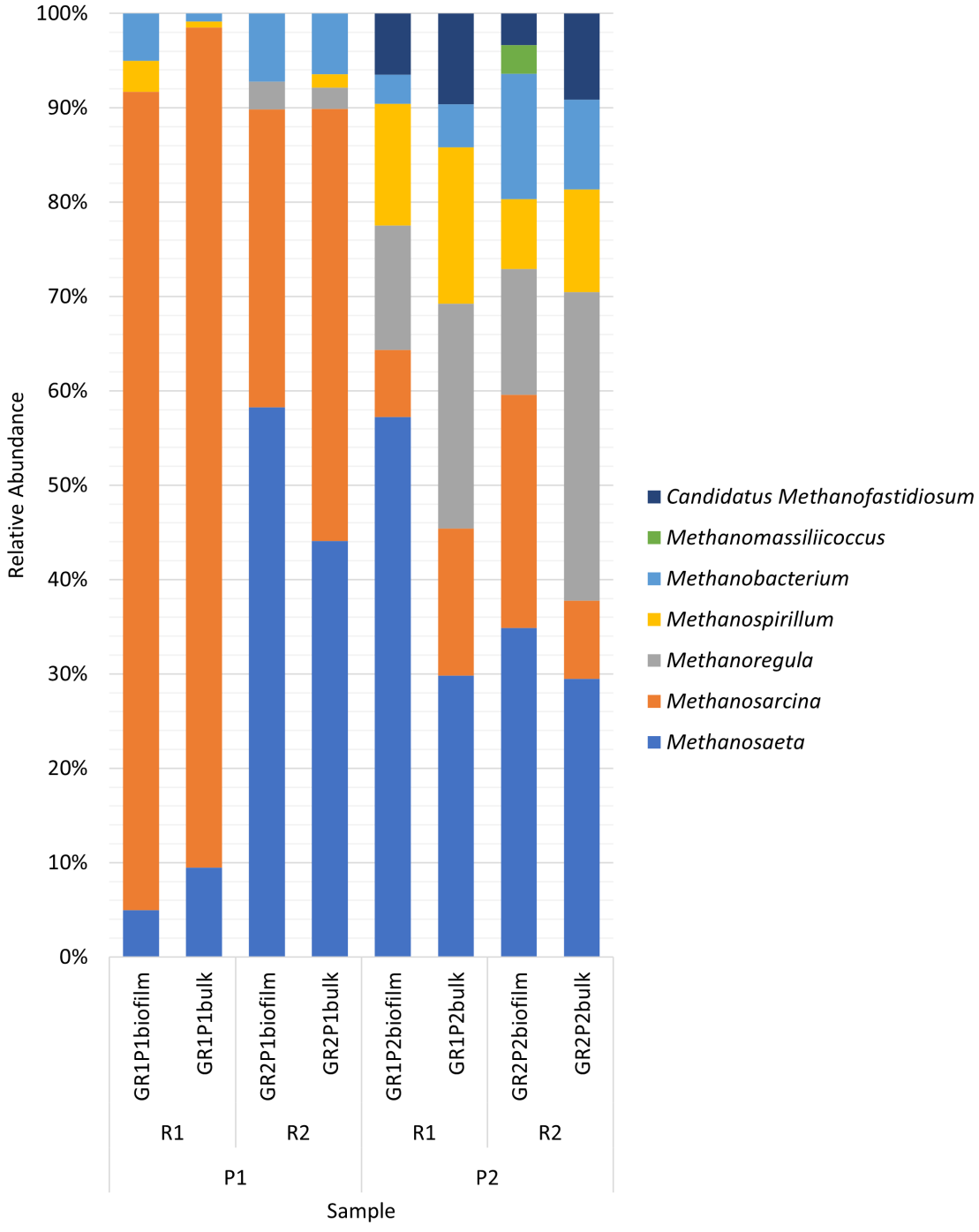


Figure 34: Assembly-free taxonomic profiles - archaeal genera

their respective bulks, indicating that biofilms had finally been successfully formed. Additionally, the read counts in R1 were lower than those in R2 at both sampling points, which indicates successful substrate cycling amongst fewer microbes therein.

5.2 Bacterial Taxonomic Profile

5.2.1 Dominant Genera

The most surprising factor revealed by the bacterial profile was the intense dominance by two genera: *Aeromonas* and *Sulfurospirillum*. At their highest relative abundances, *Aeromonas* accounted for 31.33 % in GR2P2bulk and *Sulfurospirillum* 46.62 % in GR2P1bulk. They are easily distinguished as the large orange and pale green bars, respectively, in Figure 33.

According to Bergey's Manual of Systematics of Archaea and Bacteria, species in the *Aeromonas* genus are facultatively anaerobic chemoorganotrophs, capable of oxidation and fermentation of glucose. Metabolism of glucose, as well as other carbohydrates, is accompanied by acid production and often gas production. They are typically oxidase positive (contain *c*-cyts) and catalase positive (release O_2 from hydrogen peroxide). Additionally, they are capable of denitratation (reducing NO_3^- to NO_2^-) and produce a variety of exoenzymes (Martin-Carnahan and Joseph 2015). The Manual describes species in the *Sulfurospirillum* genus as microaerobic (up to 4 % oxygen) sulphur reducers that benefit from metabolic versatility. They do not oxidise or ferment carbohydrates, rather they oxidise succinate, fumarate, malate, lactate, or pyruvate, but not acetate. Oxidising agents that *Sulfurospirillum* species can use include NO_3^-, thiosulfate, fumarate, selenate, and arsenate. They are also oxidase positive (Stolz et al. 2015).

At both sampling points, the relative abundance of *Aeromonas* was higher in the bulk samples compared to their respective biofilms. Nevertheless, at P2, the relative abundances had increased by a factor greater than 4 in the biofilms and greater than 10 in the bulk solutions, becoming the most dominant genera in the latter. As facultative anaerobes, their preference for the bulk is likely to be associated with the presence of O_2 in the headspace, which is more easily accessible whilst suspended. On the other hand, *Sulfurospirillum* was by far the most dominant genera in almost all samples, except where they were outcompeted by *Aeromonas* in the bulk samples at P2. This is despite a decrease in their relative abundances by roughly half between P1 and P2. Similarly to *Aeromonas*, *Sulfurospirillum* also showed a preference for the bulk solution, presumably for the same reason, as the DO was not high enough to be inhibitory.

5.2.2 Syntrophs

The taxonomic profiles of the syntroph populations are shown in Figure 35, which include a total of 7 syntrophic genera: *Longilinea*, *Syntrophus*, *Syntrophorhabdus*, *Syntrophobacter*, *Smithella*, *Pelotomaculum*, and *Clostridium*. The relative abundance of syntrophs was low across every sample, and extremely so at the P1 sampling stage, reaching a maximum of 0.86 % in GR1P1biofilm. Nevertheless, at the P2 sampling stage, the syntrophic community had substantially increased: more tripled in R1 (up to 3.36 % in GR1P2biofilm and 0.99 % in GR1P2 bulk, up from 0.26 %); doubled in GR2P2bulk (1.18 %, up from 0.58 %); and by a factor of 13 in GR2P2biofilm (4.49 %, up from 0.33 %).

The only individual syntrophic genus to surpass 1 % relative abundance was *Longilinea* in the P2 biofilms, representing 1.63 % and 1.76 % in GR1P2biofilm and GR2P2biofilm, respectively. This genus is a facultative syntroph that specialises in sucrose/yeast extract utilisation in co-operation with hydrogenotrophic methanogens (Fujimoto et al. 2019; Yamada et al. 2007). Hence, the inclusion of yeast extract in the synthetic feed is the best explanation for the dominance of this particular genus.

5.2.3 Exoelectrogens

The story is quite similar for the exoelectrogenic community. The confirmed exoelectrogenic genera found in this study were: *Geobacter*, *Shewanella*, *Desulfovibrio*, *Rhodoferax*, and *Syntrophus* (Akram et al. 2024). In addition, *Desulfobulbus*, *Pseudomonas*, *Thauera*, and *Thiobacillus* are also being included as part of this community, the taxonomic profiles of which are shown in Figure 36.

At the P1 sampling point, the communities as a whole showed a distinct preference for the biofilms in both reactors, with relative abundances of 2.03 % and 2.71 % in GR1P1biofilm and GR2P1biofilm, respectively, compared to 0.99 % and 1.99 % in GR1P1bulk and GR2P1bulk, respectively. This indicates that exoelectrogens were beginning to find their advantages on the media. However, there were no dominant individual exoelectrogenic genera in any of the samples. By the P2 sampling point, just like for the syntrophic community, there had also been a significant increase in the relative abundance of the exoelectrogenic community. In R2, the community had roughly doubled its proportion, with 6.22 % and 3.46 % in GR2P2biofilm and GR2P2bulk, respectively. While in GR1P2biofilm it had tripled, up to 6.42 %, and in GR1P2bulk it had increased by a factor of more than 5, up to 5.34 %.

Within the biofilms at P2, the most abundant exoelectrogens were *Desulfobulbus* (2.42 % and 2.96 % in GR1P2biofilm and GR2P2biofilm, respectively) and *Desulfovibrio* (2.43 % and 0.85 % in GR1P2biofilm and GR2P2biofilm, respectively). Ordinarily, these two genera both utilise sulphur compounds as their terminal

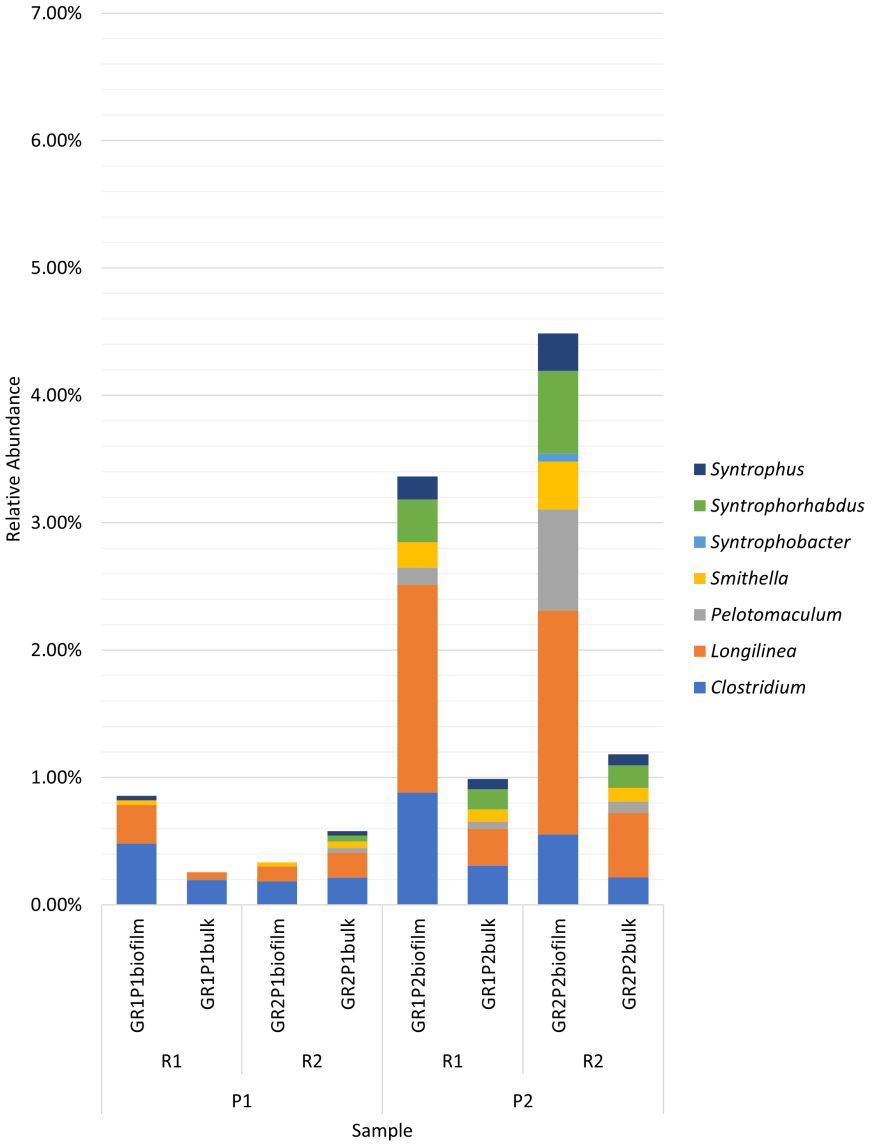


Figure 35: Assembly-free taxonomic profiles - syntrophic bacterial genera

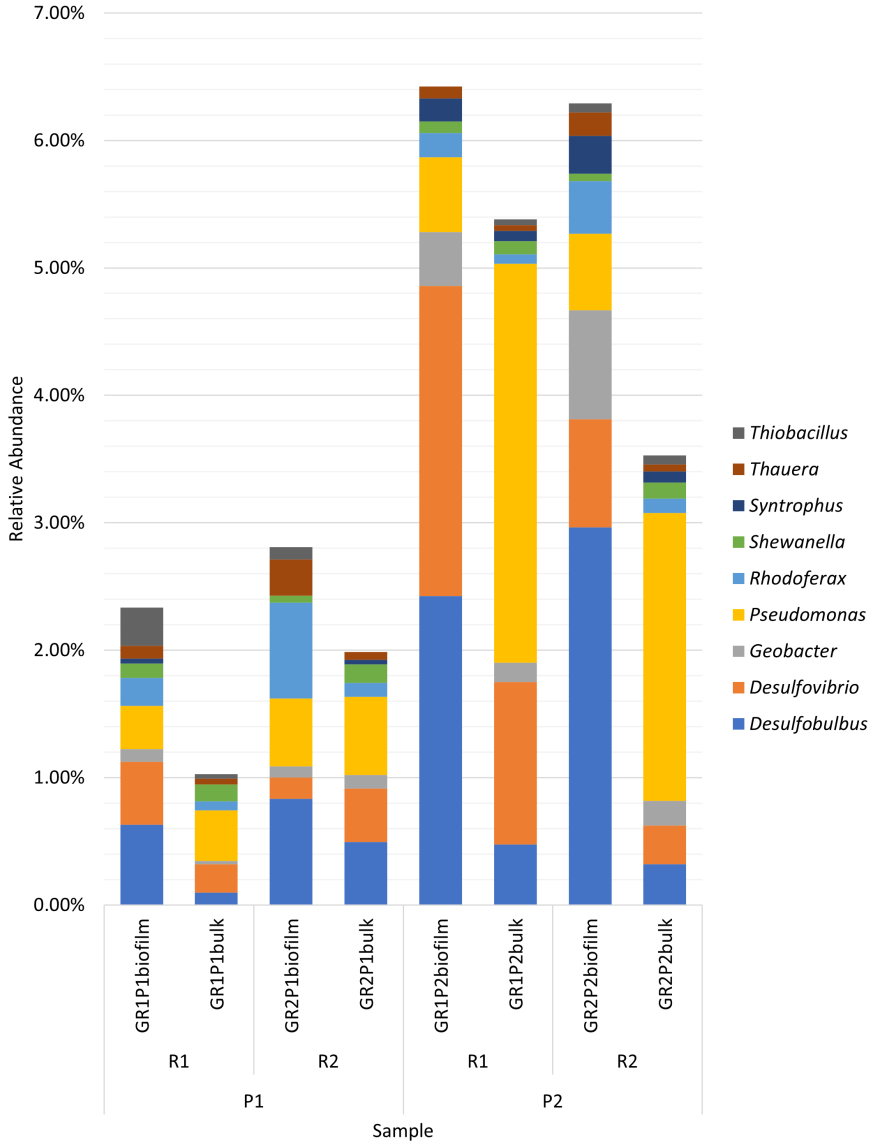


Figure 36: Assembly-free taxonomic profiles - electroactive bacterial genera

e^- acceptors (Galushko and Kuever 2019a,b). Since sulphur was not provided as part of the synthetic feed solution, this is a good indication that these genera were indeed taking advantage of the alternative e^- sharing mechanisms available in an electroactive biofilm.

5.2.4 Methanotrophs

Given the presence of O_2, it is possible that methanotrophs could have proliferated and reduced the CH_4 yields. Indeed, 8 methanotrophic genera were identified. However, as individuals, they were all well below the significance threshold. Furthermore, their largest collective relative abundance was 1.08 % in GR1P1biofilm and the second largest was 0.39 % in GR2P1biofilm. Hence, they are not considered to have a strong influence on the microbial community or reactor performance.

5.2.5 Nitrogen Cycling Community

Not including *Aeromonas* and *Sulfurospirillum*, there were 23 N-cycling genera identified, whose taxonomic profiles are shown in Figure 37. Given the mixture of NH_3, NO_3^-, and low DO, microbes associated with different parts of the N-cycle were present.

There was a small presence of 3 NH_3 oxidising genera, amounting to no more than 0.57 % combined relative abundance in any sample. These were the AOB *Nitrosomonas* and *Nitrosospira*, and the comammox genus *Nitrospira*. There were no NOB, nor anammox bacteria. From this, is can be concluded that nitrification was far from significant. In addition, there were 4 "conventional" denitrifying genera, in the sense that none of them have been association with DIET, DNRA, or NOD. These were *Comamonas*, *Denitratisoma*, *Nitratiruptor*, and *Nitrosophilus*. The maximum relative abundance of this community was 0.25 % in GR1P1biofilm. Hence, none of these genera will be considered moving forwards, as they are well below significance thresholds. On the other hand, *Aeromonas* falls into this category, becoming the most significant "conventional" denitrifier.

Referring to the list of DNRA microbes in Table 5 (subsubsection 2.5.2), a total of 17 genera were found, of which, only *Desulfobulbus*, *Desulfovibrio*, *Pseudomonas*, and *Sulfurospirillum* surpassed 1 % relative abundance. It is worth noting that among the other 13 low abundance microbes are the syntroph *Clostridium* and the electroactive genera *Shewanella* and *Thiobacillus*, both of which have been associated with DIET-assisted denitrification (He et al. 2023; Kato et al. 2012). However, even combined, these three didn't surpass the significance threshold in any sample.

Bergey's manual describes *Pseudomonas* species as aerobes, but some can also use NO_3^- as the terminal

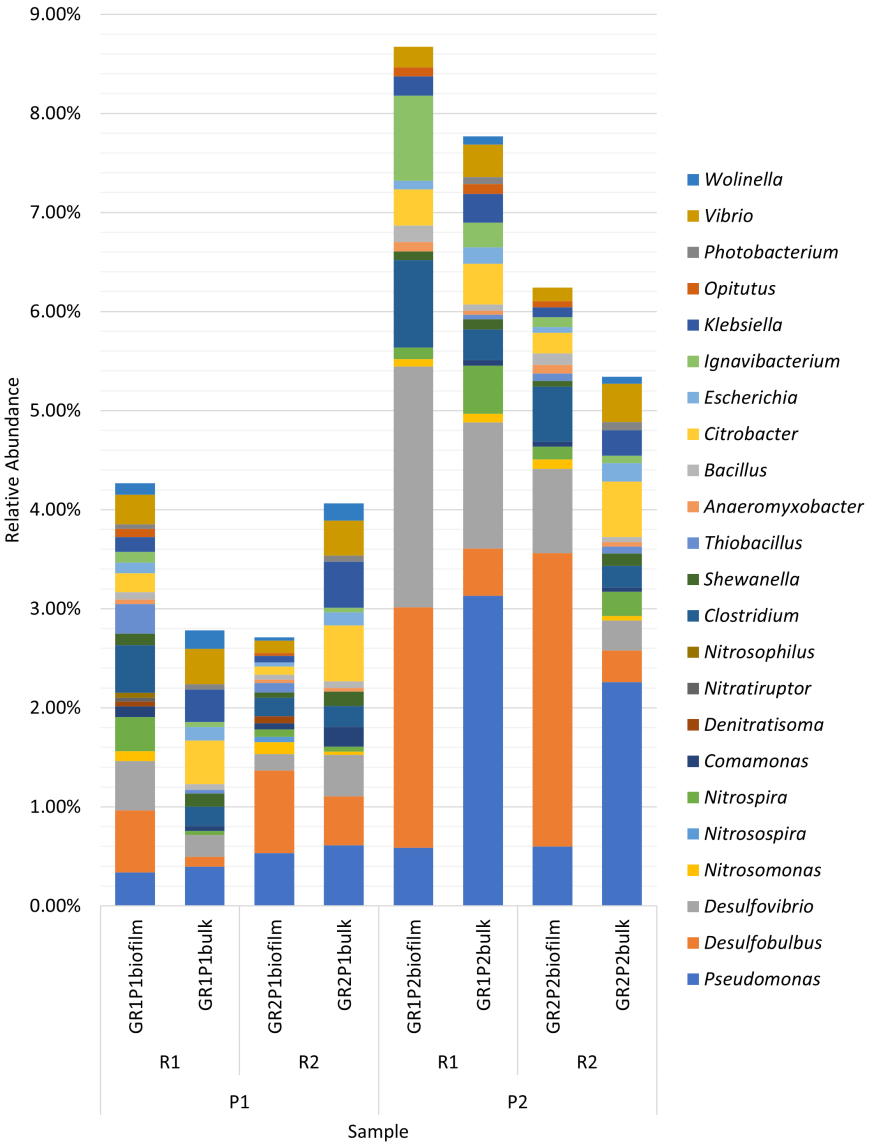


Figure 37: Assembly-free taxonomic profiles - nitrogen cycling bacterial genera

e^- acceptor, hence their association with denitrification (Palleroni 2015). Furthermore, various species have been associated with NOD (Lichtenberg et al. 2021), electroactive denitrification (He et al. 2023), and DNRA (Huang et al. 2023). Whereas the DIET capacity of *Desulfobulbus* and *Desulfovibrio* has not previously been associated with their N-cycling capabilities, much less with any DNRA capacity. Hence, *Pseudomonas*, *Aeromonas*, and *Sulfurospirillum* are the most significant NO_3^- reducers in this study.

Similar to the development of *Aeromonas*, the relative abundances of *Pseudomonas* increased in the bulk samples between P1 and P2. Ultimately, these 3 genera represented 58.07 % and 57.17 % in GR1P2bulk and GR2P2bulk, respectively, over double their presence in the biofilms (20.78 % and 18.04 % in GR1P2biofilm and GR2P2biofilm, respectively). As they are all, at minimum, oxygen tolerant, this suggests that their metabolism is better supported by the presence of O_2 than by any e^- sharing capacities of the biofilms or PANI.

5.3 Archaeal Taxonomic Profile

5.3.1 Electrotrophs

As shown in Figure 34, the archaeal community is comprised entirely of methanogens in all samples. Dominance of acetotrophic species in AD is common, hence the observation that the Methanosarcinales - *Methanosaeta* and *Methanosarcina* - are the most dominant genera. Of course, as well as being acetotrophic, these two genera are the methanogens most often associated with DIET. Although other genera, such as *Methanoregula* and *Methanospirillum*, have also been implicated in previous DIET studies (Valero et al. 2018), there is only one other confirmed electrotrophic methanogen, *M. electrotrophus* (Akram et al. 2024). While the *Methanobacterium* genus may be present, at this level, it cannot be confirmed if the electrotrophic species is present. Hence, this analysis will consider only the *Methanosaeta* and *Methanosarcina*, both of which have multiple confirmed electrotrophic species.

At the P1 sampling point, both reactors were dominated by these two, representing 91.71 %, 98.53 %, 89.86 % and 89.89 % in GR1P1biofilm, GR1P1bulk, GR2P1biofilm, and GR2P1bulk, respectively. However, by the P2 sampling point, the methanogenic community had substantially diversified. As a result, the relative abundance of the electrotrophic methanogens reduced by roughly a third in the biofilms (down to 64.36 % and 59.60 % in GR1P2biofilm and GR2P2biofilm, respectively) and more than half in the bulk solutions (down to 45.39 % and 37.74 % in GR1P2bulk and GR2P2 bulk, respectively).

Another interesting change to note is the distribution between the two electrotrophs. In GR1P1biofilm and GR1P1bulk, *Methanosarcina* commanded almost the entire archaeal community, whereas in GR2P1bulk, the balance was more even, and *Methanosaeta* pulled ahead in GR2P1biofilm. However, by the P2 sampling point, *Methanosaeta* outweighed *Methanosarcina* in every sample, most of all in GR1P2biofilm. This result is interesting, as there is no clear reason for either genera to have such distinct advantages at either stage.

5.3.2 Oxygen Tolerant Methanogens

In this study, 4 genera within methanogenic orders that have previously been shown to be oxygen tolerant were detected (Fu et al. 2023). These were *Methanosaeta* and *Methanosarcina* from the Methanosarcinales order and *Methanoregula* and *Methanospirillum* from the Methanomicrobiales order. Although the dominance of the Methanosarcinales had somewhat diminished by the P2 sampling point, the emergence of the Methanomicrobiales makes it clear that oxygen tolerance is a desirable characteristic for methanogens in the AFBRs. Collectively, they represent 90.42 %, 85.81 %, 80.34 %, and 81.37 % of the archaeal communities in GR1P2biofilm, GR1P2bulk, GR2P2biofilm, and GR2P2bulk, respectively.

5.4 Diversity Analysis

5.4.1 Alpha Diversity

The whole community richness and the diversity indices are shown in Table 16. As this analysis is based on the assembly-free taxonomic profile, the richness includes counts of both bacterial and archaeal genera that had relative abundances above the significance threshold of 0.01 %, as set in Kaiju.

Table 16: Alpha diversity analysis of bacteria and archaea

Point	Sample	Richness	Shannon	Simpson	Inv Simpson
P1	GR1P1biofilm	238	3.12	0.203	4.94
	GR1P1bulk	150	2.30	0.240	4.16
	GR2P1biofilm	331	3.68	0.109	9.19
	GR2P1bulk	209	2.93	0.215	4.65
P2	GR1P2biofilm	234	4.25	0.038	26.50
	GR1P2bulk	193	2.92	0.158	6.32
	GR2P2biofilm	273	4.34	0.037	27.10
	GR2P2bulk	198	2.95	0.159	6.31

The Shannon index sums the contributions of each genus to overall diversity, capturing both richness and evenness by weighting each genus' abundance. Values typically range from 0 to around 4.5, depending on the community size, where a value of 0 indicates a community with only one genus (no diversity) and higher values indicate greater diversity, with both high richness and evenness. As the Shannon index offers more balance between richness and evenness, a graphical representation of those results is shown in Figure 38.

Simpson's index measures the probability that two individuals randomly selected from a sample will belong to the same genus, producing values between 0 (infinite diversity) and 1 (no diversity, genera picked will always be the same). Unlike the Shannon Index, Simpson's Index gives more weight to abundant genera and is less sensitive to rare genera. The inverted Simpson's index is a transformation of Simpson's index that provides a more intuitive interpretation of diversity, ranging from 1 to a theoretical maximum equal to the number of genera in the sample when all genera are equally abundant. This version is included because it aligns more intuitively: as the diversity increases, the index also increases.

Across both sampling points and reactors, the biofilms were consistently more diverse than their associated bulk samples. This is to be expected, as biofilms offer protection from washout and therefore slower growing microbes can establish themselves. In addition, the biofilm communities in R1 were less

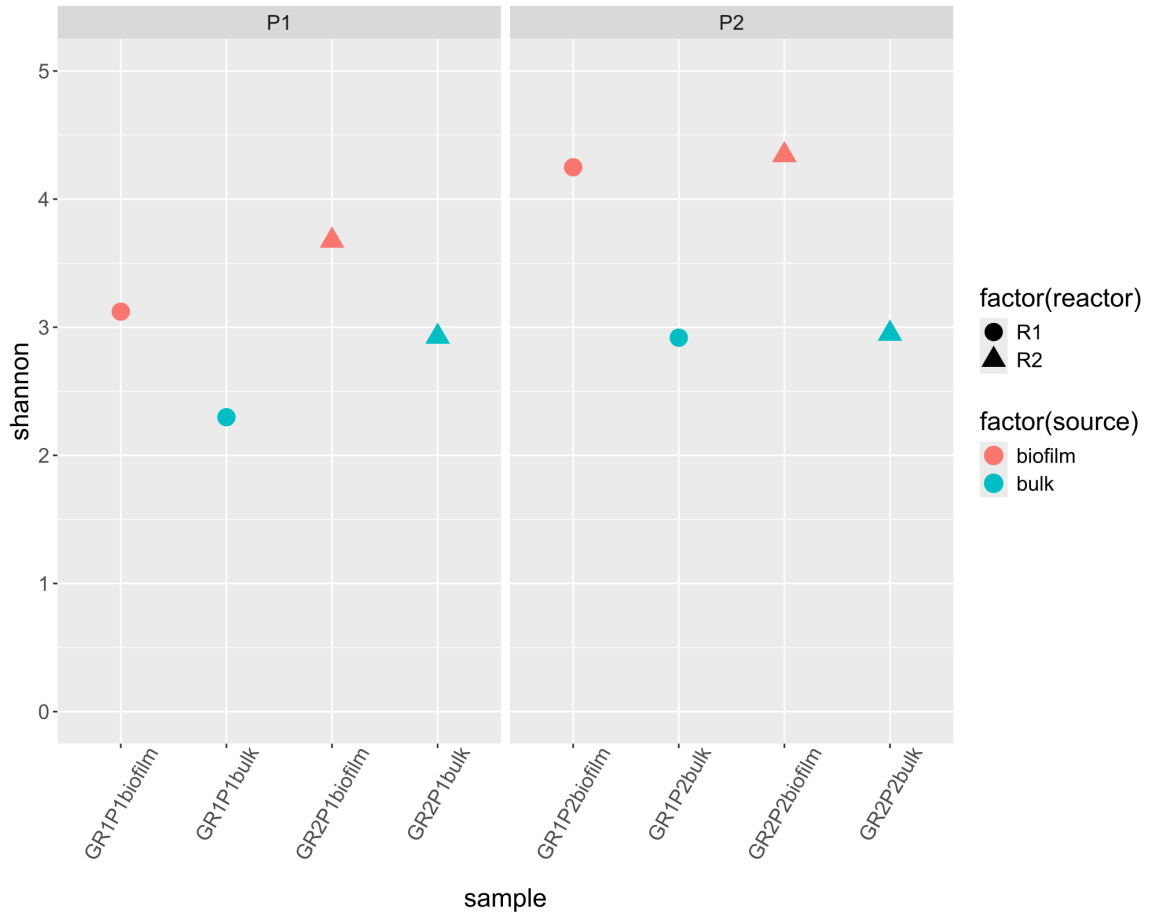


Figure 38: Shannon diversity index. Red shapes are biofilm samples, blue shapes are bulk samples. Circles are R1 samples, triangles are R2 samples.

rich and less diverse at both sampling points than those in R2. Similar to the lower read counts in R1, this further suggests efficient substrate cycling among fewer specialised microbes. Furthermore, despite decreasing richness in the biofilms between the sampling points, both the Shannon and Simpson's indices showed increased diversity. This is most likely to be associated with the re-balancing of *Sulfurospirillum* in those samples, which improved the evenness. Hence the significant impact on the Simpson indices, which are sensitive to dominant species. This increase in diversity demonstrates that the biofilms had indeed matured between the P1 and P2 sampling points, with more complex microbial interactions being supported.

On the other hand, while the bulk communities had some changes to the richness between the sampling points, the Shannon diversity index remained the same in GR2P2bulk, whereas GR1P2bulk seemed to "catch up". In the bulk samples, rather than a increase in evenness, the singular dominance by *Sulfurospirillum* was replaced by the co-dominance of *Aeromonas* and *Sulfurospirillum*. This explains why the Shannon index remained largely unchanged, whereas the Simpson indices indicated slightly improved diversity. Lastly, the lower alpha diversity in bulks suggests that the bulk solutions did not foster complex metabolic syntrophy, rather microbes with individually advantageous capacities were favoured.

5.4.2 Beta Diversity

The results of the Bray-Curtis dissimilarity analysis are shown in Table 17, and the 2D summary of the PCoA is shown in Figure 39. The exact coordinates are shown in Table 38 in subsubsection A3.3.2. Bray-Curtis dissimilarity analysis quantifies the compositional dissimilarity between two samples based on the abundance and presence/absence of genera. It ranges from 0 (samples are identical) to 1 (samples have no species in common). PCoA then condenses the dissimilarity values of multiple samples into n dimensions that capture up to 100 % of the dissimilarity. In this case, the 2 dimensional analysis captures 74.75 % of the sample-to-sample dissimilarity, shown on the X and Y axis of Figure 39.

Table 17: Bray-Curtis dissimilarity analysis of bacteria and archaea

	GR1P1 biofilm	GR1P1 bulk	GR1P2 biofilm	GR1P2 bulk	GR2P1 biofilm	GR2P1 bulk	GR2P2 biofilm
GR1P1bulk	0.3721						
GR1P2biofilm	0.4721	0.7020					
GR1P2bulk	0.4441	0.5873	0.4653				
GR2P1biofilm	0.3538	0.5161	0.6262	0.5878			
GR2P1bulk	0.3161	0.2432	0.6008	0.5317	0.4174		
GR2P2biofilm	0.4859	0.6828	0.3765	0.5409	0.4036	0.5247	
GR2P2bulk	0.4139	0.5256	0.5175	0.1869	0.5422	0.4460	0.5230

The clustering of samples from biofilms/bulks at each sampling point into almost perfectly separate quadrants highlights that those microbial communities are significantly distinct in their community structure. While the distribution of biofilm and bulk samples across the X-axis (with the exception of GR2P1bulk) underscores the distinction of those communities, the distribution of the P1 and P2 samples across the Y-axis has an important implication: that there was a significant shift in the microbial community between the period of unstable biogas composition, and the stabilised phase.

Of the samples from the P1 stage, GR2P1biofilm is the most isolated, falling much higher on the Y-axis. This is likely to be associated with the relative abundances of *Sulfurospirillum*, as this sample had 29.46 %, whereas the others had 42.40 - 46.62 %. With such large community proportions, this would impact the sample-to-sample dissimilarity. This also explains the particular closeness of GR2P1bulk and GR1P1biofilm, which would otherwise be considered highly unusual, as by reasonable estimations, these two should be highly dissimilar. However, by the P2 sampling point, with the increased community evenness, the bulk samples had become far more distinct from the biofilm samples.

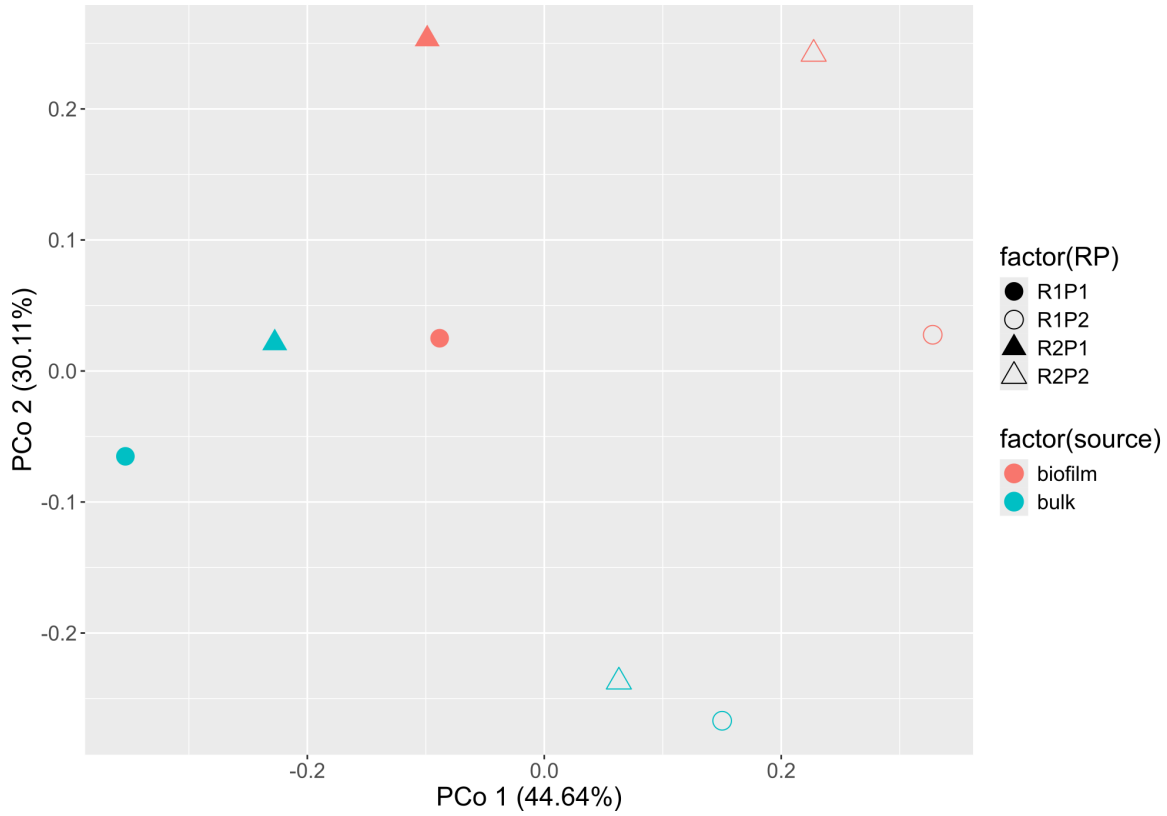


Figure 39: Principal coordinates analysis of Bray-Curtis dissimilarity. Red shapes are biofilm samples, blue shapes are bulk samples. Circles are R1 samples, triangles are R2 samples. Filled shapes are P1 samples, hollow shapes are P2 samples.

Interestingly, the bulk samples across R1 and R2 at each sampling point had the 2 lowest dissimilarity scores: GR1P1bulk-GR2P1bulk scored 0.2432; GR1P2bulk-GR2P2bulk scored 0.1869. On the other hand, the biofilm samples had larger dissimilarity scores: GR1P1biofilm-GR2P1biofilm scored 0.3538; GR1P2biofilm-GR2P2biofilm scored 0.3765. This shows that, at both sampling points, access to the PANI coating had a significant impact on the structure of the microbial community.

5.5 Community Comparison to Other Anaerobic Wastewater Treatment Reactors

5.5.1 Anaerobic Fluidised-bed Membrane BioReactors

The most relevant comparison to make is to the AFMBRs operated by Kwon et al. (2022). Their AFMBRs were fed an acetate and propionate based synthetic feed that contained NH_4^+ but not NO_3^-. The omic samples were taken on day 263 and day 420 for coated and uncoated media reactors, respectively. The taxonomic profiles of dominant bacterial and archaeal genera obtained from 16S rRNA gene sequencing are shown in Figures 40a and 40b, respectively.

As mentioned in subsubsection 2.2.5, the archaeal profiles from AFMBRs with PANI-coated media

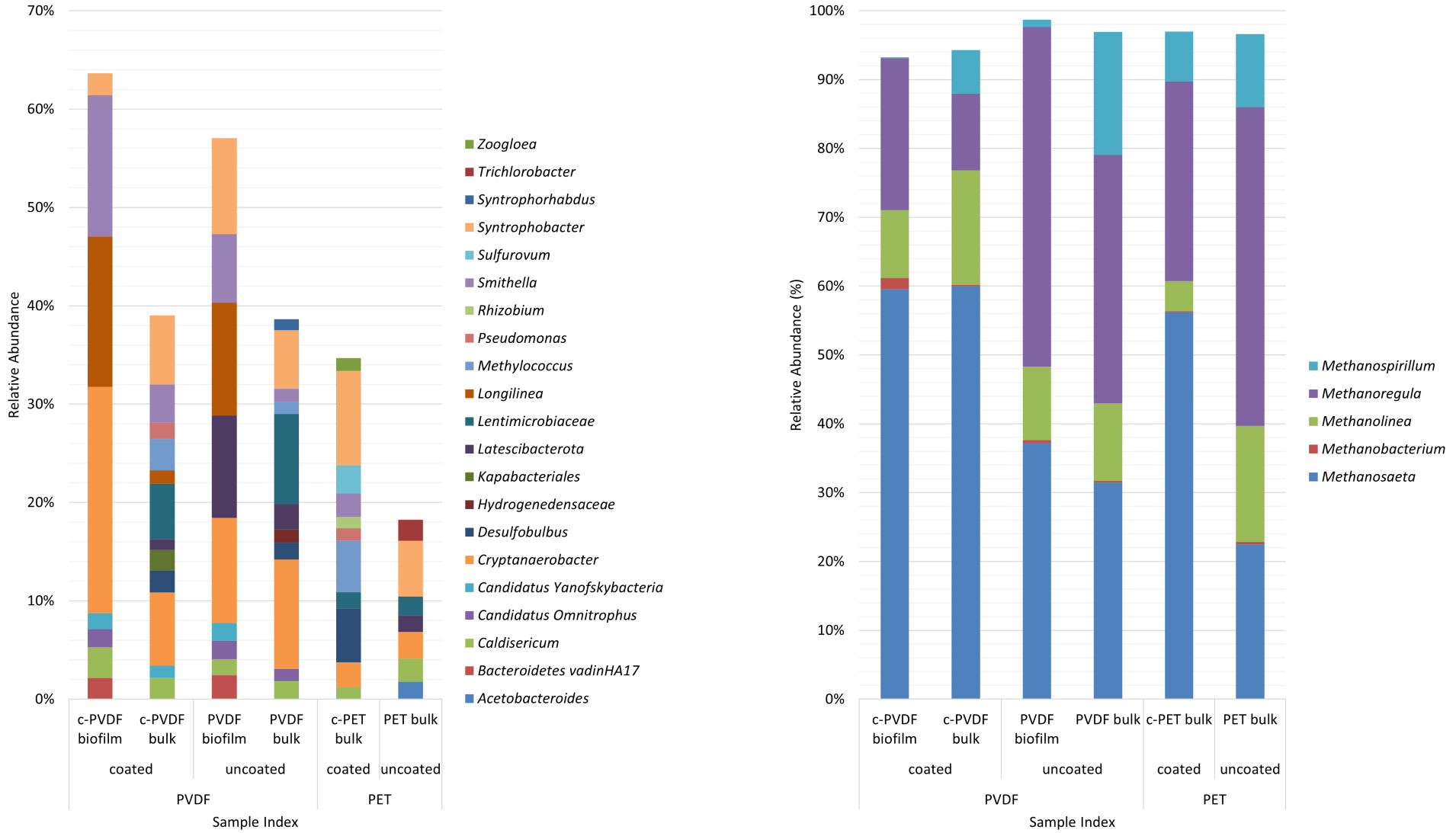


Figure 40: Taxonomic profiles from anaerobic fluidised-bed membrane bioreactors with uncoated and polyaniline coated media, adapted from Kwon et al. (2022): (a) dominant bacterial genera; (b) dominant archaeal genera

had high relative abundances of *Methanosaeta*, whereas the abundances were much lower in the reactors without. This indicated that those microbes are able to take advantage of the semi-conductor to utilise DIET and proliferate. Interestingly, there was a complete absence of *Methanosarcina* from all samples. Regarding the bacterial profile, the use of more simple organic-C molecules to form the COD of the synthetic wastewater meant that many of the hydrolytic genera present in this experiment were absent from those AFMBRs. Hence, the relative abundances of syntrophs were much higher therein, reaching 31.96 % and 28.71 % as a collective community in the coated and uncoated PVDF biofilms, respectively. *Longilinea* again was the most abundant syntroph, representing 15.29 % and 11.47 % in the same biofilm samples.

The only significantly abundant exoelectrogens were *Desulfobulbus* and *Pseudomonas*, reaching 3.90 %, 2.04 %, 6.71 %, and 1.09 % in the bulks from coated PVDF, uncoated PVDF, coated PET, and uncoated PET, respectively. However, their relative abundances in the biofilm samples were no more than 0.04 %. These two are also the only significant N-cycling genera in the AFMBRs, and no NH_3-oxidising genera were found. Due to the absence of known exoelectrogenic genera in the biofilms, attention turned to *Cryptoanaerobacter* which had relative abundances of 23.01 % and 10.69 % in the coated and uncoated PVDF biofilms, respectively. As the dominant genus, it was ultimately proposed that *Cryptoanaerobacter* could be a novel exoelectrogen cooperating with *Methanosaeta*.

The comparison to these AFMBRs reinforces the notion that a PANI coating doesn't foster a strong presence of "typical" exoelectrogens, such as *Geobacter* or *Shewanella*. However, the larger presence of electrotrophic methanogens in PANI-coated biofilms, especially *Methanosaeta*, implies that it instead encourages electroactive syntrophic relationships with novel exoelectrogens that have not been previously reported. Exemplified by *Cryptoanaerobacter* and *Sulfurospirillum*. It also shows that the low NO_3^- dosing did encourage the presence of a greater diversity of N-cycling microbes.

5.5.2 Staged Anaerobic Fluidised-bed Membrane BioReactors

Unpublished 16S rRNA gene sequencing data from a pilot-scale SAF-MBR treating real wastewater on a domestic WWTP in Bucheon, South Korea was kindly shared with us by the team at Inha University, South Korea who manage and operate this reactor. The three samples in this comparison were taken on days 342, 436, and 555 of operation, and their taxonomic profiles of bacterial and archaeal genera are shown in Figures 41a and 41b, respectively. These reactors used GAC as the fluidised media in both stages.

As this reactor was treating real wastewater, containing a complex matrix of substrates, the microbial community is substantially more diverse, with greater opportunities for metabolically diverse microbes to

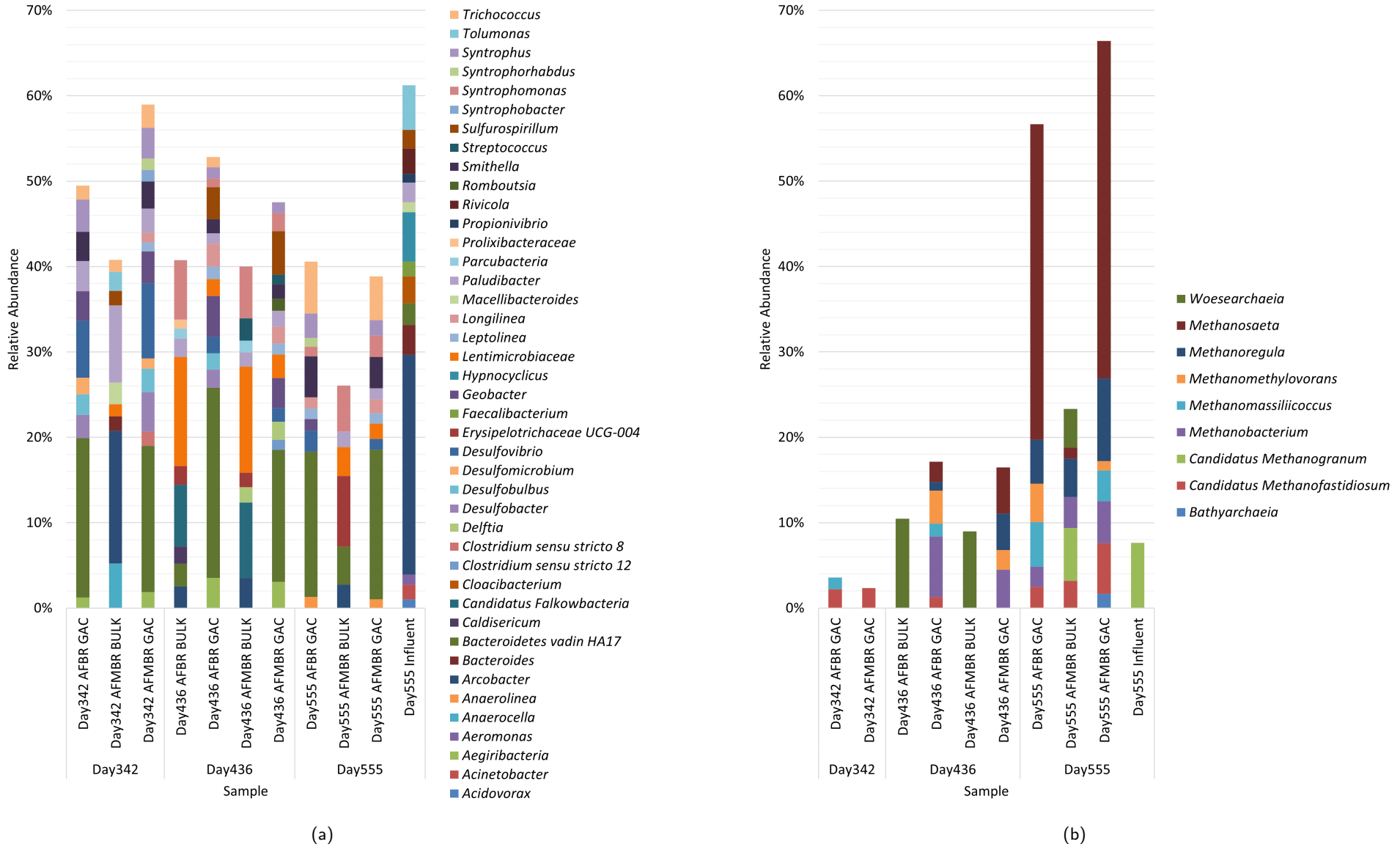


Figure 41: Taxonomic profiles from Inha staged anaerobic fluidised-bed membrane bioreactor: (a) dominant bacterial genera; (b) dominant archaeal genera

thrive. The archaeal communities in particular are much more diverse. However, this meant that the majority of that community was unclassified. Nevertheless, as operation continued, more recognisable methanogens began to dominate, *Methanosaeta* in particular, which reached 36.95 % and 39.55 % relative abundance in the AFBR and AFMBR biofilms, respectively, by day 555. This slow establishment of *Methanosaeta* when exposed to complex influents is accordant with the findings from the P1 and P2 samples in this experiment.

Naturally, as an anaerobic treatment technology, there are significant syntrophic communities, representing 9.13 % to 12.38 % in GAC biofilm samples, and 0.53 % to 7.81 % in bulk samples across all 3 sampling points. This demonstrates that the community as a whole preferred the media, presumably associated with the methanogens therein, classified or otherwise. The greater relative abundances of syntrophs compared to the AFBRs in this experiment is likely to be associated with the more diverse archaeal communities.

As a well studied conductor used to stimulate DIET in methanogenic environments, the relative abundance of exoelectrogens showed a surprising tendency. There were 10 electroactive genera found, the most significant of which were *Geobacter* and *Desulfovibrio*, which were most abundant in the GAC samples, as anticipated. However, across the three sampling points, the relative abundances of these exoelectrogens decreased. Meanwhile, there was a consistent presence of *Bacteroidetes vadin HA17*, also in the biofilms, 15.46 % to 22.29 %, compared to 2.67 % to 4.45 % in the bulks. Hence, it is hypothesised that this could also be a novel exoelectrogen. Overall, this also highlights the different electroactive communities that can be stimulated using GAC instead of PANI, with more typically-associated genera having a stronger presence.

Lastly, the community of N-cycling genera is well below significance thresholds. The highest collective relative abundance in the bacterial community was 0.29 %, and 0.04 % in the archaeal community. Hence, despite the uncontrolled influent, it can be concluded that N-cycling is not a substantial process in this reactor, emphasising the impact of NO_3^- dosing on the microbial community structure of the AFBRs in this experiment.

5.5.3 Anaerobic Digesters

Following successful sequencing, the number of clean reads obtained for each of the 3 ADs sampled is shown in Table 18. Just like for the SAF-MBR previously described, these reactors received highly complex influent, containing organic-C far more complex than acetate or glucose. In addition, each of these plants used a different heated pre-treatment before sludge digestion, which are also described in Table 18. The taxonomic profiles of dominant bacterial and archaeal genera are shown in Figures 42a and 42b, respectively. Although not collected at the same time, the sample for WWTP-1 was collected from the same WWTP

as the seed sludge for the AFBRs.

Table 18: Clean read counts from anaerobic digester 16S rRNA sequencing. THP = thermal hydrolysis plant

	WWTP-1	WWTP-2	WWTP-3
Heat treatment	THP	None	Pasteurisation
Average sludge temp (°C)	160	36	58
Archaea	126,981	135,138	143,938
Bacteria	63,902	32,829	55,694

The archaeal communities in all of the ADs are overwhelmingly dominated by *Methanosaeta* and *Methanosarcina*, especially WWTP-1 and WWTP-3. However, the treatment of waste sludge as opposed to raw influent can be assumed to make a significant difference to the substrate matrix as well as the retention times. The highly concentrated feed and extended retention times may explain the simplified archaeal community in these ADs, which is more similar to the bench-scale AFMBRs from Kwon et al. (2022) and the AFBRs in this experiment than the pilot-scale SAF-MBR.

The relative abundances of the syntrophic communities were also similar to those obtained at the P2 sampling stage in this experiment - 4.68 %, 2.67 %, and 2.29 % in WWTP-1, WWTP-2, and WWTP-3, respectively. The individual syntrophs that surpassed the significance threshold were *Syntrophomonas* and *Clostridium sensu stricto 1* in WWTP-1 and WWTP-2. Besides the syntrophic community, very few of significant bacterial genera from the AFBRs were found in the ADs. There was no *Sulfurospirillum* in any sample and only a small amount of *Aeromonas*, below 0.1 % in WWTP-1 and WWTP-2. As for N cycling genera and exoelectrogens, the only significantly abundant genera found was *Pseudomonas*, which had a relative abundance of 12.61 % in WWTP-1 and 1.97 % in WWTP-2. As *Pseudomonas* has a very diverse metabolic capabilities, it could be acting as an exoelectrogen and/or denitrifier. However, the lack of other genera that are also associated with these processes makes this seem unlikely.

The comparison to these ADs treating sludge from real wastewater emphasises the unique processes that were stimulated in the AFBRs through the attached-growth technology and the NO_3^- dosing. The lack of exoelectrogenic bacteria despite the presence of electrotrophic methanogens highlights the impact of, not just attached-growth technologies, but the benefit of the PANI coating.

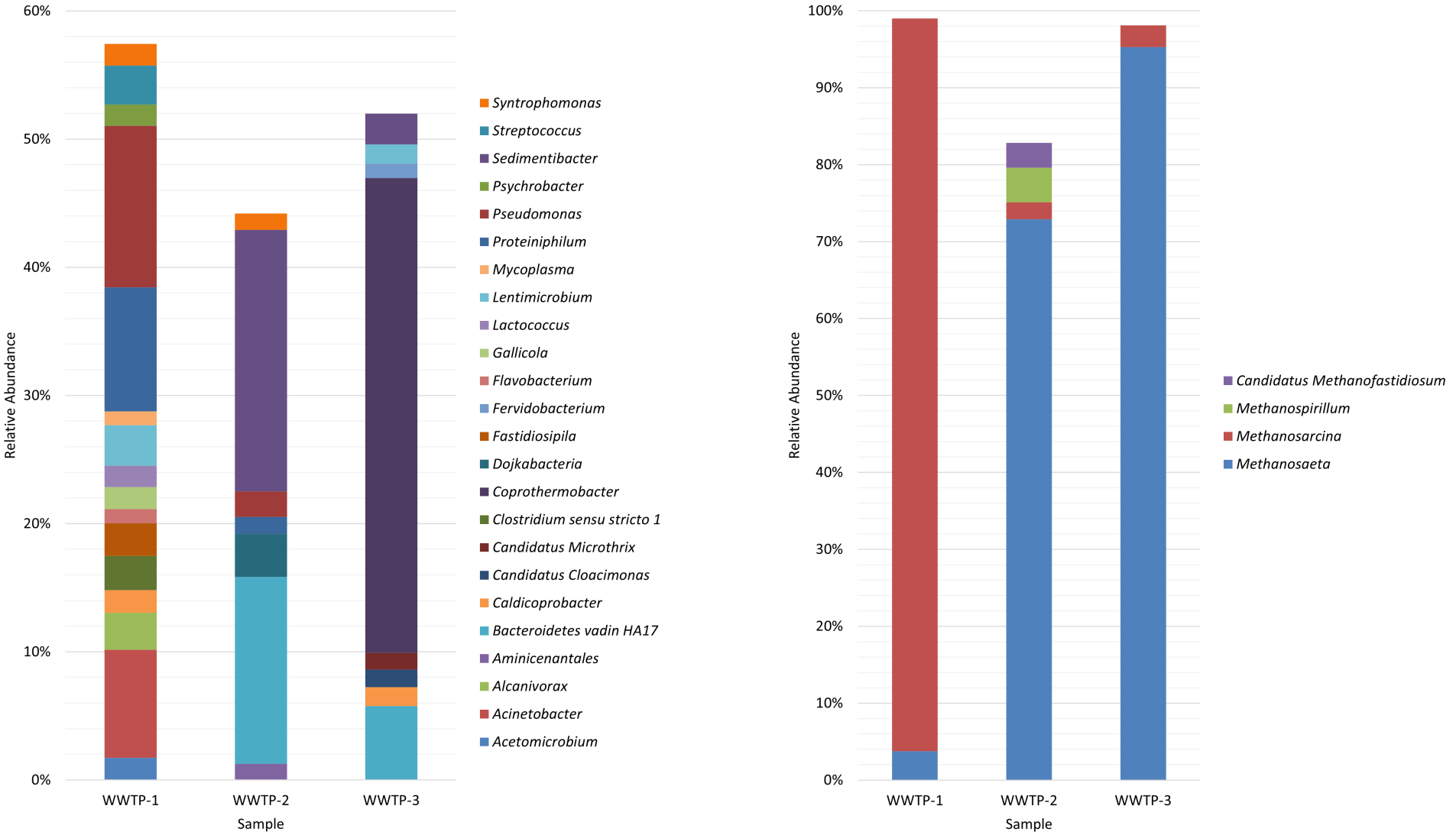


Figure 42: Taxonomic profiles from UK anaerobic digesters: (a) dominant bacterial genera; (b) dominant archaeal genera

5.6 Discussion

5.6.1 Changing Communities

The results from the P1 sampling stage certainly reflect the ongoing unstable biogas composition at that time. The similarity between the read counts and alpha diversity indices of the bulk and biofilm samples suggest that the biofilm was not yet fully adhered to the media. An idea that is reinforced by the closeness of all the P1 samples in the Bray-Curtis PCoA analysis. Moreover, the lower relative abundances of the syntrophic, exoelectrogenic, and N-cycling communities indicate that these functions were not yet strongly established.

Nevertheless, between the P1 and P2 sampling points, there were two important changes. Firstly, the biogas composition reached stabilisation, producing consistent portions of each component. Secondly, there was a measurable change in the composition of the microbial communities within the AFBRs, as confirmed by the Bray-Curtis dissimilarity analysis. This has a clear, significant implication: that the change in the biogas composition wasn't just due to equilibration of atmospheric-N_2 in the headspace. The greater distinction between the biofilm and bulk samples at P2 are discernable from the read counts and both the alpha and beta diversity indices, indicating that the biofilms had indeed matured and were successfully adhered. This is probably in large part responsible for the stabilisation of the performance data.

The large increase in the relative abundances of the syntrophs and exoelectrogens explains the stabilisation of the CH_4 component, as the firm establishment of these cooperative communities in the biofilms would support the methanogens also growing there. Meanwhile, the consistent presence of O_2 appears to have had two significant impacts: the diversification of the archaeal community, with increased relative abundances of oxygen tolerant methanogens; and the dramatic increase of *Aeromonas* relative abundance. The source of the consistent presence of O_2 can be linked with the increased N-cycling community, which, of course, stabilised the N_2 component of the biogas as well. With all of these other important communities increasing their presence, the relative abundance of *Sulfurospirillum* simply decreased with increased diversity. Nevertheless, it maintained its dominant status, signifying its importance in the microbial community.

5.6.2 Direct Interspecies Electron Transfer Community

Both the bacterial and archaeal communities suggest that DIET was active in both R1 and R2. The electrotrophic methanogens held the majority of the archaeal community in the biofilm samples, and exoelectrogenic bacterial genera were more relatively abundant than syntrophs at both sampling points. Hence, DIET-mediated methanogenesis can reasonably be anticipated. Evidence for the modality of DIET

- microbe-microbe or microbe-electrode - between the reactors was more complex.

The lower read counts, lower richness, and lower alpha diversity in R1 at both sampling points suggest that the PANI coating enabled effective substrate cycling amongst a more select group of microbes. However, analysis of the community structure at P1 suggests that the PANI coating did not provide an advantage to the electroactive community during acclimatisation. At the P1 stage, R1 had a lesser exoelectrogenic community and a greater syntrophic community than R2, suggesting that methanogenesis in R1 was more supported by conventional syntrophy than DIET.

With that being said, unlike the final results from the performance data, the results at P2 provide indications that DIET ultimately was enhanced in the presence of the PANI coating. Once at the stabilised phase, R1 did indeed have the greater exoelectrogenic community and lesser syntrophic community. This indicates that the PANI coating provided some advantage to the stabilised version of the electroactive community. The reason for this delayed development is unclear, however, similar to the changing taxonomic profile from the Inha SAF-MBR, this could simply be associated with the length of operation.

The two most likely genera to be fulfilling the role of exoelectrogens are *Desulfobulbus* and *Desulfovibrio*, as their usual terminal e^- acceptor (sulphur) was not available. While *Pseudomonas* has also been reported as electroactive, it was not significantly abundant in the biofilms, hence it is unlikely to be associated with DIET in this case. On the other hand, the fact that *Sulfurospirillum* was the single most dominant genus in every biofilm sample suggests that this genera may also have some DIET-capability, stimulated by the surrounding electroactive community. This would be in line with the proposals of other novel exoelectrogens, *Cryptanaerobacter* or *Bacteroidetes vadin HA17*, from the other AFBR-type reactors described in the previous subsection.

5.6.3 Nitrogen Cycling Community

As determined from the performance data, conventional denitrification was not the only N-cycling process in the AFBRs in this experiment. In R1, N-cycling is predominantly incomplete denitrification, with smaller contributions from DNRA and NOD. Whereas R2 had an almost even split between DNRA, complete and incomplete denitrification, plus higher rates of NOD. From the analysis in this chapter, the differences found between the microbial communities structures in the AFBRs and the three other relevant anaerobic reactors considered show that the community of N-cycling microbes is unique. Hence, it is clear that the low NO_3^- dose had a meaningful impact on the microbial community structure and therefore reactor performance.

The taxonomic profiles revealed that the three most significant genera producing these results are *Pseudomonas*, *Aeromonas*, and *Sulfurospirillum*, which had collective relative abundances of 58.07 % and 57.17 % in GR1P2bulk and GR2P2bulk, respectively. The dominance of the bulk communities indicates one of two things. Either, that the various denitrification processes were less competitive than DIET-assisted methanogenesis, which dominated the biofilm communities. Or, that the presence of O_2 was more advantageous to these genera than enhanced e^- sharing facilities.

Of these three, *Pseudomonas* has the most metabolic diversity, having been associated with denitrification, DNRA, and NOD. *Sulfurospirillum* has NO_3^--reducing capacity and has also been associated with DNRA. Moreover, although it is the most abundant genus in the biofilms, its relative abundances were higher in the bulks at the P2 sampling stage, suggesting that it may have a flexible metabolism. Meanwhile, *Aeromonas* has only been previously associated with denitratation. Since their metabolism remains unclear, their genome bins will be investigated in order to get a clearer understanding of their metabolic capabilities.

6 Genome Bin Interrogation

6.1 Metagenome Assembled Genomes

6.1.1 Results of Resolution

The first step of the resolution into MAGs process - contig assembly - produced contigs that followed normal patterns of individual and cumulative lengths, a summary of which can be seen in Table 39 in subsection A3.4. Subsequent alignment of the clean short reads to the contigs produced overall alignment rates above 90 % for all samples, showing that the majority of the reads were included in the contigs. Final resolution into MAGs resulted in 100 - 233 bins, accounting for a minimum of 68.57 % of the total community. A summary of the resolution process is shown in Table 19. The community composition differs from the relative abundances in the assembly-free taxonomic profile due to the different natures of these analytical approaches, and is therefore included to give an indication of weight only.

Table 19: Summary of metagenome resolution into reconstructed genome bins. C. = community

Point	Sample name	Overall alignment	Total bins	Archaea		Bacteria		unbinned
		(%)		C. (%)	bins	C. (%)	bins	C. (%)
P1	GR1P1biofilm	91.81	156	0.43	2	75.34	154	24.23
	GR1P1bulk	93.83	115	0.40	3	68.17	112	31.43
	GR2P1biofilm	94.94	100	0.17	2	87.38	98	12.45
	GR2P1bulk	94.02	183	0.19	3	77.19	180	22.62
P2	GR1P2biofilm	92.85	187	0.90	7	78.47	180	20.63
	GR1P2bulk	90.47	152	0.09	1	76.93	151	22.98
	GR2P2biofilm	92.23	233	3.01	16	74.47	217	22.52
	GR2P2bulk	92.27	148	0.15	1	78.88	147	20.97

6.1.2 Selection of Bins for Interrogation

Across all samples, there was a collective total of 112 bins for *Aeromonas*, *Sulfurospirillum*, and *Pseudomonas*. In order for a bin to be selected for interrogation, quality tolerances were set at completeness above 80 % and contamination below 20 %, the result of which was the ultimate selection of 14 high quality bins.

For *Aeromonas*, 19 of 20 bins were identified as *Aeromonas media*, 2 of which were high enough quality for selection, found in GR1P1biofilm and GR1P2biofilm. Unfortunately, the sole bin for *Aeromonas taiwanensis* was not high enough quality to be selected. For *Pseudomonas*, there were a total of 10 bins,

including 4 species: 7 *Pseudomonas putida* bins and 1 bin each for *Pseudomonas baetica*, *Pseudomonas argentinensis*, and *Pseudomonas chlororaphis*. Only *P. putida* had genome bins that were high enough quality: 1 in GR1P2bulk and 1 in GR2P2bulk. For *Sulfurospirillum*, there were a total of 82 bins, distributed over 9 species. Of those, 10 bins were high enough quality to be selected, encompassing 4 species: 2 *Sulfurospirillum arsenophilum* bins, 4 *Sulfurospirillum cavolei* bins, 2 *Sulfurospirillum* sp. JPD-1 bins, and 2 *Sulfurospirillum* sp. UCH001 bins. All but 2 of those bins were from biofilm samples.

These results, as well as the community proportion of those bins in their respective samples, is shown in Table 20. Sourcing *Aeromonas* and *Sulfurospirillum* bins from biofilm samples may seem incongruous with the assembly-free taxonomic profile, which clearly showed that these two genera were the most dominant in the bulks. However, by assessing multiple bins and the reference sequences of each species, the role of a species in the environment as a whole can be inferred. The reference genomes of these species were downloaded from the following NCBI links: A. media, P. putida, S. arsenophilum, S. cavolei, S. sp. JPD-1, and S. sp. UCH001.

Table 20: Genome bins for interrogation. Comp = completeness, Con = contamination, Comm = community

Point	Sample	Bin no.	Species	Comp (%)	Con (%)	Comm (%)
P1	GR1P1biofilm	135	*A. media*	92.95	0.88	0.10
	GR2P1biofilm	32	*S. cavolei*	92.01	1.57	1.20
	GR2P1biofilm	36	*S. sp. JPD-1*	89.85	5.17	4.84
	GR2P1biofilm	14	*S. sp. UCH001*	88.81	12.13	3.42
	GR2P1biofilm	42	*S. sp. UCH001*	85.27	10.85	1.87
	GR2P1bulk	144	*S. cavolei*	81.82	1.36	0.21
P2	GR1P2biofilm	127	*A. media*	84.18	0.00	0.73
	GR1P2biofilm	115	*S. arsenophilum*	84.17	13.18	0.55
	GR1P2biofilm	177	*S. cavolei*	93.79	1.36	0.15
	GR1P2bulk	131	*S. arsenophilum*	86.66	5.97	0.41
	GR1P2bulk	29	*P. putida*	81.68	1.15	0.45
	GR2P2biofilm	179	*S. cavolei*	98.33	0.65	0.57
	GR2P2biofilm	71	*S. sp. JPD-1*	85.08	2.48	0.60
	GR2P2bulk	93	*P. putida*	91.82	1.2	0.33

6.2 Metabolic Pathway Reconstruction

6.2.1 Genome Annotation

Following submission to KEGG BlastKOALA, all of the selected bins and reference sequences achieved 50.2 % - 64.7 % annotation, shown in Table 21. The genome bins of each species had similar numbers of entries (amino acid sequences included in the bin) and achieved similar annotations to their respective reference sequences, reflecting their high quality and suitability for comparison. The annotated metabolism pathway maps generated by KEGG can be found in Appendix A4, listed in the order shown in Table 21. Figures 58 - 77 in subsection A4.1 show the carbon metabolism maps and Figures 78 - 97 in subsection A4.2 show the nitrogen metabolism maps.

Table 21: Summary of KEGG genome annotation

Genome bin	Species	Entries	KEGG annotation
GR1P1biofilm.135	*A. media*	3812	61.6%
GR1P2biofilm.127	*A. media*	3460	63.3%
Ref seq.	*A. media*	3926	64.7%
GR1P2bulk.29	*P. putida*	4830	54.1%
GR2P2bulk.93	*P. putida*	5130	56.2%
Ref seq.	*P. putida*	5359	58.2%
GR1P2biofilm.115	*S. arsenophilum*	2597	50.2%
GR1P2bulk.131	*S. arsenophilum*	2485	54.2%
Ref seq.	*S. arsenophilum*	2591	57.5%
GR1P2biofilm.177	*S. cavolei*	2490	51.9%
GR2P1biofilm.32	*S. cavolei*	2151	54.3%
GR2P1bulk.144	*S. cavolei*	1858	51.8%
GR2P2biofilm.179	*S. cavolei*	2547	54.9%
Ref seq.	*S. cavolei*	2682	54.0%
GR2P1biofilm.36	*S. sp. JPD-1*	2362	54.3%
GR2P2biofilm.71	*S. sp. JPD-1*	2265	52.5%
Ref seq.	*S. sp. JPD-1*	2793	55.4%
GR2P1biofilm.14	*S. sp. UCH001*	2950	52.9%
GR2P1biofilm.42	*S. sp. UCH001*	2505	50.3%
Ref seq.	*S. sp. UCH001*	2538	55.7%

6.2.2 Carbon Metabolism Pathways

Referencing the carbon metabolism, glycolysis/gluconeogenesis, and pyruvate metabolism pathways, it was found that all of the bins submitted contained sequences for glycolysis, the pentose phosphate pathway, acetate production, and the tricarboxylic acid cycle, as well as metabolism of other sugars and carboxylic acids. Methane metabolism was also reviewed and confirmed that none of these species were methanotrophic.

The *A. media* bins and reference sequence contained sequences for glycolysis, as well as D-lactate, acetate, pyruvate, and succinate metabolism, in line with their genus-level description in Bergey's Manual (Martin-Carnahan and Joseph 2015). Further to being fermentative, species in this genus also produce acids, including acetic acid (Namdarit and Cabelli 1990). It is therefore possible that *A. media* could be an important C-cycling species in the AFBRs, releasing acetate into the bulk solution.

P. putida is a fluorescent species of *Pseudomonas* with remarkable biochemical versatility. As a fluorescent pseudomonad, glucose is typically degraded via the Entner-Doudoroff pathway. This pathway is an alternative pathway for fermentative glucose catabolism that produces the same number of reducing equivalents as the Embden–Meyerhof–Parnas pathway (glycolysis), but only 1 ATP instead of 2 (Gupta and Gupta 2021). Furthermore, *P. putida* specifically has a unique process, involving the accumulation of gluconate outside of the cell, which is then reabsorbed through a separate transport system (Palleroni 2015). Indeed, sequences for gluconate metabolism were found in the *P. putida* bins and reference sequence. Hence, although there are energetic differences, this species is glucose-consuming.

At the genus level, *Sulfurospirillum* is known to not oxidise or ferment carbohydrates, instead succinate, fumarate, malate, lactate, or pyruvate can be oxidised, and acetate can be used as the carbon source when hydrogen or formate are used as the e^- donors (Stolz et al. 2015). Indeed, sequences for those processes were found. However, despite no reports of glucose metabolism by any of these *Sulfurospirillum* species, all 10 of the bins and the reference sequences also have the complete pathways for glycolysis. Hence, it is assumed that none of them are expressing those enzymes. Concurrently, it is proposed that they are taking advantage of the acetic acid production by *A. media* as a source of acetate and sourcing their electrons from either consuming hydrogen ions or microbe-microbe DIET in the bulk.

6.2.3 Nitrate Reduction Pathways

The dissimilatory NO_3^- reducing pathways found in the bins and reference sequences are shown in Table 22. None of the bins had sequences for nitrification, except the *S. cavolei* reference sequence, which had Nxr,

only. The most immediate observation is that NirS, NirK, and Nor are absent from every bin, which implies that conventional denitrification is not carried out by any of these species. However, with the exception of *P. putida* and 2 *Sulfurospirillum* bins, they all have Nos. The presence of N_2O reducing capacity in the absence of the majority of the conventional denitrification pathway suggests that this could be associated with N_2O detoxification.

Table 22: Dissimilatory nitrate reducing genes from selected bins and reference sequences

		Denitratation		Denitritation				DNRA	
Genome bin	Species	Nap	Nar	NirK	NirS	Nor	Nos	Nrf	NirBD
GR1P1biofilm.135	*A. media*	+	-	-	-	-	+	+	+
GR1P2biofilm.127	*A. media*	+	-	-	-	-	+	-	+
Ref seq.	*A. media*	+	-	-	-	-	+	+	+
GR1P2bulk.29	*P. putida*	-	-	-	-	-	-	-	+
GR2P2bulk.93	*P. putida*	-	-	-	-	-	-	-	+
Ref seq.	*P. putida*	-	-	-	-	-	-	-	+
GR1P2biofilm.115	*S. arsenophilum*	+	-	-	-	-	+	+	-
GR1P2bulk.131	*S. arsenophilum*	+	-	-	-	-	-	+	-
Ref seq.	*S. arsenophilum*	+	-	-	-	-	+	+	-
GR1P2biofilm.177	*S. cavolei*	+	-	-	-	-	+	+	-
GR2P1biofilm.32	*S. cavolei*	+	-	-	-	-	+	+	-
GR2P1bulk.144	*S. cavolei*	+	-	-	-	-	+	+	-
GR2P2biofilm.179	*S. cavolei*	+	-	-	-	-	+	+	-
Ref seq.	*S. cavolei*	+	+	-	-	-	+	+	-
GR2P1biofilm.36	*S. sp. JPD-1*	-	-	-	-	-	+	-	-
GR2P2biofilm.71	*S. sp. JPD-1*	-	-	-	-	-	+	+	-
Ref seq.	*S. sp. JPD-1*	+	-	-	-	-	+	+	-
GR2P1biofilm.14	*S. sp. UCH001*	+	-	-	-	-	+	+	-
GR2P1biofilm.42	*S. sp. UCH001*	+	-	-	-	-	+	+	-
Ref seq.	*S. sp. UCH001*	+	-	-	-	-	-	+	-

From the genus level, *Aeromonas* species are known to undertake denitratation, hence the consistent presence of Nap and the absence of subsequent denitritation genes is expected. However, they have not been previously associated with DNRA. Thus, the presence of both NirBD and Nrf (except in GR1P2biofilm.127) is a novel finding. Additionally, given that GR1P1biofilm.135 and the reference sequence have Nrf, its absence in GR1P2biofilm.127 could be attributed to sequencing error.

Despite having been previously associated with heterotrophic nitrification-aerobic denitrification (Zhang et al. 2019), the only NO_3^- reducing sequence found in *P. putida* was NirBD. Sequences for conventional denitrification were not found in either the bins or the reference sequence. With that being, they do all have sequences for extracellular NO_2^- transport, which can be seen in Figures 81 - 83 in subsection A4.2. It is therefore possible that these microbes scavenge excess NO_2^- produced by *A. media* to be reduced to NH_3.

Bins for *S. arsenophilum*, *S. cavolei*, and *S. sp. UCH001* were largely consistent, containing the periplasmic Nap/Nrf DNRA enzyme pair. On the other hand, there were inconsistencies between the *S. sp. JPD-1* bins. While the reference sequence has Nap and Nrf, GR2P2biofilm.71 has only Nrf, GR2P1biofilm.36 has neither. Hence, *S. arsenophilum*, *S. cavolei*, and *S. sp. UCH001* can be considered as enactors of DNRA, while the evidence for *S. sp. JPD-1* is less conclusive.

Given the universal absence of Nor and the fact that putative Nod sequences are in the qNor family, it is possible that this pathway has been missed by KEGG, which doesn't include any Nod sequences in its database. As such, the next step is to search for those genes using sequence similarity searching.

6.3 Sequence Similarity Scoring

The query sequences input into the NCBI blastp server were the same set of sequences used by Zhu et al. (2017) in the course of their *nod* PCR primer design. These were (accession numbers and links to NCBI in brackets): DAMO_2434 (CBE69496) and DAMO_2437 (CBE69502) from Ettwig et al. (2010); HDN1F_02620 (CBL43845) from Zedelius et al. (2011); KX364454 (APP93282) and KX364455 (APP93283) from Ettwig et al. (2016). The results from the similarity scoring are shown in Table 23.

The maximum score is the highest alignment score calculated from the sum of the rewards for matched nucleotides and penalities for mismatches and gaps. The total score is then the sum of alignment scores of all segments from the same subject sequence. Query coverage is the percent of the query length that is included in the aligned segments. Expect values (E values) are the number of alignments expected by chance with the calculated score or better. Identity is the the extent to which two sequences have the same residues at the same positions in an alignment. The important metrics include the identity (which should be above 35 %), E value (which should be very close to zero), and query coverage (which should be above 50 %). These tolerances are fairly low due to function retention of proteins even with amino acid substitutions.

Further reinforcing the notion that *A. media* does not undertake denitritation, neither of the bins nor the reference sequence had any matches to the query Nod sequences. GR2P1bulk.144 (*S. cavolei*) and GR2P1biofilm.36 (*S. sp. JPD-1*) also had zero matches. Of the matches that were found, the highest

Table 23: Putative nitric oxide dismutase enzyme sequence similarity scoring. Sorted by identity %, green-to-red colour grading applied to identity % (largest to smallest) and E value (smallest to largest)

Subject (bin)	Species	Query (acc.)	Matches	Max score	Total score	E value	Coverage (%)	Identity (%)
GR1P2biofilm.115	S.arsenophilum	CBL43845.1	1	62.0	62.0	2.00E-12	16	32.58
Ref seq.	P.putida	CBL43845.1	1	34.3	34.3	4.40E-02	10	32.58
GR1P2biofilm.115	S.arsenophilum	APP93283.1	1	50.8	50.8	1.00E-08	12	31.63
GR1P2bulk.29	P.putida	CBL43845.1	1	34.3	34.3	3.90E-02	10	31.46
GR2P2bulk.93	P.putida	CBL43845.1	1	34.3	34.3	4.20E-02	10	31.46
GR1P2biofilm.115	S.arsenophilum	CBE69502.1	1	45.4	45.4	8.00E-07	11	30.93
GR1P2biofilm.115	S.arsenophilum	APP93282.1	1	48.1	48.1	1.00E-07	11	29.59
GR2P2biofilm.71	S.sp.JPD-1	APP93282.1	1	39.7	39.7	1.00E-04	8	28.57
GR2P2biofilm.71	S.sp.JPD-1	APP93283.1	1	39.7	39.7	1.00E-04	8	28.57
GR2P2biofilm.71	S.sp.JPD-1	CBE69502.1	1	39.3	39.3	2.00E-04	8	28.57
GR2P2biofilm.71	S.sp.JPD-1	CBE69496.1	1	38.9	38.9	3.00E-04	8	28.57
GR2P2biofilm.71	S.sp.JPD-1	CBL43845.1	1	37.0	37.0	1.00E-03	8	28.57
GR1P2bulk.29	P.putida	APP93282.1	1	34.7	34.7	2.90E-02	18	26.32
GR2P2bulk.93	P.putida	APP93282.1	1	34.7	34.7	3.10E-02	18	26.32
Ref seq.	P.putida	APP93282.1	1	34.7	34.7	3.30E-02	18	26.32
GR1P2biofilm.115	S.arsenophilum	CBE69496.1	1	51.2	51.2	8.00E-09	16	26.28
GR1P2bulk.29	P.putida	CBE69502.1	1	35.8	35.8	1.30E-02	18	25.00
GR2P2bulk.93	P.putida	CBE69502.1	1	35.8	35.8	1.40E-02	18	25.00
Ref seq.	P.putida	CBE69502.1	1	35.8	35.8	1.50E-02	18	25.00
GR1P2bulk.131	S.arsenophilum	CBE69496.1	1	39.7	39.7	5.00E-04	18	24.68
GR1P2bulk.29	P.putida	APP93283.1	1	34.7	34.7	3.60E-02	18	24.34
GR2P2bulk.93	P.putida	APP93283.1	1	34.7	34.7	3.80E-02	18	24.34
Ref seq.	P.putida	APP93283.1	1	34.7	34.7	4.20E-02	18	24.34
GR1P2bulk.131	S.arsenophilum	CBL43845.1	1	40.8	40.8	2.00E-04	18	24.32
GR2P1biofilm.14	S.sp.UCH001	CBL43845.1	1	42.0	42.0	9.00E-05	18	24.32
Ref seq.	S.sp.UCH001	CBL43845.1	1	42.0	42.0	8.00E-05	18	24.32
GR2P1biofilm.14	S.sp.UCH001	CBE69496.1	1	39.7	39.7	5.00E-04	18	24.03
Ref seq.	S.sp.UCH001	CBE69496.1	1	39.7	39.7	5.00E-04	18	24.03

Continued...

Table 23 Continued.

Subject (bin)	Species	Query (acc.)	Matches	Max score	Total score	E value	Coverage (%)	Identity (%)
GR1P2bulk.131	S.arsenophilum	CBE69502.1	1	40.4	40.4	2.00E-04	18	23.87
GR1P2bulk.131	S.arsenophilum	APP93283.1	1	40.4	40.4	2.00E-04	18	23.87
GR1P2bulk.131	S.arsenophilum	APP93282.1	1	39.7	39.7	4.00E-04	18	23.87
Ref seq.	S.arsenophilum	CBL43845.1	1	40.8	40.8	2.00E-04	18	23.65
Ref seq.	S.sp.JPD-1	CBL43845.1	1	40.0	40.0	4.00E-04	18	23.65
GR2P1biofilm.42	S.sp.UCH001	CBL43845.1	1	40.0	40.0	3.00E-04	18	23.65
Ref seq.	S.arsenophilum	CBE69496.1	1	38.5	38.5	1.00E-03	18	23.38
Ref seq.	S.sp.JPD-1	CBE69496.1	1	36.6	36.6	5.00E-03	18	23.38
GR2P1biofilm.42	S.sp.UCH001	CBE69496.1	1	37.7	37.7	1.00E-03	18	23.38
GR2P1biofilm.14	S.sp.UCH001	CBE69502.1	1	40.8	40.8	2.00E-04	18	23.23
GR2P1biofilm.14	S.sp.UCH001	APP93283.1	1	41.2	41.2	2.00E-04	18	23.23
GR2P1biofilm.14	S.sp.UCH001	APP93282.1	1	40.0	40.0	4.00E-04	18	23.23
Ref seq.	S.sp.UCH001	CBE69502.1	1	40.8	40.8	2.00E-04	18	23.23
Ref seq.	S.sp.UCH001	APP93283.1	1	40.8	40.8	2.00E-04	18	23.23
Ref seq.	S.sp.UCH001	APP93282.1	1	39.7	39.7	4.00E-04	18	23.23
Ref seq.	S.arsenophilum	CBE69502.1	1	39.7	39.7	4.00E-04	18	22.58
Ref seq.	S.arsenophilum	APP93283.1	1	39.7	39.7	4.00E-04	18	22.58
Ref seq.	S.arsenophilum	APP93282.1	1	38.5	38.5	1.00E-03	18	22.58
Ref seq.	S.sp.JPD-1	CBE69502.1	1	37.4	37.4	2.00E-03	18	22.58
Ref seq.	S.sp.JPD-1	APP93283.1	1	37.7	37.7	2.00E-03	18	22.58
Ref seq.	S.sp.JPD-1	APP93282.1	1	36.6	36.6	4.00E-03	18	22.58
GR2P1biofilm.42	S.sp.UCH001	CBE69502.1	1	38.9	38.9	6.00E-04	18	22.58
GR2P1biofilm.42	S.sp.UCH001	APP93283.1	1	38.9	38.9	6.00E-04	18	22.58
GR2P1biofilm.42	S.sp.UCH001	APP93282.1	1	38.1	38.1	1.00E-03	18	22.58
GR1P2biofilm.177	S.cavolei	CBE69502.1	1	38.1	38.1	1.00E-03	18	21.94
GR1P2biofilm.177	S.cavolei	APP93283.1	1	37.7	37.7	2.00E-03	18	21.94
GR2P1biofilm.32	S.cavolei	CBE69502.1	1	38.1	38.1	1.00E-03	18	21.94
GR2P1biofilm.32	S.cavolei	APP93283.1	1	37.7	37.7	1.00E-03	18	21.94
GR2P2biofilm.179	S.cavolei	CBE69502.1	1	39.3	39.3	5.00E-04	18	21.94
GR2P2biofilm.179	S.cavolei	APP93283.1	1	38.9	38.9	7.00E-04	18	21.94

Continued...

Table 23 Continued.

Subject (bin)	Species	Query (acc.)	Matches	Max score	Total score	E value	Coverage (%)	Identity (%)
Ref seq.	S.cavolei	CBE69502.1	1	38.1	38.1	1.00E-03	18	21.94
Ref seq.	S.cavolei	APP93283.1	1	37.7	37.7	2.00E-03	18	21.94
GR2P2biofilm.179	S.cavolei	CBE69496.1	1	35.8	35.8	7.00E-03	18	21.43
GR1P2biofilm.177	S.cavolei	CBL43845.1	1	35.8	35.8	7.00E-03	18	20.95
GR2P1biofilm.32	S.cavolei	CBL43845.1	1	35.8	35.8	6.00E-03	18	20.95
GR2P2biofilm.179	S.cavolei	CBL43845.1	1	37.0	37.0	3.00E-03	18	20.95
Ref seq.	S.cavolei	CBL43845.1	1	35.8	35.8	6.00E-03	18	20.95
GR1P2biofilm.177	S.cavolei	APP93282.1	1	34.3	34.3	1.80E-02	18	20.65
GR1P2biofilm.177	S.cavolei	CBE69496.1	1	33.9	33.9	2.40E-02	18	20.65
GR2P1biofilm.32	S.cavolei	APP93282.1	1	34.3	34.3	1.60E-02	18	20.65
GR2P1biofilm.32	S.cavolei	CBE69496.1	1	33.9	33.9	2.00E-02	18	20.65
GR2P2biofilm.179	S.cavolei	APP93282.1	1	35.4	35.4	9.00E-03	18	20.65
Ref seq.	S.cavolei	APP93282.1	1	34.7	34.7	1.80E-02	18	20.65
Ref seq.	S.cavolei	CBE69496.1	1	34.3	34.3	2.40E-02	18	20.65

identity score was 32.58 %, achieved by GR1P2biofilm.115 (*S. arsenophilum*) and the reference sequence for *P. putida*, both matched to HDN1F_02620 (CBL43845). The match with GR1P2biofilm.115 had a max score of 62.0, an E value of 2.00E-12 (the lowest of all the matches found), and a coverage of 16 %. Whereas, the match with *P. putida* had a max score of 34.3, an E value of 4.40E-02 (the highest of all the matches found), and a coverage of 10 %. Hence, the match between GR1P2biofilm.115 and HDN1F_02620 is the strongest match found.

With this result, it seems that there are no significantly strong matches to any of the five Nod sequences queried. Indeed, the highest coverage was 18 %, achieved by 59 matches, none of which had an identity score above 26.32 %. Nevertheless, this could be due to the very small number of query sequences or simply the existence of alternative Nod sequences that have yet to be characterised. For example, the study that demonstrated NOD in *P. aeruginosa* despite a lack of Nod genes (Lichtenberg et al. 2021).

6.4 Discussion

6.4.1 Cooperative Glucose Metabolism

From the microbial taxonomic profiling in the previous chapter, it was shown that the bulk samples at the P2 sampling stage were co-dominated by *Aeromonas* and *Sulfurospirillum*. This distinctive characteristic may be explained by a mutually beneficial relationship between species in these genera. Previous studies have shown that "suicidal" *Aeromonas* strains will continue to produce acetic acid from glucose to the point of cell death, even in highly aerobic conditions. Hence, it is proposed that the *A. media* in the AFBRs perform glycolysis via the conventional Embden–Meyerhof–Parnas pathway and release acetic acid into the bulk solution. The various *Sulfurospirillum* spp. then consume the acetate as their C source, using alternative e^- donors. This proposed relationship is shown in Figure 43.

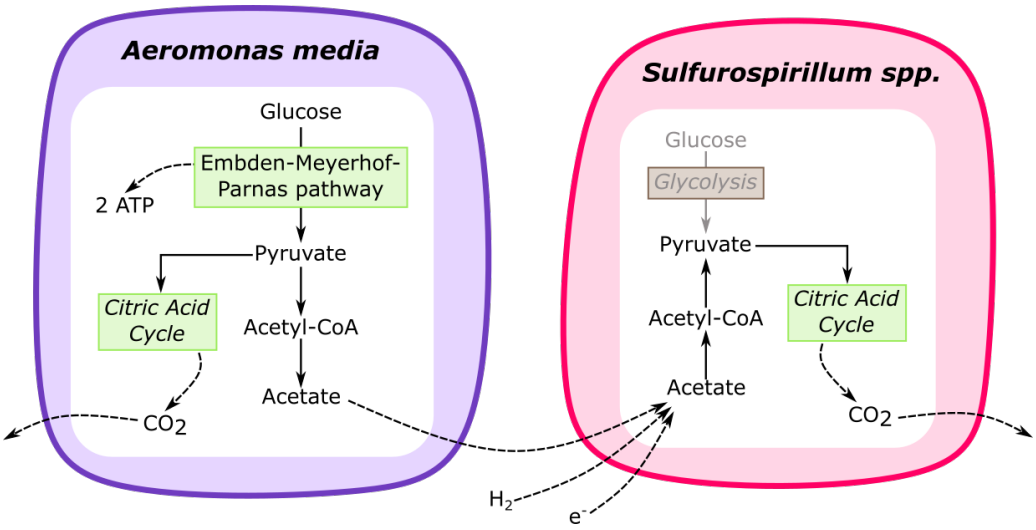


Figure 43: Proposed syntrophic relationship between *Aeromonas media* and *Sulfurospirillum* spp. for glucose metabolism. Sequences for glycolysis in *Sulfurospirillum* spp. are presumed to be inactive

The e^- donors to *Sulfurospirillum* in this situation are unclear. It could be conventional hydrogen and formate mediated e^- transfer, or there may be microbe-microbe DIET between *Sulfurospirillum* and *Pseudomonas*. Given that *Sulfurospirillum* was also dominant in the biofilms, there is the possibility that this genus is a novel electrotroph, and is receiving electrons from *Pseudomonas* in the bulk, which is already established as electroactive.

While *A. media* was able to cooperate with *Sulfurospirillum* spp., it was in competition with *P. putida* for substrate, and evidently had a substantial advantage. While the exact reason for this may not be clear, a syntrophic relationship with *Sulfurospirillum* spp. would certainly provide leverage. Alternatively, the different energy yields of the glucose metabolic pathways used by these species offer the best explanation. The Embden–Meyerhof–Parnas pathway in *A. media* generates 2 ATP, whereas the Entner-Doudoroff pathway in *P. putida* only generates 1 ATP (Gupta and Gupta 2021). Incidently, this could be further

evidence of an electroactive relationship between *Sulfurospirillum* spp. and *P. putida*, as the latter seeks to reduce the energy expenditure of reducing hydrogen.

6.4.2 Conventional Denitrification

The incomplete N mass balance from the performance results provided evidence that incomplete conventional denitrification led to the generation of N_2O, necessitating that the process was at least partially active. However, the metabolic pathway reconstruction firmly establishes that none of the species assessed in this chapter are conducting conventional denitrification, as they are all missing crucial denitritation enzymes, except Nos in *A. media* and the *Sulfurospirillum* spp. This has two indications. Firstly, that other, perhaps less oxygen tolerant, microbes were performing conventional denitrification, and the presence of a small concentration of DO prevented them from completing the process. Secondly, if neither *Aeromonas* nor *Sulfurospirillum* were performing conventional denitrification, then the function of Nos in those microbes may have been for N_2O detoxification.

6.4.3 Unconventional Nitrate Metabolism

Pathway reconstruction showed that most of the bins assessed had the periplasmic Nap/Nrf DNRA enzyme pair, which is strong evidence that they are responsible for the increase in the NH_3 concentrations. Furthermore, the preference for Nap over Nar (which was only found in the reference sequence for *S. cavolei*) for denitratation is likely to be due to the insensitivity of Nap to O_2. The presence of NirBD and Nrf sequences in *A. media* is intriguing, as the *Aeromonas* genus has not previously been associated with N-cycling beyond NO_3^- reduction to NO_2^-. The exclusive presence of NirBD in *P. putida* is also strange. The combination of these factors could suggest an interesting dynamic. While *A. media* has genes for NO_2^- reduction to NH_3, it may not be using them. On the other hand, the presence of extracellular NO_2^- transport enzymes in *P. putida* with genes only for its reduction to NH_3 suggests that these two might undertake cooperative DNRA. Despite their competition for glucose.

In order to perform NOD, either NirK or NirS enzymes are still required to transform NO_2^- to NO. The absence of these sequences in every bin assessed suggests that these species are either scavenging external NO from incomplete denitrification, or they are not undertaking NOD. At the same time, sequence similarity searching unfortunately also provided weak evidence for NOD by these species, with poor quality matches to five putative Nod sequences. Nevertheless, recent studies have shown that the knowledge of NOD is still in its early development. Such as the alternative model for NOD to 2 N_2O and 1 O_2 (Kraft et al. 2022) and the demonstration of NOD performance without detection of putative Nod sequences (Lichtenberg et al. 2021). Hence, the poor matches in this experiment may be associated with the state of the field, as

the presence of O_2 in the biogases strongly indicates oxygenic denitrification.

7 General Discussion

7.1 Performance Summary

7.1.1 Effective High-Rate Treatment of Low-Strength Wastewater

As stated in the introduction, WWTPs must contribute to the global effort to mitigate climate change by reducing their direct and indirect GHG emissions, most importantly, CH_4, N_2O, and CO_2. This is in addition to efficiently removing COD and N from domestic wastewaters. The application of anaerobic treatment technologies, and more specifically attached-growth technologies, offer the greatest opportunities for doing so, due to their low energy demand, low sludge production, and opportunity for energy recovery. The design evolution of the AFBR technology can be traced back as far as 1957, with the ACP design by Coulter et al. (1957). After 67 years of development, this experiment provides further evidence of the suitability of the AFBR technology for the high-rate treatment of low-strength wastewater using 7-channel PVDF beads as the fluidised media, chosen for its operational sustainability and prior success with (R1) and without (R2) a PANI coating (Kwon et al. 2022).

In this experiment, the two AFBRs were operated at low HRTs of 6.00 and 6.05 h, and at an ambient temperature of 21 °C. Treating 8.51 and 8.43 l/d of a synthetic wastewater with an average COD concentration of 339.13 mg COD/l, the results were COD removal rates of 2467.85 and 2529.46 mg COD/d, equating to removal efficiencies of 85.65 % and 87.66 %. Moreover, sludge production was negligible and acidification was minimal. The quick and effective treatment of this synthetic wastewater generated 0.19 and 0.23 l/d of a CH_4-rich biogas. However, the inclusion of a low NO_3^- dose produced more complex BNR performance than anticipated. Both of which are discussed in detail below.

7.1.2 Acclimatisation Time

Despite the stabilisation of the COD concentrations in the effluents by day 88 of reactor operation, the biogas composition remained volatile until day 228. Prior to that point, there were distinct alternations between CH_4-CO_2 and N_2-O_2 in the biogases, suggesting that there was competition between two distinct microbial communities during the destabilised period. Multiple factors from the two meta-genomic samples - taken on day 193 (P1) and day 290 (P2) - confirm that there was indeed a significant change in the microbial communities. Including changes to read counts, diversity indices, and taxonomic profiles. As such, the P1 samples, taken roughly a month before the biogas composition stabilised, are considered to show a snap shot of one version of the unsettled community. Whereas the P2 samples show the mature community that produced the final stabilised results.

The reason for the over 200 day maturation period for the biofilms can be attributed to the slow growing nature of anaerobic microbes as well as the nature of complex microbial communities. For example, the taxonomic profiles from the pilot-scale SAF-MBR discussed in subsubsection 5.5.2 showed that, even after 555 days of operation, the microbial communities can continue to exhibit significant population changes.

7.2 Methanogenesis

7.2.1 Review of Performance

Ultimately, the performance of methanogenesis was good, as determined from its dominant proportion of the biogases and satisfactory yields from COD removal. However, based on the performance data, it can be concluded that any microbe-electrode DIET enabled by the PANI coating didn't provide a measurable benefit to methanogenesis in this experiment, which is in contradiction to previous study (Kwon et al. 2022).

7.2.2 Stimulation

At both sampling points, the archaeal taxonomic profiles consisted entirely of methanogens. By the time the biogas composition stabilised, the kingdom-level community assessment shown in Table 15 in subsection 5.1 revealed that the biofilms at the P2 sampling point contained larger proportions of archaea than the bulks. This demonstrates that the application of an attached-growth technology facilitated the retention of slow-growing methanogens in the AFBRs, improving their performance in a high-rate reactor treating a low-strength wastewater. Since the archaeal community was consistently methanogenic, the shift towards the ultimate performance of methanogenesis must have been associated with changes in the bacterial community. Indeed, the substantial increase in the relative abundances of the syntroph and exoelectrogen bacterial sub-communities in both AFBRs confirm that this is the case.

In the P2 samples, total sub-community relative abundances in the biofilms were 3.36 % and 4.49 % syntrophs, and 6.42 % and 6.22 % exoelectrogens in GR1P2biofilm and GR2P2biofilm. In both reactors, the exoelectrogens had larger relative abundances that the syntrophs, suggesting that DIET metabolism was favourable. In the case of R2, this must be in the form of microbe-microbe DIET, as no conductive materials were included. On the other hand, the lower syntrophs and higher exoelectrogens in R1 suggest that methanogenesis was more supported by DIET than conventional syntrophic partnerships in the presence of the PANI coating. This indicates some amount of microbe-electrode DIET.

7.2.3 Inhibition

There are several possible factors that could have negatively impacted the observed performance of methanogenesis in this experiment. The most important of which being the impact of the presence of O_2. Although oxygen-tolerant methanogens - *Methanosaeta*, *Methanosarcina*, *Methanoregula*, and *Methanospirillum* (Fu et al. 2023) - held over 80 % of the archaeal communities at P2, it is unclear exactly how the DO impacted the dynamics within the reactors. Nevertheless, it was confirmed that there were not any significant populations of typical methanotrophs.

Another critical factor is the incomplete carbon mass balance, which could contain substantial quantities of CH_4. From the performance monitoring and calculations of dissolved gas using the unitless Henry's law with temperature corrections applied, the carbon mass balances established in subsection 4.2 were 62.26 % and 59.84 % complete. Moreover, in the absence of measurements of dissolved gases, the CH_4 supersaturation degree could have been higher, meaning that additional CH_4 could have been lost in the effluent without detection.

While the AFMBR study by Kwon et al. (2022) provides a strong baseline for CH_4 yield comparison, there were important experimental differences that may have inflated those CH_4 yields, primarily the more simple organic-C, longer HRT, and application of membranes. The use of acetate and propionate as the sources of COD reduced the microbial diversity as hydrolytic microbes were not be able to survive, such that there was less competition for syntrophs. Longer HRTs, the shortest being 8 h, protected microbes from washout and stimulated more complete substrate utilisation. Lastly, the membranes would have reduced dissolved CH_4 losses.

All of these factors affect R1 and R2 in equal measure, as they were true for both. However, the weaker performance of methanogenesis in R1 is especially surprising, as the presence of PANI was expected to accelerate acclimation time and boost CH_4 yields. Furthermore, the changes in the bacterial exoelectrogenic communities suggest that the DIET community initially struggled to establish itself. Unfortunately, the reason for the absence of expected performance in this case is not apparent from the available data.

7.3 Nitrogen Cycling Pathways

7.3.1 Review of Performance

The aim of this study was to investigate the impact of a low NO_3^- dose on anaerobic reactor performance, including investigating the feasibility of DIET and NOD coupling, as NOD has gained interest for its potential to curb N_2O emissions. A key, albeit predictable, finding was that anammox bacteria were not

found in any of the microbial samples, and NH_3-oxidising microbes were well below significance thresholds, as would be expected from current understandings. Beyond this, the primary finding from this experiment is that N-cycling was extremely complex.

Removal rates of oxidised inorganic-N (NO_3^- + NO_2^-) were over 95 % in both reactors, achieved with only the low COD concentration of the synthetic influent wastewater. Alone, this would be interpreted as conventional denitrification transforming these substrates into N_2 gas. However, multiple factors establish that this cannot be the case in this experiment, namely the production of O_2 and NH_3, associated with oxygenic denitrification and DNRA, respectively. Nevertheless, there is evidence that conventional denitrification is an active process in both AFBRs, the most important of which is the incomplete nitrogen mass balances, which imply N_2O accumulation from incomplete conventional denitrification.

7.3.2 Conventional Denitrification

During the initial review of the dominant genera *Aeromonas* and *Sulfurospirillum*, it was found that both typically have NO_3^- reducing capabilities (Martin-Carnahan and Joseph 2015; Stolz et al. 2015). Furthermore, the well known denitrifying genera *Pseudomonas* was above the significance threshold in the bulks at P2. Hence, MAGs of species in these genera were interrogated to ascertain their roles in N-cycling. Although *A. media* and most of the *Sulfurospirillum* bins had sequences for NO_3^- reduction, pathway mapping found that all of the high quality genome bins, as well as the reference sequences obtained from NCBI, were missing most of the critical denitritation genes, except for Nos. Moreover, the *P. putida* bins had no conventional denitrification sequences at all. Hence, none of these species are likely to be the primary enactors of conventional denitrification in the AFBRs.

Nevertheless, in the absence of the necessary preceding denitritation capacities, the function of Nos sequences in these microbes could be for N_2O detoxification. As a consequence, this indicates that partial denitrification is undertaken by other microbes, releasing N_2O into the bulks, some of which is then transformed into N_2 by *Aeromonas* and *Sulfurospirillum* to avoid toxicity. Concurrently, while *Pseudomonas* was more abundant in the bulk, it also had a small presence in the biofilms. *Pseudomonas* has been associated with electroactive denitrification (He et al. 2023), hence low-abundance *Pseudomonas* spp. taking advantage of DIET could be undertaking this partial denitrification. Moreover, both of the *P. putida* bins interrogated were from bulk samples, meaning that alternative pathways by other *Pseudomonas* spp. in the biofilms could have been missed.

The notion of incomplete DIET-mediated denitrification is further reinforced by the fact that the majority of the NO_3^- + NO_2^- removed from R1 was ultimately unaccounted for. This indicates that

the PANI coating enables an advantage to conventional denitrifiers, such that they could outcompete for substrate, but the advantage was not enough to complete the process. At this time, the potential reasons for pathway non-completion in an electroactive biofilm that should facilitate metabolism is not known.

7.3.3 Oxygenic Denitrification

Infiltration of DO from atmospheric O_2 is inevitable in any anaerobic system, however, it is not typically found in the produced biogas. As described in subsubsection 4.1.3, the design of the liquid and gaseous effluent points was such that atmospheric air ingress was not possible, and checks for leaks confirmed that there were no other entry points. Hence, the consistent presence of a small amount of O_2 in the biogases from both AFBRs is evidence that NOD is taking place. Stoichiometric formulae described in subsubsection 4.3.3, the analysis of the carbon mass balance in subsection 4.2, and sources of CO_2 in subsubsection 4.4.2 were used to determine the possible substrate consumption and output production rates. Based on a the large outstanding CO_2 balance, it was determined that glycolytic NOD was more likely than acetotrophic.

Sequence similarity scoring to five putative Nod sequences (selected from a previous PCR primer design study (Zhu et al. 2017)) found that none of the *A. media* bins had any matches to Nod sequences. As this genus is also known to not undertake denitritation (Martin-Carnahan and Joseph 2015), this is confirmation that this species is not undertaking NOD. Amongst the remaining 20 bins and reference sequences, 18 had matches. The most significant match was a *S. arsenophilum* bin (GR1P2biofilm.115), however it was low quality. Furthermore, the finding that all four of the *Sulfurospirillum* spp. and *P. putida* lack NirK and NirS indicates that, if these species are responsible for NOD, they must be scavenging NO from the bulk solution, as they have no means of generating it for themselves.

With this result, it must be considered that there is still much that is unknown about the NOD process in microbes. The majority of available *nod* sequences are classified as putative, having not be confirmed in pure/co-culture. Furthermore, recent studies highlight that there may be alternative versions of both the process and Nod genes that have yet to be characterised (Kraft et al. 2022; Lichtenberg et al. 2021). As it pertains to this experiment, it may be the case that NOD is being carried out by other less abundant microbes whose genome bins were not interrogated, hence higher quality matches may exist elsewhere in the AFBRs. Additionally, sequence similarity searches using just five query sequences is highly limiting, and expanded searches using a greater number of search sequences could provide better results.

7.3.4 Dissimilatory Nitrate Reduction to Ammonia

Testing procedure ruled out erroneous inclusion of cellular biomass during inorganic-N monitoring and there is no incentive for microbes to undertake the exorbitant thermodynamic expense of N_2 fixation. The COD/NO_3^--N ratio in this experiment was 50.19, which far exceeds the necessary ratio of 7.7 for DNRA to dominate over denitrification (van den Berg et al. 2015). Furthermore, pathway mapping confirmed that all of the bins interrogated, except 1, had at least one sequence for NO_2^- reduction to NH_3. Therefore, the increased concentration of NH_3 in the effluents from both AFBRs is attributed entirely to DNRA.

Despite this, it wouldn't be accurate to say that DNRA dominated over denitrification in either of the AFBRs. As discussed, in R1 it is likely that incomplete DIET-mediated denitrification was able to dominate due to the PANI coating. However, in P2, the various dissimilatory NO_3^- reduction processes were almost evenly split. Previous studies using acetate have shown that denitrification and DNRA are able to coexist over a range of ratios, owing to different substrate affinities (van den Berg et al. 2016). Notably, that denitrifiers have a higher affinity for organic-C than DNRA bacteria. Hence, in the AFBRs, the exoelectrogens working with methanogens may have also formed connections with denitrifiers, enhancing their organic-C consumption to out-compete DNRA bacteria, which have only been shown to associate with DIET within anammox bacteria (Wang et al. 2022a).

7.4 Novel Microbial Interactions

Based on the performance once the biogas composition stabilised and the taxonomic profiles from the P2 sampling stage, the proposed novel syntrophic relationships between key dominant microbial groups and species are shown in Figure 44. Microbes in the biofilms - methanogens, syntrophs, exoelectrogens, and denitrifiers (a small amount) - release CH_4, CO_2, N_2, N_2O, and NO into the bulk solution, most of which escapes in the gaseous and aqueous effluents. Some of the N_2O and NO released is further transformed by *Sulfurospirillum* spp. into N_2 via either N_2O detoxification or NOD, which also produces O_2. Some of the N_2O is also detoxified by *A. media* into N_2. DNRA from NO_3^- is carried out by *Sulfurospirillum* spp. and *A. media*, while *P. putida* scavenges any NO_2^- released from *A. media* to transform it into NH_3.

As proposed in Figure 43, excess acetate produced by *A. media* is consumed by *Sulfurospirillum* spp. as the C source. Compounding on Figure 43, Figure 44 shows that electrons for *Sulfurospirillum* spp. are sourced either from diffused shuttle molecules, such as H_2, or directly from *P. putida*. The lower energy yield of the Entner-Doudoroff pathway in *P. putida* compared to the Embden-Mayerhof-Parnas pathway in *A. media* (and indeed other hydrolytic microbes) may explain why *P. putida* was not more dominant. Overall, the microbial interactions in the AFBRs are unique, reflecting their unique performance.

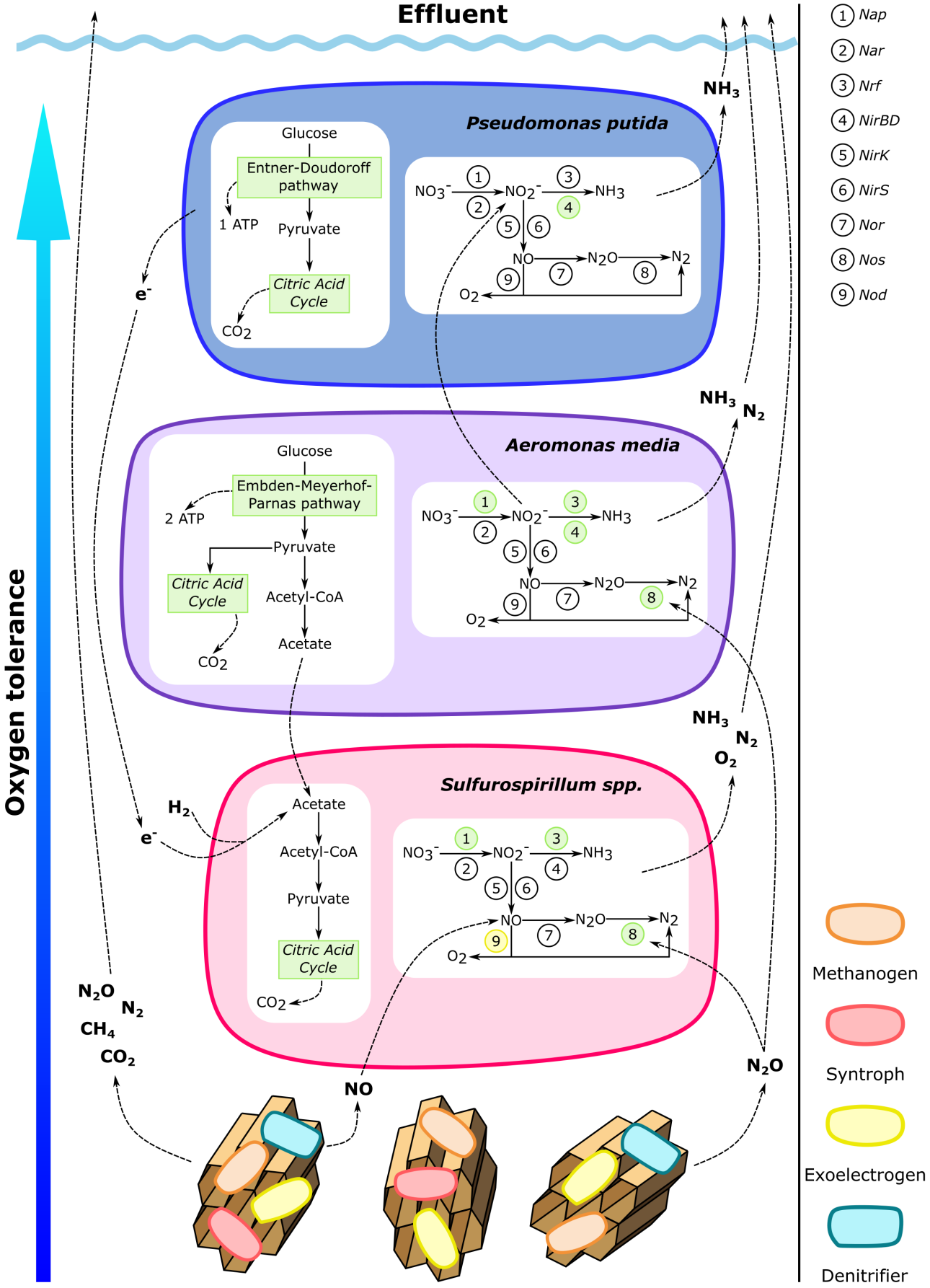


Figure 44: Proposed syntrophic relationships in AFBRs. Nitrogen cycling genes coloured in green were found within the majority of bins of those species. Nod gene in *Sulfurospirillum* spp. coloured yellow as sequence similarity match quality was low

7.5 Potential Applications

7.5.1 Auto-Aeration

The AFBR technology and its iterations (AFMBR and SAF-MBR) are indisputably established as effective primary biological treatment technologies for COD removal and CH_4 generation, reiterated again by the results of this experiment. However, the production of O_2 when exposed to a low NO_3^- dose could be leveraged to further improve performance. As demonstrated by the satisfactory CH_4 yields from both reactors, it is clear that the amount of O_2 produced was not sufficient to inhibit methanogenesis or stimulate a significant population of methanotrophs. Meanwhile, micro-aeration has been shown to stimulate methanogenesis via a combination of factors (Chen et al. 2020b). Hence, by dosing NO_3^- and stimulating NOD, an entirely autonomous mechanism for micro-aeration was provided, requiring no additional energy consumption or operational expenditure.

7.5.2 Combination with Partial-Nitrification/Anammox

Typical low strength wastewaters contain 23.1 $\pm$3.3 mg NH_3-N/l and negligible NO_3^--N (Rahman et al. 2020). Hence, in order to recreate the results of this experiment to treat real wastewater, the plant design would have to include a means to introduce NO_3^- into the AFBRs. Chemical dosing is not an attractive option, as it increases operational expenditure. Alternatively, a subsequent PN/A technology provides the ideal solution. Applied as either SHARON-anammox or CANON/OLAND, a PN/A treatment would receive an influent that has very low COD, NO_2^-, and NO_3^-, but high NH_3. This would then complete the transformation to N_2 and produce an effluent that contains extant NO_3^- which can be recycled back to the AFBRs to stimulate the desired processes.

The combination of anaerobic and PN/A technologies has been previous studied, and found to be effective for COD removal, BNR, and CH_4 recovery. Thermodynamic analysis was used to establish that anammox bacteria would be able to survive on post-anaerobic treated wastewaters, hence a modified version of a schematic proposed by Wang et al. (2018) is shown in Figure 45, including the NO_3^- recirculation proposed in this thesis.

7.5.3 Methanotrophic Denitrification

Although the high advection system of the AFBR/AFMBR enables maximum recovery of gaseous CH_4, the challenge of dissolved CH_4 in the effluents persists. As an alternative to energy intensive processes such as gas stripping or membrane filtration, WWTP layouts featuring methanotrophic denitrification have been previously proposed (Costa et al. 2022). Figure 46 shows two versions: one in which methanotrophic

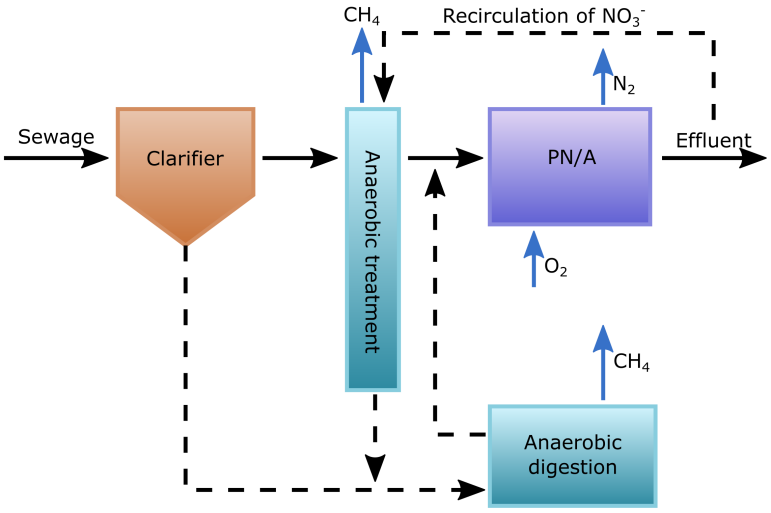


Figure 45: Proposed schematic for anaerobic treatment followed by PN/A, adapted from Wang et al. (2018)

denitrification and nitrification are undertaken in two separate reactors, and one in which the processes are completed simultaneously in one. However, both versions still rely on some amount of mechanical aeration, increasing operational expenditure and energy demand. Hence, the finding that NOD can be stimulated in an attached-growth anaerobic reactor presents an opportunity to explore auto-aeration of post-anaerobic treatment effluents, aiming to utilise autotrophic n-DAMO to remove dissolved CH_4 with minimal provision of mechanical aeration.

7.5.4 Scalability

The SAF-MBR system has already been applied at scale, with the pilot-scale plant in Bucheon, South Korea successfully operated treating real wastewater for a number of years now (Shin et al. 2014). However, this system has not previously been shown to foster NOD as the AFBRs in this experiment have. This, of course, presents the largest challenge to scalability of these results, as the exact conditions beyond presence of NO_3^- that stimulated NOD are not known. Indeed, before further experiments with subsequent treatments, a much greater understanding of NOD must be obtained in order to estimate the scalability.

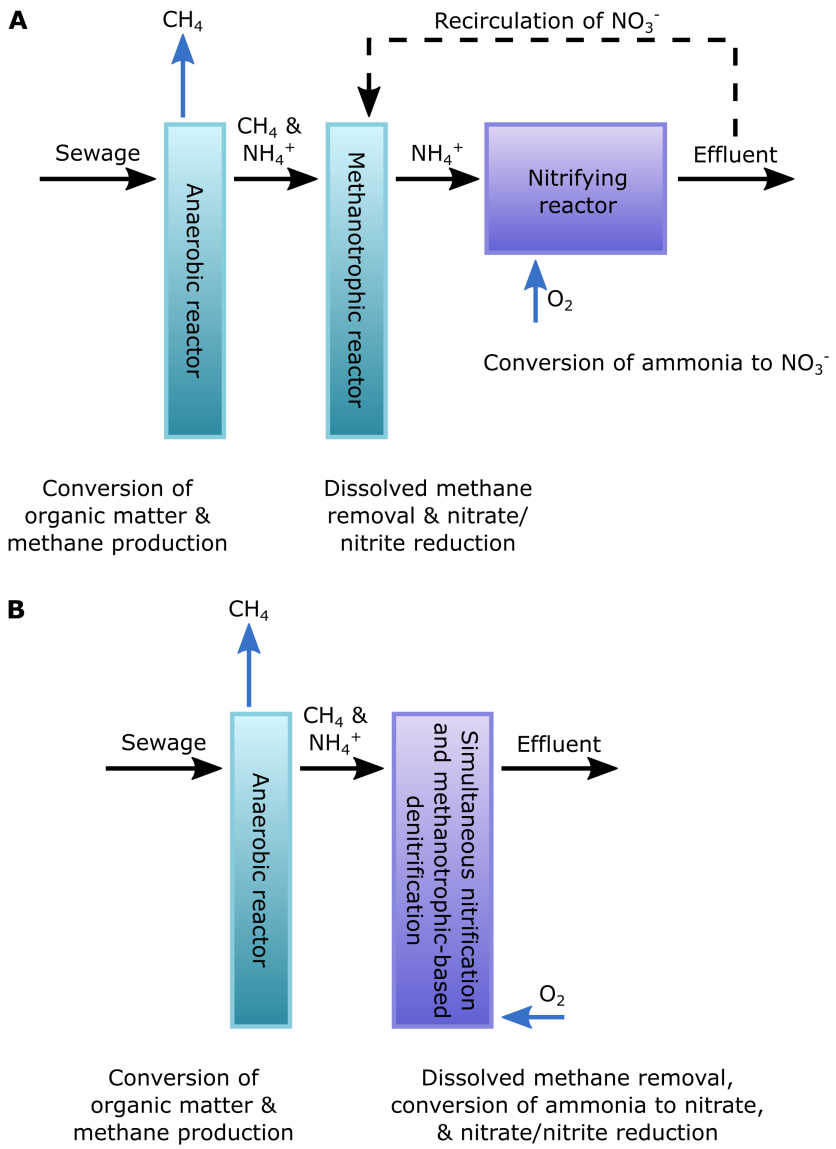


Figure 46: Proposed schematics for anaerobic treatment followed by methanotrophic denitrification, adapted from Costa et al. (2022): (a) separate nitrifying chamber with recycling of oxidised inorganic nitrogen compounds; (b) simultaneous nitrification and methanotrophic denitrification.

8 Conclusions and Recommendations

8.1 Conclusions

Based on the hypothesis that DIET and NOD can act cooperatively, the aim of this research project was to investigate the impact of a low NO_3^- dose on an anaerobic system that has previously been shown to accommodate DIET via a PANI coating on PVDF beads (Kwon et al. 2022). By following the objectives and work packages, both reactors achieved good performance and distinct microbial communities were successfully enriched in the presence and absence of the semi-conductive coating. Thus, the feasibility of DIET and NOD coupling can be assessed.

One of the most significant observations from this experiment was that the impact of the PANI coating was not as expected, i.e. stimulating microbe-electrode DIET, leading to reduced acclimatisation times and enhanced CH_4 yields. Instead, even after 290 days of reactor operation, those benefits were not realised, and the performance data showed no significant difference between R1 and R2 for these metrics. Nevertheless, the meta-genomic data suggests that microbe-microbe DIET, at least, is active in both. The strongest evidence for this being the significant relative abundances of the exoelectrogens *Desulfobulbus* and *Desulfovibrio* in the biofilms, despite the absence of their primary e^- acceptor. Further inspection of the meta-genomic data also suggests that the PANI coating influenced the microbial community structure, favouring exoelectrogenic bacteria over syntrophs in R1 and enabling the similar methanogenic performance as observed in R2 with fewer microbes.

Hence, it may be the case that the PANI coating didn't accelerate reactor start-up time, but continued operation may reveal the anticipated boost to methanogenesis. In the mean time, the performance and meta-genomic data obtained in this experiment lead to the conclusion that further study of PANI-coated media is required before it can be recommended as a mechanism for boosting methanogenesis via DIET in full scale applications. On the other hand, the PANI coating did appear to have a substantial impact on N-cycling, with distinct differences in the N-cycling performance between R1 and R2.

Under the high COD/NO_3^--N ratio created in both reactors, DNRA should have outcompeted denitrification for substrate (van den Berg et al. 2015). However, no more than a third of the NO_3^-+NO_2^- removed was transformed into NH_3 (see Table 11 in subsubsection 4.3.2). Furthermore, the generation of N_2 and the incomplete mass balances indicate both complete and incomplete denitrification. Hence, it was concluded that the electroactive biofilms provided a boost to the small community of denitrifying microbes therein. Most likely to be *Pseudomonas* spp., which have been previously associated with DIET-mediated denitrification (He et al. 2023).

As for the performance differences, lower rates of NH_3 production in R1 indicate a greater advantage to denitrification in terms of NO_3^- substrate consumption, potentially due to any microbe-electrode DIET that was anticipated for methanogenesis. However, concurrent lesser N_2 generation and a greater gap in the N mass balance indicate greater rates of process non-completion. It can therefore be concluded that the semi-conductive properties of the PANI coating encouraged incomplete DIET-mediated denitrification, which has not been previously studied. This again demonstrates that further research into the impact of PANI as a means of boosting desired microbial metabolism is required, especially if it has the counter-productive impact of increasing N_2O emissions when exposed to a low NO_3^- dose.

This study is also an application of meta-omics to further the literature and understanding of how NOD functions in complex environments. Although distinguishing the exact contributions of conventional and oxygenic denitrification to the generated N_2 is not possible from the data in this experiment, the presence of O_2 in the biogas determines that oxygenic denitrification was active. Notwithstanding the weak matches from sequence similarity searches, which could be because the microbes undertaking NOD were not interrogated, or alternative versions of Nod could have provided better matches. Lastly, determined on the basis that incomplete conventional denitrification dominated in the presence of the PANI coating, it can be concluded that NOD is not coupled with DIET, potentially because NOD is an e^- neutral reaction, and therefore wouldn't derive benefit from an external e^- sink/source.

While previous studies have identified the presence of putative *nod* genes in wastewater treatment plants (Zhu et al. 2017), this study is among the first to demonstrate that NOD can make significant contributions to denitrification during wastewater treatment (Lv et al. 2024). With that being said, the exact reasons for this are unclear, not aided by the unintentional discovery of its presence. However, as discussed in the previous chapter, there is substantial potential for *nod* in industrial wastewater treatment processes if it can be intentionally fostered. Suggestions will now be discussed.

8.2 Recommendations for Future Research

8.2.1 Improvements to Experimental Design

As mentioned in subsubsection 4.1.4, at the outset of this programme, there was no intention to measure inorganic-N or assess N-cycling. It wasn't until unusual biogas readings were detected that the aim of the project shifted to investigate. While high quality data and thorough analysis were still attainable, there were several metrics that would have facilitated a better understanding of the performance from the AFBRs that were not taken. The most important of these being to develop methodologies for measuring various gaseous and dissolved components, such as dissolved gases (CH_4 and O_2 in particular), N_2O, TOC, VFAs,

and SS. This would help to resolve the incomplete mass balances, and in turn provide a lot more certainty to the assessment of substrate cycling, such as distribution among the N-cycling processes, and dissolved CH_4 losses.

As described in subsubsection 2.5.1, the development of specific PCR primers to amplify putative *nod* sequences has lead to an exponential increase in the number of sequences being added to the NCBI database (Bhattacharjee et al. 2016; Hu et al. 2019; Zhu et al. 2017). Hence, expanded sequence similarity searches and motif filtering (unique combinations of amino acids that have specific physical functions) would improve the quality of matches found, as the substitutions that distinguish Nod from qNor could be filtered (Ettwig et al. 2012; Zhu et al. 2017). Not just for Nod, but for *c*-cyt and e-pili genes, too.

At the same times that the meta-genomic samples were taken, meta-transcriptomic samples were also taken, however those samples all failed the quality control checks at Novogene and were not sequenced. Successful meta-transcriptomic sequencing would have provided stronger evidence for the proposed activity in the important microbes in this experiment, as gene activity could have been quantified. Hence, repeating attempts to obtain meta-transcriptomic are recommended.

8.2.2 Continued Experiments

Even though performance monitoring for this thesis was concluded on day 290 of operation, the same AFBRs are still active in the Roger Perry lab (on day 848 at time of submission on 16th Dec 2024). Under the care of new students, there are plenty of opportunities to further the experiment and examine different components in greater detail. For example, the further development of the electroactive microbial community and performance of methanogenesis. Outside of ongoing reactor operation, batch cultures or pure culture experiments to further explore the impact of PANI on conventional denitrification are highly recommended.

One of the most important factors to assess will likely be the impact of the COD/NO_3^--N ratio. This feature is already known to impact the substrate consumption between conventional denitrification and DNRA, however, it is not known how this may impact NOD. Similarly, the impact of NH_3/NO_3^- could also be assessed to investigate changes to DNRA. Both of these could be supplemented by stable isotope probing using $\delta^{15}N$ and $\delta^{18}O$ in NO_3^- (Roberts et al. 2023). Lastly, longevity testing of PANI coating, as the durability of the coating is under its own abrasion has not yet been examined.

9 References

Ajunwa, Obinna M. et al. (2021). "Electrotrophs and Electricigens; Key Players in Microbial Electrophysiology". In: *Bioelectrochemical Systems: Vol.1 Principles and Processes*. Ed. by Prasun Kumar and Chandrasekhar Kuppam. Springer Singapore, pp. 299–326. DOI: 10.1007/978-981-15-6872-5_13.

Akram, Jehangir et al. (2024). "Advances in microbial community, mechanisms and stimulation effects of direct interspecies electron transfer in anaerobic digestion". In: *Biotechnology Advances*. DOI: 10.1016/j.biotechadv.2024.108398.

Alavi-Borazjani, S. Azadeh et al. (2020). "Over-acidification control strategies for enhanced biogas production from anaerobic digestion: A review". In: *Biomass and Bioenergy* 143. DOI: 10.1016/J.BIOMBIOE.2020.105833.

Allahkarami, Esmaeil and Abolfazl Dehghan Monfared (2024). "Chapter 5 - Activated carbon adsorbents for the removal of emerging pollutants and its adsorption mechanisms". In: *Sustainable Remediation Technologies for Emerging Pollutants in Aqueous Environment*. Ed. by Mohammad Hadi Dehghani et al. Elsevier, pp. 79–109. ISBN: 978-0-443-18618-9.

Altschul, Stephen F. et al. (1990). "Basic local alignment search tool". In: *Journal of Molecular Biology* 215 (3), pp. 403–410. DOI: 10.1016/S0022-2836(05)80360-2.

Altschul, Stephen F. et al. (1997). "Gapped BLAST and PSI-BLAST: a new generation of protein database search programs". In: *Nucleic Acids Research* 25 (17), pp. 3389–3402. DOI: 10.1093/NAR/25.17.3389.

An, Zeming et al. (2024). "Nitrous oxide emissions in novel wastewater treatment processes: A comprehensive review". In: *Bioresource Technology* 391. DOI: 10.1016/J.BIORTECH.2023.129950.

Aslam, Muhammad et al. (2017). "Membrane bioreactors for wastewater treatment: A review of mechanical cleaning by scouring agents to control membrane fouling". In: *Chemical Engineering Journal* 307, pp. 897–913. DOI: 10.1016/J.CEJ.2016.08.144.

Asnicar, Francesco et al. (2020). "Precise phylogenetic analysis of microbial isolates and genomes from metagenomes using PhyloPhlAn 3.0". In: *Nature Communications* 11 (1). DOI: 10.1038/s41467-020-16366-7.

Babraham Bioinformatics (2023). *FastQC*. URL: www.bioinformatics.babraham.ac.uk/projects/fastqc/ (visited on 01/02/2024).

Baek, Gahyun et al. (2023). "Challenges in engineering direct interspecies electron transfer for enhanced methanogenesis". In: *Renewable and Sustainable Energy Reviews* 183. DOI: 10.1016/J.RSER.2023.113503.

Bahram, Mohammad et al. (2019). "Newly designed 16S rRNA metabarcoding primers amplify diverse and novel archaeal taxa from the environment". In: *Environmental Microbiology Reports* 11 (4), pp. 487–494. DOI: 10.1111/1758-2229.12684.

Bai, Mengwei et al. (2024). "Gene cloning, expression and performance validation of nitric oxide dismutase". In: *Science of The Total Environment* 935. DOI: 10.1016/J.SCITOTENV.2024.173455.

Baird, Rodger and Laura Bridgewater (2017). *Standard Methods for the Examination of Water and Wastewater*. 23rd ed. American Public Health Association. ISBN: 9780875532875.

Barber, W.P.F. (2016). "Thermal hydrolysis for sewage treatment: A critical review". In: *Water Research* 104, pp. 53–71. DOI: 10.1016/J.WATRES.2016.07.069.

Batstone, D.J. et al. (2002). *Anaerobic digestion model no. 1 (ADM1)*. IWA. ISBN: 1900222787.

Bendall, Derek S. (2016). "Keilin, Cytochrome and Its Nomenclature". In: *Cytochrome Complexes: Evolution, Structures, Energy Transduction, and Signaling*. Ed. by William A. Cramer and Toivo Kallas. 1st ed. Springer Netherlands, pp. 3–11. DOI: 10.1007/978-94-017-7481-9.

Benomar, Saida et al. (2015). "Nutritional stress induces exchange of cell material and energetic coupling between bacterial species". In: *Nature Communications 2015 6:1* 6 (1). DOI: 10.1038/ncomms7283.

Benson, Gary (1999). "Tandem repeats finder: a program to analyze DNA sequences". In: *Nucleic Acids Research* 27 (2), pp. 573–580. DOI: 10.1093/NAR/27.2.573.

Besson, Stéphane et al. (2022). "Nitrite reduction in bacteria: A comprehensive view of nitrite reductases". In: *Coordination Chemistry Reviews* 464. DOI: 10.1016/J.CCR.2022.214560.

Bhattacharjee, Ananda Shankar et al. (2016). "Methane dependent denitrification- from ecosystem to laboratory-scale enrichment for engineering applications". In: *Water Research* 99, pp. 244–252. DOI: 10.1016/J.WATRES.2016.04.070.

Boesen, Thomas et al. (2021). "Pili for nanowires". In: *Nature Microbiology* 6 (11), pp. 1347–1348. DOI: 10.1038/s41564-021-00990-0.

Bokulich, Nicholas A. et al. (2018). "Optimizing taxonomic classification of marker-gene amplicon sequences with QIIME 2's q2-feature-classifier plugin". In: *Microbiome* 6 (90). DOI: 10.1186/S40168-018-0470-Z.

Bolger, Anthony M. et al. (2014). "Trimmomatic: a flexible trimmer for Illumina sequence data". In: *Bioinformatics* 30 (15). DOI: 10.1093/BIOINFORMATICS/BTU170.

Bolyen, Evan et al. (2019). "Reproducible, interactive, scalable and extensible microbiome data science using QIIME 2". In: *Nature Biotechnology* 37 (8), pp. 852–857. DOI: 10.1038/s41587-019-0209-9.

Bonfield, James K. et al. (2021). "HTSlib: C library for reading/writing high-throughput sequencing data". In: *GigaScience* 10 (2). DOI: 10.1093/GIGASCIENCE/GIAB007.

Boone, David R. et al. (1993). "Diversity and Taxonomy of Methanogens". In: *Methanogenesis: ecology, physiology, biochemistry & genetics*. Ed. by James G. Ferry. Chapman & Hall, pp. 35–80. DOI: 10.1007/978-1-4615-2391-8_2.

Buan, Nicole R. (2018). "Methanogens: Pushing the boundaries of biology". In: *Emerging Topics in Life Sciences* 2 (4), pp. 629–646. DOI: 10.1042/ETLS20180031.

Burlat, B. et al. (2005). "Cytochrome c nitrite reductase: from structural to physicochemical analysis". In: *Biochemical Society Transactions* 33 (1), pp. 137–140. DOI: 10.1042/BST0330137.

Cai, Mingwei et al. (2016). "Metagenomic reconstruction of key anaerobic digestion pathways in municipal sludge and industrial wastewater biogas-producing systems". In: *Frontiers in Microbiology* 7. DOI: 10.3389/FMICB.2016.00778.

Callahan, Benjamin J. et al. (2016). "DADA2: High-resolution sample inference from Illumina amplicon data". In: *Nature Methods* 13 (7), pp. 581–583. DOI: 10.1038/nmeth.3869.

Campos, J. L. et al. (2016). "Greenhouse Gases Emissions from Wastewater Treatment Plants: Minimization, Treatment, and Prevention". In: *Journal of Chemistry* 2016. DOI: 10.1155/2016/3796352.

Cao, Shenbin et al. (2021). "Coupling anammox with heterotrophic denitrification for enhanced nitrogen removal: A review". In: *Critical Reviews in Environmental Science and Technology* 51 (19), pp. 2260–2293. DOI: 10.1080/10643389.2020.1778394.

Caranto, Jonathan D. and Kyle M. Lancaster (2017). "Nitric oxide is an obligate bacterial nitrification intermediate produced by hydroxylamine oxidoreductase". In: *Proceedings of the National Academy of Sciences* 114 (31), pp. 8217–8222. DOI: 10.1073/pnas.1704504114.

Castro-Barros, Celia M. et al. (2017). "Evaluating the potential for dissimilatory nitrate reduction by anammox bacteria for municipal wastewater treatment". In: *Bioresource Technology* 233, pp. 363–372. DOI: 10.1016/J.BIORTECH.2017.02.063.

Chang, Yin Ru et al. (2019). "Membrane fouling during water or wastewater treatments: Current research updated". In: *Journal of the Taiwan Institute of Chemical Engineers* 94, pp. 88–96. DOI: 10.1016/J.JTICE.2017.12.019.

Chen, Hongbo et al. (2020a). "Recent advances in nitrous oxide production and mitigation in wastewater treatment". In: *Water Research* 184. DOI: 10.1016/J.WATRES.2020.116168.

Chen, Qing et al. (2020b). "Review on microaeration-based anaerobic digestion: State of the art, challenges, and prospectives". In: *Science of The Total Environment* 710. DOI: 10.1016/J.SCITOTENV.2019.136388.

Chen, Jian Jhih et al. (2021). "Denitrification, anammox, and dissimilatory nitrate reduction to ammonium across a mosaic of estuarine benthic habitats". In: *Limnology and Oceanography* 66 (4), pp. 1281–1297. DOI: 10.1002/LNO.11681.

Chicano, Tadeo Moreno et al. (2021). "Structural and functional characterization of the intracellular filament-forming nitrite oxidoreductase multiprotein complex". In: *Nature Microbiology* 6 (9), pp. 1129–1139. DOI: 10.1038/s41564-021-00934-8.

Clark, Ian M. et al. (2021). "Metagenomic approaches reveal differences in genetic diversity and relative abundance of nitrifying bacteria and archaea in contrasting soils". In: *Scientific Reports* 11. DOI: 10.1038/s41598-021-95100-9.

Clément, Jean Christophe et al. (2005). "Ammonium oxidation coupled to dissimilatory reduction of iron under anaerobic conditions in wetland soils". In: *Soil Biology and Biochemistry* 37 (12), pp. 2323–2328. DOI: 10.1016/J.SOILBIO.2005.03.027.

Conrad, Ralf (2020). "Importance of hydrogenotrophic, aceticlastic and methylotrophic methanogenesis for methane production in terrestrial, aquatic and other anoxic environments: A mini review". In: *Pedosphere* 30 (1), pp. 25–39. DOI: 10.1016/S1002-0160(18)60052-9.

Costa, R. B. et al. (2022). "Methanotrophic denitrification in wastewater treatment: microbial aspects and engineering strategies". In: *Critical Reviews in Biotechnology* 42 (1), pp. 145–161. DOI: 10.1080/07388551.2021.1931014.

Costas, Amaya M.G. et al. (2017). "Defining Electron Bifurcation in the Electron-Transferring Flavoprotein Family". In: *Journal of Bacteriology* 199 (21). DOI: 10.1128/jb.00440-17.

Coulter, J.B. et al. (1957). "Anaerobic Contact Process for Sewage Disposal". In: *Sewage and Industrial Wastes* 29 (4), pp. 468–477.

Crone, Brian C. et al. (2016). "Significance of dissolved methane in effluents of anaerobically treated low strength wastewater and potential for recovery as an energy product: A review". In: *Water Research* 104, pp. 520–531. DOI: 10.1016/J.WATRES.2016.08.019.

Dahiya, Shikha et al. (2023). "Understanding acidogenesis towards green hydrogen and volatile fatty acid production – Critical analysis and circular economy perspective". In: *Chemical Engineering Journal* 464. DOI: 10.1016/J.CEJ.2023.141550.

Daims, Holger et al. (2015). "Complete nitrification by Nitrospira bacteria". In: *Nature* 528. DOI: 10.1038/NATURE16461.

Daims, Holger et al. (2016). "A New Perspective on Microbes Formerly Known as Nitrite-Oxidizing Bacteria". In: *Trends in Microbiology* 24 (9), pp. 699–712. DOI: 10.1016/J.TIM.2016.05.004.

Danecek, Petr et al. (2021). "Twelve years of SAMtools and BCFtools". In: *GigaScience* 10 (2). DOI: 10.1093/GIGASCIENCE/GIAB008.

Daverey, Achlesh et al. (2019). "Recent advances in energy efficient biological treatment of municipal wastewater". In: *Bioresource Technology Reports* 7. DOI: 10.1016/J.BITEB.2019.100252.

de Haas, David and John Andrews (2022). "Nitrous oxide emissions from wastewater treatment - Revisiting the IPCC 2019 refinement guidelines". In: *Environmental Challenges* 8. DOI: 10.1016/J.ENVC.2022.100557.

Deng, Lijuan et al. (2022). "Recent advances in attached growth membrane bioreactor systems for wastewater treatment". In: *Science of The Total Environment* 808. DOI: 10.1016/J.SCITOTENV.2021.152123.

Deng, Panbo et al. (2023). "Geobacter grbiciae—A New Electron Donor in the Formation of Co-Cultures via Direct Interspecies Electron Transfer". In: *Microbiology Research* 14 (4), pp. 1774–1787. DOI: 10.3390/MICROBIOLRES14040122.

Di Capua, Francesco et al. (2019). "Electron donors for autotrophic denitrification". In: *Chemical Engineering Journal* 362, pp. 922–937. DOI: 10.1016/J.CEJ.2019.01.069.

Di Capua, Francesco et al. (2022). "Simultaneous nitrification–denitrification in biofilm systems for wastewater treatment: Key factors, potential routes, and engineered applications". In: *Bioresource Technology* 361. DOI: 10.1016/J.BIORTECH.2022.127702.

Duan, Haoran et al. (2022a). "Achieving robust mainstream nitrite shunt at pilot-scale with integrated sidestream sludge treatment and step-feed". In: *Water Research* 223. DOI: 10.1016/J.WATRES.2022.119034.

Duan, Shoupeng et al. (2022b). "Heterotrophic nitrifying bacteria in wastewater biological nitrogen removal systems: A review". In: *Critical Reviews in Environmental Science and Technology* 52 (13), pp. 2302–2338. DOI: 10.1080/10643389.2021.1877976.

Dubé, Charles-David and Serge R Guiot (2015). "Direct Interspecies Electron Transfer in Anaerobic Digestion: A Review". In: *Biogas Science and Technology*. Ed. by Georg M Guebitz et al. Springer International Publishing, pp. 101–115. DOI: 10.1007/978-3-319-21993-6_4.

Dubey, Gyanendra P. and Sigal Ben-Yehuda (2011). "Intercellular Nanotubes Mediate Bacterial Communication". In: *Cell* 144 (4). DOI: 10.1016/J.CELL.2011.01.015.

Dutta, Kasturi et al. (2014). "Removal of pharmaceuticals and organic matter from municipal wastewater using two-stage anaerobic fluidized membrane bioreactor". In: *Bioresource Technology* 165, pp. 42–49. DOI: 10.1016/j.biortech.2014.03.054.

Edwards, Marcus J. et al. (2020). "Role of multiheme cytochromes involved in extracellular anaerobic respiration in bacteria". In: *Protein Science* 29 (4). DOI: 10.1002/PRO.3787.

Ersever, Ilknur et al. (2014). "Modeling and design of anaerobic fluidized bed reactor with recycling for denitrification of reverse osmosis concentrates". In: *Chemical Engineering Science* 108, pp. 111–122. DOI: 10.1016/J.CES.2013.12.036.

Ettwig, Katharina F. et al. (2010). "Nitrite-driven anaerobic methane oxidation by oxygenic bacteria". In: *Nature* 464 (7288), pp. 543–548. DOI: 10.1038/nature08883.

Ettwig, Katharina F. et al. (2012). "Bacterial oxygen production in the dark". In: *Frontiers in Microbiology* 3 (AUG). DOI: 10.3389/FMICB.2012.00273/BIBTEX.

Ettwig, Katharina F. et al. (2016). "Archaea catalyze iron-dependent anaerobic oxidation of methane". In: *Proceedings of the National Academy of Sciences of the United States of America* 113 (45), pp. 12792–12796. DOI: 10.1073/PNAS.1609534113.

Feng, Dong et al. (2021). "How can ethanol enhance direct interspecies electron transfer in anaerobic digestion?" In: *Biotechnology Advances* 52. DOI: 10.1016/J.BIOTECHADV.2021.107812.

Ferry, J. G. (2010). "Biochemistry of Acetotrophic Methanogenesis". In: *Handbook of Hydrocarbon and Lipid Microbiology*. Ed. by Kenneth N. Timmis. Springer, pp. 357–367. DOI: 10.1007/978-3-540-77587-4_23.

Fu, Shanfei et al. (2023). "Micro-aeration: an attractive strategy to facilitate anaerobic digestion". In: *Trends in Biotechnology* 41 (5), pp. 714–726. DOI: 10.1016/J.TIBTECH.2022.09.008.

Fujimoto, Masanori et al. (2019). "Syntroph diversity and abundance in anaerobic digestion revealed through a comparative core microbiome approach". In: *Applied Microbiology and Biotechnology* 103 (15), pp. 6353–6367. DOI: 10.1007/S00253-019-09862-4.

Galushko, Alexander and Jan Kuever (2019a). "Desulfobulbus". In: *Bergey's Manual of Systematics of Archaea and Bacteria*. DOI: 10.1002/9781118960608.GBM01023.pub2.

— (2019b). "Desulfovibrio". In: *Bergey's Manual of Systematics of Archaea and Bacteria*. DOI: 10.1002/9781118960608.GBM01035.pub2.

Guerrero-Cruz, Simon et al. (2021). "Methanotrophs: Discoveries, Environmental Relevance, and a Perspective on Current and Future Applications". In: *Frontiers in Microbiology* 12. DOI: 10.3389/FMICB.2021.678057.

Guo, Jingbo et al. (2021). "Nitrous oxide emission in a laboratory anoxic-oxic process at different influent pHs: Generation pathways and the composition and function of bacterial community". In: *Bioresource Technology* 328. DOI: 10.1016/J.BIORTECH.2021.124844.

Guo, Wei et al. (2023). "Interspecies electron transfer between Geobacter and denitrifying bacteria for nitrogen removal in bioelectrochemical system". In: *Chemical Engineering Journal* 455. DOI: 10.1016/J.CEJ.2022.139821.

Gupta, Rani and Namita Gupta (2021). "Entner–Doudoroff Pathway". In: *Fundamentals of Bacterial Physiology and Metabolism*. Springer Singapore, pp. 307–326. DOI: 10.1007/978-981-16-0723-3_11.

Gurevich, Alexey et al. (2013). "QUAST: quality assessment tool for genome assemblies". In: *Bioinformatics* 29 (8), pp. 1072–1075. DOI: 10.1093/bioinformatics/btt086.

Hao, Zhen Le et al. (2022). "A mechanistic review on aerobic denitrification for nitrogen removal in water treatment". In: *Science of The Total Environment* 847. DOI: 10.1016/J.SCITOTENV.2022.157452.

Al-Hazmi, Hussein E. et al. (2023). "An advanced synergy of partial denitrification-anammox for optimizing nitrogen removal from wastewater: A review". In: *Bioresource Technology* 381. DOI: 10.1016/J.BIORTECH.2023.129168.

He, Lei et al. (2023). "Accelerating denitrification and mitigating nitrite accumulation by multiple electron transfer pathways between Shewanella oneidensis MR-1 and denitrifying microbial community". In: *Bioresource Technology* 368. DOI: 10.1016/j.biortech.2022.128336.

Heidrich, E. S. et al. (2011). "Determination of the internal chemical energy of wastewater". In: *Environmental Science and Technology* 45 (2), pp. 827–832. DOI: 10.1021/ES103058W.

Hoehler, Tori et al. (2019). "Environmental Constraints That Limit Methanogenesis". In: *Biogenesis of Hydrocarbons*. Ed. by Alfons J.M. Stams and Diana Z. Sousa. Springer, pp. 153–178. DOI: 10.1007/978-3-319-78108-2_17.

Holmes, Dawn E. et al. (2022). "Different outer membrane c-type cytochromes are involved in direct interspecies electron transfer to Geobacter or Methanosarcina species". In: *mLife* 1 (3), pp. 272–286. DOI: 10.1002/MLF2.12037.

Hospenthal, Manuela K. et al. (2017). "A comprehensive guide to pilus biogenesis in Gram-negative bacteria". In: *Nature Reviews Microbiology* 15 (6), pp. 365–379. DOI: 10.1038/nrmicro.2017.40.

Hu, Qian et al. (2017). "Conductive polyaniline nanorods enhanced methane production from anaerobic wastewater treatment". In: *Polymer* 120, pp. 236–243. DOI: 10.1016/J.POLYMER.2017.05.073.

Hu, Qian Qian et al. (2019). "High microbial diversity of the nitric oxide dismutation reaction revealed by PCR amplification and analysis of the nod gene". In: *International Biodeterioration and Biodegradation* 143. DOI: 10.1016/j.ibiod.2019.05.025.

Hu, Bo et al. (2023). "A critical review of heterotrophic nitrification and aerobic denitrification process: Influencing factors and mechanisms". In: *Journal of Water Process Engineering* 54. DOI: 10.1016/J.JWPE.2023.103995.

Huang, Xuejiao et al. (2023). "Dissimilatory nitrate reduction to ammonium in four Pseudomonas spp. under aerobic conditions". In: *Heliyon* 9 (4). DOI: 10.1016/j.heliyon.2023.e14983.

IUPAC (2019). "disproportionation". In: *Compendium of Chemical Terminology*. 3.0.1 ed. DOI: doi:10.1351/goldbook.D01799. URL: doi.org/10.1351/goldbook.D01799 (visited on 09/06/2024).

Jiang, Meng et al. (2020). "Enhancement of denitrification performance with reduction of nitrite accumulation and N2O emission by Shewanella oneidensis MR-1 in microbial denitrifying process". In: *Water Research* 169. DOI: 10.1016/j.watres.2019.115242.

Jin, Hong Yu et al. (2022). "Current advances and challenges for direct interspecies electron transfer in anaerobic digestion of waste activated sludge". In: *Chemical Engineering Journal* 450. DOI: 10.1016/j.cej.2022.137973.

Kanehisa, Minoru et al. (2016). "BlastKOALA and GhostKOALA: KEGG Tools for Functional Characterization of Genome and Metagenome Sequences". In: *Journal of molecular biology* 428 (4), pp. 726–731. DOI: 10.1016/J.JMB.2015.11.006.

Kang, Dongwan D. et al. (2019). "MetaBAT 2: An adaptive binning algorithm for robust and efficient genome reconstruction from metagenome assemblies". In: *PeerJ*. DOI: 10.7717/peerj.7359.

Kang, Hyun Jin et al. (2021). "Recent advances in methanogenesis through direct interspecies electron transfer via conductive materials: A molecular microbiological perspective". In: *Bioresource Technology* 322. DOI: 10.1016/J.BIORTECH.2020.124587.

Kato, Souichiro et al. (2012). "Microbial interspecies electron transfer via electric currents through conductive minerals". In: *Proceedings of the National Academy of Sciences of the United States of America* 109 (25), pp. 10042–10046. DOI: 10.1073/pnas.1117592109.

Kim, Byung Hong and Geoffrey Michael Gadd (2008). "Anaerobic respiration". In: *Bacterial Physiology and Metabolism*. Cambridge University Press, pp. 298–353. DOI: 10.1017/CBO9780511790461.010.

Kim, Jeonghwan et al. (2011). "Anaerobic fluidized bed membrane bioreactor for wastewater treatment". In: *Environmental Science and Technology* 45 (2), pp. 576–581. DOI: 10.1021/es1027103.

Kim, Minseok et al. (2020). "Use of polymeric scouring agent as fluidized media in anaerobic fluidized bed membrane bioreactor for wastewater treatment: System performance and microbial community". In: *Journal of Membrane Science* 606 (April), pp. 118–121. DOI: 10.1016/j.memsci.2020.118121.

Kleerebezem, Robbert and Sebastian Lücker (2021). "Cyclic Conversions in the Nitrogen Cycle". In: *Frontiers in Microbiology* 12. DOI: 10.3389/FMICB.2021.622504.

Kraft, Beate et al. (2022). "Oxygen and nitrogen production by an ammonia-oxidizing archaeon". In: *Science* 375 (6576). DOI: 10.1126/science.abe6733.

Kurth, Julia M. et al. (2021). "Methanogenic archaea use a bacteria-like methyltransferase system to demethoxylate aromatic compounds". In: *The ISME Journal* 15 (12), pp. 3549–3565. DOI: 10.1038/s41396-021-01025-6.

Kuypers, Marcel M.M. et al. (2018). "The microbial nitrogen-cycling network". In: *Nature Reviews Microbiology* 16 (5), pp. 263–276. DOI: 10.1038/nrmicro.2018.9.

Kwon, Daeeun and Jeonghwan Kim (2022). "Surface modification of polymeric media coated with conductive polyaniline to enhance methane production for anaerobic low-strength wastewater treatment". In: *Applied Surface Science* 577. DOI: 10.1016/J.APSUSC.2021.151859.

Kwon, Daeeun et al. (2022). "Polyaniline-coated conductive media promotes direct interspecies electrons transfer (DIET) and kinetics enhancement of low-strength wastewater treatment in anaerobic fluidized bed membrane bioreactor (AFMBR)". In: *Chemical Engineering Journal* 446 (2). DOI: 10.1016/j.cej.2022.136711.

Labatut, Rodrigo A. et al. (2014). "Conventional mesophilic vs. thermophilic anaerobic digestion: A trade-off between performance and stability?" In: *Water Research* 53, pp. 249–258. DOI: 10.1016/J.WATRES.2014.01.035.

Langmead, Ben and Steven L. Salzberg (2012). "Fast gapped-read alignment with Bowtie 2". In: *Nature Methods* 9 (4), pp. 357–359. DOI: 10.1038/nmeth.1923.

Leang, Ching et al. (2010). "Alignment of the c-type cytochrome OmcS along pili of Geobacter sulfurreducens". In: *Applied and Environmental Microbiology* 76 (12), pp. 4080–4084. DOI: 10.1128/AEM.00023-10.

Lee, Hyung Sool et al. (2018). "Anaerobic oxidation of methane coupled to denitrification: fundamentals, challenges, and potential". In: *Critical Reviews in Environmental Science and Technology* 48 (19-21), pp. 1067–1093. DOI: 10.1080/10643389.2018.1503927.

Lehtovirta-Morley, Laura E. (2018). "Ammonia oxidation: Ecology, physiology, biochemistry and why they must all come together". In: *FEMS Microbiology Letters* 365 (9). DOI: 10.1093/FEMSLE/FNY058.

Li, Dinghua et al. (2015). "MEGAHIT: an ultra-fast single-node solution for large and complex metagenomics assembly via succinct de Bruijn graph". In: *Bioinformatics* 31 (10), pp. 1674–1676. DOI: 10.1093/BIOINFORMATICS/BTV033.

Li, Dinghua et al. (2016). "MEGAHIT v1.0: A fast and scalable metagenome assembler driven by advanced methodologies and community practices". In: *Methods* 102. DOI: 10.1016/J.YMETH.2016.02.020.

Li, Xuesong et al. (2021). "State-of-the-art management technologies of dissolved methane in anaerobically-treated low-strength wastewaters: A review". In: *Water Research* 200. DOI: 10.1016/J.WATRES.2021.117269.

Lichtenberg, Mads et al. (2021). "Nitric-oxide-driven oxygen release in anoxic Pseudomonas aeruginosa". In: *iScience* 24 (12). DOI: 10.1016/J.ISCI.2021.103404.

Lier, J. B. van et al. (2015). "Celebrating 40 years anaerobic sludge bed reactors for industrial wastewater treatment". In: *Reviews in Environmental Science and Biotechnology* 14 (4), pp. 681–702. DOI: 10.1007/S11157-015-9375-5/TABLES/4.

Light, Samuel H. et al. (2018). "A flavin-based extracellular electron transfer mechanism in diverse Gram-positive bacteria". In: *Nature* 562. DOI: 10.1038/s41586-018-0498-z.

Liu, Fanghua et al. (2012). "Promoting direct interspecies electron transfer with activated carbon". In: *Energy and Environmental Science* 5 (10), pp. 8982–8989. DOI: 10.1039/c2ee22459c.

Liu, Yimo et al. (2014a). "A trans-outer membrane porin-cytochrome protein complex for extracellular electron transfer by Geobacter sulfurreducens PCA". In: *Environmental Microbiology Reports* 6 (6), pp. 776–785. DOI: 10.1111/1758-2229.12204.

Liu, Ze Hua et al. (2014b). "Dissolved methane: A hurdle for anaerobic treatment of municipal wastewater". In: *Environmental Science and Technology* 48 (2), pp. 889–890. DOI: 10.1021/ES405553J.

Liu, Fanghua et al. (2014c). "Magnetite compensates for the lack of a pilin-associated c-type cytochrome in extracellular electron exchange". In: *Environmental Microbiology* 17 (3), pp. 648–655. DOI: 10.1111/1462-2920.12485.

Liu, Tao et al. (2024). "Sustainable wastewater management through nitrogen-cycling microorganisms". In: *Nature Water* 2 (10), pp. 936–952. DOI: 10.1038/s44221-024-00307-5.

Lofrano, Giusy and Jeanette Brown (2010). "Wastewater management through the ages: A history of mankind". In: *Science of The Total Environment* 408 (22), pp. 5254–5264. DOI: doi.org/10.1016/j.scitotenv.2010.07.062.

Logan, Bruce E. et al. (2019). "Electroactive microorganisms in bioelectrochemical systems". In: *Nature Reviews Microbiology* 17 (5), pp. 307–319. DOI: 10.1038/s41579-019-0173-x.

Lovley, Derek R. (2011). "Live wires: Direct extracellular electron exchange for bioenergy and the bioremediation of energy-related contamination". In: *Energy and Environmental Science* 4 (12), pp. 4896–4906. DOI: 10.1039/c1ee02229f.

Lovley, Derek R. (2017a). "Happy together: microbial communities that hook up to swap electrons". In: *ISME Journal* 11, pp. 327–336. DOI: 10.1038/ismej.2016.136.

— (2017b). "Syntrophy Goes Electric: Direct Interspecies Electron Transfer". In: *Annual Review of Microbiology* 71, pp. 643–664. DOI: 10.1146/annurev-micro-030117-020420.

Lovley, Derek R. and Dawn E. Holmes (2020). "Protein nanowires: The electrification of the microbial world and maybe our own". In: *Journal of Bacteriology* 202 (20). DOI: 10.1128/JB.00331-20.

— (2022). "Electromicrobiology: the ecophysiology of phylogenetically diverse electroactive microorganisms". In: *Nature Reviews Microbiology* 20 (1). DOI: 10.1038/s41579-021-00597-6.

Lv, Sini et al. (2024). "Unveiling novel pathways and key contributors in the nitrogen cycle: Validation of enrichment and taxonomic characterization of oxygenic denitrifying microorganisms in environmental samples". In: *Science of The Total Environment* 908. DOI: 10.1016/J.SCITOTENV.2023.168339.

Maktabifard, Mojtaba et al. (2018). "Achieving energy neutrality in wastewater treatment plants through energy savings and enhancing renewable energy production". In: *Reviews in Environmental Science and Biotechnology* 17 (4), pp. 655–689. DOI: 10.1007/S11157-018-9478-X.

Maktabifard, Mojtaba et al. (2023). "Net-zero carbon condition in wastewater treatment plants: A systematic review of mitigation strategies and challenges". In: *Renewable and Sustainable Energy Reviews* 185. DOI: 10.1016/J.RSER.2023.113638.

Mand, Thomas D. and William W. Metcalf (2019). "Energy Conservation and Hydrogenase Function in Methanogenic Archaea, in Particular the Genus Methanosarcina". In: *Microbiology and Molecular Biology Reviews* 83 (4). DOI: 10.1128/MMBR.00020-19.

Mannina, Giorgio et al. (2016). "Greenhouse gases from wastewater treatment - A review of modelling tools". In: *Science of the Total Environment* 551-552, pp. 254–270. DOI: 10.1016/j.scitotenv.2016.01.163.

Martikainen, Pertti J. (2022). "Heterotrophic nitrification – An eternal mystery in the nitrogen cycle". In: *Soil Biology and Biochemistry* 168. DOI: 10.1016/J.SOILBIO.2022.108611.

Martin-Carnahan, Amy and Samuel W. Joseph (2015). "Aeromonas". In: *Bergey's Manual of Systematics of Archaea and Bacteria*. DOI: 10.1002/9781118960608.GBM01081.

McCarty, Perry L. (2018). "What is the Best Biological Process for Nitrogen Removal: When and Why?" In: *Environmental Science and Technology* 52 (7), pp. 3835–3841. DOI: 10.1021/ACS.EST.7B05832/SUPPL_FILE/ES7B05832_SI_001.PDF.

McIlroy, Simon J. et al. (2023). "Anaerobic methanotroph 'Candidatus Methanoperedens nitroreducens' has a pleomorphic life cycle". In: *Nature Microbiology* 8 (2), pp. 321–331. DOI: 10.1038/s41564-022-01292-9.

Meegoda, Jay N. et al. (2018). "A Review of the Processes, Parameters, and Optimization of Anaerobic Digestion". In: *International Journal of Environmental Research and Public Health* 15. DOI: 10.3390/IJERPH15102224.

Menzel, Peter et al. (2016). "Fast and sensitive taxonomic classification for metagenomics with Kaiju". In: *Nature Communications* 7 (1). DOI: 10.1038/ncomms11257.

Mishra, Saurabh et al. (2022). "Nitrogen removal from wastewater: A comprehensive review of biological nitrogen removal processes, critical operation parameters and bioreactor design". In: *Journal of Environmental Chemical Engineering* 10 (3). DOI: 10.1016/J.JECE.2022.107387.

Nagoya, Misa et al. (2020). "Isolation of an Obligate Mixotrophic Methanogen That Represents the Major Population in Thermophilic Fixed-Bed Anaerobic Digesters". In: *Microorganisms* 8 (2). DOI: 10.3390/MICROORGANISMS8020217.

Namdarit, Hassan and Victor J Cabelli (1990). "Glucose-Mediated Catabolite Repression of the Tricarboxylic Acid Cycle as an Explanation for Increased Acetic Acid Production in Suicidal Aeromonas Strains". In: *Journal of Bacteriology* 172 (8), pp. 4721–4724. DOI: 10.1128/jb.172.8.4721-4724.1990.

Oksanen, Jari et al. (2024). *vegan: Community Ecology Package*. R package version 2.7-0, github.com/vegandevs/vegan. URL: vegandevs.github.io/vegan/ (visited on 11/10/2024).

Oliveira, Lorena Lima de et al. (2010). "Anaerobic degradation of linear alkylbenzene sulfonate (LAS) in fluidized bed reactor by microbial consortia in different support materials". In: *Bioresource Technology* 101 (14), pp. 5112–5122. DOI: 10.1016/J.BIORTECH.2010.01.141.

Omena, Sylvia P.F. et al. (2013). "Simultaneous removal of phenol and nitrate in an anoxic fluidized bed reactor". In: *Journal of Environmental Science and Health, Part A* 48 (5), pp. 581–591. DOI: 10.1080/10934529.2013.730459.

Palleroni, Norberto J. (2015). "Pseudomonas". In: *Bergey's Manual of Systematics of Archaea and Bacteria*. DOI: 10.1002/9781118960608.GBM01210.

Pan, Yuan et al. (2023). "Carbon source shaped microbial ecology, metabolism and performance in denitrification systems". In: *Water Research* 243. DOI: 10.1016/J.WATRES.2023.120330.

Pandey, C. B. et al. (2020). "DNRA: A short-circuit in biological N-cycling to conserve nitrogen in terrestrial ecosystems". In: *Science of The Total Environment* 738. DOI: 10.1016/J.SCITOTENV.2020.139710.

Park, Heesu et al. (1999). "Flux enhancement with powdered activated carbon addition in the membrane anaerobic bioreactor". In: *Separation Science and Technology* 34 (14), pp. 2781–2792. DOI: 10.1081/SS-100100804.

Park, Jeong Hoon et al. (2018). "Direct interspecies electron transfer via conductive materials: A perspective for anaerobic digestion applications". In: *Bioresource Technology* 254, pp. 300–311. DOI: 10.1016/j.biortech.2018.01.095.

Parks, Donovan H. et al. (2015). "CheckM: assessing the quality of microbial genomes recovered from isolates, single cells, and metagenomes". In: *Genome Research* 25 (7), pp. 1043–1055. DOI: 10.1101/GR.186072.114.

Pozzebon, Elizabeth A. and Lars Seifert (2023). "Emerging environmental health risks associated with the land application of biosolids: a scoping review". In: *Environmental Health: A Global Access Science Source* 22 (1). DOI: 10.1186/S12940-023-01008-4.

Preetham, Veeravalli et al. (2024). "Enhancement of simultaneous nitrification denitrification (SND) and simultaneous nitrification-anammox-denitrification (SNAD) via 3D printed carriers: Insights into critical factors, functional microbes, and potential solutions". In: *Journal of Cleaner Production* 458. DOI: 10.1016/J.JCLEPRO.2024.142520.

Qu, Bo et al. (2014). "Anaerobic ammonium oxidation with an anode as the electron acceptor". In: *Environmental Microbiology Reports* 6 (1), pp. 100–105. DOI: 10.1111/1758-2229.12113.

Quast, Christian et al. (2013). "The SILVA ribosomal RNA gene database project: Improved data processing and web-based tools". In: *Nucleic Acids Research* 41 (D1), pp. D590–D596. DOI: 10.1093/nar/gks1219.

Quince, Christopher et al. (2017). "Shotgun metagenomics, from sampling to analysis". In: *Nature Biotechnology* 35 (9), pp. 833–844. DOI: 10.1038/nbt.3935.

Ragsdale, Stephen W. and Elizabeth Pierce (2008). "Acetogenesis and the Wood–Ljungdahl pathway of CO2 fixation". In: *Biochimica et Biophysica Acta (BBA) - Proteins and Proteomics* 1784, pp. 1873–1898. DOI: 10.1016/j.bbapap.2008.08.012.

Rahman, Arifur et al. (2020). "Moving forward with A-stage and high-rate contact-stabilization for energy efficient water resource recovery facility: Mechanisms, factors, practical approach, and guidelines". In: *Journal of Water Process Engineering* 36. DOI: 10.1016/J.JWPE.2020.101329.

Reguera, Gemma et al. (2005). "Extracellular electron transfer via microbial nanowires". In: *Nature* 435 (7045), pp. 1098–1101. DOI: 10.1038/nature03661.

Reineke, Walter and Michael Schlömann (2023). "The Microbial Nitrogen Cycle". In: *Environmental Microbiology*. Springer Spektrum, pp. 291–305. DOI: 10.1007/978-3-662-66547-3_7.

Ritchie, Hannah et al. (2023). *CO_2 and Greenhouse Gas Emissions*. URL: ourworldindata.org/co2-and-greenhouse-gas-emissions (visited on 01/24/2024).

Rittmann, Bruce E. and Perry L. McCarty (2020). "Chapter 5: Stoichiometry and Energetics". In: *Environmental Biotechnology: Principles and Applications*. 2nd ed. McGraw-Hill, pp. 143–180. ISBN: 9781260441604.

Roberts, Keryn et al. (2023). "Stable isotopes of nitrate (δ15N and δ18O) as functional indicators of nitrogen processing in constructed wetlands". In: *Science of The Total Environment* 899. DOI: 10.1016/J.SCITOTENV.2023.165246.

Robertson, Lesley A. and J. Gijs Kuenen (1984). "Aerobic denitrification: a controversy revived". In: *Archives of Microbiology* 139 (4), pp. 351–354. DOI: 10.1007/BF00408378/METRICS.

Robeson, Michael S. et al. (2020). "RESCRIPt: Reproducible sequence taxonomy reference database management for the masses". In: *bioRxiv*. DOI: 10.1101/2020.10.05.326504.

Rotaru, Amelia Elena et al. (2014). "A new model for electron flow during anaerobic digestion: direct interspecies electron transfer to Methanosaeta for the reduction of carbon dioxide to methane". In: *Energy and Environmental Science* 7, pp. 408–415. DOI: 10.1039/c3ee42189a.

Rotaru, Amelia Elena et al. (2015). "Link between capacity for current production and syntrophic growth in Geobacter species". In: *Frontiers in Microbiology* 6. DOI: 10.3389/FMICB.2015.00744.

Rother, Michael (2010). "Methanogenesis". In: *Handbook of Hydrocarbon and Lipid Microbiology*. Ed. by Kenneth N. Timmis. Springer-Verlag, pp. 481–499. DOI: 10.1007/978-3-540-77587-4_36.

Ruiz-Urigüen, Melany et al. (2018). "Electrode colonization by the Feammox bacterium Acidimicrobiaceae sp. strain A6". In: *Applied and Environmental Microbiology* 84 (24). DOI: 10.1128/AEM.02029-18.

Sayers, Eric W. et al. (2022). "Database resources of the National Center for Biotechnology Information". In: *Nucleic Acids Research* 50 (D1). DOI: 10.1093/NAR/GKAB1112.

Schöne, Christian and Michael Rother (2019). "Methanogenesis from Carbon Monoxide". In: *Biogenesis of Hydrocarbons*. Ed. by Alfons J.M. Stams and Diana Z. Sousa. Springer, pp. 123–151. DOI: 10.1007/978-3-319-78108-2_4.

Shaw, Dario R. et al. (2020). "Extracellular electron transfer-dependent anaerobic oxidation of ammonium by anammox bacteria". In: *Nature Communications* 11 (1). DOI: 10.1038/S41467-020-16016-Y.

Shin, Chungheon et al. (2011). "Effects of influent DO/COD ratio on the performance of an anaerobic fluidized bed reactor fed low-strength synthetic wastewater". In: *Bioresource Technology* 102 (21), pp. 9860–9865. DOI: 10.1016/j.biortech.2011.07.109.

Shin, Chungheon et al. (2014). "Pilot-scale temperate-climate treatment of domestic wastewater with a staged anaerobic fluidized membrane bioreactor (SAF-MBR)". In: *Bioresource Technology* 159. DOI: 10.1016/j.biortech.2014.02.060.

Shrestha, Pravin Malla and Amelia Elena Rotaru (2014). "Plugging in or going wireless: Strategies for interspecies electron transfer". In: *Frontiers in Microbiology* 5 (MAY). DOI: 10.3389/fmicb.2014.00237.

Sieber, Jessica R. et al. (2018). "Methanogens: Syntrophic Metabolism". In: *Biogenesis of Hydrocarbons*. Ed. by Alfons J.M. Stams and Diana Z. Souza. Springer, Cham, pp. 1–31. DOI: 10.1007/978-3-319-53114-4_2-1.

Silver, Whendee L et al. (2001). "Dissimilatory Nitrate Reduction to Ammonium in Upland Tropical Forest Soils". In: *Ecology* 82 (9), pp. 2410–2416. DOI: 10.1890/0012-9658(2001)082.

Slobodkina, Galina B. et al. (2017). "Respiratory ammonification of nitrate coupled to anaerobic oxidation of elemental sulfur in deep-sea autotrophic thermophilic bacteria". In: *Frontiers in Microbiology* 8. DOI: 10.3389/FMICB.2017.00087.

Soler-Jofra, Aina et al. (2021). "Hydroxylamine and the nitrogen cycle: A review". In: *Water Research* 190. DOI: 10.1016/J.WATRES.2020.116723.

Song, Young Chae et al. (2019). "Direct interspecies electron transfer in bulk solution significantly contributes to bioelectrochemical nitrogen removal". In: *International Journal of Hydrogen Energy* 44 (4), pp. 2180–2190. DOI: 10.1016/J.IJHYDENE.2018.08.188.

Sravan, J. Shanthi et al. (2021). "Chapter 1 - Status of biogas production and biogas upgrading: A global scenario". In: *Emerging Technologies and Biological Systems for Biogas Upgrading*. Ed. by Nabin Aryal et al. Academic Press, pp. 3–26. DOI: doi.org/10.1016/B978-0-12-822808-1.00002-7.

Stams, Alfons J. M. et al. (2019). "Ecophysiology of Acetoclastic Methanogens". In: *Biogenesis of Hydrocarbons*. Ed. by Alfons J.M. Stams and Diana Z. Sousa. Springer, Cham, pp. 109–121. DOI: 10.1007/978-3-319-78108-2_21.

Stanford, George et al. (1975). "Denitrification and Associated Nitrogen Transformations in Soils". In: *Soil Science* 120 (2), pp. 147–152.

Stazi, Valentina and Maria Concetta Tomei (2018). "Enhancing anaerobic treatment of domestic wastewater: State of the art, innovative technologies and future perspectives". In: *Science of The Total Environment* 635, pp. 78–91. DOI: 10.1016/J.SCITOTENV.2018.04.071.

Stein, Lisa Y. (2019). "Insights into the physiology of ammonia-oxidizing microorganisms". In: *Current Opinion in Chemical Biology* 49, pp. 9–15. DOI: 10.1016/J.CBPA.2018.09.003.

Stolz, John F. et al. (2015). "Sulfurospirillum". In: *Bergey's Manual of Systematics of Archaea and Bacteria*. DOI: 10.1002/9781118960608.GBM01072.

Strock, J.S. (2008). "Ammonification". In: *Encyclopedia of Ecology*. Ed. by Sven Erik Jørgensen and Brian D. Fath. 1st ed. Academic Press, pp. 162–165. DOI: 10.1016/B978-008045405-4.00256-1.

Strous, Marc et al. (1999). "Missing lithotroph identified as new planctomycete". In: *Nature* 400 (6743), pp. 446–449. DOI: 10.1038/22749.

Su, Bensheng et al. (2022). "Simultaneous partial nitrification, anammox, and denitrification in an upflow microaerobic membrane bioreactor treating middle concentration of ammonia nitrogen wastewater with low COD/TN ratio". In: *Chemosphere* 295. DOI: 10.1016/J.CHEMOSPHERE.2022.133832.

Summers, Zarath M. et al. (2010). "Direct Exchange of Electrons Within Aggregates of an Evolved Syntrophic Coculture of Anaerobic Bacteria". In: *Science* 330, pp. 1413–1416. DOI: 10.1126/science.1196526.

Switzenbaum, Michael S. and William J. Jewell (1978). "The anaerobic attached film expanded bed reactor for the treatment of dilute organic wastes". Cornell University. DOI: 10.2172/6085589.

— (1980). "Anaerobic Attached-Film Expanded-Bed Reactor Treatment". In: *Water Pollution Control Federation* 52 (7), pp. 1953–1965.

Tchobanoglous, George et al. (2014). 5th ed. New York, NY: McGraw-Hill Education. ISBN: 9780073401188.

Thauer, Rudolf K. et al. (2008). "Methanogenic archaea: ecologically relevant differences in energy conservation". In: *Nature Reviews Microbiology* 6 (8), pp. 579–591. DOI: 10.1038/nrmicro1931.

The Huttenhower Lab (2023). *KneadData*. URL: huttenhower.sph.harvard.edu/kneaddata/ (visited on 01/02/2024).

Tiedje, James M. et al. (1982). "Denitrification: ecological niches, competition and survival". In: *Antonie van Leeuwenhoek* 48 (6), pp. 569–583. DOI: 10.1007/BF00399542.

Ueki, Toshiyuki (2021). "Cytochromes in Extracellular Electron Transfer in Geobacter". In: *Applied and Environmental Microbiology* 87 (10). DOI: 10.1128/AEM.03109-20.

Valero, David et al. (2018). "Enhancing Biochemical Methane Potential and Enrichment of Specific Electroactive Communities from Nixtamalization Wastewater using Granular Activated Carbon as a Conductive Material". In: *Energies* 11. DOI: 10.3390/EN11082101.

van de Graaf, A. A. et al. (1995). "Anaerobic oxidation of ammonium is a biologically mediated process". In: *Applied and Environmental Microbiology* 61 (4), pp. 1246–1251. DOI: 10.1128/AEM.61.4.1246-1251.1995.

van den Berg, Eveline M. et al. (2015). "Enrichment of DNRA bacteria in a continuous culture". In: *The ISME Journal* 9 (10), pp. 2153–2161. DOI: 10.1038/ISMEJ.2015.26.

van den Berg, Eveline M. et al. (2016). "DNRA and denitrification coexist over a broad range of acetate/N-NO3- ratios, in a chemostat enrichment culture". In: *Frontiers in Microbiology* 7 (1842). DOI: 10.3389/fmicb.2016.01842.

Venturin, Bruno et al. (2022). "Key enzymes involved in anammox-based processes for wastewater treatment: An applied overview". In: *Water Environment Research* 94 (9). DOI: 10.1002/WER.10780.

Wagner, Tristan et al. (2018). "Hydrogenotrophic Methanogenesis". In: *Biogenesis of Hydrocarbons*. Ed. by Alfons J.M. Stams and Diana Z. Sousa. Springer, pp. 79–107. DOI: 10.1007/978-3-319-53114-4_3-1.

Walker, David J.F. et al. (2020). "Syntrophus conductive pili demonstrate that common hydrogen-donating syntrophs can have a direct electron transfer option". In: *The ISME Journal* 14 (3), pp. 837–846. DOI: 10.1038/s41396-019-0575-9.

Wan, Yuxuan et al. (2018). "Syntrophic growth of Geobacter sulfurreducens accelerates anaerobic denitrification". In: *Frontiers in Microbiology* 9. DOI: 10.3389/fmicb.2018.01572.

Wang, Qian et al. (2018). "Insights into the roles of anammox bacteria in post-treatment of anaerobically-treated sewage". In: *Critical Reviews in Environmental Science and Technology* 48 (6), pp. 655–684. DOI: 10.1080/10643389.2018.1474679.

Wang, Wei et al. (2019a). "Bacterial Extracellular Electron Transfer Occurs in Mammalian Gut". In: *Analytical Chemistry* 91 (19). DOI: 10.1021/ACS.ANALCHEM.9B03176/ASSET/IMAGES/LARGE/AC9B03176_0003.JPEG.

Wang, Xiaoguang et al. (2019b). "The role of the NADH-dependent nitrite reductase, Nir, from Escherichia coli in fermentative ammonification". In: *Archives of Microbiology* 201 (4), pp. 519–530. DOI: 10.1007/S00203-018-1590-3.

Wang, Wei and Duu Jong Lee (2021). "Direct interspecies electron transfer mechanism in enhanced methanogenesis: A mini-review". In: *Bioresource Technology* 330. DOI: 10.1016/J.BIORTECH.2021.124980.

Wang, Weigang et al. (2022a). "Biochar-mediated DNRA pathway of anammox bacteria under varying COD/N ratios". In: *Water Research* 212. DOI: 10.1016/j.watres.2022.118100.

Wang, Zhibin et al. (2022b). "Enrichment of DNRA bacteria: Shift of microbial community and its combination with anammox to promote TN removal". In: *Journal of Environmental Chemical Engineering* 10 (6). DOI: 10.1016/J.JECE.2022.108867.

Wang, Cerong et al. (2024). "Review of the mechanisms involved in dissimilatory nitrate reduction to ammonium and the efficacies of these mechanisms in the environment". In: *Environmental Pollution* 345. DOI: 10.1016/J.ENVPOL.2024.123480.

Water UK (2021). *Annual Emissions Report 2021*. URL: www.water.org.uk/wp-content/uploads/2021/10/Water-UK-Annual-Emissions-Report-2021.pdf (visited on 01/29/2024).

Wei, Wei et al. (2015). "Higher diversity and abundance of denitrifying microorganisms in environments than considered previously". In: *The ISME Journal* 9 (9), pp. 1954–1965. DOI: 10.1038/ismej.2015.9.

Whittaker, Mark et al. (2000). "Electron transfer during the oxidation of ammonia by the chemolithotrophic bacterium Nitrosomonas europaea". In: *Biochimica et Biophysica Acta (BBA) - Bioenergetics* 1459 (2), pp. 346–355. DOI: doi.org/10.1016/S0005-2728(00)00171-7.

Woods, Donald Devereux (1938). "The reduction of nitrate to ammonia by Clostridium welchii". In: *Biochemical Journal* 32 (11), pp. 2000–2012. DOI: 10.1042/BJ0322000.

Wrage-Mönnig, Nicole et al. (2018). "The role of nitrifier denitrification in the production of nitrous oxide revisited". In: *Soil Biology and Biochemistry* 123. DOI: 10.1016/J.SOILBIO.2018.03.020.

Wu, Kejia et al. (2024). "Isolation of a methyl-reducing methanogen outside the Euryarchaeota". In: *Nature*. DOI: 10.1038/s41586-024-07728-y.

Xia, Yinglin and Jun Sun (2023). "Beta Diversity Metrics and Ordination". In: *Bioinformatic and Statistical Analysis of Microbiome Data: From Raw Sequences to Advanced Modeling with QIIME 2 and R*. Springer, Cham, pp. 335–395. DOI: 10.1007/978-3-031-21391-5_10.

Xiao, Leilei et al. (2020). "Methane production by acetate dismutation stimulated by Shewanella oneidensis and carbon materials: An alternative to classical CO2 reduction". In: *Chemical Engineering Journal* 389. DOI: 10.1016/J.CEJ.2020.124469.

Xing, Wei et al. (2024). "Cooperation between autotrophic and heterotrophic denitrifiers under low C/N ratios revealed by individual-based modelling". In: *Science of The Total Environment* 921. DOI: 10.1016/J.SCITOTENV.2024.171091.

Yamada, Takeshi et al. (2007). "Bellilinea caldifistulae gen. nov., sp. nov and Longilinea arvoryzae gen. nov., sp. nov., strictly anaerobic, filamentous bacteria of the phylum Chloroflexi isolated from methanogenic

propionate-degrading consortia". In: *International Journal of Systematic and Evolutionary Microbiology* 57 (10), pp. 2299–2306. DOI: 10.1099/IJS.0.65098-0.

Yang, Yonggang et al. (2012). "Bacterial extracellular electron transfer in bioelectrochemical systems". In: *Process Biochemistry* 47 (12), pp. 1707–1714. DOI: 10.1016/J.PROCBIO.2012.07.032.

Yang, Peixian et al. (2019). "Metatranscriptomic evidence for classical and RuBisCO-mediated CO2 reduction to methane facilitated by direct interspecies electron transfer in a methanogenic system". In: *Scientific Reports* 9 (4116). DOI: 10.1038/s41598-019-40830-0.

Yang, Jixian et al. (2020a). "A critical review of aerobic denitrification: Insights into the intracellular electron transfer". In: *Science of The Total Environment* 731. DOI: 10.1016/J.SCITOTENV.2020.139080.

Yang, Ting et al. (2020b). "Characterization on the aerobic denitrification process of Bacillus strains". In: *Biomass and Bioenergy* 140. DOI: 10.1016/J.BIOMBIOE.2020.105677.

Yee, Mon Oo and Amelia Elena Rotaru (2020). "Extracellular electron uptake in Methanosarcinales is independent of multiheme c-type cytochromes". In: *Scientific Reports* 10 (1). DOI: 10.1038/s41598-019-57206-z.

Yeshanew, M.M. et al. (2018). "Anaerobic Digestion Processes". In: *Advances in Wastewater Treatment*. Ed. by Giorgio Mannina et al. 1st ed. IWA Publishing. ISBN: 978-1-78040-970-2.

Yoo, Rihye et al. (2012). "Anaerobic treatment of municipal wastewater with a staged anaerobic fluidized membrane bioreactor (SAF-MBR) system". In: *Bioresource Technology* 120, pp. 133–139. DOI: 10.1016/J.BIORTECH.2012.06.028.

Young, James C. and Perry L. McCarty (1969). "The Anaerobic Filter for Waste Treatment". In: *Journal (Water Pollution Control Federation)*.

Zedelius, Johannes et al. (2011). "Alkane degradation under anoxic conditions by a nitrate-reducing bacterium with possible involvement of the electron acceptor in substrate activation". In: *Environmental Microbiology Reports* 3 (1), pp. 125–135. DOI: 10.1111/J.1758-2229.2010.00198.X.

Zhang, Wenjie et al. (2018). "Effects of inorganic carbon on the nitrous oxide emissions and microbial diversity of an anaerobic ammonia oxidation reactor". In: *Bioresource Technology* 250, pp. 124–130. DOI: 10.1016/J.BIORTECH.2017.11.027.

Zhang, Ni et al. (2019). "Nitrogen removal by a metal-resistant bacterium, Pseudomonas putida ZN1, capable of heterotrophic nitrification–aerobic denitrification". In: *Journal of Chemical Technology & Biotechnology* 94 (4), pp. 1165–1175. DOI: 10.1002/JCTB.5863.

Zhang, Tianqi et al. (2020). "Autotrophic nitrogen removal and potential microbial interactions in anammox systems with different ammonia and organic carbon concentrations". In: *Journal of Water Process Engineering* 37. DOI: 10.1016/J.JWPE.2020.101493.

Zhang, Yao et al. (2023). "Syntrophy mechanism, microbial population, and process optimization for volatile fatty acids metabolism in anaerobic digestion". In: *Chemical Engineering Journal* 452. DOI: 10.1016/J.CEJ.2022.139137.

Zhang, Xinzheng et al. (2024). "Towards energy conservation and carbon reduction for wastewater treatment processes: A review of carbon-neutral anaerobic biotechnologies". In: *Journal of Water Process Engineering* 59. DOI: 10.1016/J.JWPE.2024.105026.

Zheng, Shiling et al. (2021). "Desulfovibrio feeding Methanobacterium with electrons in conductive methanogenic aggregates from coastal zones". In: *Water Research* 202. DOI: 10.1016/J.WATRES.2021.117490.

Zhou, Miaomiao et al. (2018). "Enhanced volatile fatty acids production from anaerobic fermentation of food waste: A mini-review focusing on acidogenic metabolic pathways". In: *Bioresource Technology* 248, pp. 68–78. DOI: 10.1016/J.BIORTECH.2017.06.121.

Zhou, Qinmao et al. (2021). "Electrode-dependent ammonium oxidation with different low C/N ratios in single-chambered microbial electrolysis cells". In: *Bioelectrochemistry* 142. DOI: 10.1016/j.bioelechem.2021.107889.

Zhou, Zhuo et al. (2022). "Non-syntrophic methanogenic hydrocarbon degradation by an archaeal species". In: *Nature* 601 (7892), pp. 257–262. DOI: 10.1038/s41586-021-04235-2.

Zhou, Yifan et al. (2023a). "A Comprehensive Review on Wastewater Nitrogen Removal and Its Recovery Processes". In: *International Journal of Environmental Research and Public Health* 20 (4). DOI: 10.3390/IJERPH20043429.

Zhou, Jinjie et al. (2023b). "Methane production by Methanothrix thermoacetophila via direct interspecies electron transfer with Geobacter metallireducens". In: *mBio* 14 (4). DOI: 10.1128/MBIO.00360-23.

Zhu, Baoli et al. (2017). "Unexpected diversity and high abundance of putative nitric oxide dismutase (Nod) genes in contaminated aquifers and wastewater treatment systems". In: *Applied and Environmental Microbiology* 83 (4). DOI: 10.1128/AEM.02750-16.

A1 AFBR Performance Data

A1.1 Operation

A1.1.1 Influent Flow Rate and Hydraulic Retention Times

Table 24: Influent flow rate and hydraulic retention times

	Flow (ml/h)		HRT (h)	
Day	R1	R2	R1	R2
9	43.16	65.79	49.12	32.22
10	71.61	68.39	29.60	31.00
11	58.26	67.83	36.39	31.26
12	84.00	81.00	25.24	26.17
15	85.50	88.50	25.17	24.13
16	96.00	96.00	22.08	22.08
17	102.75	111.25	20.63	19.07
19	127.78	129.63	16.59	16.35
22	145.00	140.00	14.62	15.14
25	159.10	157.60	13.35	13.46
26	205.50	189.00	10.32	11.24
29	224.25	216.79	9.45	9.80
30	226.13	232.00	9.39	9.15
32	224.67	240.00	9.52	8.85
33	250.00	260.00	8.48	8.15
37	141.82	114.55	14.95	18.51
38	285.00	290.00	7.44	7.31
39	280.00	280.00	7.57	7.57
44	302.50	288.50	7.01	7.35
46	330.00	324.00	6.42	6.54
50	339.00	342.00	6.25	6.20
52	353.57	355.71	6.00	5.96
57	360.00	354.00	5.89	5.99
59	348.00	348.00	6.09	6.09
61	346.36	355.91	6.12	5.96
64	354.00	354.00	5.99	5.99
66	351.43	351.43	6.03	6.03
74	360.00	312.00	5.89	6.79
75	336.00	372.00	6.31	5.70
79	348.00	354.00	6.09	5.99
85	355.19	337.16	5.97	6.34
86	342.00	384.00	6.20	5.52
88	384.00	378.00	5.52	5.61
93	354.55	346.36	5.98	6.12
95	346.67	303.33	6.12	6.99
100	378.00	378.00	5.61	5.61
102	354.00	360.00	5.99	5.89
107	350.00	360.00	6.06	5.89
109	336.00	342.00	6.31	6.20
116	341.54	350.77	6.21	6.04

	Flow (ml/h)		HRT (h)	
Day	R1	R2	R1	R2
121	354.00	348.00	5.99	6.09
123	348.00	330.00	6.09	6.42
135	366.32	360.00	5.79	5.89
137	354.00	348.00	5.99	6.09
142	340.00	350.00	6.24	6.06
144	360.00	336.00	5.89	6.31
149	366.00	354.00	5.79	5.99
151	330.00	372.00	6.42	5.70
158	393.00	354.00	5.67	6.02
163	336.00	360.00	6.31	5.89
165	354.00	318.00	5.99	6.67
172	318.00	318.00	6.67	6.67
179	330.00	336.00	6.42	6.31
184	366.00	342.00	5.79	6.20
186	366.00	348.00	5.79	6.09
191	360.00	360.00	5.89	5.89
192	312.00	336.00	6.79	6.31
206	336.00	348.00	6.31	6.09
207	384.00	360.00	5.52	5.89
212	348.00	360.00	6.09	5.89
214	378.00	354.00	5.61	5.99
219	384.00	360.00	5.52	5.89
221	378.00	354.00	5.61	5.99
226	360.00	330.00	5.89	6.42
228	360.00	366.00	5.89	5.79
233	365.45	321.82	5.80	6.59
235	366.00	372.00	5.79	5.70
240	366.00	366.00	5.79	5.79
242	360.00	336.00	5.89	6.31
247	354.00	360.00	5.99	5.89
256	360.00	372.00	5.89	5.70
261	360.00	324.00	5.89	6.54
263	348.00	348.00	6.09	6.09
268	360.00	365.00	5.89	5.81
270	360.00	360.00	5.89	5.89
275	360.00	366.00	5.89	5.79
277	300.00	360.00	7.07	5.89
282	372.00	366.00	5.70	5.79
286	342.00		6.20	



Figure 47: Hydraulic retention times

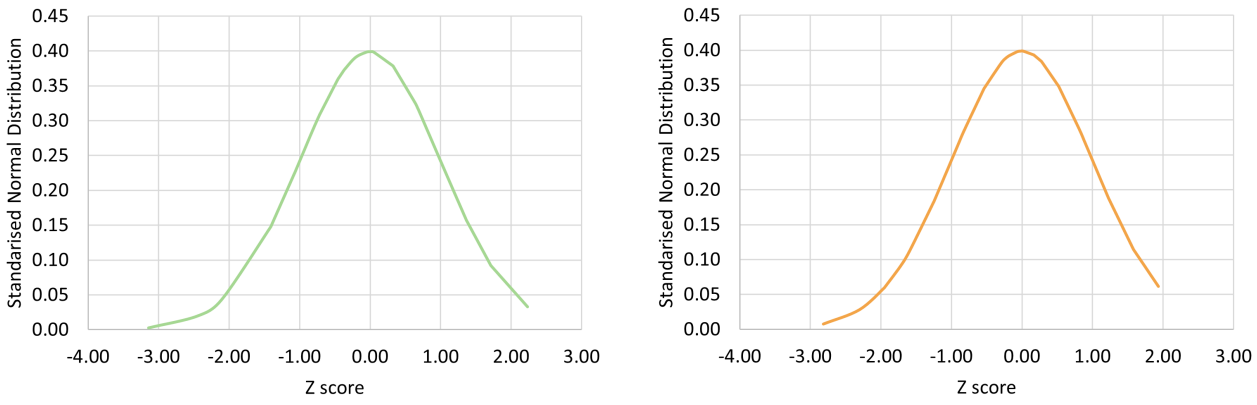


Figure 48: Steady-state hydraulic retention time standardised normal distributions: (a) R1; (b) R2

A1.1.2 pH

Table 25: pH results

Day	Feed	R1	R2
10		6.13	6.59
11		6.43	6.70
12		7.00	7.10
15		7.50	7.50
16		7.40	7.50
22		7.40	7.40
25		7.60	7.50
26		7.40	7.50
30		7.39	7.30
32		7.26	7.38
33		7.28	7.42
37		7.21	7.39
38		6.80	6.90
39		7.01	7.07
44		7.13	7.27
50		7.01	7.33
52		7.08	7.12
53		7.10	7.20
57		7.12	7.33
59		7.14	7.38
64		7.09	7.44
66		7.16	7.14
72		7.20	7.26
75		7.17	7.30
79		7.29	7.24
81		7.10	7.27
85	7.82	7.11	7.24
86		7.12	7.32
87	7.86		
88		7.16	7.34
93		7.22	7.41
94	7.78		
95		7.05	7.38
100		7.03	7.17
101	7.78		
102		7.04	7.14
106	7.75		
107		7.21	7.20
108	7.78		
109		7.17	7.24
113	7.77		
114		7.29	7.02
115	7.79		
116		6.98	7.30
117		7.13	7.38
121		7.13	7.43
122	7.78		
123		7.24	7.13
135		7.00	7.36
136	7.78		
141	7.83		
142		7.08	7.23
144		7.11	7.20
148	7.76		
149		7.16	7.22
151		7.13	7.22
155	7.76		
158		7.10	7.27
162	7.84		
163		7.05	7.16
165		7.08	7.24
172		7.14	7.28
179		7.14	7.32
184		7.20	7.30
186		7.04	7.18
190	7.82		
191		7.01	6.99
192		7.08	7.15
204	7.78		
207		7.00	7.16
211	7.78		
212		7.06	7.16
214		7.04	7.22
219		7.00	7.29
221	7.84	7.06	7.21
226		7.22	7.22
228		7.19	7.24
232	7.79		
233		7.18	7.36
234	7.83		
240		7.21	7.24
241	7.81		
242		7.13	7.23
247		7.17	7.27
248	7.82		
253		7.31	7.36
255	7.84		
256		7.16	7.17
260	7.82		
261		7.18	7.14
262	7.81		
263		7.10	7.25
267	7.82		
268		7.08	7.26
270		7.14	7.18
274	7.77		
275		7.19	7.19
277		7.16	7.21
282		7.14	7.18

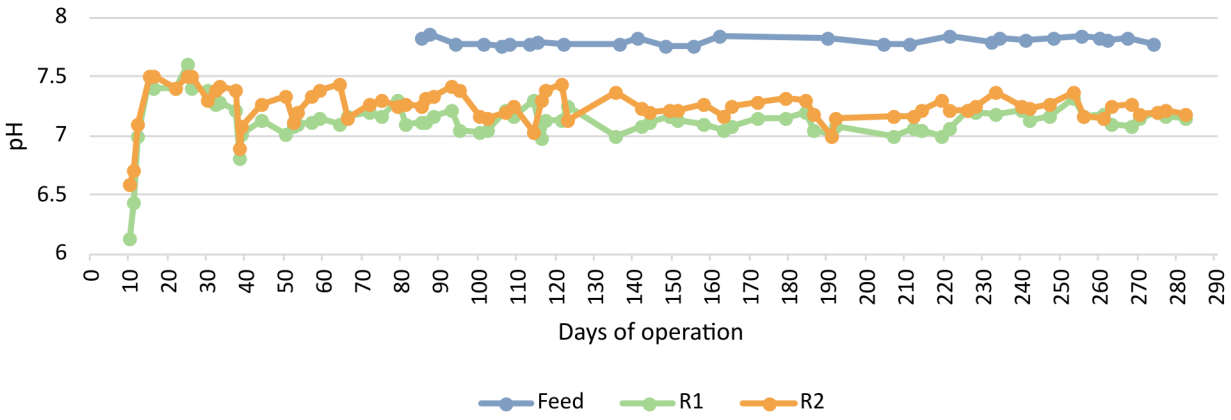
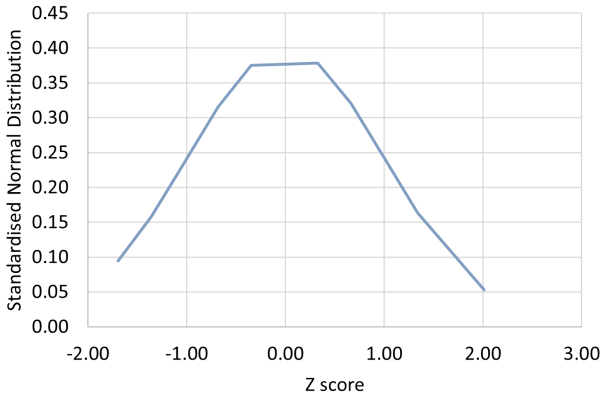
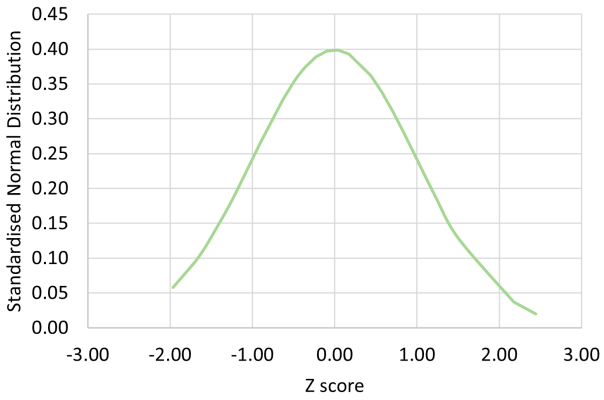


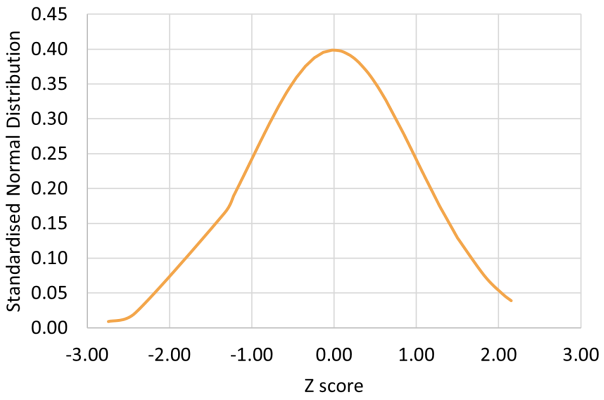
Figure 49: pH results



(a)



(b)



(c)

Figure 50: pH standardised normal distributions: (a) feed; (b) R1; (c) R2

A1.2 Chemical Oxygen Demand Data

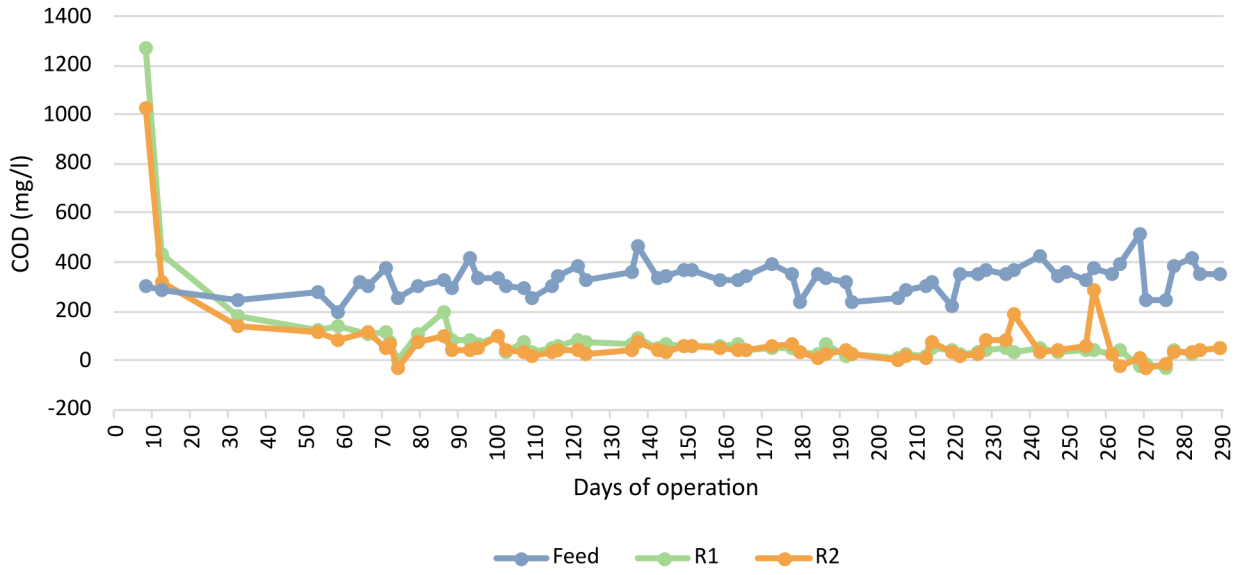
Table 26: Chemical oxygen demand results. conc.=concentration, rmvd.=concentration removed, rmvl.=removal efficiency. Rows coloured red show removal percentages > 100 %, rows coloured yellow show readings that fell outside of the normal distribution curve

	Feed	R1			R2		
	conc.	conc.	rmvd.	rmvl.	conc.	rmvd	rmvl
Day	(mg/l)	(mg/l)	(mg/l)	(%)	(mg/l)	(mg/l)	(%)
8	303.03	1272.73	-969.70	-320.00	1030.30	-727.27	-240.00
12	284.66	431.90	-147.24	-51.72	320.65	-35.99	-12.64
32	243.62	177.78	65.84	27.03	138.27	105.35	43.24
53	275.27	126.16	149.10	54.17	114.70	160.57	58.33
58	195.05	140.19	54.86	28.13	85.33	109.71	56.25
64	319.43						
66	302.32	105.53	196.79	65.09	111.23	191.09	63.21
71	372.09	111.63	260.47	70.00	49.61	322.48	86.67
72		78.10			69.66		
74	251.69	0.00	251.69	100.00	-29.96	281.65	111.90
79	305.20	110.98	194.22	63.64	70.91	234.30	76.77
86	327.75	199.63	128.12	39.09	95.34	232.40	70.91
88	297.87	79.43	218.44	73.33	42.55	255.32	85.71
93	419.27	80.15	339.11	80.88	43.16	376.11	89.71
95	330.86	66.67	264.20	79.85	46.91	283.95	85.82
100	337.41	97.96	239.46	70.97	97.96	239.46	70.97
102	301.89	35.22	266.67	88.33	40.25	261.64	86.67
107	294.60	76.19	218.41	74.14	35.56	259.05	87.93
109	253.16	30.38	222.78	88.00	20.25	232.91	92.00
114	303.80	50.63	253.16	83.33	35.44	268.35	88.33
116	344.30	60.76	283.54	82.35	45.57	298.73	86.76
121	380.71	82.32	298.39	78.38	41.16	339.55	89.19
123	324.18	73.20	250.98	77.42	26.14	298.04	91.94
135	360.13	66.88	293.25	81.43	41.16	318.97	88.57
137	463.02	92.60	370.42	80.00	72.03	391.00	84.44
142	333.12	50.47	282.65	84.85	40.38	292.74	87.88
144	343.22	65.62	277.60	80.88	32.81	310.41	90.44
149	363.41	55.52	307.89	84.72	55.52	307.89	84.72
151	363.85	55.98	307.87	84.62	55.98	307.87	84.62
158	326.53	60.64	265.89	81.43	51.31	275.22	84.29
163	326.53	69.97	256.56	78.57	41.98	284.55	87.14
165	340.43	38.91	301.52	88.57	43.77	296.66	87.14
172	389.06	53.50	335.56	86.25	58.36	330.70	85.00
177	350.15	53.50	296.66	84.72	63.22	286.93	81.94
179	235.79	31.66	204.13	86.57	31.66	204.13	86.57
184	353.68	27.44	326.24	92.24	10.55	343.13	97.02
186	336.84	69.66	267.19	79.32	27.44	309.40	91.85
191	320.00	14.78	305.22	95.38	40.11	279.89	87.47
193	235.79	27.44	208.35	88.36	27.44	208.35	88.36
205	252.63	6.33	246.30	97.49	-2.11	254.74	100.84
207	286.32	23.22	263.10	91.89	19.00	267.32	93.36
212	303.16	19.00	284.16	93.73	10.55	292.60	96.52
214	318.32	50.66	267.66	84.09	78.10	240.22	75.47

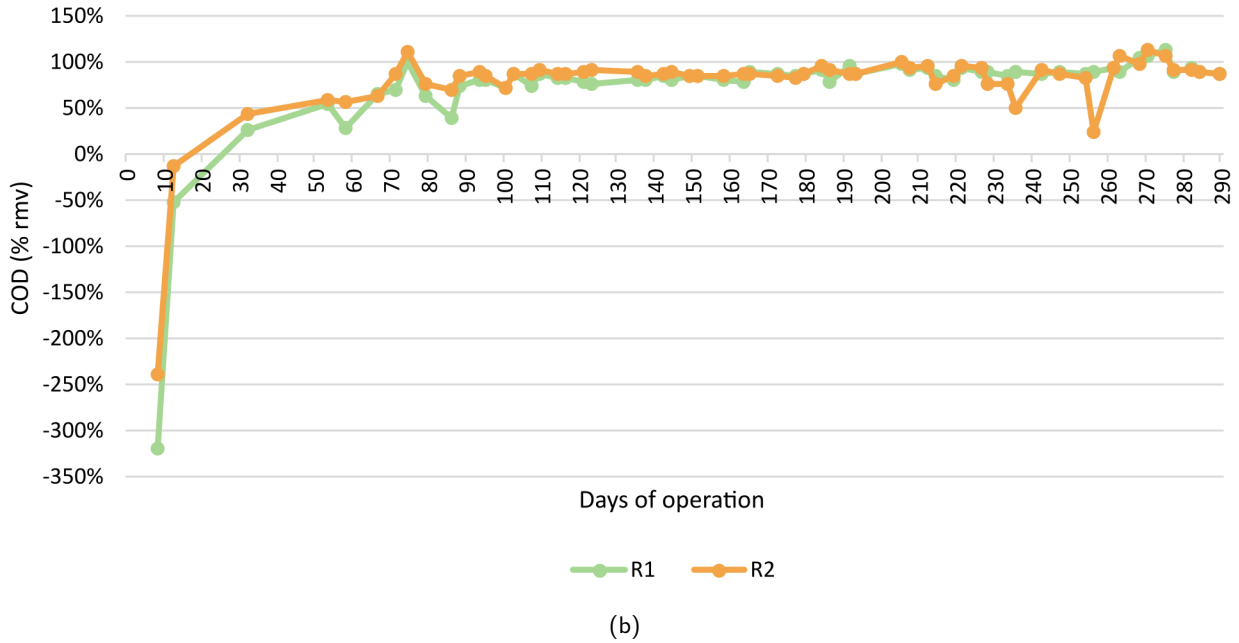
Continued...

Table 26 Continued.

	Feed	R1			R2		
	conc.	conc.	rmvd.	rmvl.	conc.	rmvd.	rmvl.
Day	(mg/l)	(mg/l)	(mg/l)	(%)	(mg/l)	(mg/l)	(%)
219	217.80	41.88	175.92	80.77	33.51	184.29	84.62
221	351.83	25.13	326.70	92.86	16.75	335.08	95.24
226	351.83	33.51	318.32	90.48	25.13	326.70	92.86
228	368.59	41.88	326.70	88.64	83.77	284.82	77.27
233	351.83	50.26	301.57	85.71	83.77	268.06	76.19
235	371.13	37.11	334.02	90.00	185.57	185.57	50.00
242	420.62	49.48	371.13	88.24	32.99	387.63	92.16
247	346.39	37.11	309.28	89.29	41.24	305.15	88.10
249	362.89						
254	329.90	41.24	288.66	87.50	57.73	272.16	82.50
256	379.38	41.24	338.14	89.13	288.66	90.72	23.91
261	348.19	24.87	323.32	92.86	24.87	323.32	92.86
263	389.64	41.45	348.19	89.36	-24.87	414.51	106.38
268	513.99	-24.87	538.86	104.84	8.29	505.70	98.39
270	248.70	-16.58	265.28	106.67	-33.16	281.87	113.33
275	248.70	-33.16	281.87	113.33	-16.58	265.28	106.67
277	384.00	40.00	344.00	89.58	32.00	352.00	91.67
282	416.00	24.00	392.00	94.23	32.00	384.00	92.31
284	352.00	40.00	312.00	88.64	40.00	312.00	88.64
289	352.00	48.00	304.00	86.36	48.00	304.00	86.36



(a)



(b)

Figure 51: Chemical oxygen demand results: (a) influent and effluent COD concentration (mg/l); (b) effluent COD removal efficiency (%)

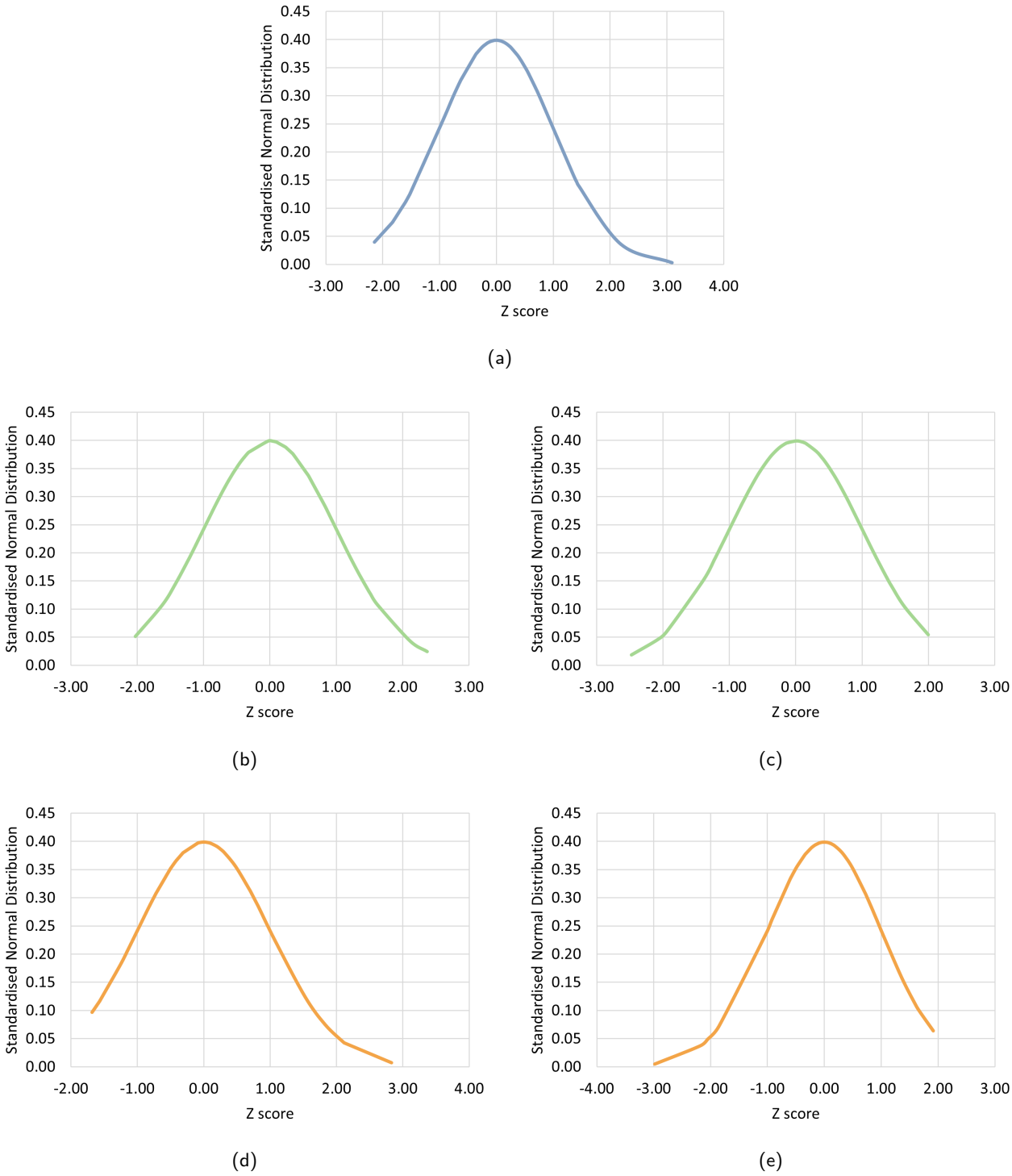


Figure 52: Steady-state chemical oxygen demand standardised normal distributions: (a) feed concentration; (b) R1 concentration; (c) R1 removal efficieny; (d) R2 concentration; (e) R2 removal efficiency

A1.3 Biogas Production Data

Table 27: Biogas production results. Rows coloured grey were taken using the gas bottle collection method

Day	R1	R2
31		0.83
37	0.12	
53	0.21	0.56
54	0.33	0.38
96	3.37	4.67
100	0.60	1.40
101	0.73	1.58
103	1.23	1.07
107	1.37	2.30
109	0.63	1.26
114	0.14	2.14
122	1.21	1.68
135	1.89	1.83
137	0.18	-0.18
138	1.18	0.51
142	0.86	0.86
145	0.13	1.17
149	0.00	1.57
151	0.50	1.15
157	-0.02	0.51
159	9.20	10.91
162	2.09	11.56
164	14.10	9.80
165	8.29	8.68
166	7.59	3.41
172	5.57	9.65
173	6.60	7.87
176	7.11	8.63
177	7.02	8.32
178	9.79	8.67
179	6.57	2.04
180	8.83	1.04
184	7.71	5.86
187	6.32	8.04
192	6.82	10.43
198	9.25	8.70
199	8.89	6.59
200	10.80	9.50
201	9.42	9.71
204	9.97	10.57
206	9.35	9.47
207	7.90	7.85
211	12.26	11.31
212	8.68	9.20
213	11.15	11.96
215	7.66	11.08
219	9.13	16.23
220	8.96	10.58
221	6.86	11.06
222	9.91	11.95
228	5.86	9.86
229	9.82	13.44
232	1.36	6.82
233	4.93	10.13
234	10.00	13.74
235	3.52	8.57
236	6.08	13.45
241	6.15	13.60
242	4.31	7.81
247	2.42	5.96
248	7.81	13.26
249	12.70	19.63
255	6.71	10.09
257	11.43	11.83
261	17.48	20.29
263	4.10	6.99
264	12.58	14.97
268	12.57	9.29
269	5.95	6.94
270		9.53
271	8.58	8.92
276	9.07	10.52
277	8.83	7.52
278	7.96	6.39
282	8.04	9.48
284	2.64	7.52

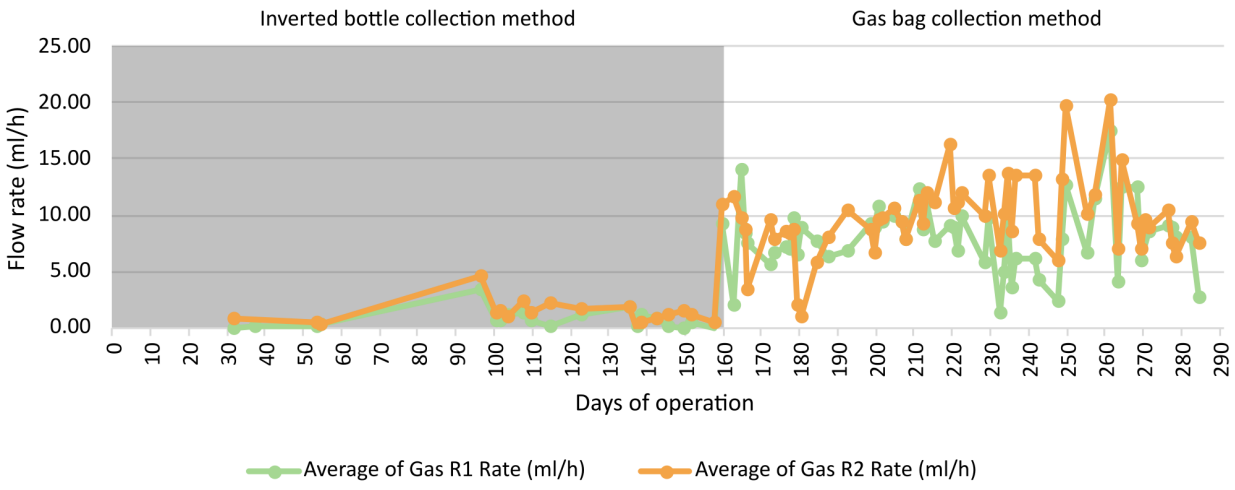
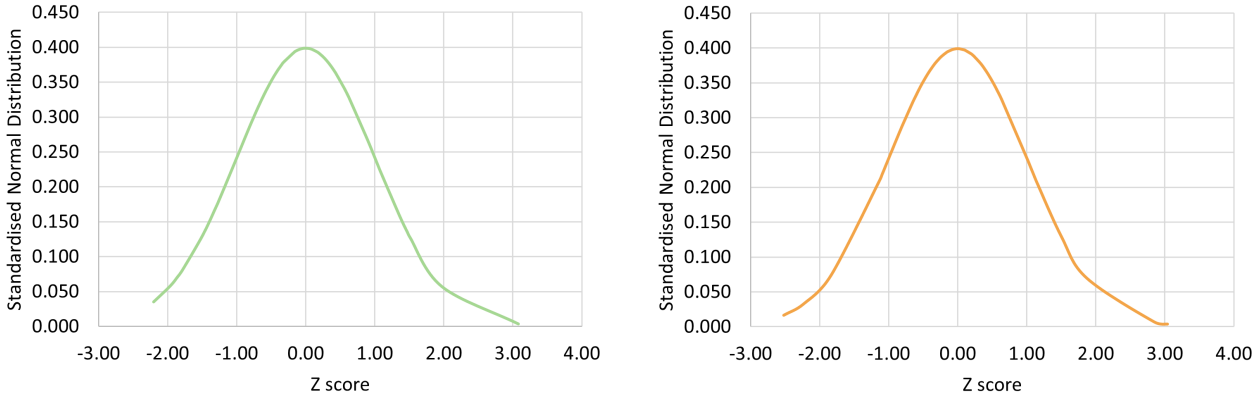


Figure 53: Biogas production results



(a) (b)

Figure 54: Gas bag biogas production standardised normal distributions: (a) R1; (b) R2

A1.4 Biogas Composition Data

Table 28: Biogas composition results. Rows coloured grey were taken using the Geotech GA2000 Infrared Gas Analyser

	R1				R2			
Day	Methane	Nitrogen	CO2	Oxygen	Methane	Nitrogen	CO2	Oxygen
22					0.10%	81.20%	0.10%	18.60%
29					0.20%	80.80%	0.10%	18.90%
44	4.30%	78.10%	0.20%	17.40%	8.20%	73.90%	0.50%	17.40%
50	5.90%	80.70%	5.30%	8.00%	8.20%	83.80%	5.30%	2.80%
52	1.00%	81.60%	0.50%	16.90%	0.90%	82.00%	0.60%	16.50%
53	2.90%	81.20%	0.60%	15.30%	7.80%	75.40%	1.00%	15.90%
57	0.40%	80.40%	0.10%	19.10%	6.70%	77.30%	0.60%	15.40%
61	1.00%	80.10%	0.00%	18.90%	8.70%	74.50%	0.60%	16.20%
74	1.12%	90.10%	5.05%	2.41%	19.59%	72.72%	5.72%	1.96%
122	23.30%	64.73%	1.27%	10.70%	37.12%	53.32%	2.93%	6.62%
135	34.24%	55.92%	2.96%	5.97%	16.36%	68.40%	0.59%	13.81%
136	37.23%	53.20%	3.57%	5.58%	8.40%	74.29%	0.62%	16.69%
142	10.89%	56.40%	0.52%	11.53%	52.58%	37.30%	6.92%	2.08%
158	18.29%	70.24%	1.64%	8.98%	55.67%	33.22%	8.89%	1.74%
162					16.31%	66.82%	0.74%	15.31%
165	17.69%	50.60%	0.61%	10.83%				
172	31.02%	56.80%	1.15%	10.11%	33.84%	40.30%	2.96%	6.89%
179	51.18%	32.31%	8.77%	1.21%				
180					5.21%	75.74%	0.30%	17.97%
184					30.46%	55.98%	0.97%	11.32%
185	30.11%	50.64%	1.43%	9.16%	22.43%	62.43%	0.54%	13.69%
186	42.18%	45.55%	7.61%	4.67%	57.34%	32.49%	8.79%	1.38%
192	35.77%	53.62%	1.96%	8.66%	39.22%	48.88%	3.01%	8.56%
198	16.69%	67.46%	0.45%	14.60%	28.26%	58.88%	1.05%	11.81%
207	36.73%	39.29%	3.08%	4.93%	18.00%	66.19%	0.44%	14.90%
212	57.31%	31.59%	10.45%	0.65%	38.69%	49.83%	1.94%	9.54%
214	49.02%	39.98%	6.52%	3.94%	25.64%	59.11%	2.09%	12.63%
218	37.25%	49.36%	4.85%	7.95%				
219	39.98%	47.20%	5.25%	7.07%				
228	48.49%	29.14%	8.34%	1.21%	56.89%	32.05%	9.38%	1.20%
229	57.81%	30.36%	10.27%	0.96%	62.55%	25.43%	11.04%	0.51%
232	52.75%	38.35%	6.19%	1.61%	59.12%	32.57%	6.10%	1.06%
233	52.74%	36.47%	9.88%	0.63%	59.26%	29.24%	9.77%	0.77%
235	52.39%	35.88%	9.36%	1.28%	61.03%	27.36%	10.26%	0.71%
236	53.75%	35.46%	8.30%	1.71%	62.13%	27.51%	8.33%	1.54%
242	53.34%	35.45%	9.83%	1.38%	56.19%	33.29%	9.23%	1.29%
246	55.64%	29.19%	9.59%	1.32%	63.06%	25.21%	9.64%	1.23%
248	57.28%	33.19%	7.95%	1.58%	59.17%	31.58%	7.42%	1.84%
256	52.40%	37.11%	9.52%	0.96%	54.21%	35.81%	8.80%	1.18%
261	49.39%	38.90%	8.31%	2.12%	55.92%	33.32%	8.64%	1.30%
263	55.86%	33.37%	8.49%	1.25%	47.73%	39.87%	6.99%	4.61%
267	59.54%	29.60%	9.72%	0.62%	48.47%	40.11%	6.36%	5.06%
283	57.55%	25.34%	9.95%	0.91%	46.14%	41.65%	4.15%	7.12%
289	55.92%	32.42%	9.28%	1.31%	53.48%	35.52%	7.89%	2.30%
290	41.14%	28.25%	6.73%	2.64%	50.18%	37.34%	7.44%	4.01%

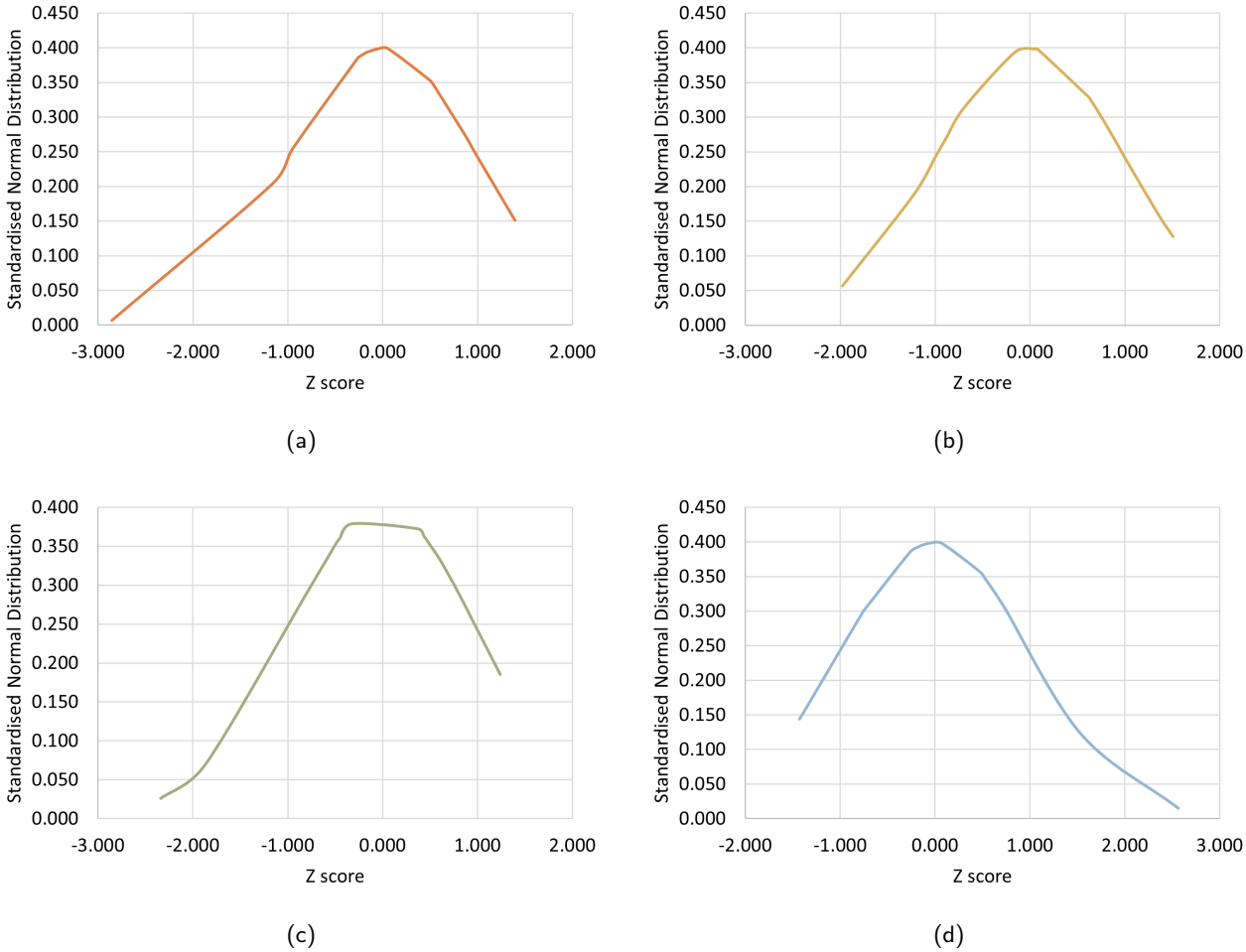


Figure 55: R1 steady-state biogas composition standardised normal distributions: (a) CH_4; (b) N_2; (c) CO_2; (d) O_2

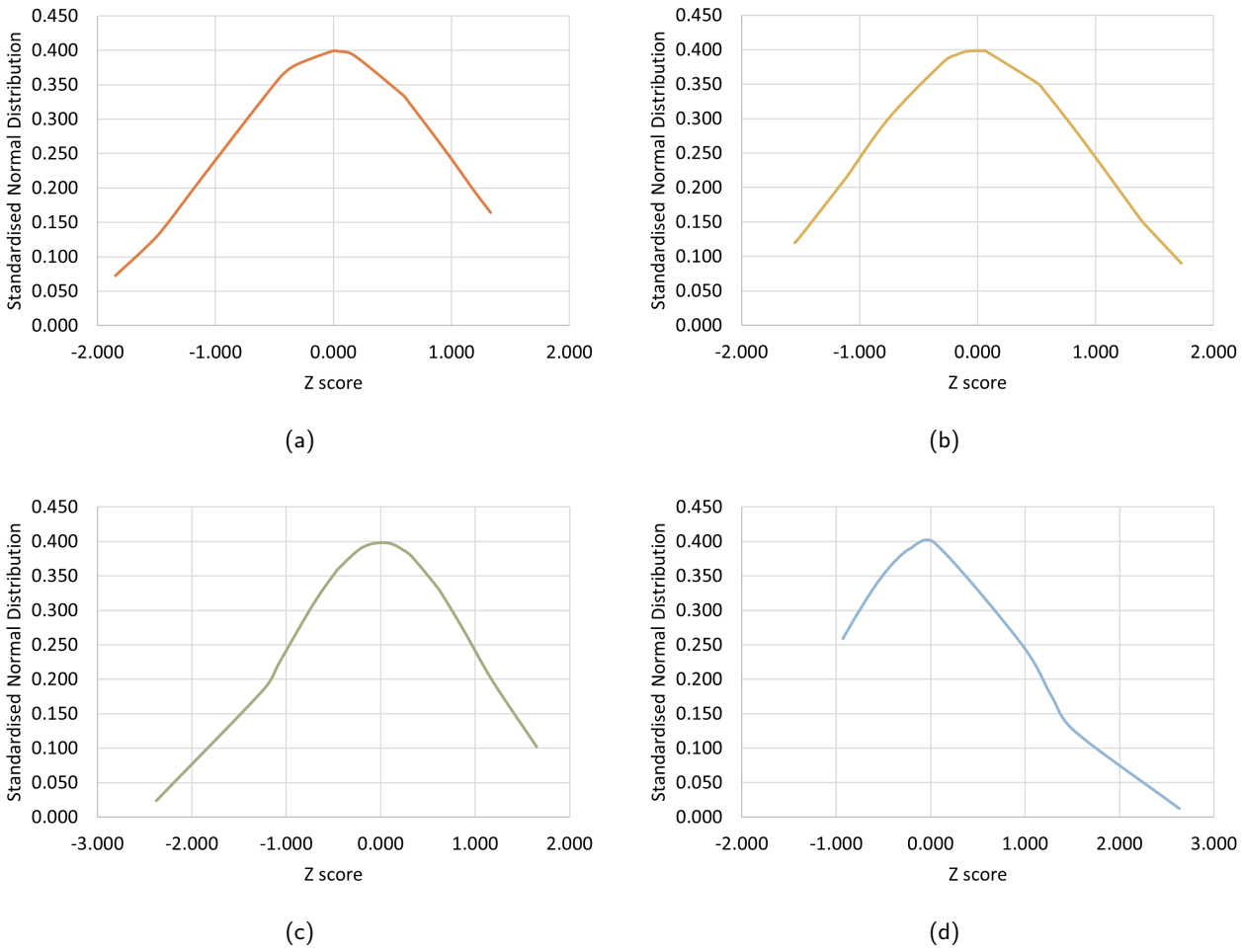


Figure 56: R2 steady-state biogas composition standardised normal distributions: (a) CH_4; (b) N_2; (c) CO_2; (d) O_2

A1.5 Dissolved Inorganic Nitrogen Data

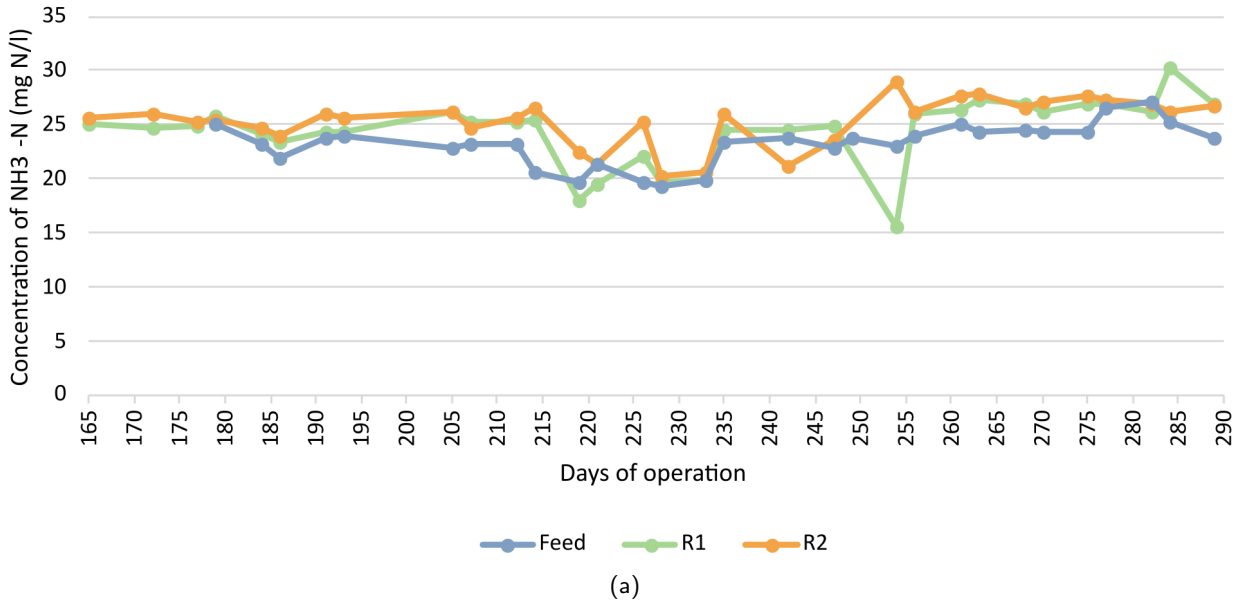
Table 29: Dissolved inorganic nitrogen results. conc.=concentration, rmvd.=concentration removed, rmvl.=removal efficiency.

	Feed	R1			R2		
Day	conc. (mg N/l)	conc. (mg N/l)	rmvd. (mg N/l)	rmvl. (%)	conc. (mg N/l)	rmvd. (mg N/l)	rmvl. (%)
Ammonia							
165		24.99			25.68		
172		24.72			25.95		
177		24.93			25.32		
179	25.08	25.80	-0.72	-2.86	25.48	-0.40	-1.60
184	23.21	24.10	-0.90	-3.86	24.68	-1.47	-6.35
186	21.98	23.39	-1.41	-6.41	24.00	-2.02	-9.19
191	23.72	24.32	-0.60	-2.51	26.09	-2.37	-9.99
193	24.00	24.27	-0.27	-1.12	25.69	-1.69	-7.03
205	22.94	26.26	-3.33	-14.51	26.27	-3.34	-14.56
207	23.14	25.30	-2.16	-9.35	24.62	-1.48	-6.38
212	23.20	25.35	-2.15	-9.27	25.59	-2.39	-10.30
214	20.53	25.43	-4.90	-23.86	26.48	-5.95	-28.96
219	19.71	18.03	1.67	8.49	22.48	-2.77	-14.06
221	21.31	19.58	1.73	8.12	21.40	-0.09	-0.40
226	19.62	22.03	-2.41	-12.27	25.34	-5.72	-29.15
228	19.27	19.65	-0.38	-1.98	20.24	-0.97	-5.06
233	19.95	19.92	0.02	0.12	20.71	-0.76	-3.80
235	23.41	24.45	-1.04	-4.43	26.07	-2.65	-11.34
242	23.74	24.52	-0.78	-3.30	21.11	2.63	11.09
247	22.83	24.91	-2.08	-9.10	23.54	-0.71	-3.09
249	23.78						
254	23.09	15.68	7.41	32.09	29.02	-5.93	-25.69
256	24.00	25.96	-1.96	-8.16	26.19	-2.19	-9.12
261	25.06	26.44	-1.38	-5.51	27.59	-2.53	-10.09
263	24.30	27.33	-3.02	-12.44	27.80	-3.50	-14.41
268	24.43	26.92	-2.49	-10.19	26.62	-2.20	-9.00
270	24.25	26.28	-2.03	-8.38	27.05	-2.80	-11.55
275	24.28	26.88	-2.61	-10.73	27.61	-3.33	-13.73
277	26.60	26.98	-0.38	-1.43	27.30	-0.70	-2.62
282	27.13	26.16	0.97	3.58	26.89	0.23	0.86
284	25.24	30.37	-5.12	-20.30	26.20	-0.96	-3.80
289	23.82	26.86	-3.05	-12.80	26.83	-3.01	-12.65
Nitrate							
235	7.23	0.53	6.70	92.74	0.37	6.86	94.91
242	6.78	0.35	6.43	94.84	0.25	6.52	96.25
247	7.02	0.29	6.74	95.91	0.36	6.67	94.93
249	6.74						
254	6.90	0.33	6.57	95.23	0.34	6.56	95.02
256	6.69	0.39	6.30	94.14	0.44	6.26	93.48
261	6.67	0.03	6.65	99.60			
263	6.86	0.04	6.82	99.45	0.26	6.61	96.27
268	6.44	0.02	6.41	99.63			
270	6.40						

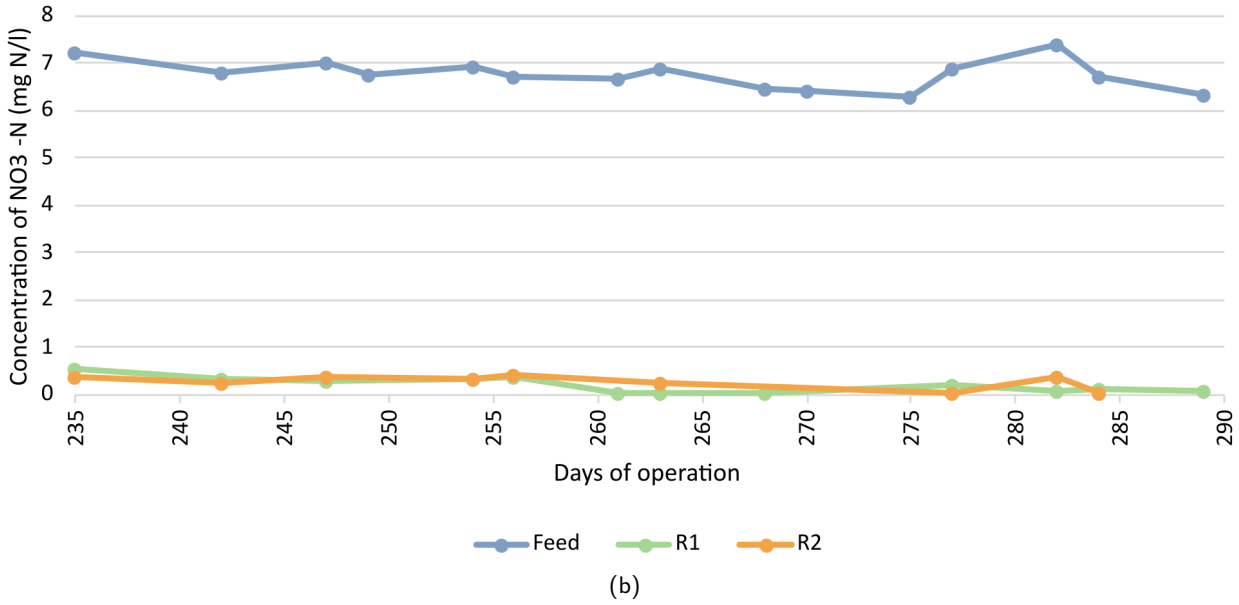
Continued...

Table 29 Continued.

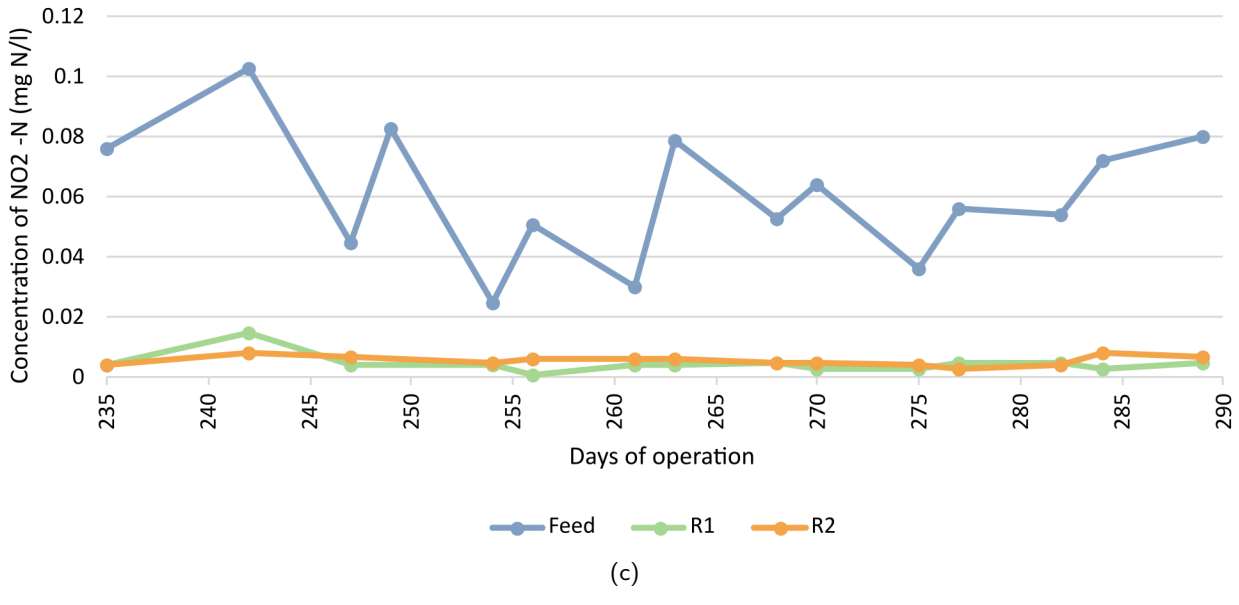
Day	Feed conc. (mg N/l)	R1 conc. (mg N/l)	R1 rmvd. (mg N/l)	R1 rmvl. (%)	R2 conc. (mg N/l)	R2 rmvd. (mg N/l)	R2 rmvl. (%)
275	6.30						
277	6.87	0.19	6.68	97.23	0.04	6.82	99.39
282	7.40	0.09	7.32	98.81	0.37	7.03	94.95
284	6.73	0.12	6.61	98.28	0.03	6.70	99.57
289	6.32	0.08	6.24	98.78			
Nitrite							
235	0.08	0.00	0.07	94.74	0.00	0.07	94.74
242	0.10	0.02	0.09	85.44	0.01	0.10	92.23
247	0.05	0.00	0.04	91.11	0.01	0.04	84.44
249	0.08						
254	0.03	0.00	0.02	84.00	0.01	0.02	80.00
256	0.05	0.00	0.05	98.04	0.01	0.05	88.24
261	0.03	0.00	0.03	86.67	0.01	0.02	80.00
263	0.08	0.00	0.08	94.94	0.01	0.07	92.41
268	0.05	0.01	0.05	90.57	0.01	0.05	90.57
270	0.06	0.00	0.06	95.31	0.01	0.06	92.19
275	0.04	0.00	0.03	91.67	0.00	0.03	88.89
277	0.06	0.01	0.05	91.07	0.00	0.05	94.64
282	0.05	0.01	0.05	90.74	0.00	0.05	92.59
284	0.07	0.00	0.07	95.83	0.01	0.06	88.89
289	0.08	0.01	0.08	93.75	0.01	0.07	91.25
Total N							
235	30.72	24.98	5.74	18.68	26.44	4.28	13.93
242	30.62	24.89	5.73	18.72	21.37	9.25	30.21
247	29.90	25.20	4.70	15.72	23.90	6.00	20.07
249	30.60						
254	30.02	16.01	14.01	46.66	29.37	0.65	2.16
256	30.75	26.36	4.39	14.28	26.64	4.11	13.37
261	31.76	26.47	5.29	16.66			
263	31.24	27.37	3.88	12.41	28.07	3.18	10.17
268	30.91	26.94	3.97	12.84			
270	30.71						
275	30.61						
277	33.52	27.17	6.35	18.93	27.34	6.18	18.44
282	34.58	26.25	8.33	24.10	27.27	7.31	21.14
284	32.04	30.48	1.56	4.85	26.24	5.80	18.11
289	30.22	26.95	3.27	10.82			



(a)



(b)



(c)

Figure 57: Dissolved inorganic nitrogen results, all readings in mg N/l: (a) ammonia; (b) nitrate; (c) nitrite

A2 Stoichiometry of Denitrification and Nitric Oxide Dismutation

A2.1 Cell Synthesis Reaction

Equation 26 describes the cell synthesis reaction (R_c) using NH_4^+ as the nitrogen source (Rittmann and McCarty 2020).

$$\frac{1}{5}CO_2 + \frac{1}{20}HCO_3^- + \frac{1}{20}NH_4^+ + H^+ + e^- \rightarrow \frac{1}{20}C_5H_7O_2N + \frac{9}{20}H_2O \tag{26}$$

A2.2 Electron Donor Reactions

Equation 27 describes the electron donor reaction (R_d) using glucose (Rittmann and McCarty 2020).

$$\frac{1}{24}C_6H_{12}O_6 + \frac{1}{4}H_2O \rightarrow \frac{1}{4}CO_2 + H^+ + e^- \qquad \Delta G^\circ = 40.95kJ/e^- \tag{27}$$

Equation 28 describes the electron donor reaction (R_d) using acetate (Rittmann and McCarty 2020).

$$\frac{1}{8}CH_3COO^- + \frac{3}{8}H_2O \rightarrow \frac{1}{8}CO_2 + \frac{1}{8}HCO_3^- + H^+ + e^- \qquad \Delta G^\circ = 27.40kJ/e^- \tag{28}$$

A2.3 Electron Acceptor Reactions

A2.3.1 Denitrification

Equation 29 describes the electron acceptor reaction (R_a) using NO_3^- via conventional denitrification (Rittmann and McCarty 2020).

$$\frac{1}{5}NO_3^- + \frac{6}{5}H^+ + e^- \rightarrow \frac{1}{10}N_2 + \frac{3}{5}H_2O \qquad \Delta G^\circ = -72.20kJ/e^- \tag{29}$$

A2.3.2 Nitric Oxide Dismutation

Table 30 describes the free energy changes for each of the NOD process steps.

Table 30: Energetics of Nitric Oxide Dismutation Reaction Steps

Reaction Step	ΔG° (kJ/mol)	Reference
$\frac{1}{2}NO_3^- + H^+ + e^- \rightarrow \frac{1}{2}NO_2^- + \frac{1}{2}H_2O$	-41.65	Rittmann and McCarty (2020)
$NO_2^- + 2H^+ + e^- \rightarrow NO + H_2O$	-38.50	Kleerebezem and Lücker (2021)
$2NO \rightarrow N_2 + O_2$	-173.10	Ettwig et al. (2012)

Table 31 shows the compilation of the NOD process steps and the combined free energy change of the complete reaction.

Table 31: Nitric Oxide Dismutation Reaction Steps

				ΔG° (kJ/mol N)
	Step 1			
R_a:	$NO_3^- + 2H^+ + 2e^-$	$\rightarrow$	$NO_2^- + H_2O$	-83.30
-R_d:	$NO_2^- + 2H^+ + e^-$	$\rightarrow$	$NO + H_2O$	-38.50
R_e:	$NO_3^- + 4H^+ + 3e^-$	$\rightarrow$	$NO + 2H_2O$	-121.80
	Step 2			
R_a:	$NO_3^- + 4H^+ + 3e^-$	$\rightarrow$	$NO + 2H_2O$	-121.80
-R_d:	NO	$\rightarrow$	$0.5N_2 + 0.5O_2$	-86.55
R_e:	$\mathbf{NO_3^- + 4H^+ + 3e^-}$	$\rightarrow$	$\mathbf{0.5N_2 + 0.5O_2 + 2H_2O}$	**-208.35**

Equation 30 describes the electron acceptor reaction (R_a) using NO_3^- via NOD.

$$\frac{1}{3}NO_3^- + \frac{4}{3}H^+ + e^- \rightarrow \frac{1}{6}N_2 + \frac{1}{6}O_2 + \frac{2}{3}H_2O \qquad \Delta G^\circ = -69.45kJ/e^- \tag{30}$$

A2.4 Half Reactions

A2.4.1 Synthesis Half Reactions

Equation 31 describes the synthesis half reaction (R_s) for stoichiometry (Rittmann and McCarty 2020).

$$R_s = R_c - R_d \tag{31}$$

Table 32 describes the assembled synthesis half reactions using glucose and acetate as both the carbon and electron sources. The free energy changes of these reactions (ΔG_s°) will be calculated in subsection A2.5 below.

Table 32: Synthesis half reactions (anabolic)

				ΔG° (kJ/e$^-$)
	Glycolytic cell synthesis			
R_c:	$\frac{1}{5}CO_2 + \frac{1}{20}HCO_3^- + \frac{1}{20}NH_4^+ + H^+ + e^-$	$\rightarrow$	$\frac{1}{20}C_5H_7O_2N + \frac{9}{20}H_2O$	
-R_d:	$\frac{1}{24}C_6H_{12}O_6 + \frac{1}{4}H_2O$	$\rightarrow$	$\frac{1}{4}CO_2 + H^+ + e^-$	-40.95
R_s:	$\mathbf{\frac{1}{24}C_6H_{12}O_6 + \frac{1}{20}HCO_3^- + \frac{1}{20}NH_4^+}$	$\rightarrow$	$\mathbf{\frac{1}{20}C_5H_7O_2N + \frac{1}{20}CO_2 + \frac{1}{5}H_2O}$	
	Acetotrophic cell synthesis			
R_c:	$\frac{1}{5}CO_2 + \frac{1}{20}HCO_3^- + \frac{1}{20}NH_4^+ + H^+ + e^-$	$\rightarrow$	$\frac{1}{20}C_5H_7O_2N + \frac{9}{20}H_2O$	
-R_d:	$\frac{1}{8}CH_3COO^- + \frac{3}{8}H_2O$	$\rightarrow$	$\frac{1}{8}CO_2 + \frac{1}{8}HCO_3^- + H^+ + e^-$	-27.40
R_s:	$\mathbf{\frac{1}{8}CH_3COO^- + \frac{3}{40}CO_2 + \frac{1}{20}NH_4^+}$	$\rightarrow$	$\mathbf{\frac{1}{20}C_5H_7O_2N + \frac{3}{40}HCO_3^- + \frac{3}{40}H_2O}$	

A2.4.2 Energy Half Reactions

Equation 32 describes the energy half reaction (R_e) for stoichiometry (Rittmann and McCarty 2020).

$$R_e = R_a - R_d \tag{32}$$

Table 33 describes the assembled energy half reactions for each of the NO_3^- reduction pathways. The ΔG° values on the final R_e equations is the free energy for the full energy reaction (ΔG_r°)

Table 33: Energy half reactions (catabolic)

				ΔG_r° (kJ/e$^-$)
	Glycolytic denitrification			
R_a:	$\frac{1}{5}NO_3^- + \frac{6}{5}H^+ + e^-$	$\rightarrow$	$\frac{1}{10}N_2 + \frac{3}{5}H_2O$	-72.20
-R_d:	$\frac{1}{24}C_6H_{12}O_6 + \frac{1}{4}H_2O$	$\rightarrow$	$\frac{1}{4}CO_2 + H^+ + e^-$	-40.95
R_e:	$\mathbf{\frac{1}{24}C_6H_{12}O_6 + \frac{1}{5}NO_3^- + \frac{1}{5}H^+}$	$\rightarrow$	$\mathbf{\frac{1}{4}CO_2 + \frac{1}{10}N_2 + \frac{7}{20}H_2O}$	**-113.15**
	Acetotrophic denitrification			
R_a:	$\frac{1}{5}NO_3^- + \frac{6}{5}H^+ + e^-$	$\rightarrow$	$\frac{1}{10}N_2 + \frac{3}{5}H_2O$	-72.20
-R_d:	$\frac{1}{8}CH_3COO^- + \frac{3}{8}H_2O$	$\rightarrow$	$\frac{1}{8}CO_2 + \frac{1}{8}HCO_3^- + H^+ + e^-$	-27.40
R_e:	$\mathbf{\frac{1}{8}CH_3COO^- + \frac{1}{5}NO_3^- + \frac{1}{5}H^+}$	$\rightarrow$	$\mathbf{\frac{1}{8}CO_2 + \frac{1}{8}HCO_3^- + \frac{1}{10}N_2 + \frac{9}{40}H_2O}$	**-99.60**
	Glycolytic nitric oxide dismutation			
R_a:	$\frac{1}{3}NO_3^- + \frac{4}{3}H^+ + e^-$	$\rightarrow$	$\frac{1}{6}N_2 + \frac{1}{6}O_2 + \frac{2}{3}H_2O$	-69.45
-R_d:	$\frac{1}{24}C_6H_{12}O_6 + \frac{1}{4}H_2O$	$\rightarrow$	$\frac{1}{4}CO_2 + H^+ + e^-$	-40.95
R_e:	$\mathbf{\frac{1}{24}C_6H_{12}O_6 + \frac{1}{3}NO_3^- + \frac{1}{3}H^+}$	$\rightarrow$	$\mathbf{\frac{1}{4}CO_2 + \frac{1}{6}N_2 + \frac{1}{6}O_2 + \frac{5}{12}H_2O}$	**-110.40**
	Acetotrophic nitric oxide dismutation			
R_a:	$\frac{1}{3}NO_3^- + \frac{4}{3}H^+ + e^-$	$\rightarrow$	$\frac{1}{6}N_2 + \frac{1}{6}O_2 + \frac{2}{3}H_2O$	-69.45
-R_d:	$\frac{1}{8}CH_3COO^- + \frac{3}{8}H_2O$	$\rightarrow$	$\frac{1}{8}CO_2 + \frac{1}{8}HCO_3^- + H^+ + e^-$	-27.40
R_e:	$\mathbf{\frac{1}{8}CH_3COO^- + \frac{1}{3}NO_3^- + \frac{1}{3}H^+}$	$\rightarrow$	$\mathbf{\frac{1}{8}CO_2 + \frac{1}{8}HCO_3 + \frac{1}{6}N_2 + \frac{1}{6}O_2 + \frac{7}{24}H_2O}$	**-96.85**

A2.5 Reaction Energetics

A2.5.1 Free Energy Change of Cell Synthesis

Equation 33 describes the energetic cost of converting the carbon source to activated acetate (acetyl coenzyme-A) (ΔG_p), where ΔG_c° is the free energy change of the electron donor reaction (R_d) (Rittmann and McCarty 2020).

$$\Delta G_p = 30.9 - \Delta G_c^\circ \tag{33}$$

Equation 34 describes the energy requirement for cell synthesis (ΔG_s) (Rittmann and McCarty 2020).

$$\Delta G_s = \frac{\Delta G_p}{\varepsilon^n} + \frac{\Delta G_{pc}}{\varepsilon} \tag{34}$$

When NH_4^+ is used as the nitrogen source (Equation 26), the energy required to convert activated actetate to cellular carbon (ΔG_{pc}) is 18.8 kJ/e$^-$. ε is included as a term for energy-transfer efficiency, as energy is always lost in the electron transfers. The exponent n is used for the energy-transfer efficiency for conversion of carbon to pyruvate. When ΔG_p is negative, n = -1. When, ΔG_p is positive, n = + 1 (Rittmann and McCarty 2020).

A2.5.2 Energetic Balance Between Energy and Synthesis Reactions

Equation 35 describes the energy balance between the anabolic and catabolic reactions (Rittmann and McCarty 2020).

$$A\varepsilon\Delta G_r + \Delta G_s = 0 \tag{35}$$

A is the amount of energy (expressed in equivalents of electron donor) required to provide ΔG_s. The energy released by donor oxidation, including the portion that is again lost through transfer inefficiencies, is then $A\varepsilon\Delta G_r$. Solving for A, the equation becomes as described in Equation 36.

$$A = -\frac{\Delta G_s}{\varepsilon\Delta G_r} \tag{36}$$

Equation 37 describes the split between energy and synthesis (Rittmann and McCarty 2020).

$$f_s^0 = \frac{1}{1+A} \qquad \text{and} \qquad f_e^0 = 1 - f_s^0 \tag{37}$$

Table 34 describes the ΔG_s, A, f_s^0, and f_e^0 values obtained at various ε values.

Table 34: Energetics with various energy transfer efficiencies

ε	1.0	0.9	0.8	0.7	0.6	0.5	0.4	0.3	0.2	0.1
Glycolytic cell synthesis: $\Delta G_p = -10.05$, $\Delta G_{pc} = 18.8$, $n = -1$										
ΔG_s	8.75	11.84	15.46	19.82	25.30	32.58	42.98	59.65	91.99	187.00
Acetotrophic cell synthesis: $\Delta G_p = 3.50$, $\Delta G_{pc} = 18.8$, $n = +1$										
ΔG_s	22.30	24.78	27.88	31.86	37.17	44.60	55.75	74.33	111.50	223.00
Glycolytic denitrification										
A	0.08	0.12	0.17	0.25	0.37	0.58	0.95	1.76	4.06	16.53
f_s^0	0.93	0.90	0.85	0.80	0.73	0.63	0.51	0.36	0.20	0.06
f_e^0	0.07	0.10	0.15	0.20	0.27	0.37	0.49	0.64	0.80	0.94
Acetotrophic denitrification										
A	0.22	0.28	0.35	0.46	0.62	0.90	1.40	2.49	5.60	22.39
f_s^0	0.82	0.78	0.74	0.69	0.62	0.53	0.42	0.29	0.15	0.04
f_e^0	0.18	0.22	0.26	0.31	0.38	0.47	0.58	0.71	0.85	0.96
Glycolytic NOD										
A	0.08	0.12	0.18	0.26	0.38	0.59	0.97	1.80	4.17	16.94
f_s^0	0.93	0.89	0.85	0.80	0.72	0.63	0.51	0.36	0.19	0.06
f_e^0	0.07	0.11	0.15	0.20	0.28	0.37	0.49	0.64	0.81	0.94
Acetotrophic NOD										
A	0.23	0.28	0.36	0.47	0.64	0.92	1.44	2.56	5.76	23.03
f_s^0	0.81	0.78	0.74	0.68	0.61	0.52	0.41	0.28	0.15	0.04
f_e^0	0.19	0.22	0.26	0.32	0.39	0.48	0.59	0.72	0.85	0.96

A2.6 Completed Equations

Equation 38 describes the complete stoichiometric reaction (R) (Rittmann and McCarty 2020).

$$R = f_e \cdot R_e + f_s \cdot R_s \tag{38}$$

Table 35 shows the final stoichiometric formulae using an ε value of 0.5.

Table 35: Completed stoichiometry

	Glycolytic denitrification		
$f_e^0 \cdot R_e$	$0.015C_6H_{12}O_6 + 0.073NO_3^- + 0.073H^+$	$\rightarrow$	$0.091CO_2 + 0.037N_2 + 0.128H_2O$
$f_s^0 \cdot R_s$	$0.026C_6H_{12}O_6 + 0.032HCO_3^- + 0.032NH_4^+$	$\rightarrow$	$0.032C_5H_7O_2N + 0.032CO_2 + 0.127H_2O$
R:	$0.042C_6H_{12}O_6 + 0.032HCO_3^- + 0.032NH_4^+ + 0.073NO_3^- + 0.073H^+$	$\rightarrow$	$0.032C_5H_7O_2N + 0.123CO_2 + 0.037N_2 + 0.255H_2O$
	Acetotrophic denitrification		
$f_e^0 \cdot R_e$	$0.059CH_3COO^- + 0.094NO_3^- + 0.094H^+$	$\rightarrow$	$0.059CO_2 + 0.059HCO_3^- + 0.047N_2 + 0.106H_2O$
$f_s^0 \cdot R_s$	$0.066CH_3COO^- + 0.040CO_2 + 0.026NH_4^+$	$\rightarrow$	$0.026C_5H_7O_2N + 0.040HCO_3^- + 0.040H_2O$
R:	$0.125CH_3COO^- + 0.040CO_2 + 0.026NH_4^+ + 0.094NO_3^- + 0.094H^+$	$\rightarrow$	$0.026C_5H_7O_2N + 0.059CO_2 + 0.099HCO_3^- + 0.047N_2 + 0.146H_2O$
	Glycolytic NOD		
$f_e^0 \cdot R_e$	$0.015C_6H_{12}O_6 + 0.124NO_3^- + 0.124H^+$	$\rightarrow$	$0.093CO_2 + 0.062N_2 + 0.155H_2O + 0.062O_2$
$f_s^0 \cdot R_s$	$0.026C_6H_{12}O_6 + 0.031HCO_3^- + 0.031NH_4^+$	$\rightarrow$	$0.031C_5H_7O_2N + 0.031CO_2 + 0.126H_2O$
R:	$0.042C_6H_{12}O_6 + 0.031HCO_3^- + 0.031NH_4^+ + 0.124NO_3^- + 0.124H^+$	$\rightarrow$	$0.031C_5H_7O_2N + 0.124CO_2 + 0.062N_2 + 0.280H_2O + 0.062O_2$
	Acetotrophic NOD		
$f_e^0 \cdot R_e$	$0.060CH_3COO^- + 0.160NO_3^- + 0.160H^+$	$\rightarrow$	$0.060CO_2 + 0.060HCO_3^- + 0.080N_2 + 0.140H_2O + 0.080O_2$
$f_s^0 \cdot R_s$	$0.065CH_3COO^- + 0.039CO_2 + 0.026NH_4^+$	$\rightarrow$	$0.026C_5H_7O_2N + 0.039HCO_3^- + 0.039H_2O$
R:	$0.125CH_3COO^- + 0.039CO_2 + 0.026NH_4^+ + 0.160NO_3^- + 0.160H^+$	$\rightarrow$	$0.026C_5H_7O_2N + 0.060CO_2 + 0.099HCO_3^- + 0.080N_2 + 0.179H_2O + 0.080O_2$

A3 Meta-Genomics Scripts and Output Details

A3.1 Library Prep

```
kneaddata \
     --input1 ${DIR}/sample_1.fq.gz \
     --input2 ${DIR}/sample_2.fq.gz \
     --output ${DIR} \
     --output-prefix sample \
     --trimmomatic ${DIR}/share/trimmomatic-0.39-2 \
     --threads 50 \
     --processes 25 \
     --run-trim-repetitive \
     --remove-intermediate-output \
     --run-fastqc-end
```

Table 36: Sequence file read counts from KneadData library prep

	Sample name	Raw Data		Post-Trimmomatic		Post-TRF	
		Forward	Reverse	Forward	Reverse	Forward	Reverse
P1	GR1P1biofilm	70,179,888	70,179,888	65,368,820	65,368,820	65,063,705	65,060,651
	GR1P1bulk	71,596,995	71,596,995	67,109,668	67,109,668	66,807,007	66,802,160
	GR2P1biofilm	93,699,670	93,699,670	84,745,329	84,745,329	84,340,920	84,329,893
	GR2P1bulk	93,669,651	93,669,651	85,283,850	85,283,850	84,879,256	84,878,026
P2	GR1P2biofilm	77,196,474	77,196,474	73,565,305	73,565,305	73,111,581	73,113,583
	GR1P2bulk	56,721,774	56,721,774	54,644,278	54,644,278	54,377,019	54,378,440
	GR2P2biofilm	103,164,616	103,164,616	98,448,451	98,448,451	97,932,698	97,932,926
	GR2P2bulk	73,117,299	73,117,299	70,332,632	70,332,632	70,027,337	70,030,971

A3.2 Assembly-Free Taxonomic Classification

```
kaiju -z 50 -v \
     -t ${DIR}/nodes.dmp \
     -f ${DIR}/kaiju_db_nr.fmi \
     -i ${DIR}/sample.trimmed.1.fastq \
     -j ${DIR}/sample.trimmed.2.fastq \
     > ${DIR}/sample_kaiju.out

kaiju2table -v \
     -t ${DIR}/nodes.dmp \
     -n ${DIR}/names.dmp \
     -r genus \
     -m 0.01 \
     -o ${DIR}/sample_tax-tab.tsv \
     -l superkingdom,phylum,class,order,family,genus \
     ${DIR}/sample_kaiju.out
```

Table 37: Read classifications from Kaiju assembly-free taxonomic profiling. BT = below threshold (belong to a (non-viral) genus with less than 0.01% of all reads). NVG = cannot be assigned to a (non-viral) genus.

Point	Sample name	Read count	Archaea	Bacteria	BT	NVG	unclassified	Viruses
P1	GR1P1biofilm	65,368,820	0.72%	31.46%	4.47%	20.87%	42.42%	0.06%
	GR1P1bulk	67,109,668	1.58%	49.05%	3.20%	18.01%	28.12%	0.03%
	GR2P1biofilm	84,745,329	0.69%	37.84%	4.58%	18.36%	38.49%	0.04%
	GR2P1bulk	85,283,850	1.23%	35.05%	4.01%	19.74%	39.91%	0.06%
P2	GR1P2biofilm	73,565,305	0.40%	16.51%	4.80%	24.83%	53.42%	0.04%
	GR1P2bulk	54,644,278	0.23%	33.07%	3.94%	22.69%	40.03%	0.03%
	GR2P2biofilm	98,448,451	1.21%	20.79%	4.99%	23.57%	49.37%	0.07%
	GR2P2bulk	70,332,632	0.32%	35.29%	4.08%	20.43%	39.85%	0.04%

A3.3 Diversity Analysis

A3.3.1 Alpha

```
library(tidyverse)
alphadata <- read.csv("DIR\\af-tax_alpha.csv")

richness <- function(x){sum(x>0)}

shannon <- function(x){rabund <- x[x>0]/sum(x)
     -sum(rabund * log(rabund))}

simpson <- function(x){rabund <- x[x>0]/sum(x)
     1-sum(rabund * rabund)}

alphadiversity <- alphadata %>%
group_by(sample) %>%
filter(superkingdom == "Bacteria" | superkingdom == ''Archaea'') %>%
summarise(richness = richness(reads),
     shannon = shannon(reads),
     simpson = simpson(reads),
     invsimpson = 1/simpson,
     n = sum(reads)
     )

alphadiversity$source <-
c("biofilm","bulk","biofilm","bulk","biofilm","bulk","biofilm","bulk")
alphadiversity_bacteria$reactor <- c("R1","R1","R1","R1","R2","R2","R2","R2")
alphadiversity_bacteria$point <- c("P1","P1","P2","P2","P1","P1","P2","P2")

alphadiversity %>% arrange(factor(sample, levels =
c("GR1P1biofilm","GR1P1bulk","GR2P1biofilm","GR2P1bulk",
"GR1P2biofilm","GR1P2bulk","GR2P2biofilm","GR2P2bulk")))

ggplot(alphadiversity,aes(x=sample, y=shannon)) +
     geom_point(aes(colour = factor(source), shape = factor(reactor)), size = 3) +
     facet_wrap(~point, scales = "free_x")
```

A3.3.2 Beta

```
library(tidyverse)
library(vegan)
betadata <- read.csv("DIR\\af-tax_beta.csv")

betaDF <- betadata %>%
group_by(sample) %>%
pivot_wider(names_from = taxon_id, values_from = reads) %>%
as.data.frame()

rownames(betaDF) <- betaDF$sample
betaDF <- betaDF[,-1]
betaMX <- as.matrix(betaDF)
dist <- vegdist(betaMX, method="bray", na.rm=TRUE)

pcoa_eig <- cmdscale(bacteriadist, eig=TRUE, add=TRUE)
positions <- pcoa_eig$points
colnames(positions) <- c("pcoa1","pcoa2")

percent <- 100 * pcoa_eig$eig / sum(pcoa_eig$eig)

pcoa_eigDF <- as.data.frame(positions)
pcoa_eigDF$source <-
c("biofilm","bulk","biofilm","bulk","biofilm","bulk","biofilm","bulk")
pcoa_eigDF$RP <- c("R1P1","R1P1","R1P2","R1P2","R2P1","R2P1","R2P2","R2P2")

ggplot(pcoa_eigDF,aes(x=pcoa1, y=pcoa2)) +
     geom_point(aes(colour = factor(source), shape = factor(RP)), size = 3) +
     scale_shape_manual(values=c(16, 21, 17, 24)) +
     labs(x = "PCo 1 (44.79%)", y = "PCo 2 (29.54%)")
```

Table 38: Principal coordinates analysis of Bray-Curtis dissimilarity

Point	Sample	pcoa1	pcoa2
P1	GR1P1biofilm	-0.08833	0.024996
	GR1P1bulk	-0.35356	-0.06514
	GR2P1biofilm	-0.09884	0.253318
	GR2P1bulk	-0.22753	0.021345
P2	GR1P2biofilm	0.327852	0.027649
	GR1P2bulk	0.150116	-0.26695
	GR2P2biofilm	0.227355	0.24196
	GR2P2bulk	0.062946	-0.23717

A3.4 Assembly

A3.4.1 MEGAHIT

```
megahit \
     -t 256 \
     -1 ${DIR}/sample.trimmed.1.fastq \
     -2 ${DIR}/sample.trimmed.2.fastq \
```

```
     --out-dir ${DIR} \
     --out-prefix sample
```

A3.4.2 QUAST

```
quast -t 56 \
     ${DIR}/sample.contigs.fa \
     -o ${DIR}/
```

A3.5 Alignment

A3.5.1 Bowtie2

```
bowtie2-build --threads 50 \
     ${DIR}/sample.contigs.fa \
     ${DIR}/sample.index

bowtie2 --threads 50 \
     -x ${DIR}/sample.index \
     -1 ${DIR}/sample.trimmed.1.fastq \
     -2 ${DIR}/sample.trimmed.2.fastq \
     -S ${DIR}/sample.aligned.sam
```

A3.5.2 SAMtools + HTSlib

```
samtools view -@25 -b --verbosity 5 \
     ${DIR}/sample.aligned.sam \
     -o ${DIR}/sample.aligned.bam

samtools sort -@25 \
     ${DIR}/sample.aligned.bam \
     -o ${DIR}/sample.sorted.bam

samtools index -@25 -b \
     ${DIR}/sample.sorted.bam \
     ${DIR}/sample.sorted.bam.bai
```

Table 39: Summary of QUAST reports from MEGAHIT assembly. All statistics are based on contigs of size >= 500 bp, unless otherwise noted (e.g., "no. contigs (>= 0 bp)" and "Total length (>= 0 bp)" include all contigs)

Point	Sample name	Total no. of contigs	of which, >= 500 bp	Total length (bp)	of those >= 500 bp	GC (%)	N50	N90	L50	L90
P1	GR1P1biofilm	760,201	417,437	868,036,819	737,221,745	51.47	2,946	646	33,341	286,916
	GR1P1bulk	567,557	302,867	634,442,996	533,198,523	49.17	2,996	645	24,736	208,306
	GR2P1biofilm	605,247	329,533	652,051,158	546,503,465	50.6	2,543	632	29,524	231,743
	GR2P1bulk	700,988	367,198	900,956,955	774,580,406	50.82	5,217	684	20,134	233,323
P2	GR1P2biofilm	790,894	441,072	1,051,830,578	923,021,343	52.02	4,534	703	27,482	284,947
	GR1P2bulk	720,622	412,060	906,050,198	788,786,416	51.38	3,634	668	28,394	275,007
	GR2P2biofilm	1,255,206	675,532	1,453,597,070	1,240,659,299	53.19	3,285	660	56,222	458,919
	GR2P2bulk	711,230	383,288	861,641,836	738,073,415	51.95	4,234	655	22,037	253,941

A3.6 Binning

```
jgi_summarize_bam_contig_depths \
     --outputDepth ${DIR}/sample.depth.txt \
     ${DIR}/sample.sorted.bam

metabat2 -t 15 \
     -i ${DIR}/sample.contigs.fa \
     -a ${DIR}/sample.depth.txt \
     -o ${DIR}
```

A3.7 Metagenome Assembled Genome Taxonomic Classification

A3.7.1 PhyloPhlAn 3.0

```
phylophlan_metagenomic --nproc 90 \
     -i ${DIR}/ \
     -e .fa \
     -d SGB.Jul20 \
     -n 1 \
     -o ${DIR} \
     --verbose 2>&1 | tee ${DIR}/sample/phylophlan_metagenomic.log
```

A3.7.2 CheckM

```
checkm lineage_wf -t 20 -x fa \
     -f ${DIR}/sample.lineage.tsv \
     ${DIR} \
     ${DIR}

checkm coverage -t 8 -x fa \
     ${DIR}/ \
     ${DIR}/sample.coverage.tsv \
     ${DIR}/sample.sorted.bam

checkm profile \
     -f ${DIR}/sample.profile.tsv \
     --tab_table \
     ${DIR}/sample.coverage.tsv
```

A3.8 16S rRNA Analysis

```
qiime tools import \
--type 'SampleData[PairedEndSequencesWithQuality]' \
--input-format PairedEndFastqManifestPhred33V2 \
--input-path ${DIR}/sample_manifest.tsv \
--output-path ${DIR}/sample_import.qza

qiime demux summarize \
--i-data ${DIR}/sample_import.qza \
--o-visualization ${DIR}/sample_demux.vis.qzv
```

```
qiime dada2 denoise-paired \
--i-demultiplexed-seqs ${DIR}/sample_import.qza \
--p-trunc-len-f 220 \
--p-trunc-len-r 220 \
--o-table ${DIR}/sample_table.qza \
--o-representative-sequences ${DIR}/sample_repseqs.qza \
--o-denoising-stats ${DIR}/sample_denoise.stats.qza

qiime feature-table summarize \
  --i-table ${DIR}/sample_table.qza \
  --o-visualization ${DIR}/sample_table.qzv \
  --m-sample-metadata-file ${DIR}/sample_metadata.tsv

qiime feature-table tabulate-seqs \
  --i-data ${DIR}/sample_repseqs.qza \
  --o-visualization ${DIR}/sample_repseqs.qzv

qiime metadata tabulate \
--m-input-file ${DIR}/sample_denoise.stats.qza \
--o-visualization ${DIR}/sample_denoise.stats.qzv

qiime feature-classifier classify-sklearn \
  --i-classifier ${DIR}/silva-138-99-nb-classifier.qza \
  --i-reads ${DIR}/sample_repseqs.qza \
  --o-classification ${DIR}/sample_taxonomy.qza

qiime metadata tabulate \
  --m-input-file ${DIR}/sample_taxonomy.qza \
  --o-visualization ${DIR}/sample_taxonomy.qzv

qiime taxa barplot \
  --i-table ${DIR}/sample_table.qza \
  --i-taxonomy ${DIR}/sample_taxonomy.qza \
  --m-metadata-file ${DIR}/sample_metadata.tsv \
  --o-visualization ${DIR}/sample_taxa.bar.plots.qzv
```

A4 Pathway Annotation

A4.1 Carbon Metabolism

A4.1.1 Aeromonas media

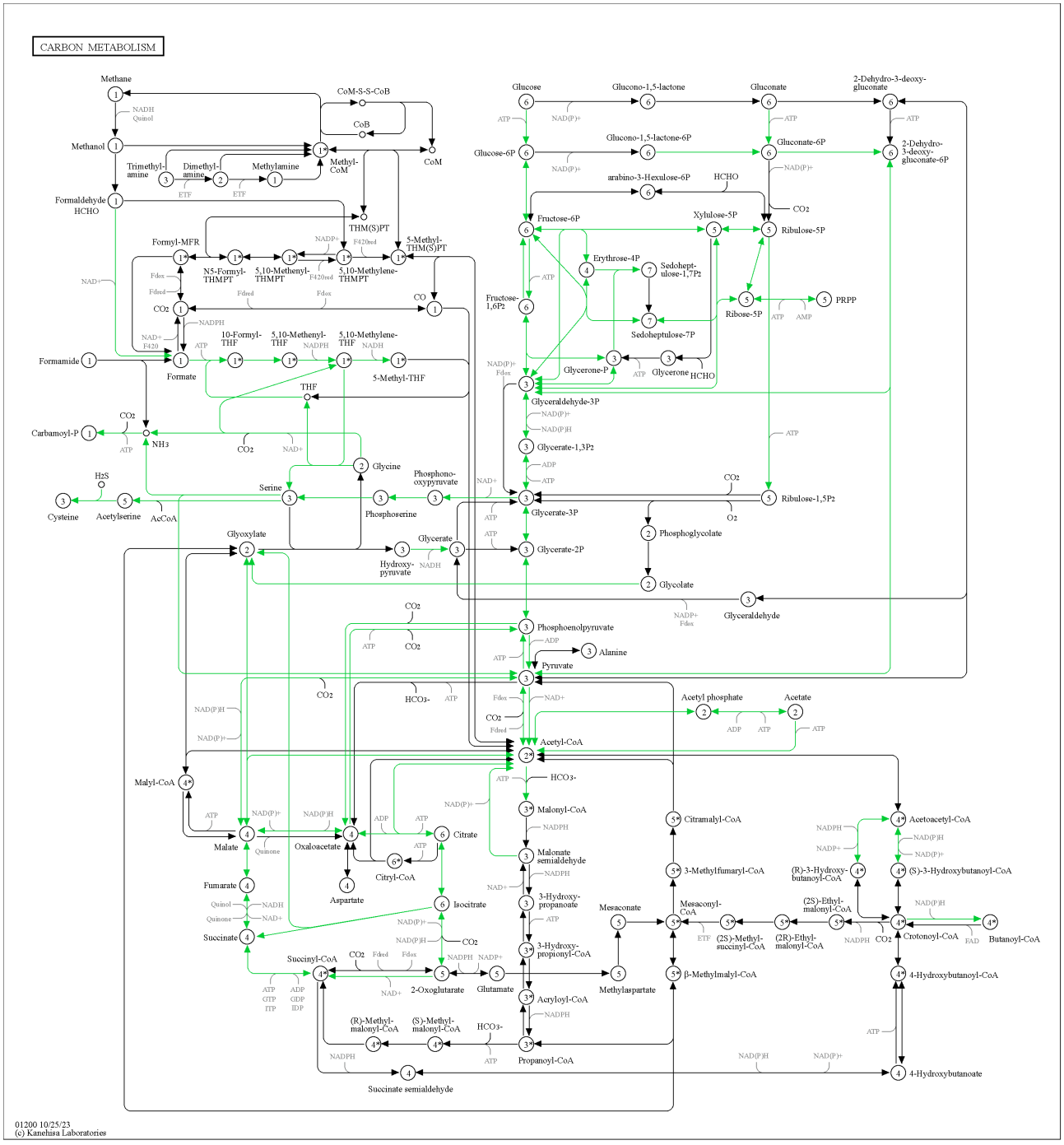


Figure 58: Carbon metabolism pathway annotation - GR1P1biofilm.135

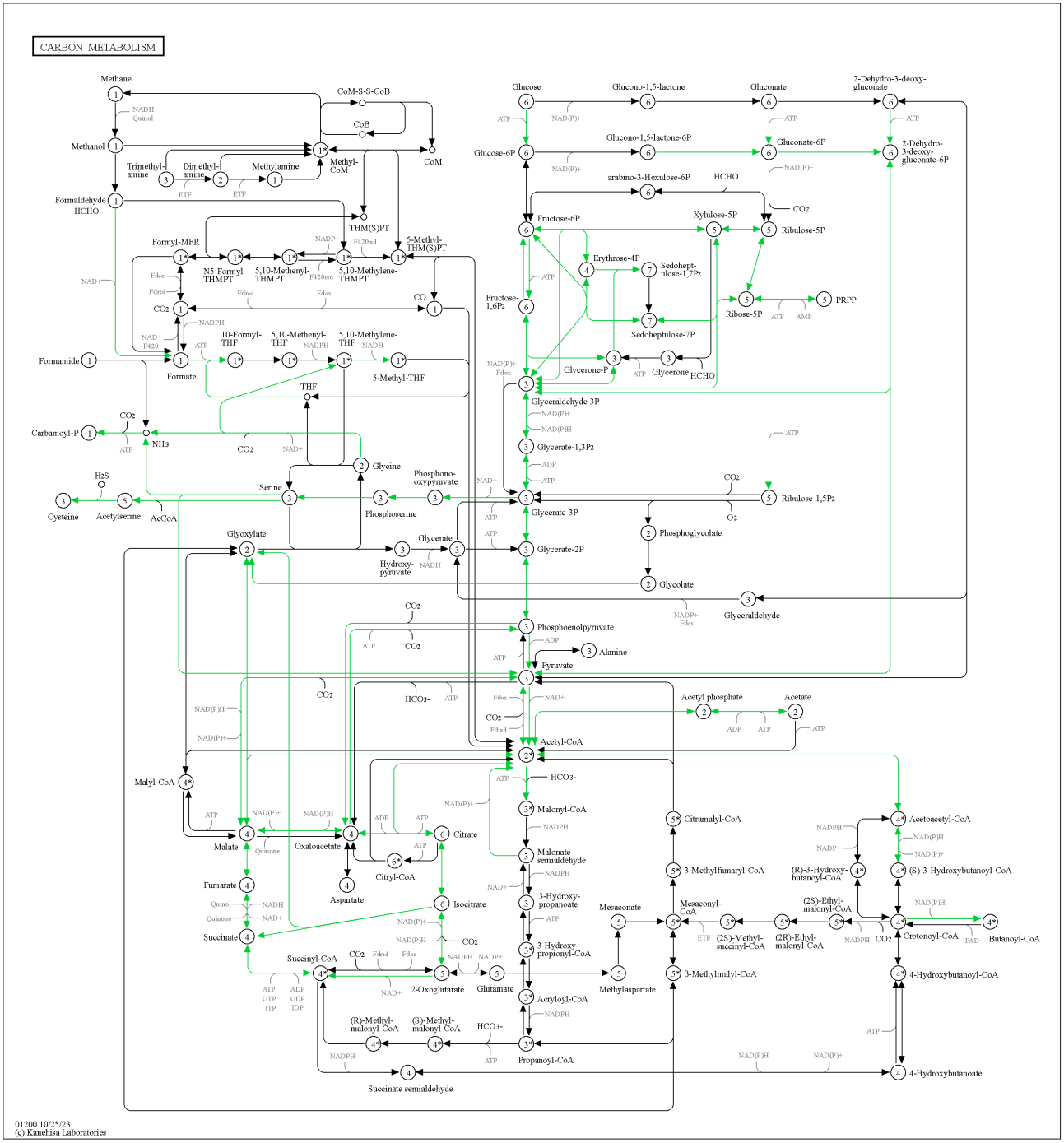


Figure 59: Carbon metabolism pathway annotation - GR1P2biofilm.127

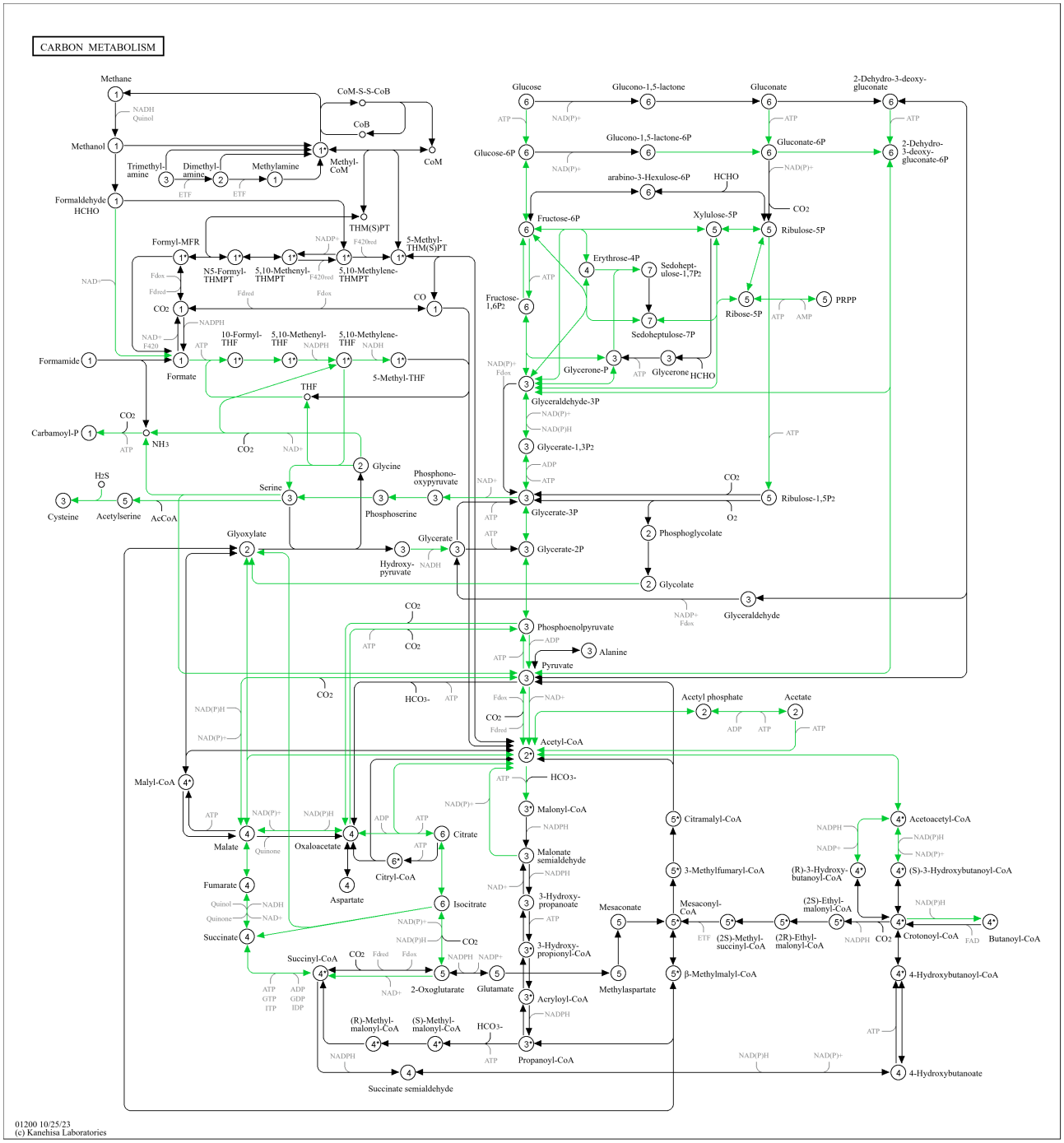


Figure 60: Carbon metabolism pathway annotation - *A. media* reference sequence (GCF_020423125.1)

A4.1.2 Pseudomonas putida

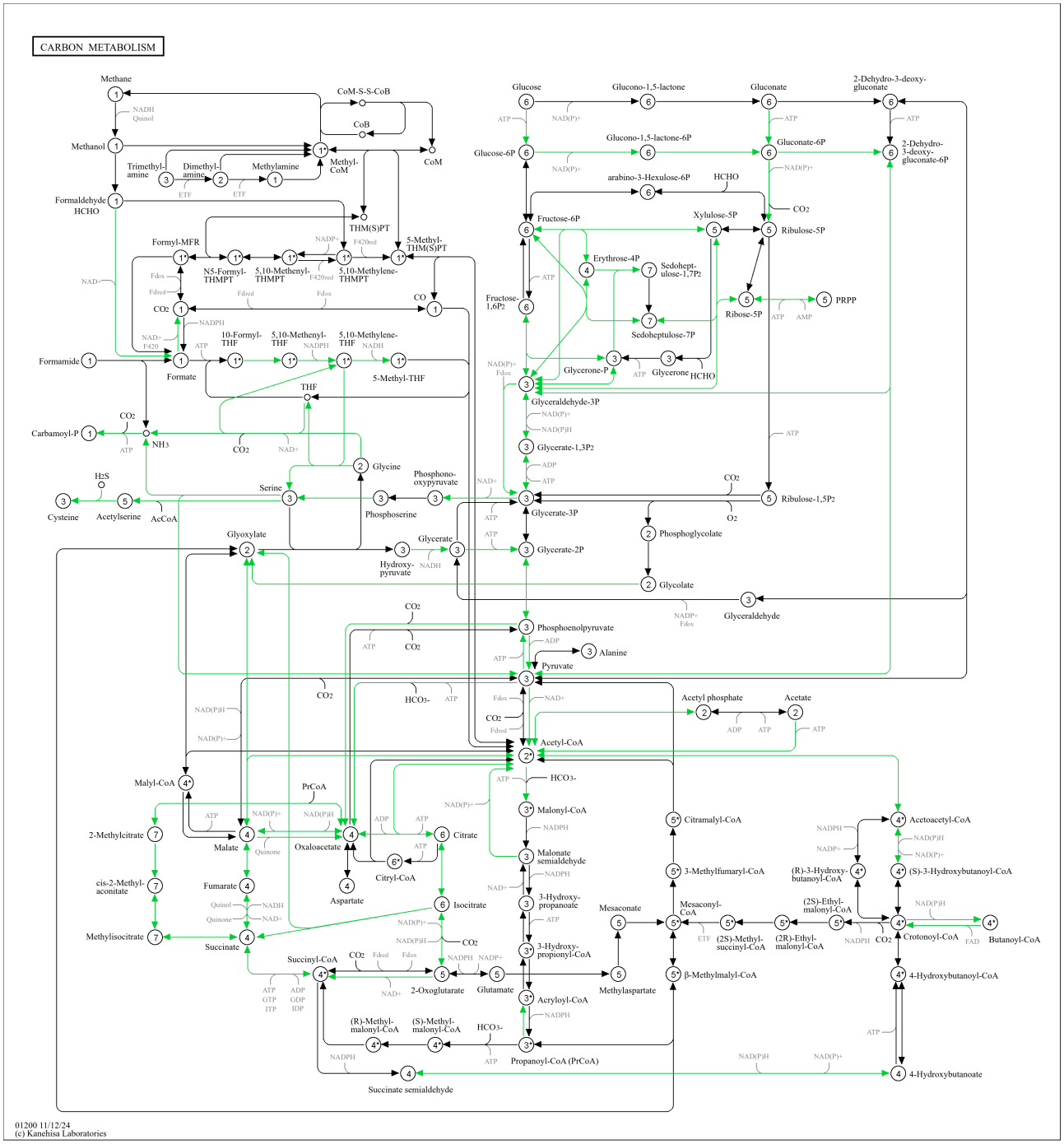


Figure 61: Carbon metabolism pathway annotation - GR1P2bulk.29

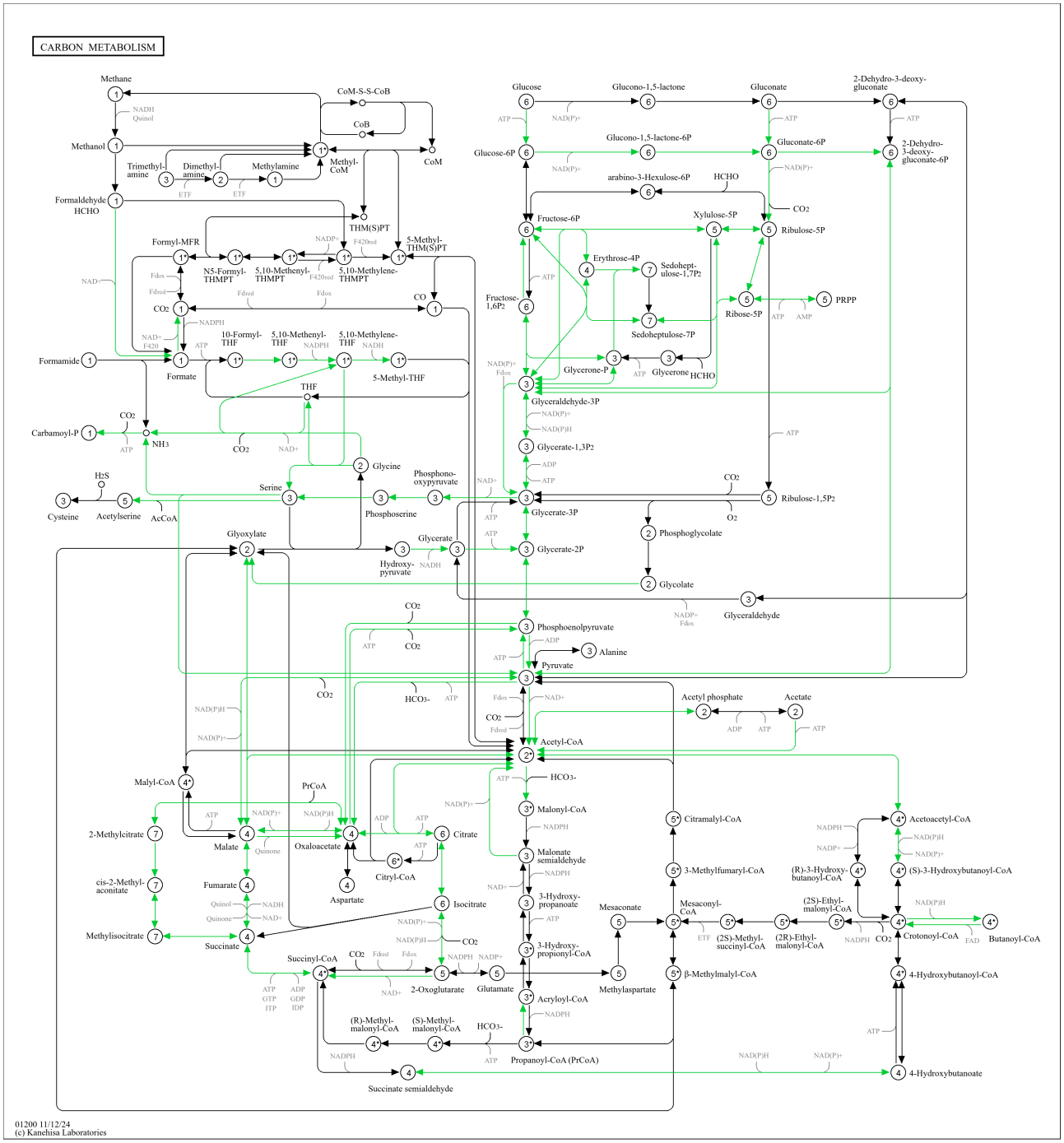


Figure 62: Carbon metabolism pathway annotation - GR2P2bulk.93

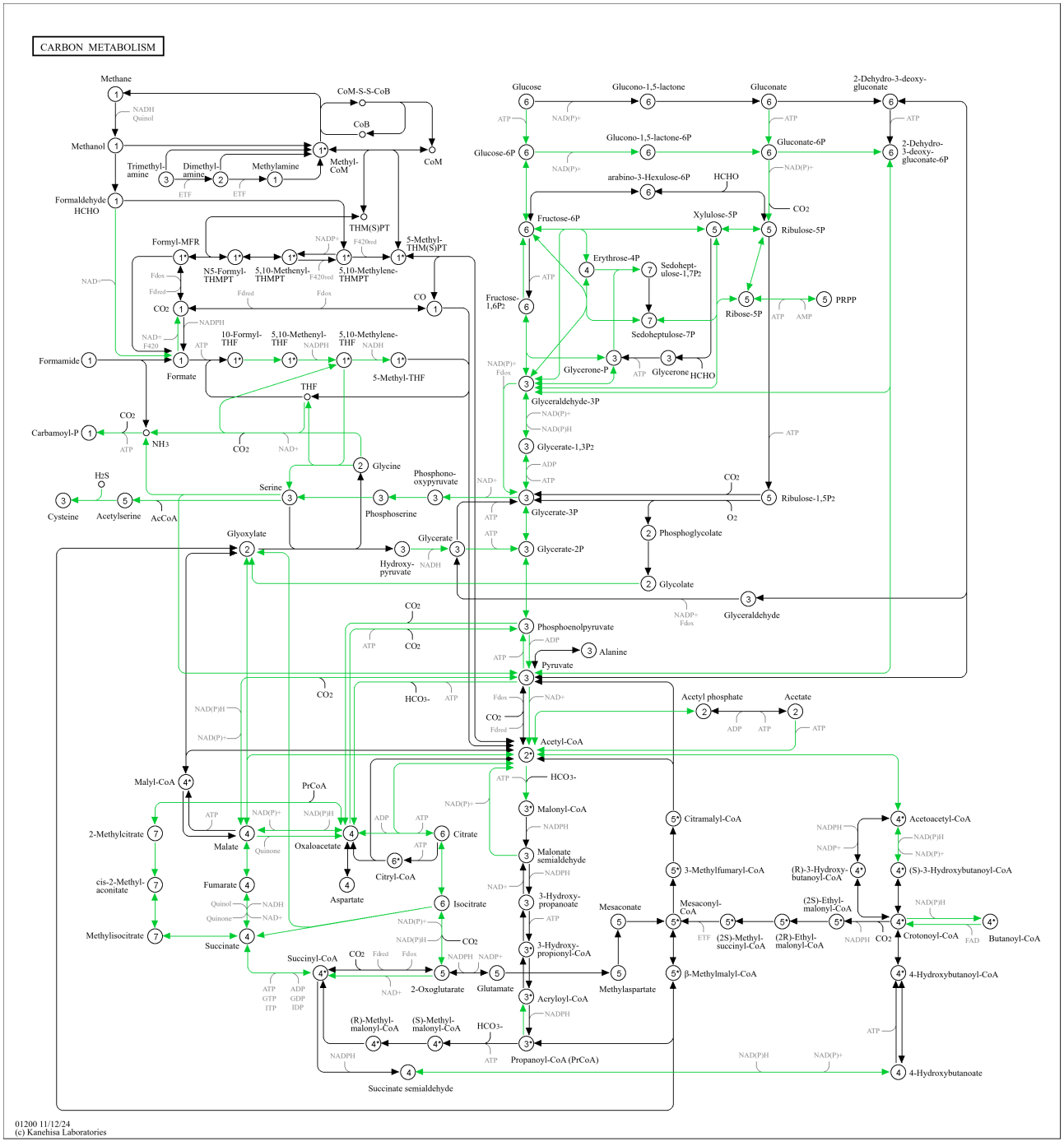


Figure 63: Carbon metabolism pathway annotation - *P. putida* reference sequence (GCF_000412675.1)

A4.1.3 Sulfurospirillum arsenophilum

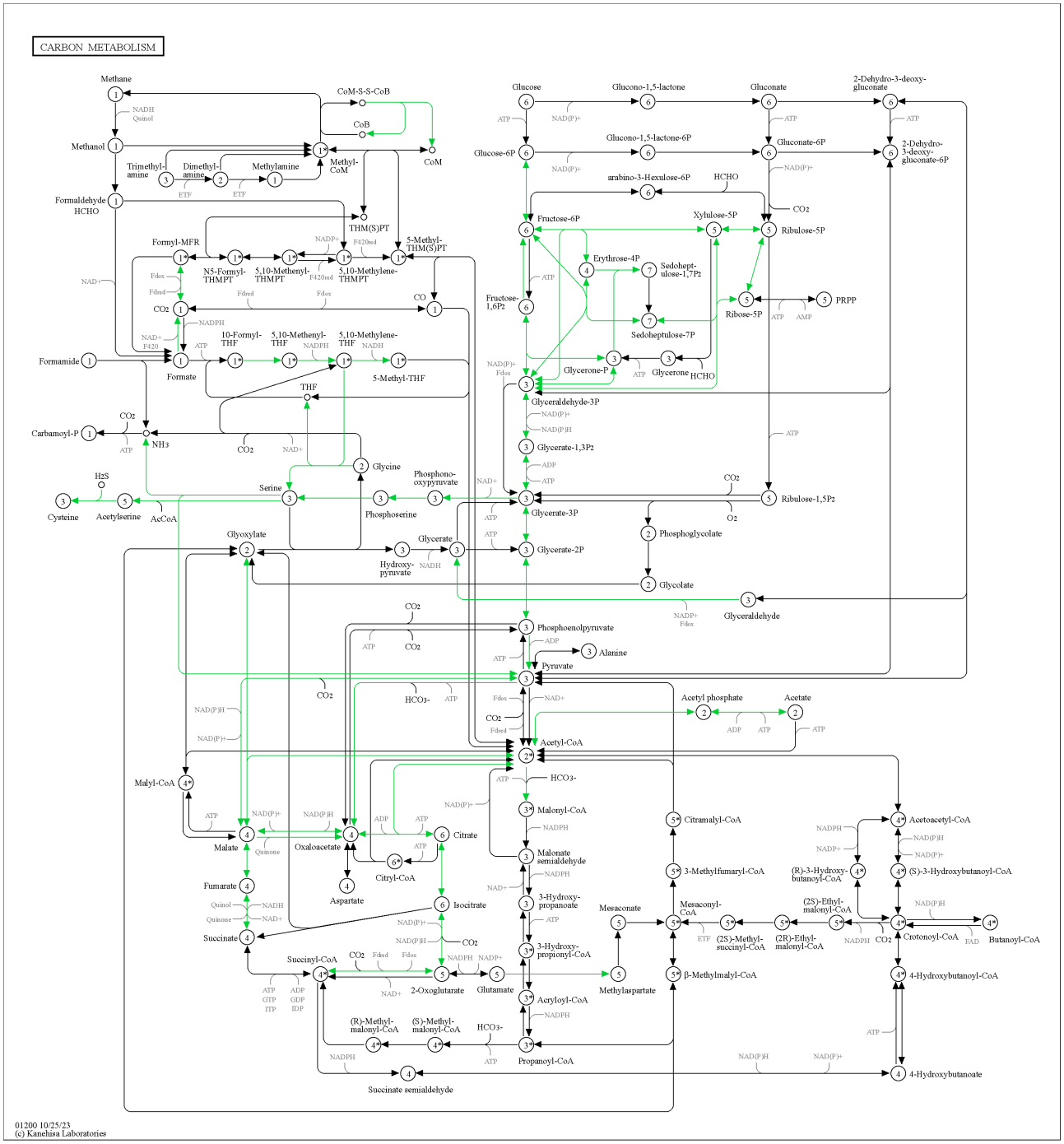


Figure 64: Carbon metabolism pathway annotation - GR1P2biofilm.115

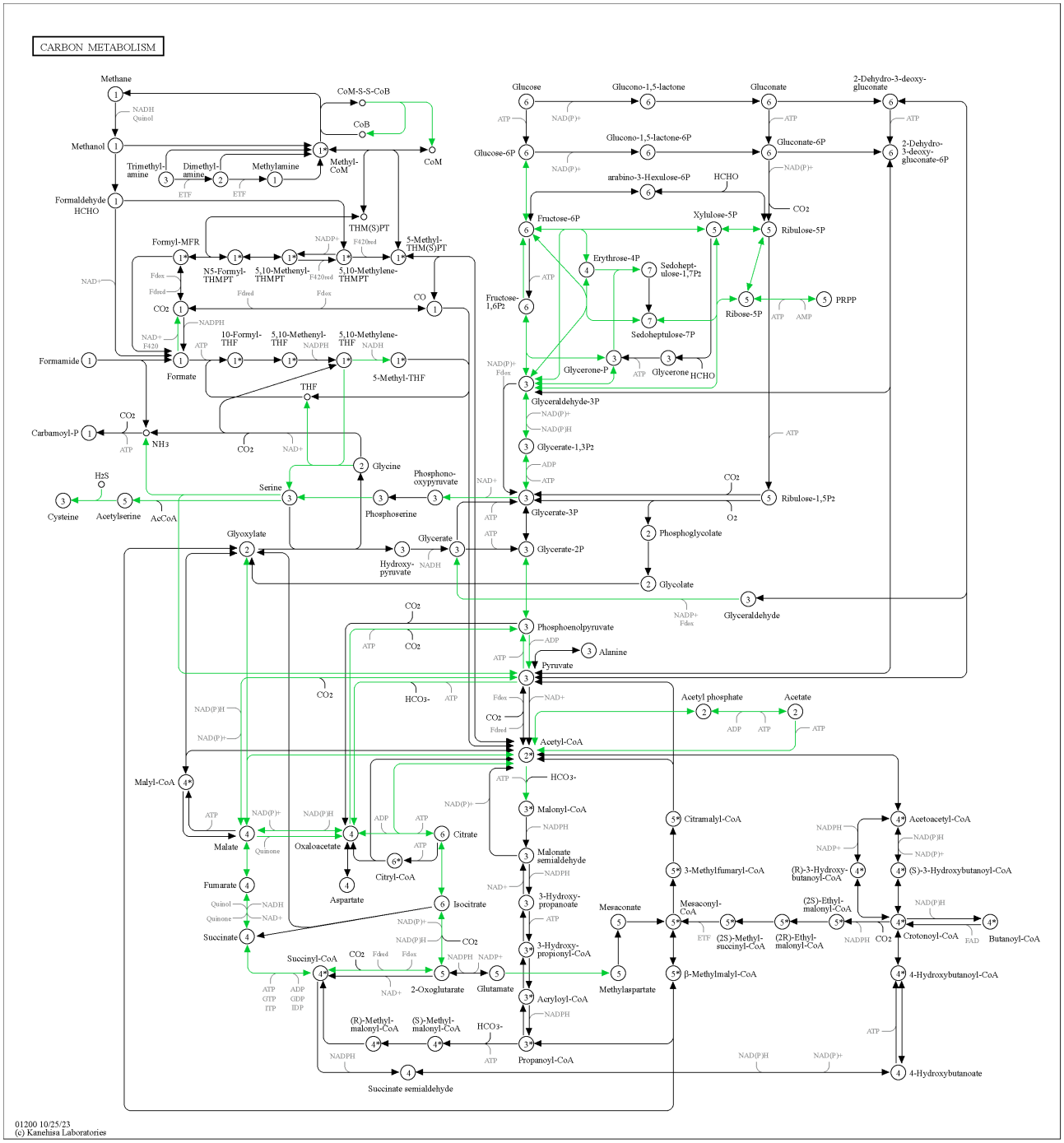


Figure 65: Carbon metabolism pathway annotation - GR1P2bulk.131

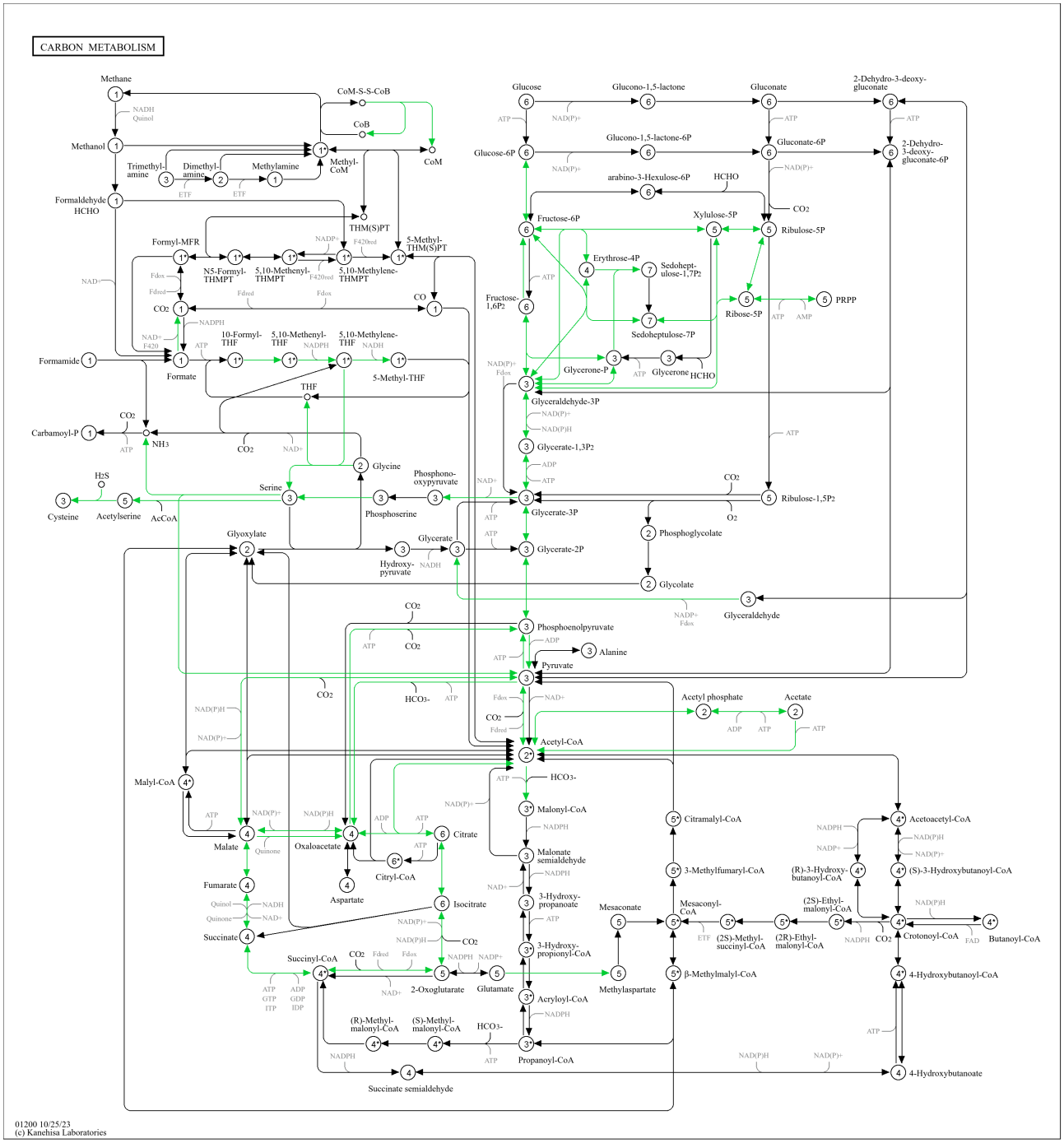


Figure 66: Carbon metabolism pathway annotation - *S. arsenophilum* reference sequence (GCF_-000813345.1)

A4.1.4 Sulfurospirillum cavolei

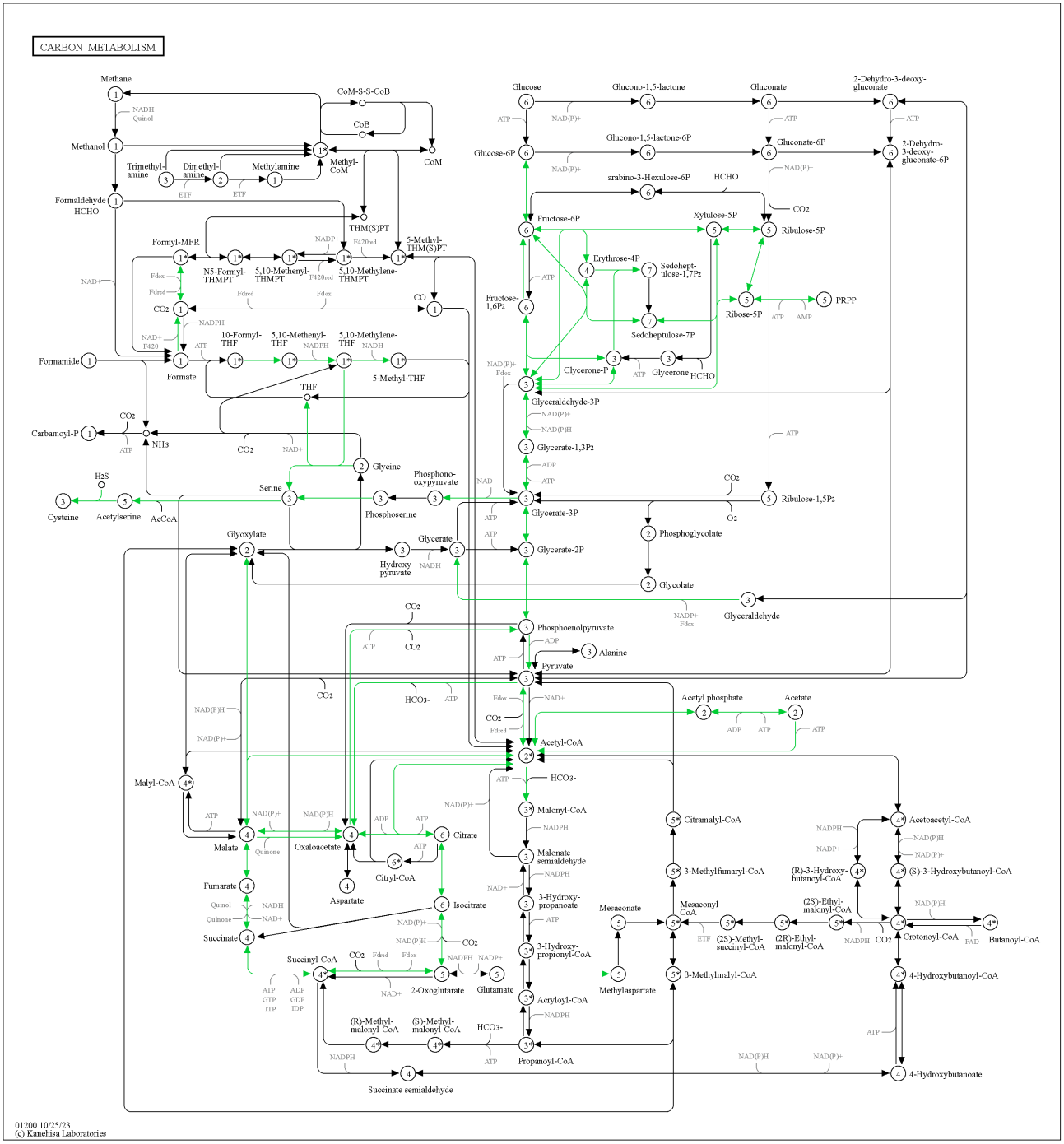


Figure 67: Carbon metabolism pathway annotation - GR1P2biofilm.177

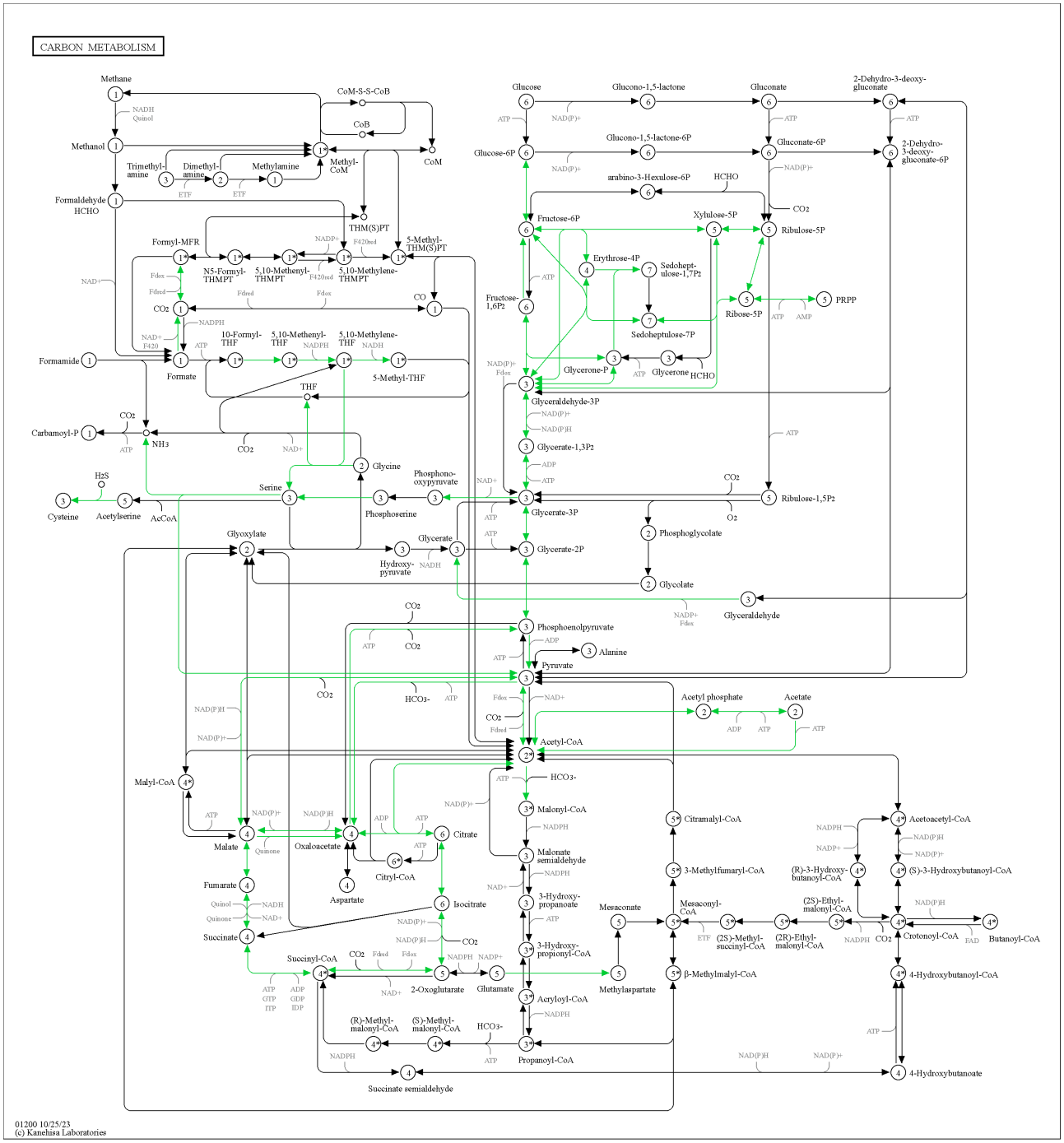


Figure 68: Carbon metabolism pathway annotation - GR2P1biofilm.32

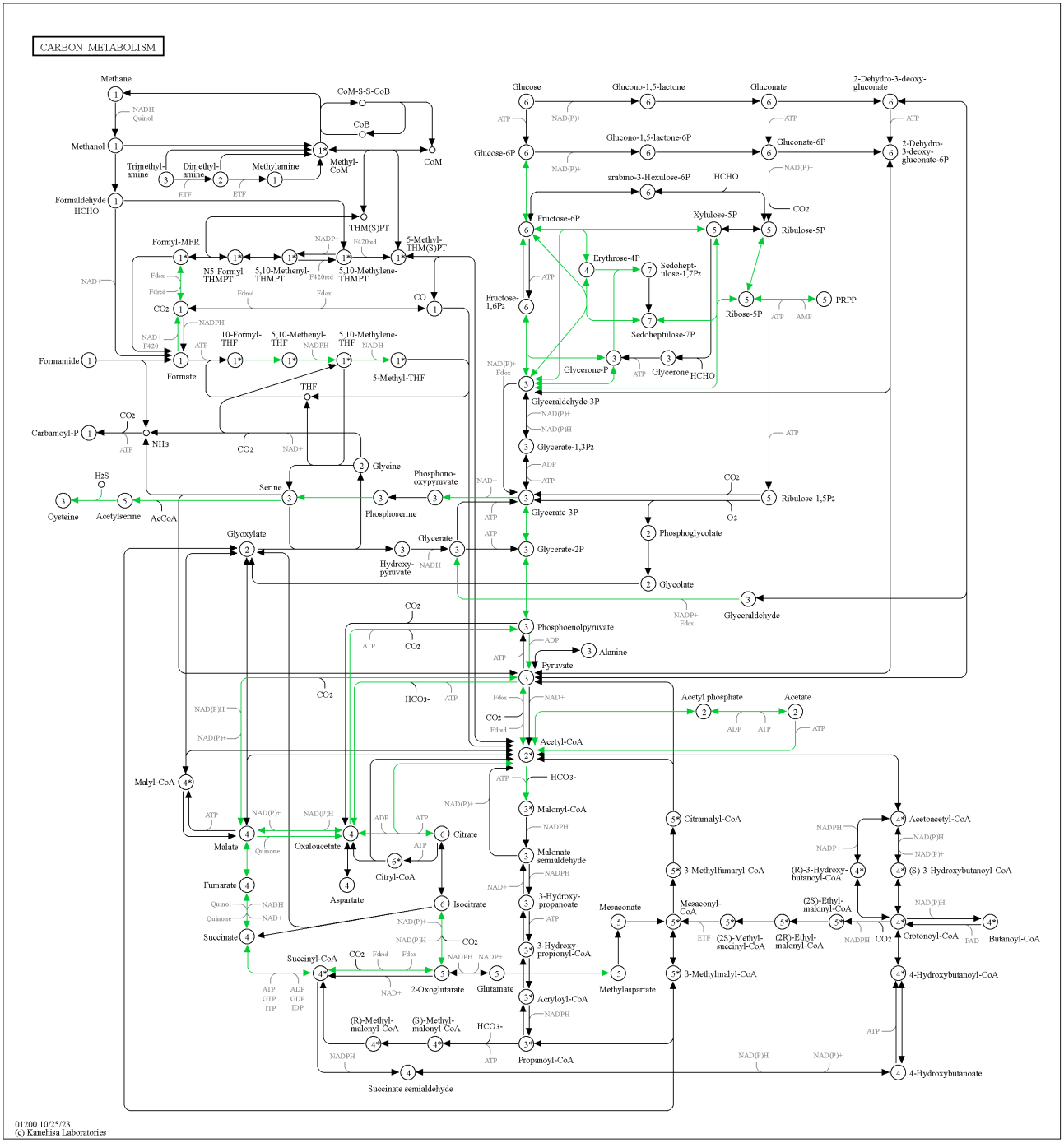


Figure 69: Carbon metabolism pathway annotation - GR2P1bulk.144

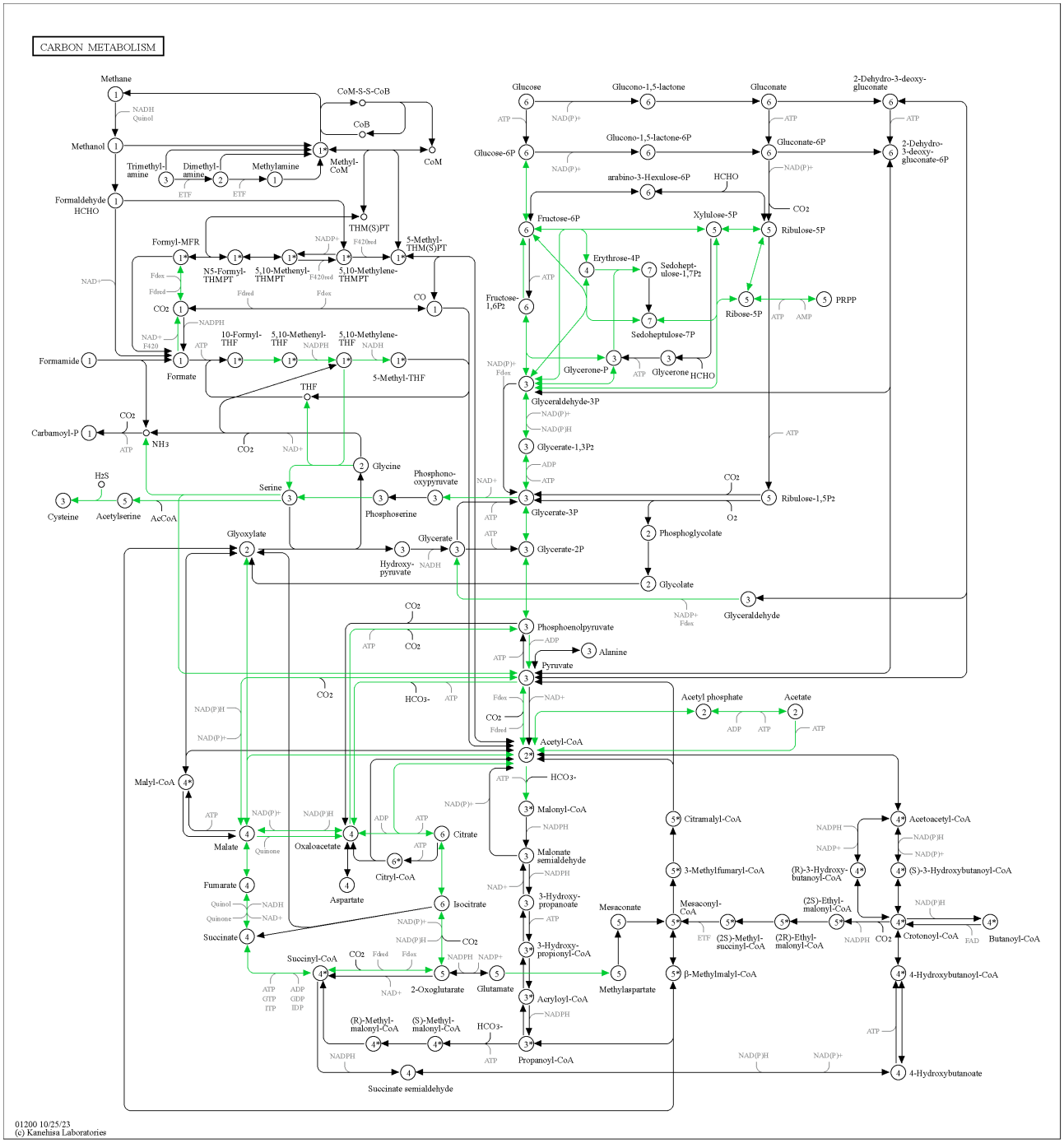


Figure 70: Carbon metabolism pathway annotation - GR2P2biofilm.179

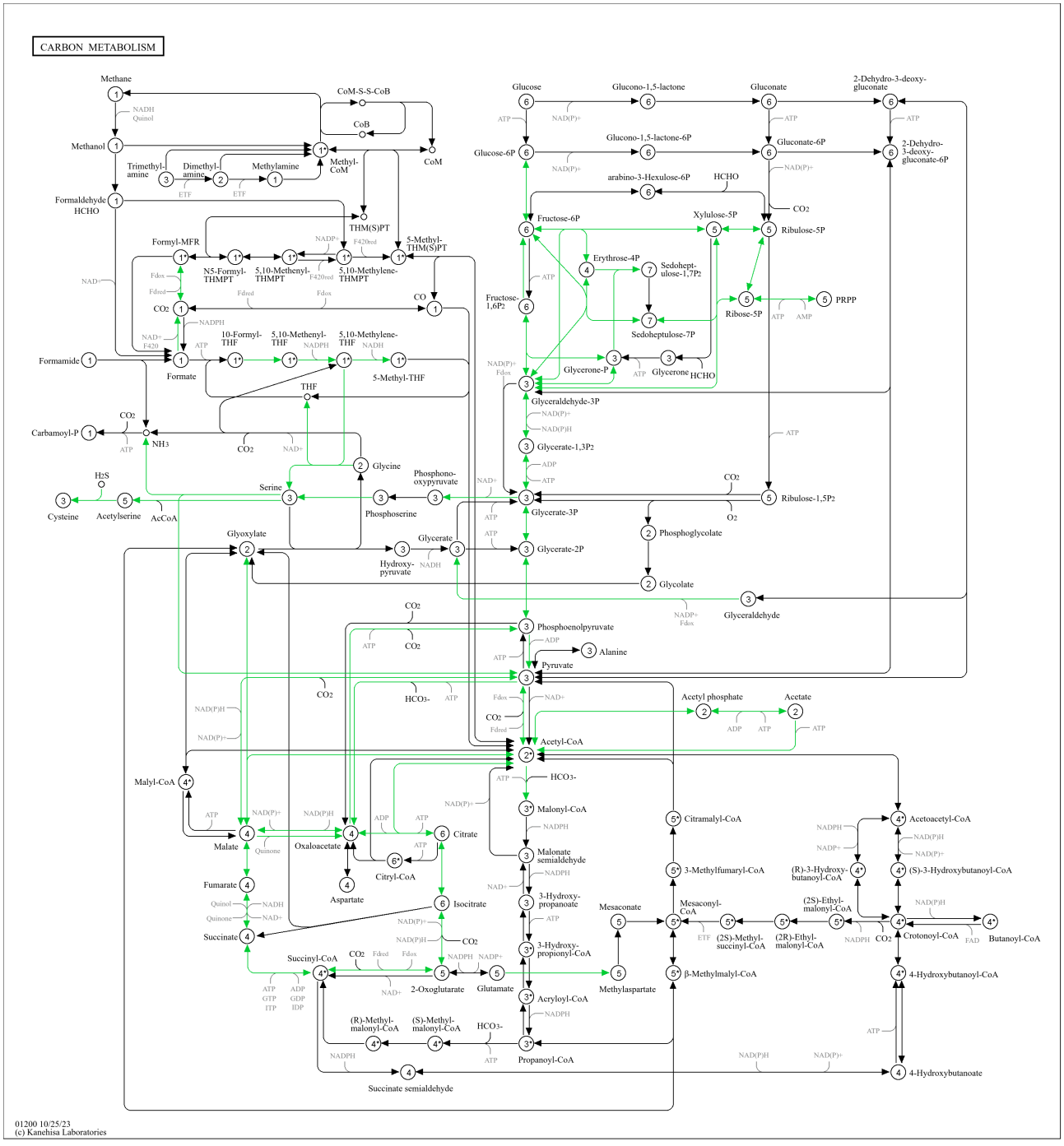


Figure 71: Carbon metabolism pathway annotation - *S. cavolei* reference sequence (GCF_000813325.1)

A4.1.5 Sulfurospirillum sp. JPD-1

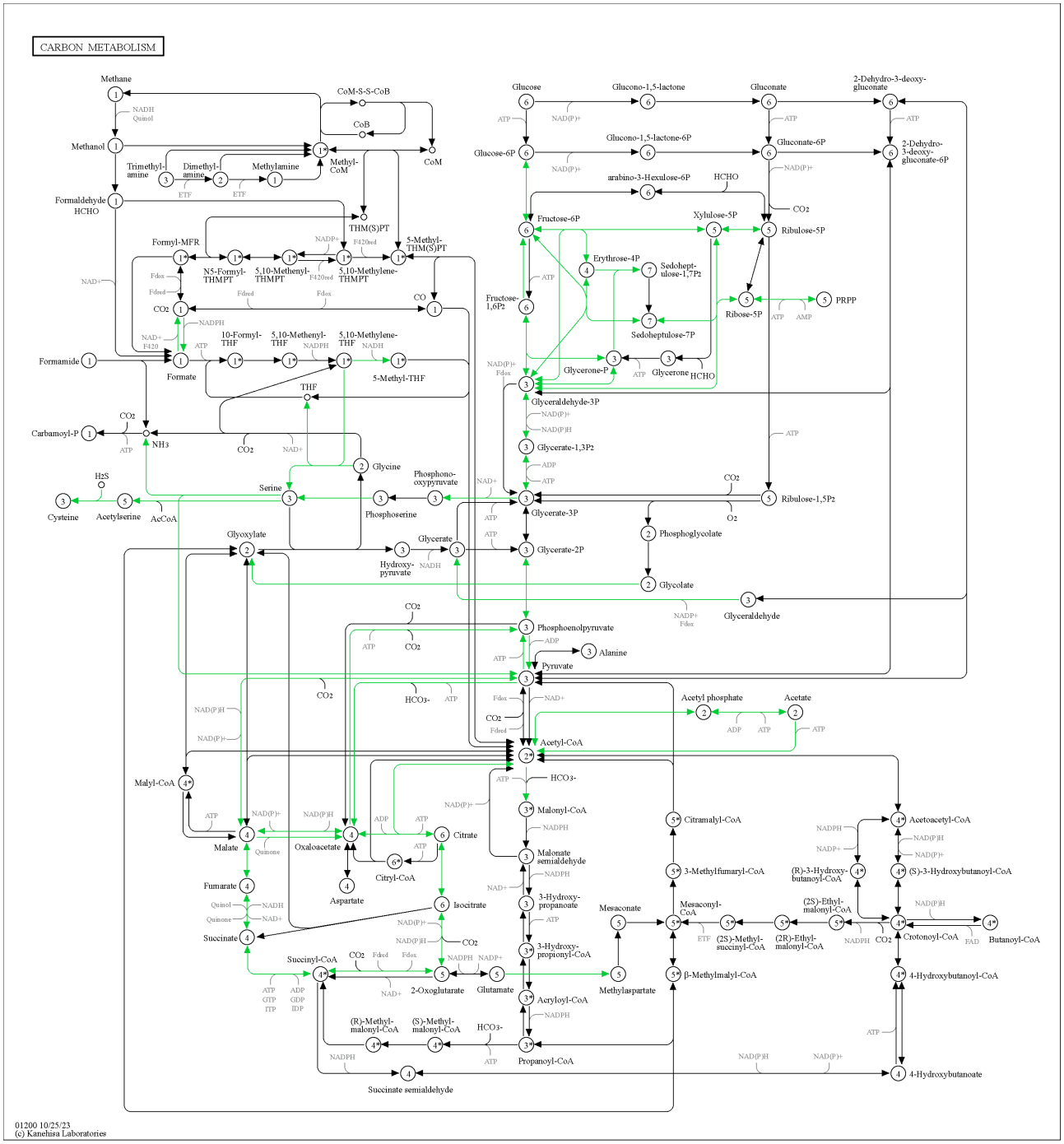


Figure 72: Carbon metabolism pathway annotation - GR2P1biofilm.36

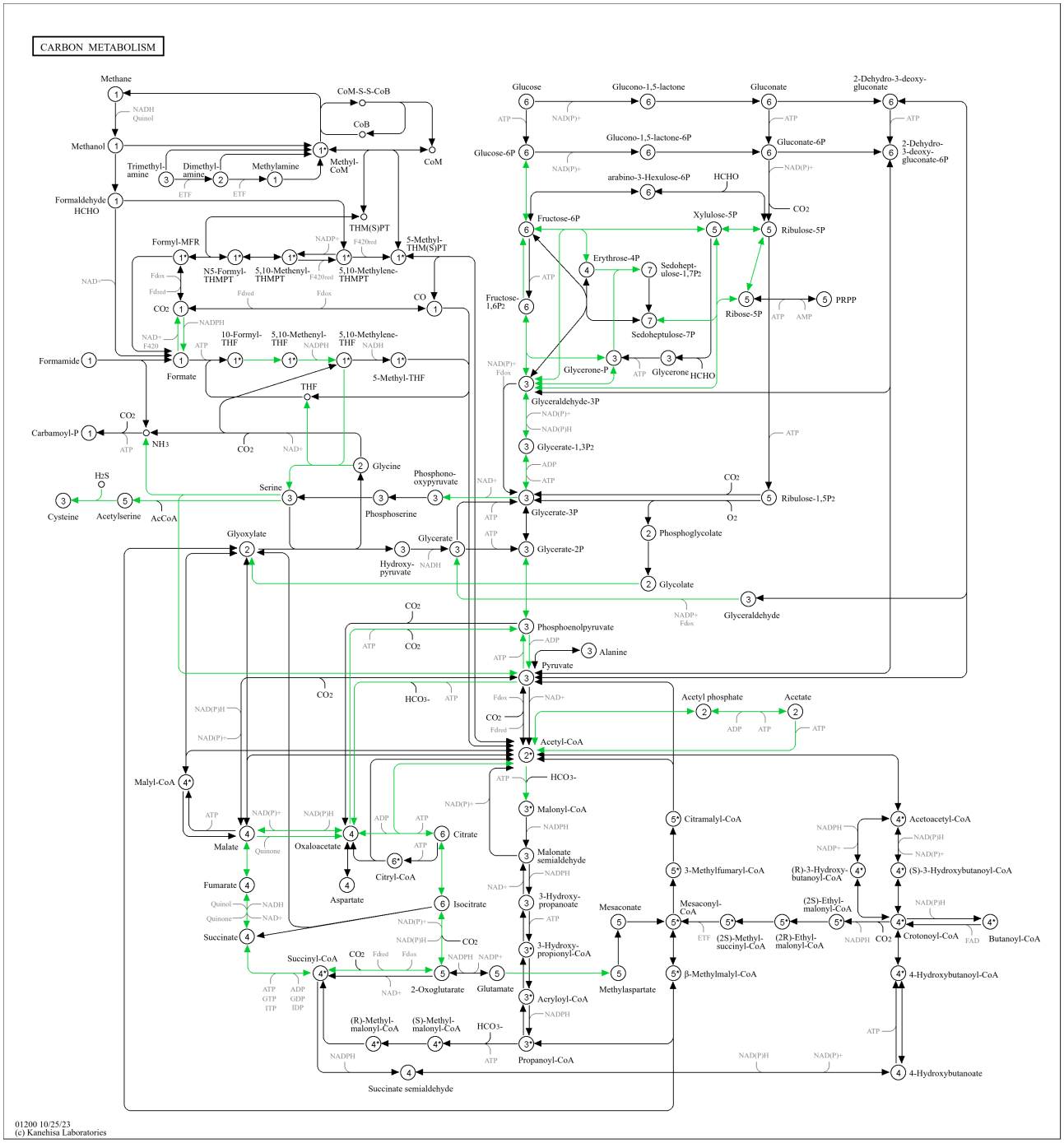


Figure 73: Carbon metabolism pathway annotation - GR2P2biofilm.71

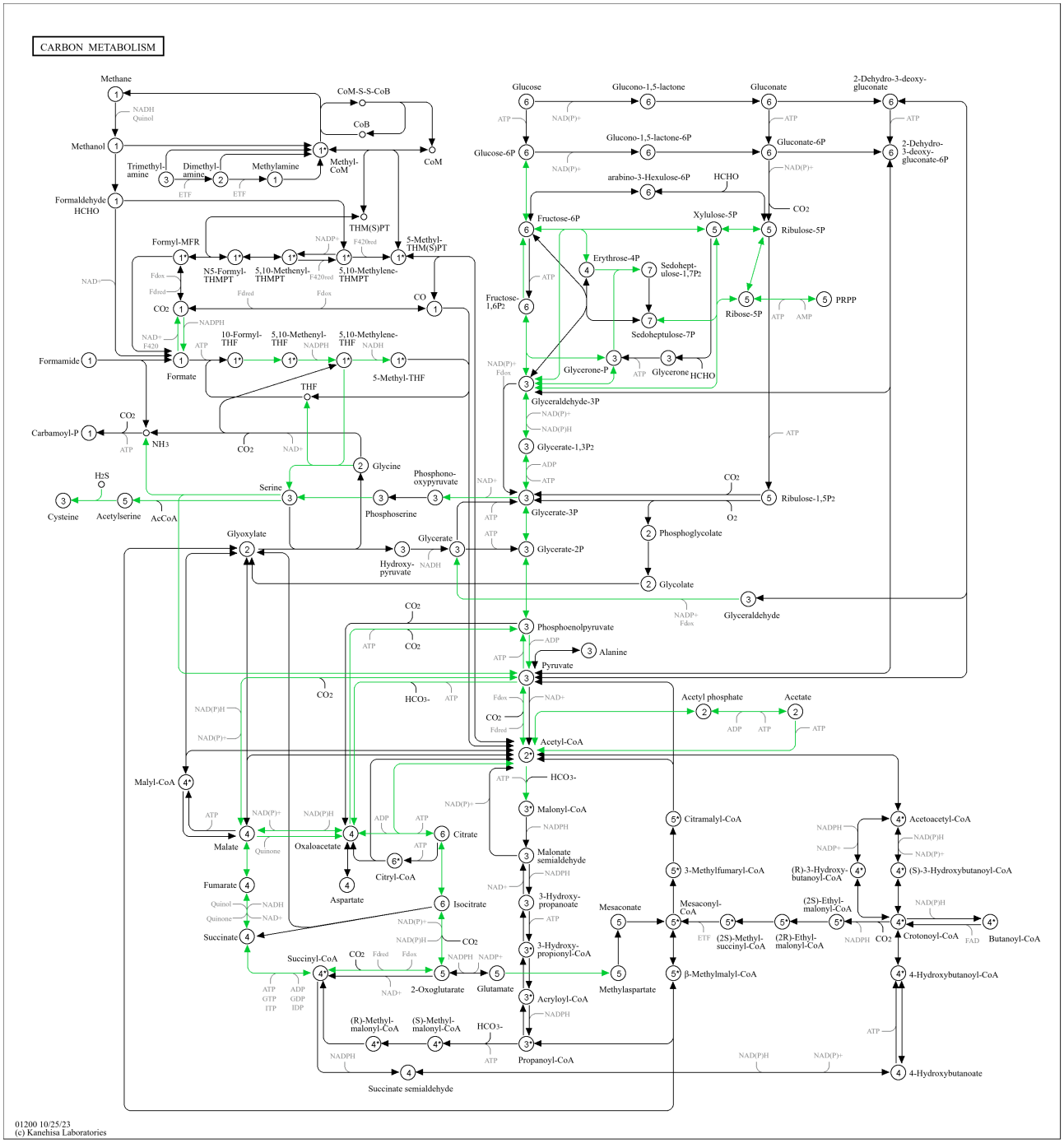


Figure 74: Carbon metabolism pathway annotation - *S. sp. JPD-1* reference sequence (GCF_002309535.1)

A4.1.6 Sulfurospirillum sp. UCH001

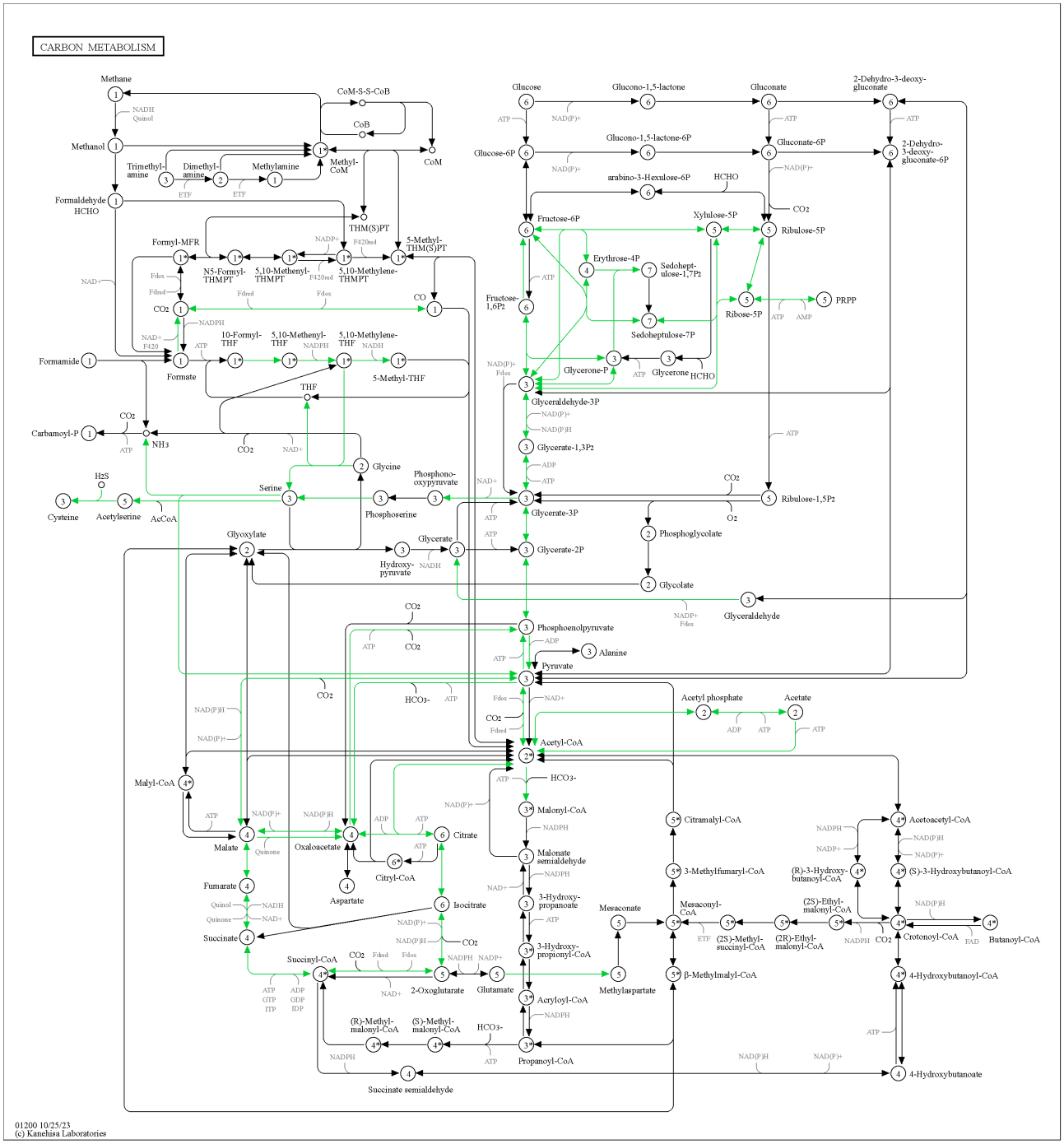


Figure 75: Carbon metabolism pathway annotation - GR2P1biofilm.14

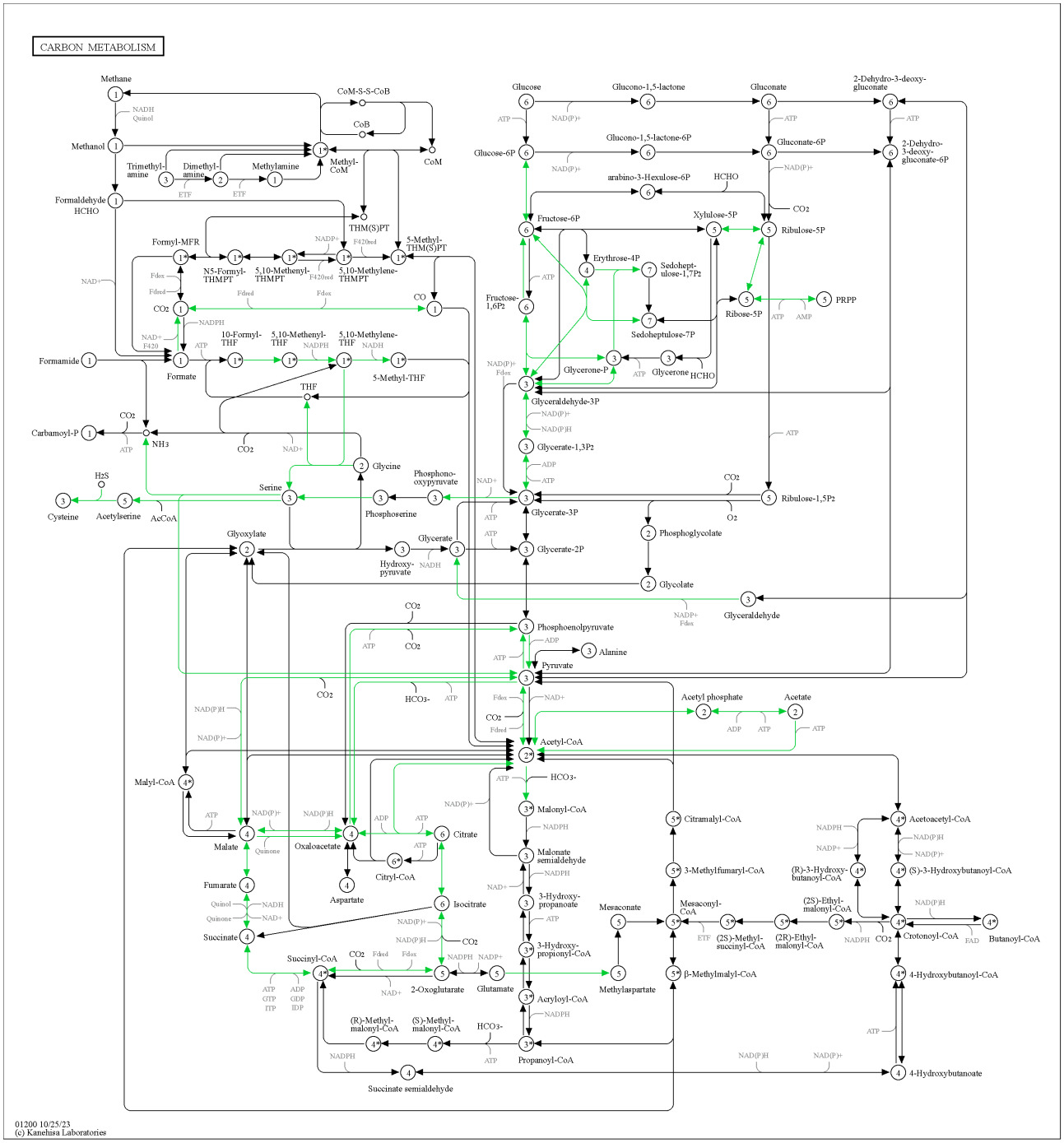


Figure 76: Carbon metabolism pathway annotation - GR2P1biofilm.42

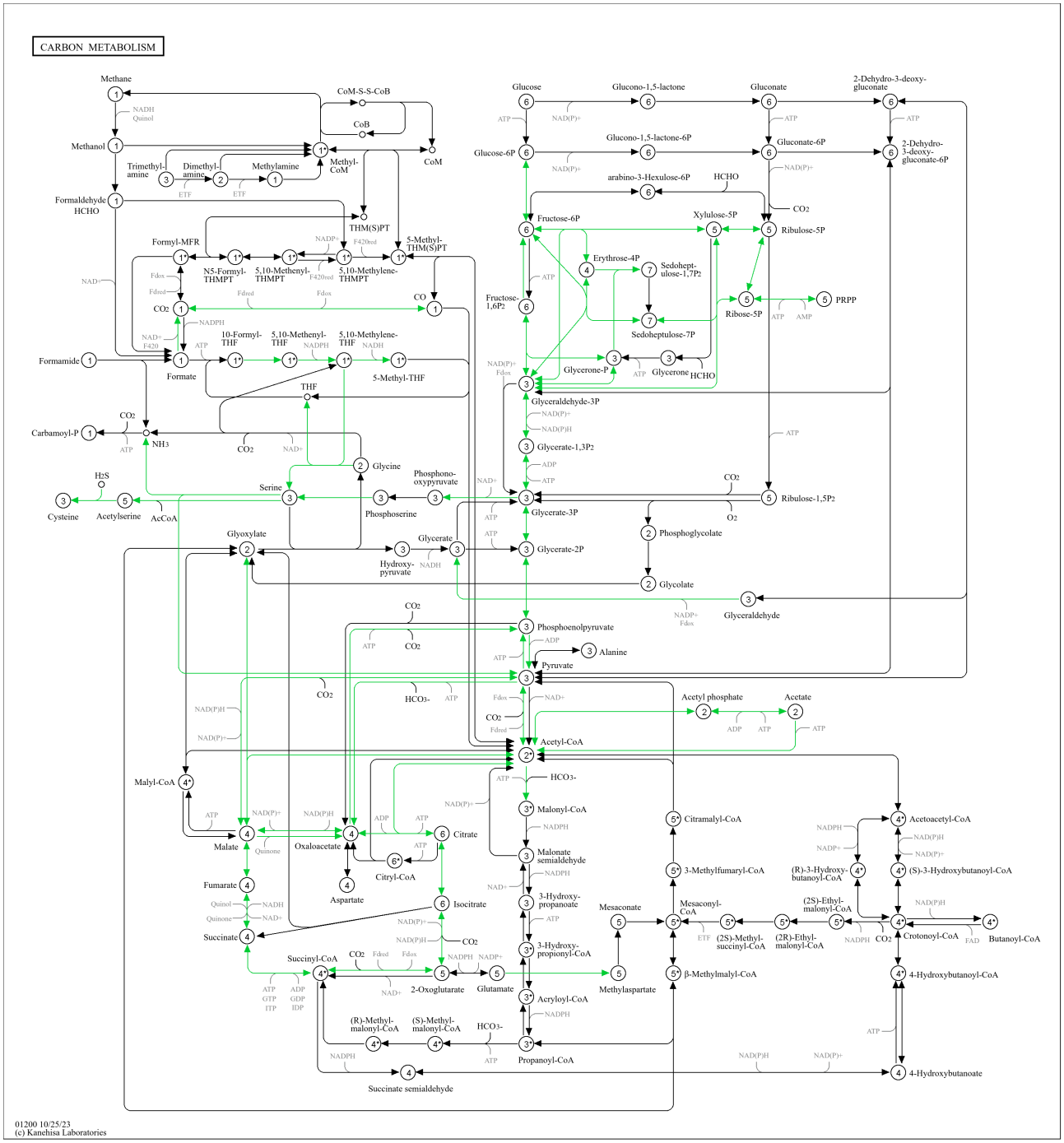


Figure 77: Carbon metabolism pathway annotation - *S. sp. UCH001* reference sequence (GCF_-001548035.1)

A4.2 Nitrogen Metabolism

A4.2.1 Aeromonas media

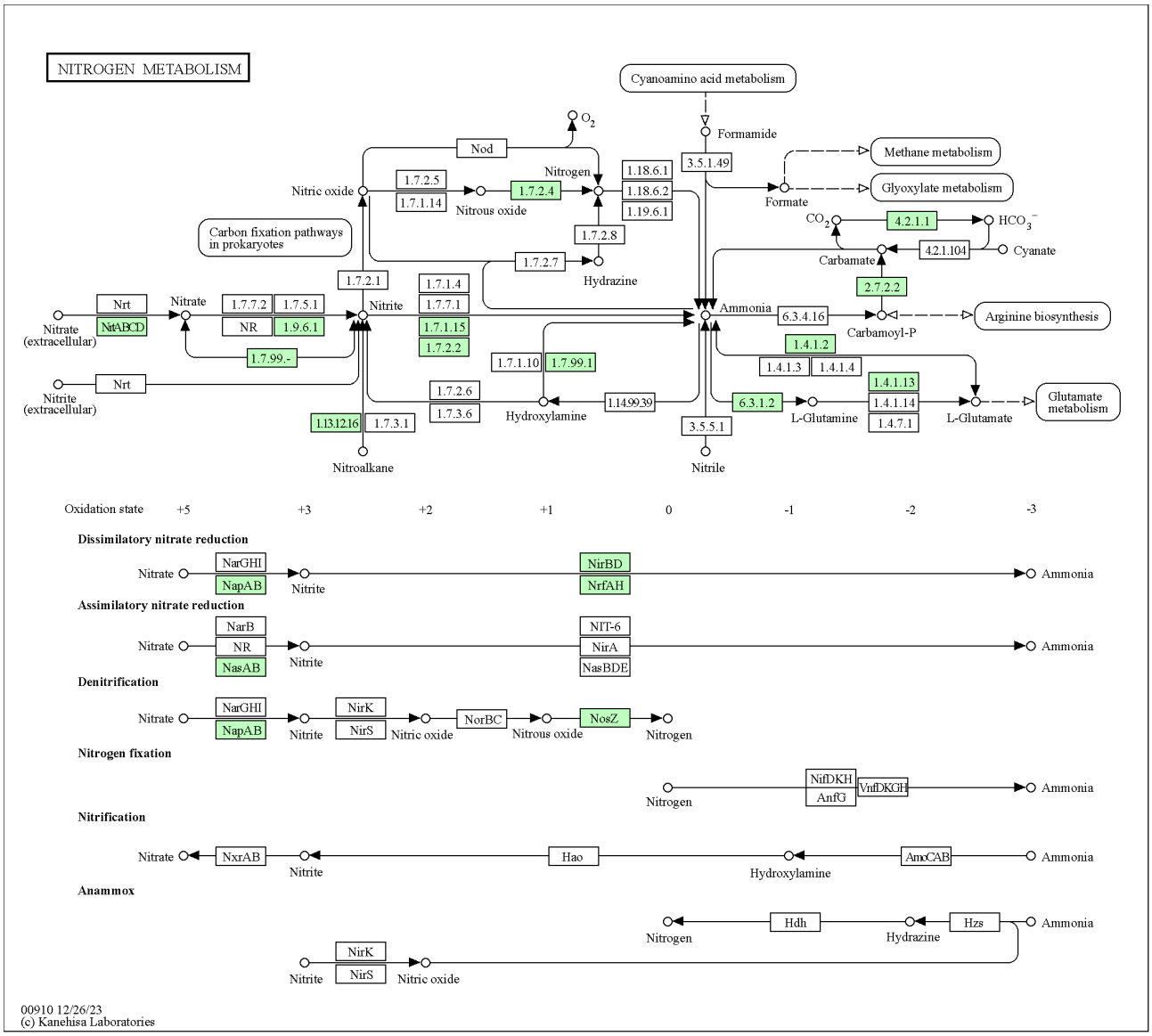


Figure 78: Nitrogen metabolism pathway annotation - GR1P1biofilm.135

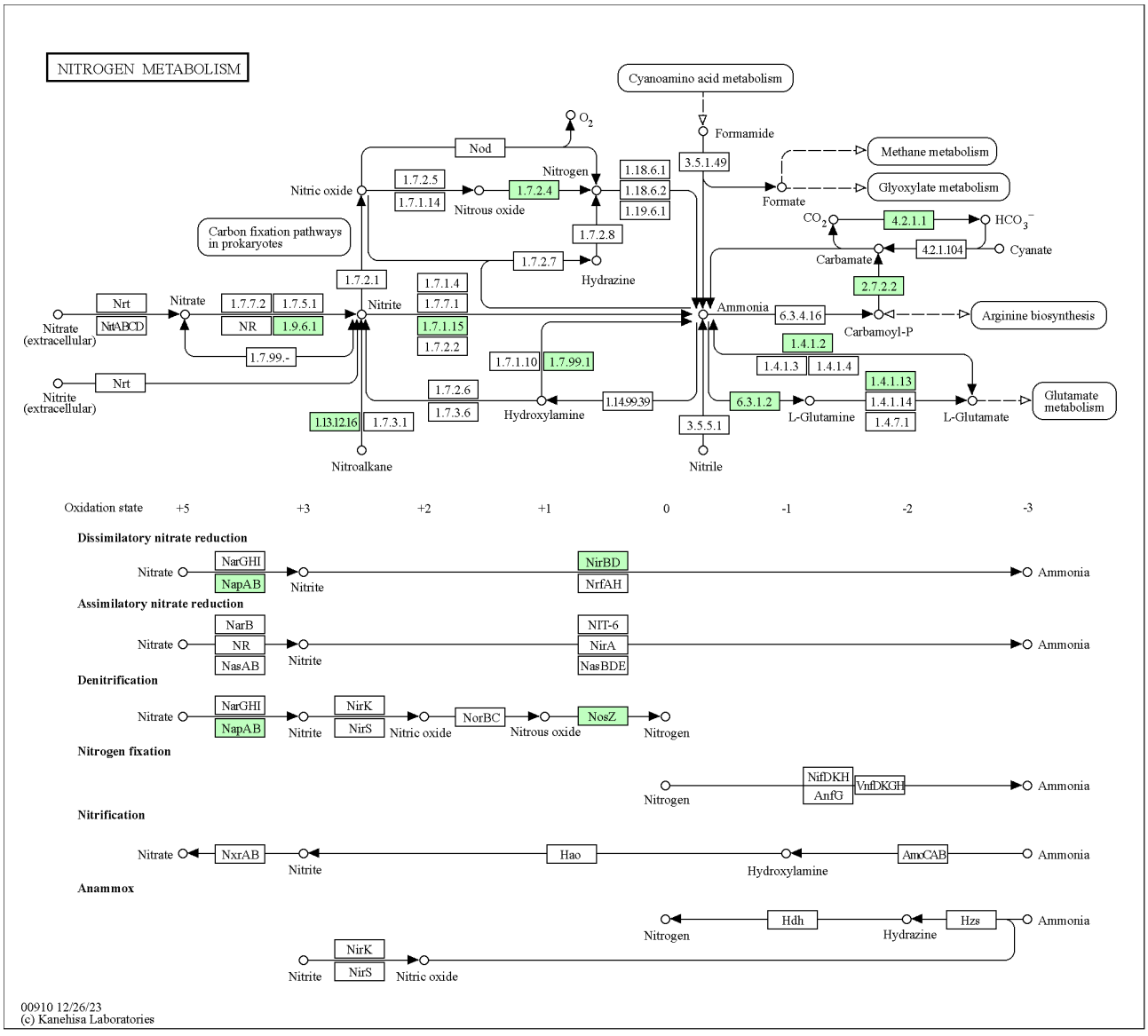


Figure 79: Nitrogen metabolism pathway annotation - GR1P2biofilm.127

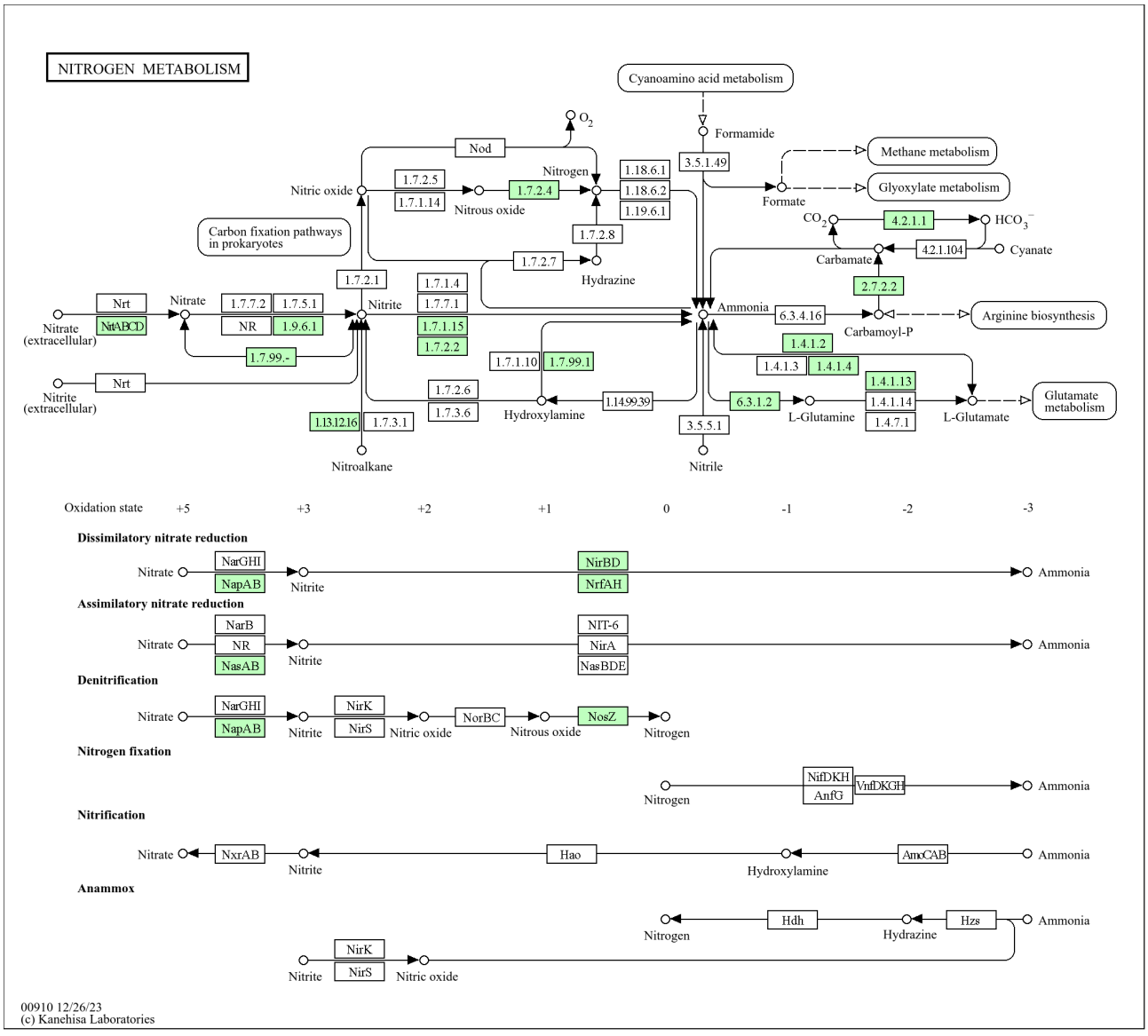


Figure 80: Nitrogen metabolism pathway annotation - *A. media* reference sequence (GCF_020423125.1)

A4.2.2 Pseudomonas putida

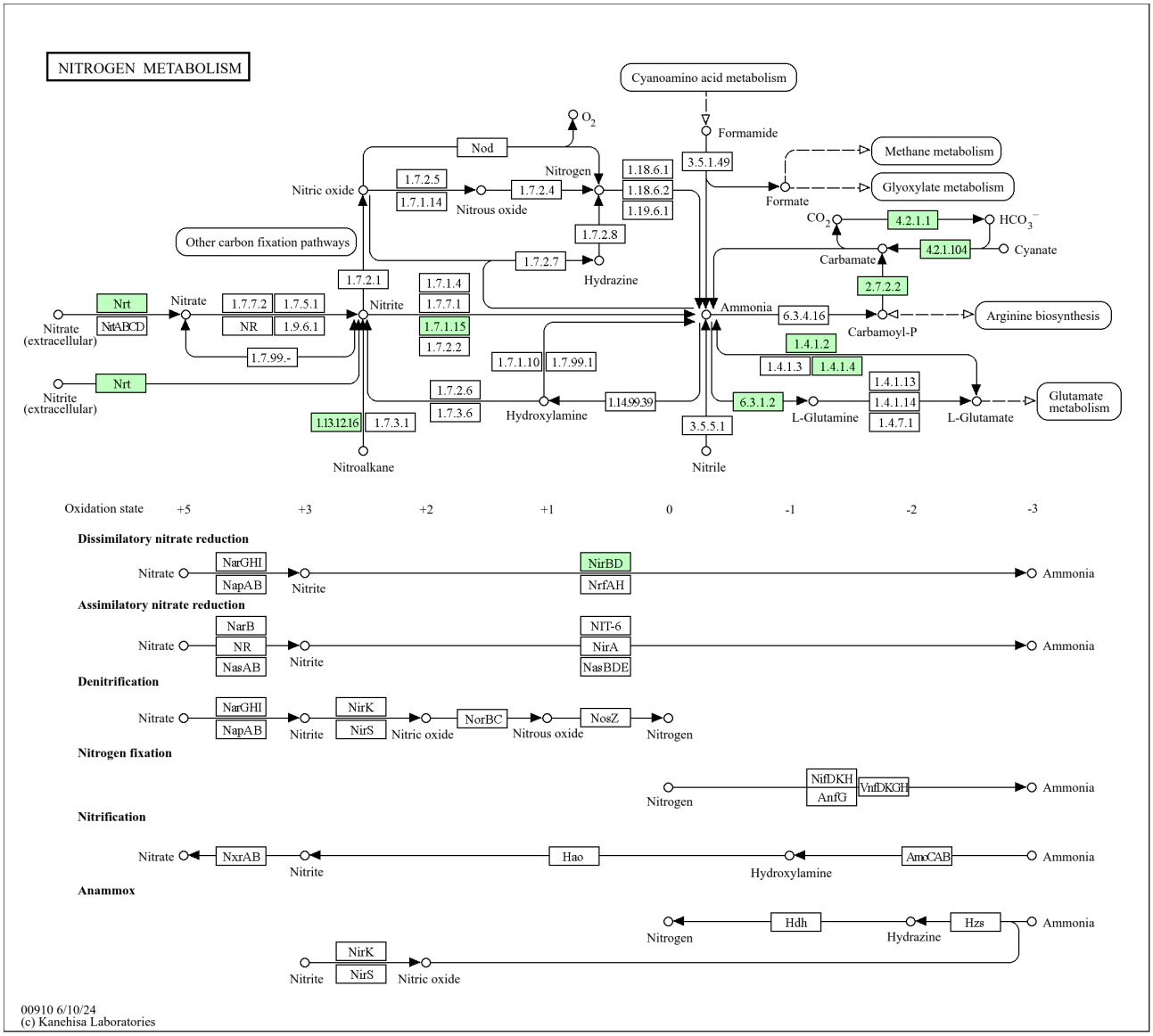


Figure 81: Nitrogen metabolism pathway annotation - GR1P2bulk.29

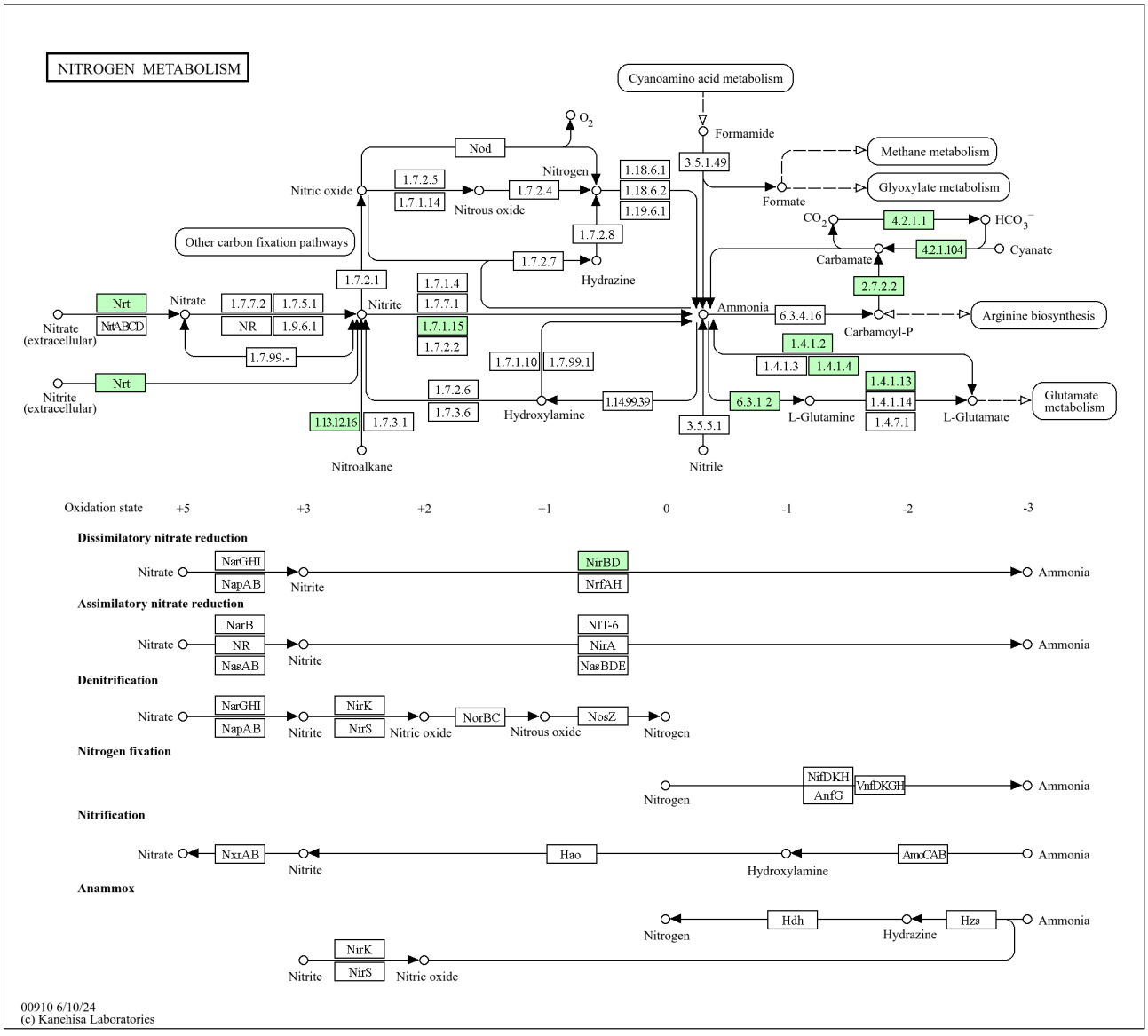


Figure 82: Nitrogen metabolism pathway annotation - GR2P2bulk.93

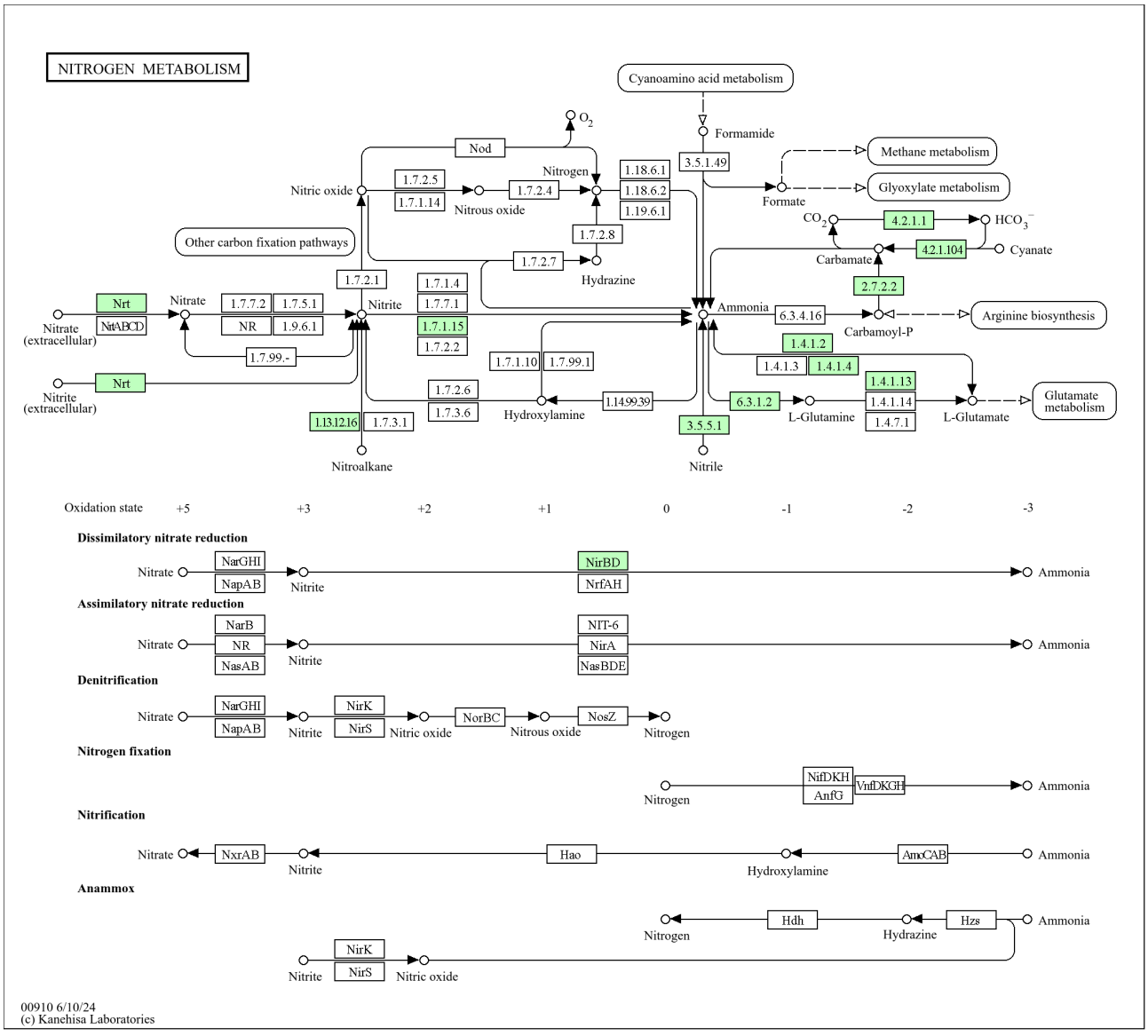


Figure 83: Nitrogen metabolism pathway annotation - *P. putida* reference sequence (GCF_000412675.1)

A4.2.3 Sulfurospirillum arsenophilum

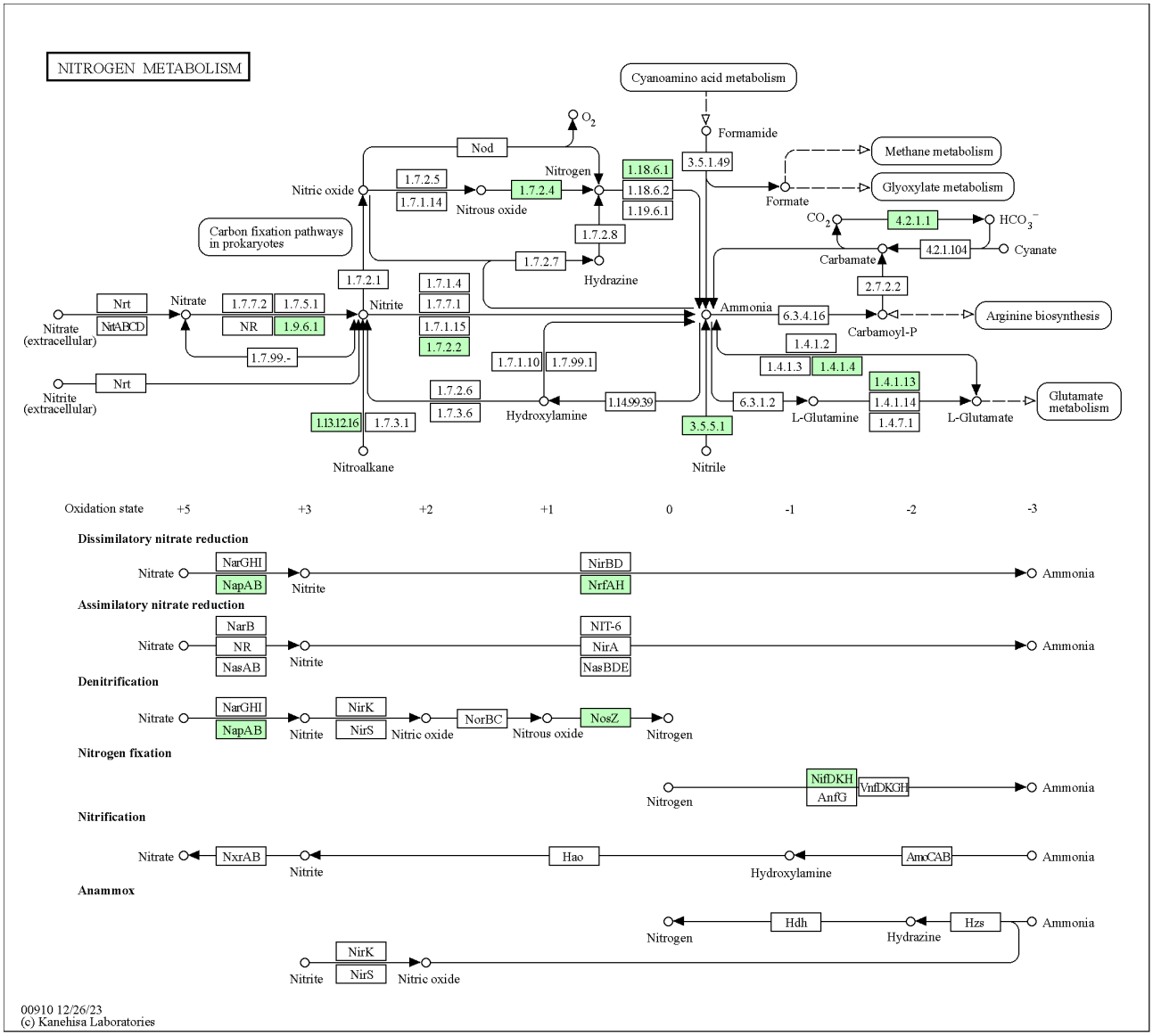


Figure 84: Nitrogen metabolism pathway annotation - GR1P2biofilm.115

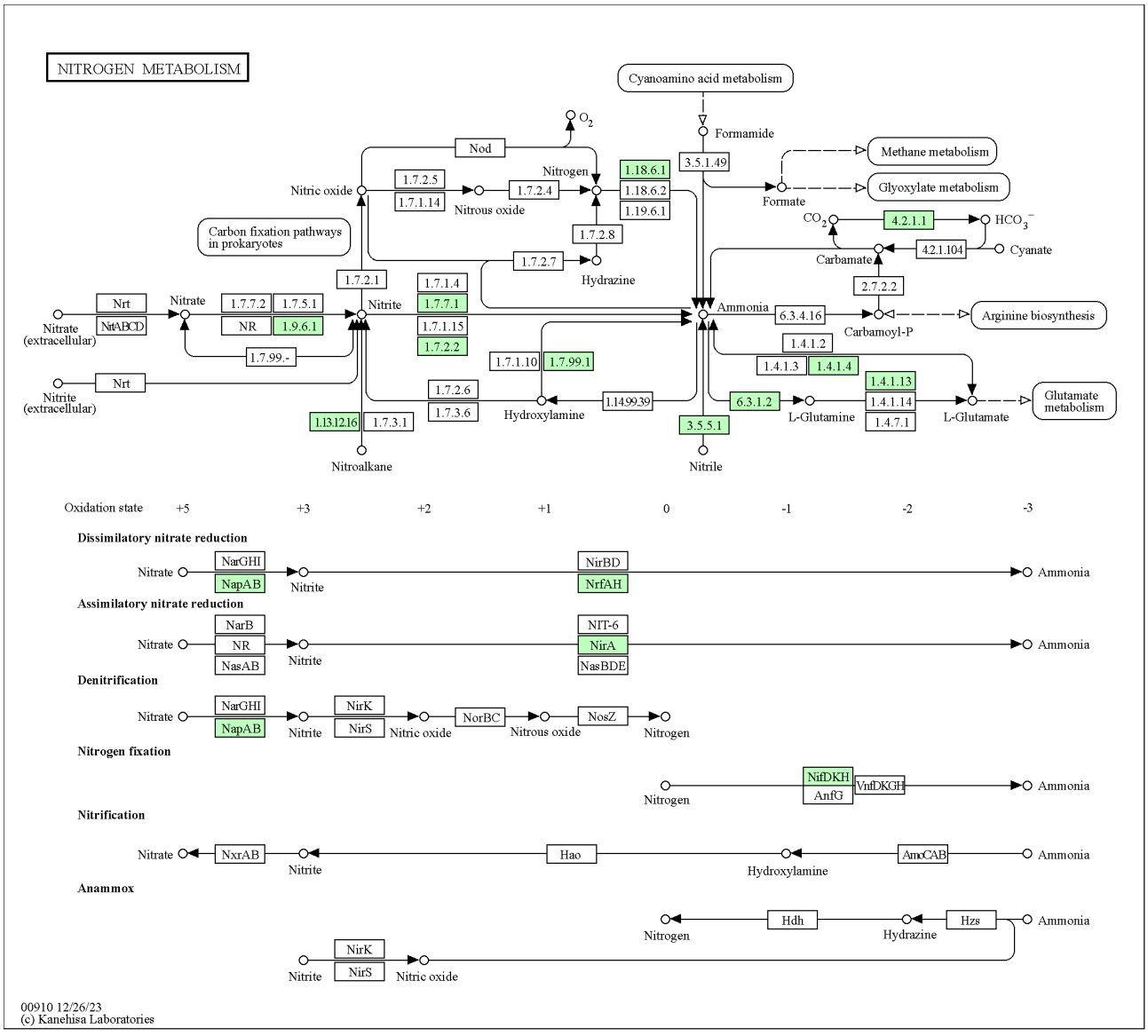


Figure 85: Nitrogen metabolism pathway annotation - GR1P2bulk.131

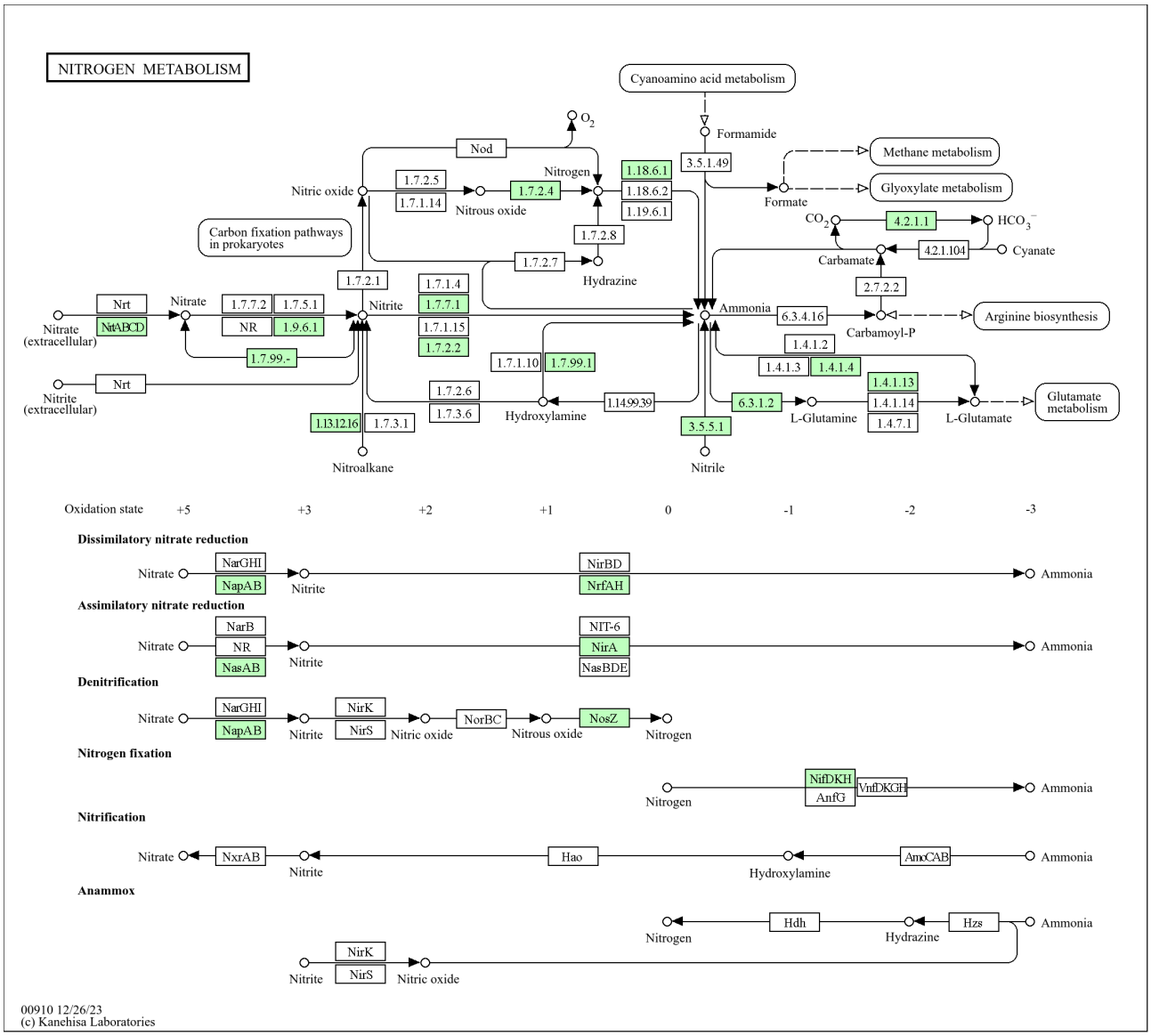


Figure 86: Nitrogen metabolism pathway annotation - *S. arsenophilum* reference sequence (GCF_-000813345.1)

A4.2.4 Sulfurospirillum cavolei

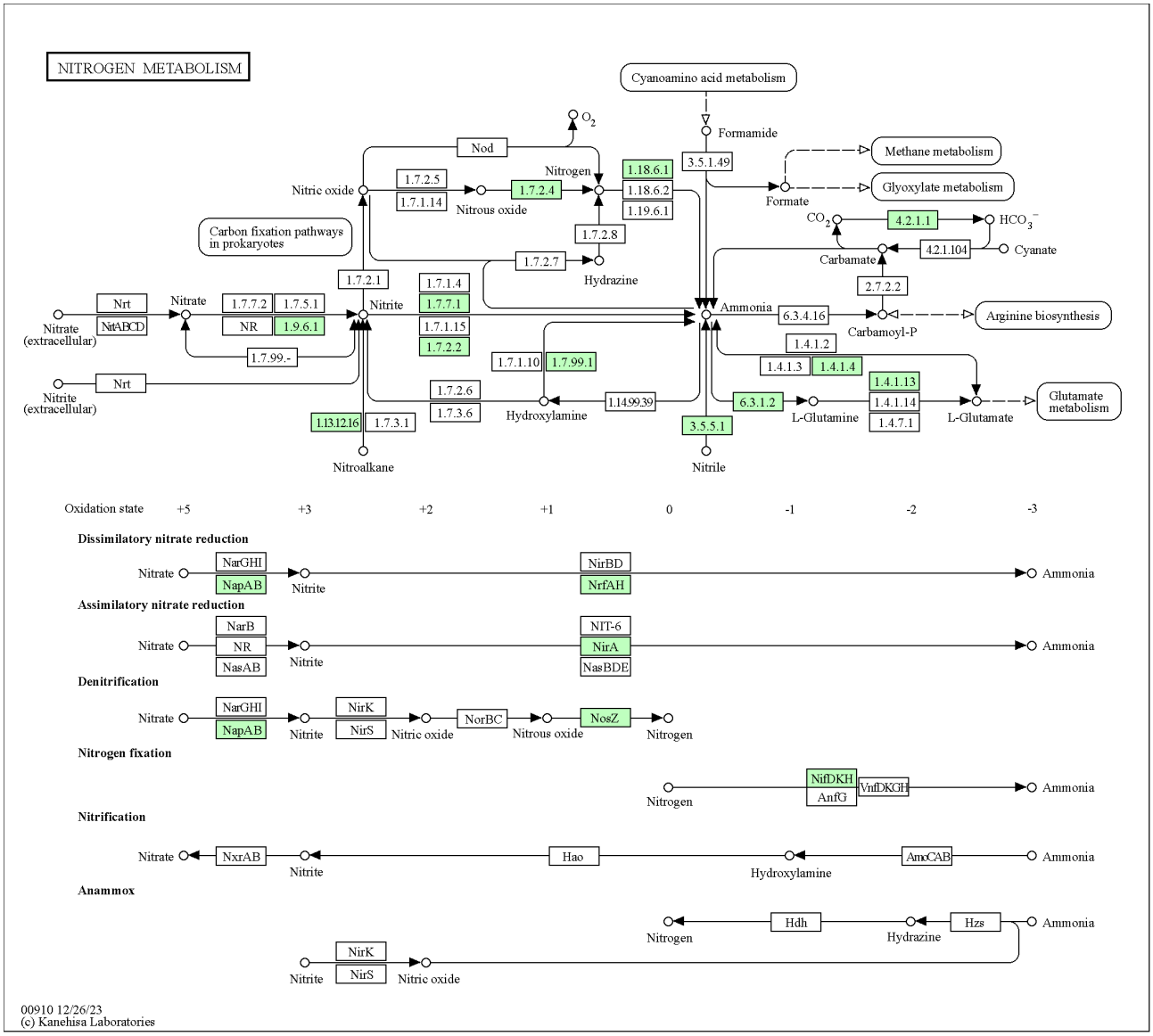


Figure 87: Nitrogen metabolism pathway annotation - GR1P2biofilm.177

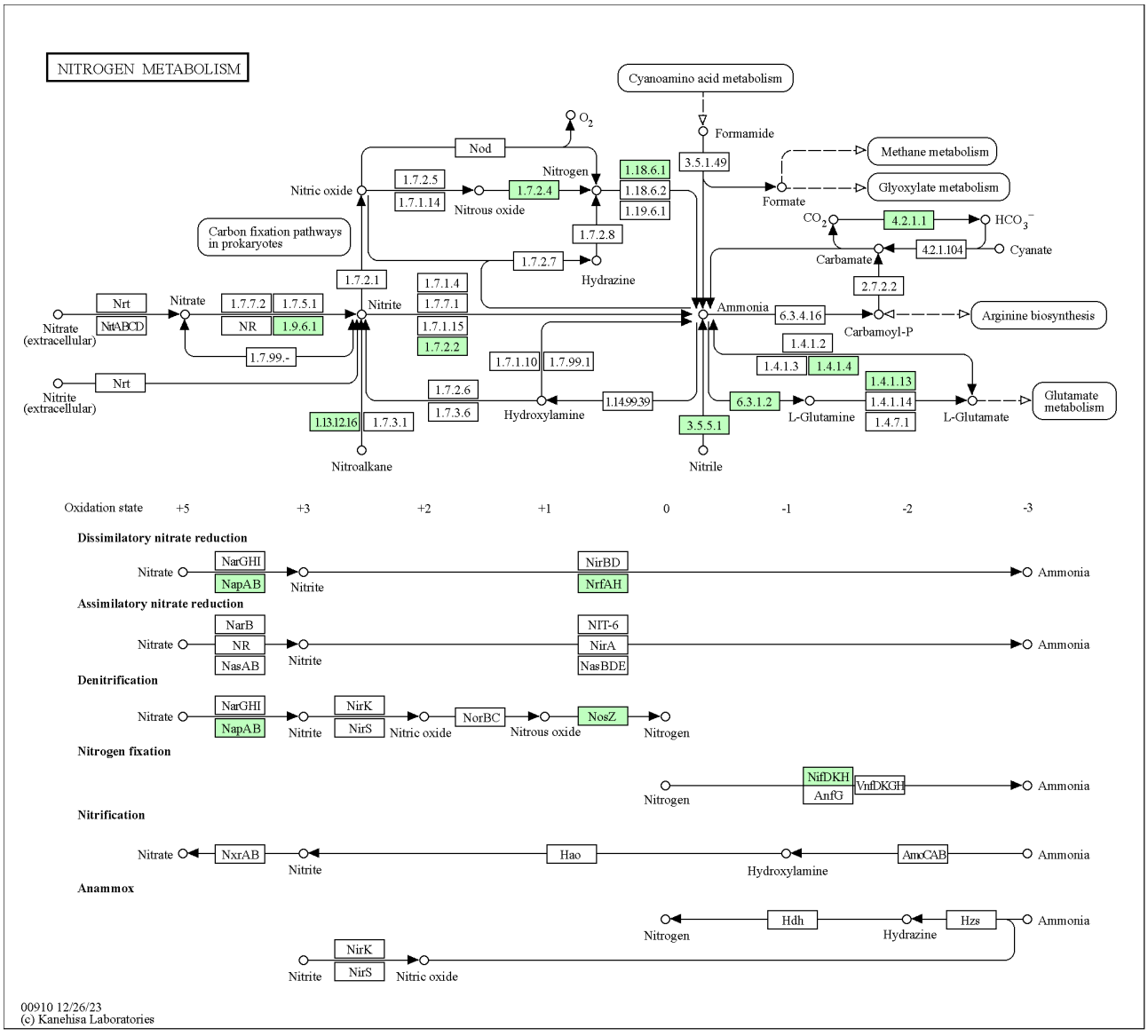


Figure 88: Nitrogen metabolism pathway annotation - GR2P1biofilm.32

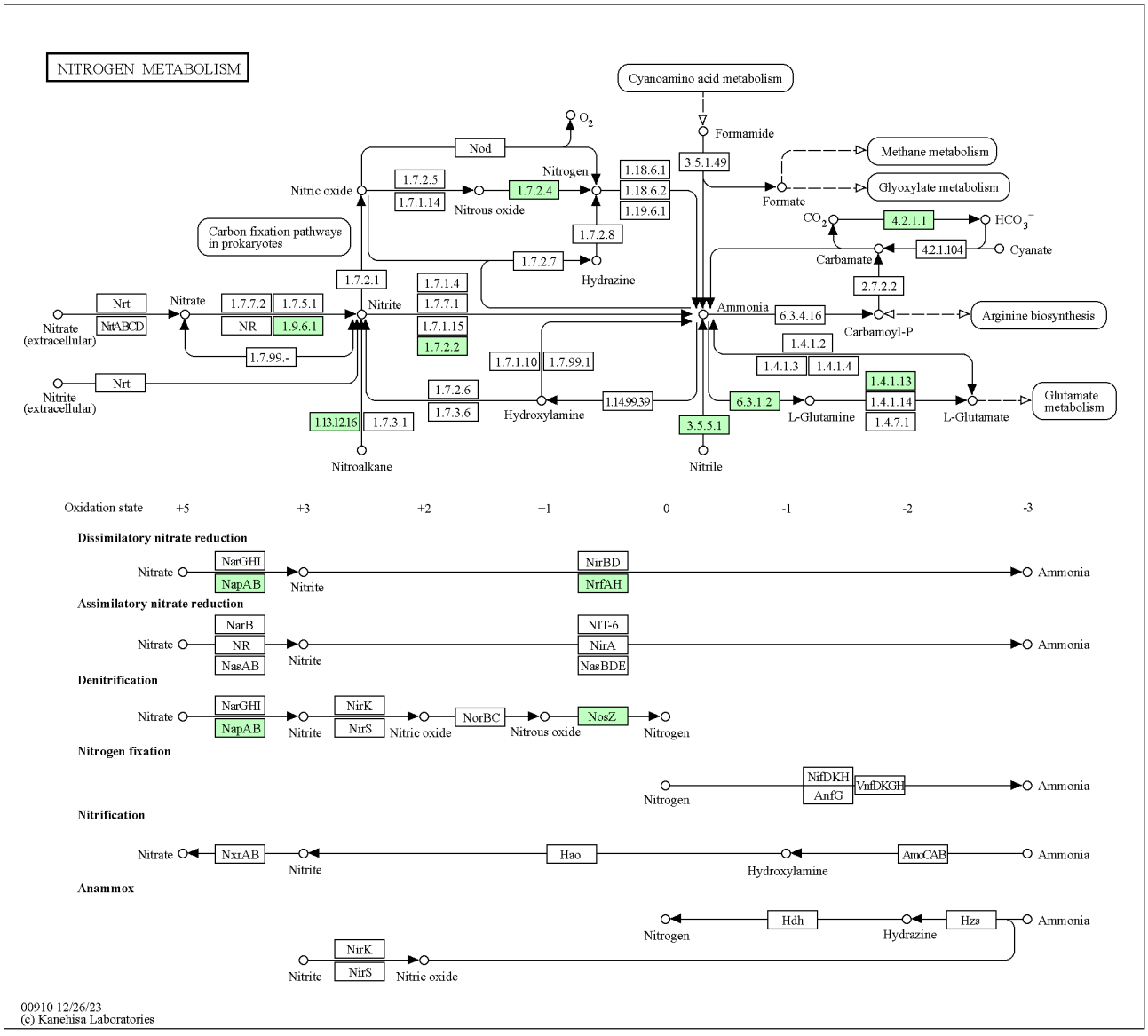


Figure 89: Nitrogen metabolism pathway annotation - GR2P1bulk.144

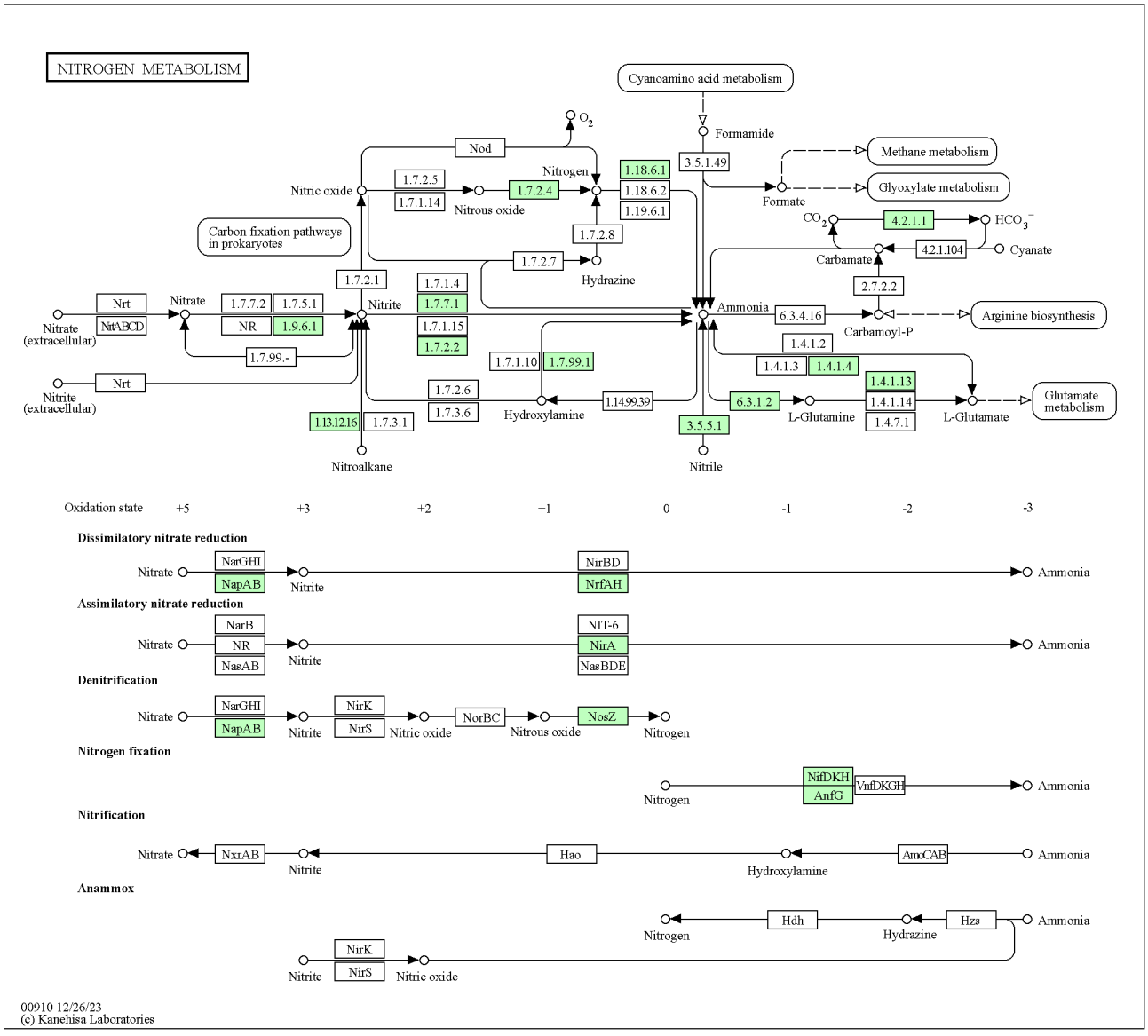


Figure 90: Nitrogen metabolism pathway annotation - GR2P2biofilm.179

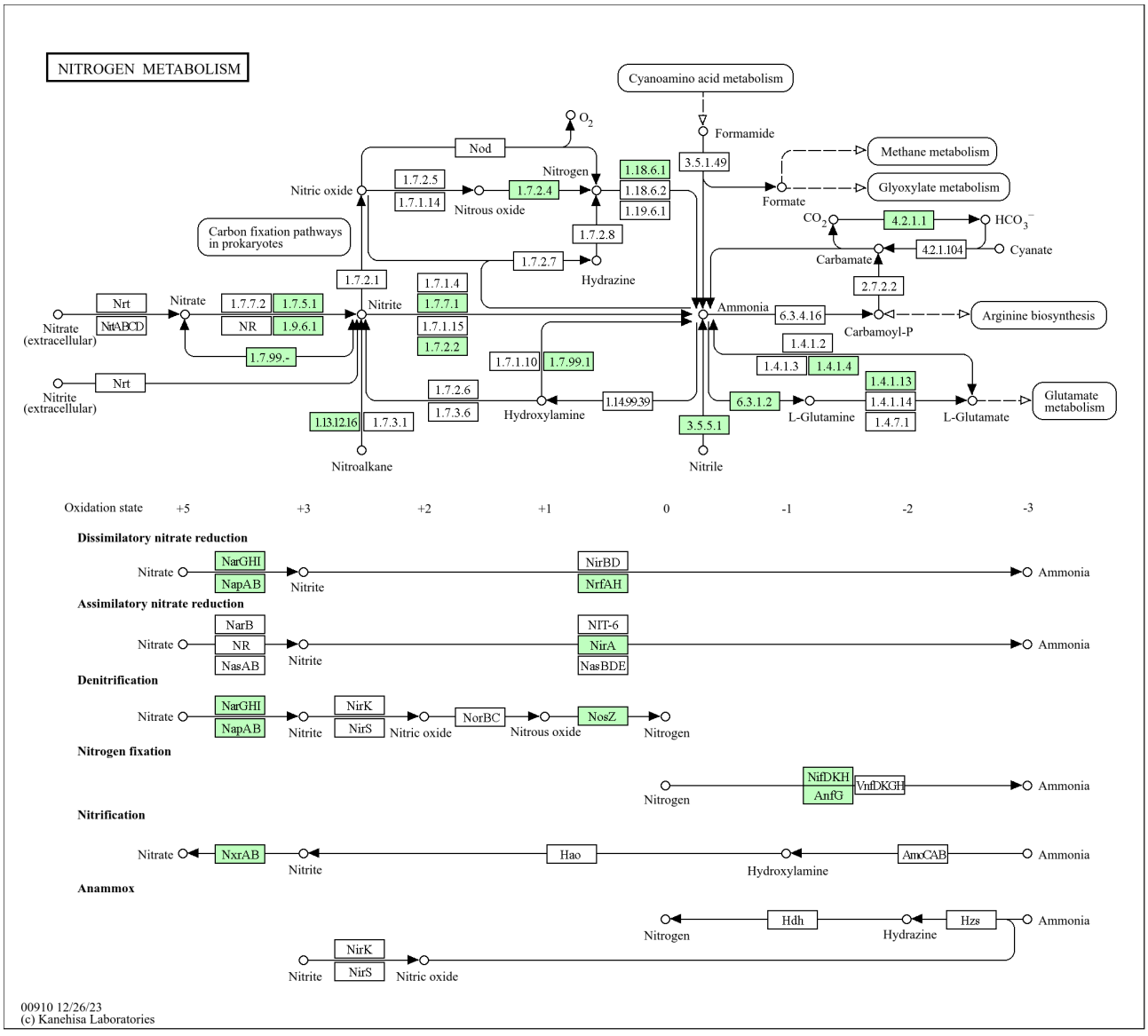


Figure 91: Nitrogen metabolism pathway annotation - *S. cavolei* reference sequence (GCF_000813325.1)

A4.2.5 Sulfurospirillum sp. JPD-1

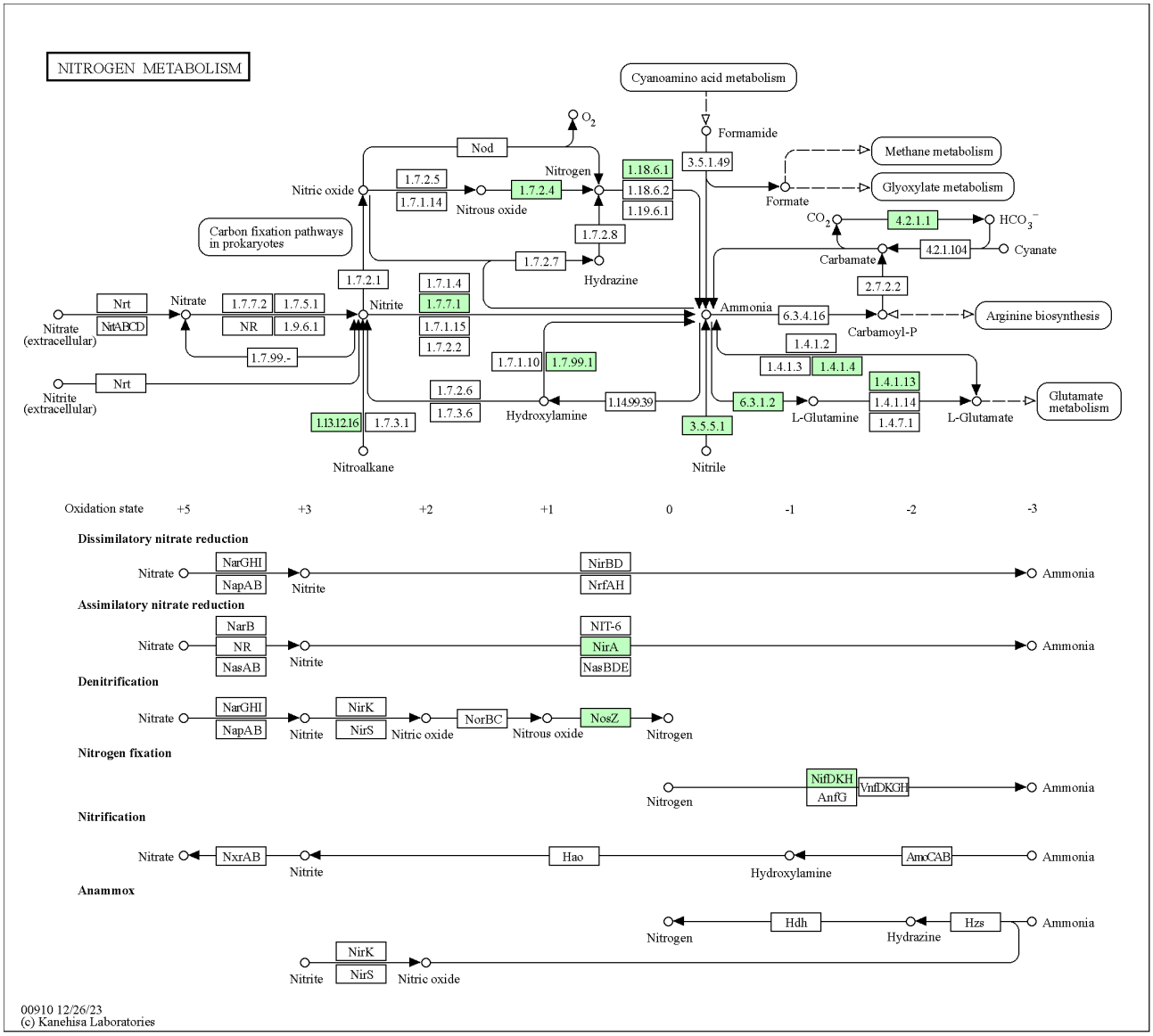


Figure 92: Nitrogen metabolism pathway annotation - GR2P1biofilm.36

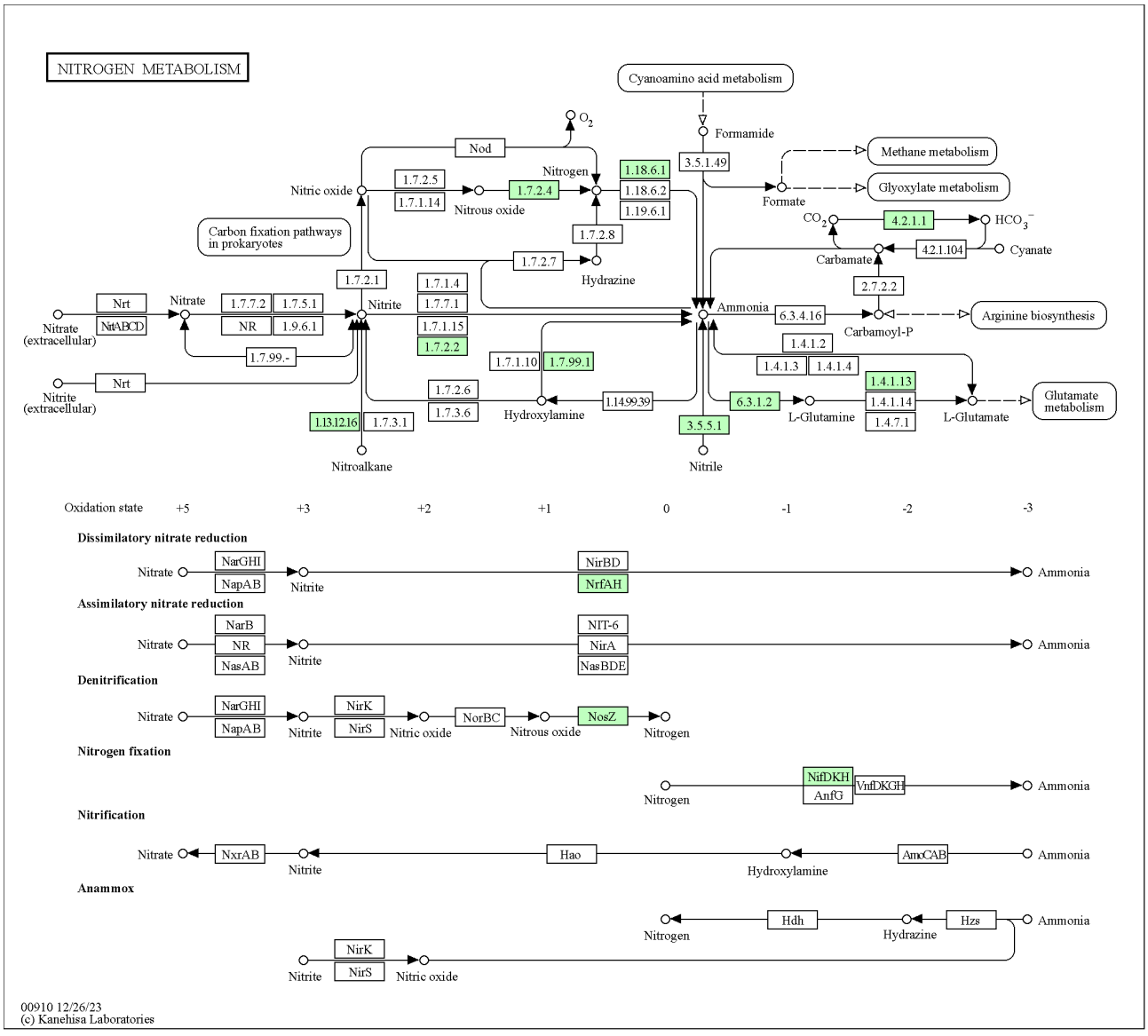


Figure 93: Nitrogen metabolism pathway annotation - GR2P2biofilm.71

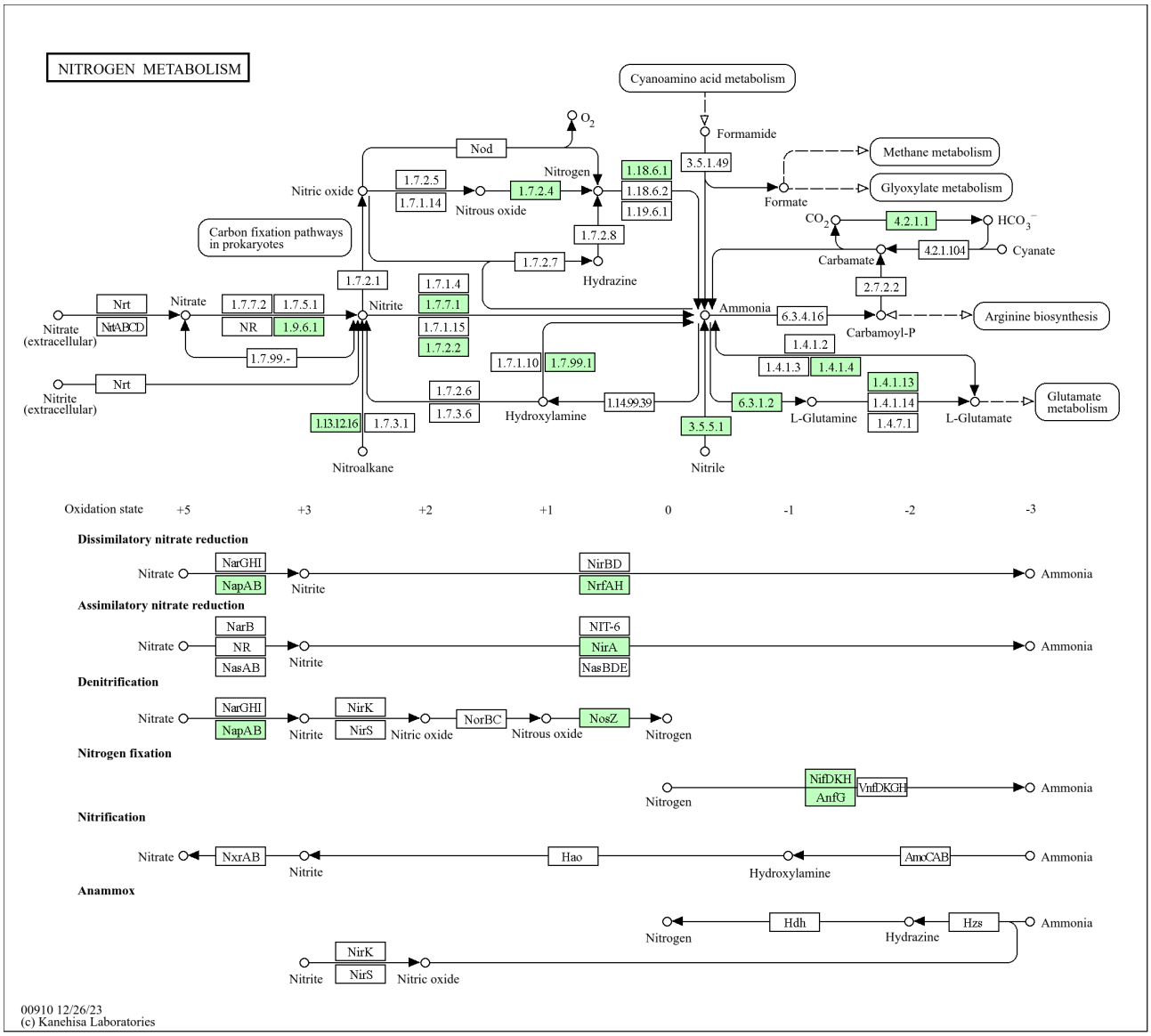


Figure 94: Nitrogen metabolism pathway annotation - *S. sp. JPD-1* reference sequence (GCF_-002309535.1)

A4.2.6 Sulfurospirillum sp. UCH001

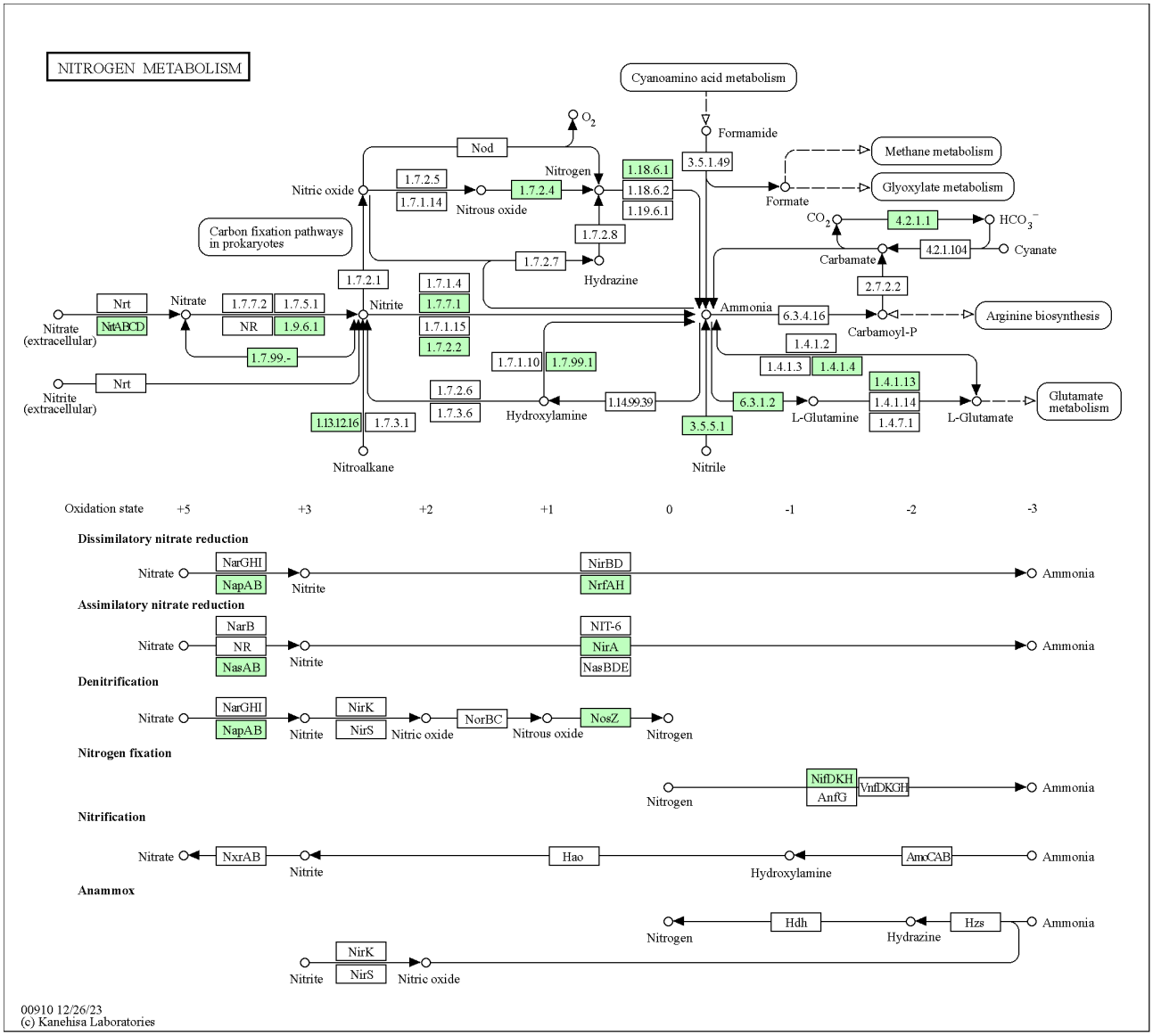


Figure 95: Nitrogen metabolism pathway annotation - GR2P1biofilm.14

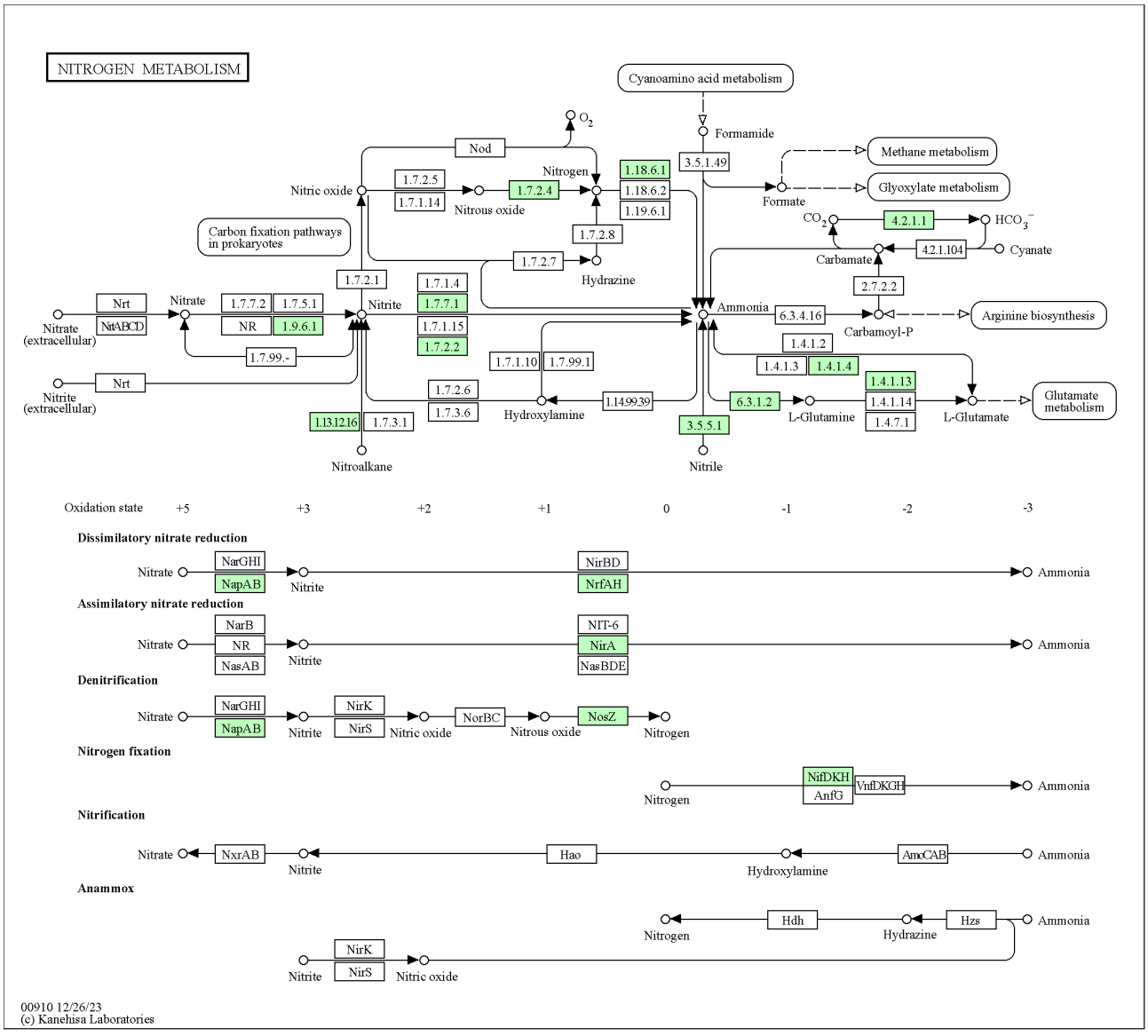


Figure 96: Nitrogen metabolism pathway annotation - GR2P1biofilm.42

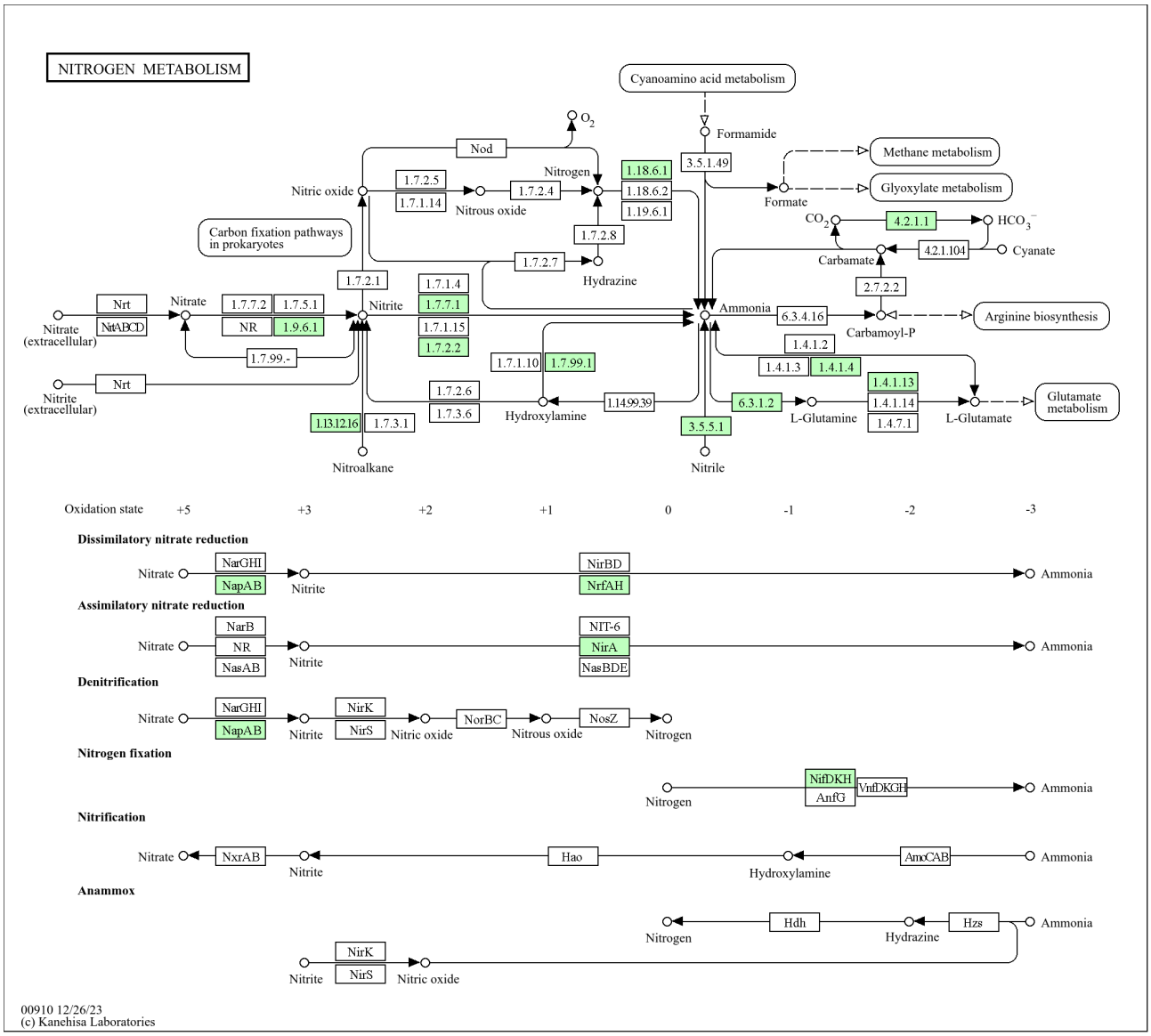


Figure 97: Nitrogen metabolism pathway annotation - *S. sp. UCH001* reference sequence (GCF_-001548035.1)

A5 Reproduction Permissions

Table 40: List of permissions for reproduction of figures

Page no.	Name of work	Source of work	Copyright holder	Permission request date	Permission obtained, yes/no	Permission note
29	Subfigure 4a Anaerobic contact process	J.B. Coulter et al. (1957). "Anaerobic Contact Process for Sewage Disposal". In: *Sewage and Industrial Wastes* 29 (4), pp. 468–477	Water Environment Federation	Mar 19, 2025	yes	Written permission obtained via LinkedIn on May 7, 2025
29	Subfigure 4b Anaerobic filter	James C. Young and Perry L. McCarty (1969). "The Anaerobic Filter for Waste Treatment". In: *Journal (Water Pollution Control Federation)*	Water Environment Federation	Mar 19, 2025	yes	Written permission obtained via LinkedIn on May 7, 2025
29	Subfigure 4c Anaerobic attached-film expanded-bed reactor	Michael S. Switzenbaum and William J. Jewell (1980). "Anaerobic Attached-Film Expanded-Bed Reactor Treatment". In: *Water Pollution Control Federation* 52 (7), pp. 1953–1965	Water Environment Federation	Mar 19, 2025	yes	Written permission obtained via LinkedIn on May 7, 2025
34	Figure 6 Phylogenetic analysis of electroactive microorganisms found in bioelectrochemical systems	Bruce E. Logan et al. (2019). "Electroactive microorganisms in bioelectrochemical systems". In: *Nature Reviews Microbiology* 17 (5), pp. 307–319. DOI: 10.1038/s41579-019-0173-x	Springer Nature	Mar 20, 2025	yes	Written permission obtained via Copyright Clearance Centre's RightsLink service
37	Subfigure 7a, Subfigure 7b, Subfigure 7c, & Subfigure 8a	Derek R. Lovley and Dawn E. Holmes (2022). "Electromicrobiology: the ecophysiology of phylogenetically diverse electroactive microorganisms". In: *Nature Reviews Microbiology* 20 (1). DOI: 10.1038/s41579-021-00597-6	Springer Nature	Mar 20, 2025	yes	Written permission obtained via Copyright Clearance Centre's RightsLink service
39	Subfigure 8b	Derek R. Lovley (2017a). "Happy together: microbial communities that hook up to swap electrons". In: *ISME Journal* 11, pp. 327–336. DOI: 10.1038/ismej.2016.136	Oxford University Press	Mar 20, 2025	yes	Written permission obtained via Copyright Clearance Centre's RightsLink service

Continued...

Table 40 Continued.

Page no.	Name of work	Source of work	Copyright holder	Permission request date	Permission obtained, yes/no	Permission note
42	Figure 9 Key anaerobic digestion pathways and genera associated with major intermediates	Mingwei Cai et al. (2016). "Metagenomic reconstruction of key anaerobic digestion pathways in municipal sludge and industrial wastewater biogas-producing systems". In: *Frontiers in Microbiology* 7. DOI: 10.3389/FMICB.2016.00778	Cai et al. 2016	N/A	yes	Article distributed under the terms of the Creative Commons Attribution License (CC BY)
44	Figure 10 Phylogeny of methanogenic archaea	Tristan Wagner et al. (2018). "Hydrogenotrophic Methanogenesis". In: *Biogenesis of Hydrocarbons*. Ed. by Alfons J.M. Stams and Diana Z. Sousa. Springer, pp. 79–107. DOI: 10.1007/978-3-319-53114-4_3-1	Springer Nature	Mar 21, 2025	yes	Written permission obtained via Copyright Clearance Centre's RightsLink service
45	Figure 11 Methanogenesis pathways and associated enzymes	Nicole R. Buan (2018). "Methanogens: Pushing the boundaries of biology". In: *Emerging Topics in Life Sciences* 2 (4), pp. 629–646. DOI: 10.1042/ETLS20180031	Portland Press	N/A	yes	Permission for non-commercial reproduction (including in a thesis) stated here
50	Figure 12 Hydrogenotrophic methanogenesis in *Methanosaeta*	Peixian Yang et al. (2019). "Metatranscriptomic evidence for classical and RuBisCO-mediated CO2 reduction to methane facilitated by direct interspecies electron transfer in a methanogenic system". In: *Scientific Reports* 9 (4116). DOI: 10.1038/s41598-019-40830-0	Yang et al. 2019	N/A	yes	Article distributed under the terms of the Creative Commons Attribution License (CC BY)
57	Figure 17 Maximum likelihood phylogeny of nitrite reductase gene clusters	Wei Wei et al. (2015). "Higher diversity and abundance of denitrifying microorganisms in environments than considered previously". In: *The ISME Journal* 9 (9), pp. 1954–1965. DOI: 10.1038/ismej.2015.9	Oxford University Press	Feb 24, 2025	yes	Written permission obtained via Copyright Clearance Centre's RightsLink service

Continued...

Table 40 Continued.

Page no.	Name of work	Source of work	Copyright holder	Permission request date	Permission obtained, yes/no	Permission note
60	Figure 19 A timeline of discoveries in the nitrogen cycle and biotechnology applications	Tao Liu et al. (2024). "Sustainable wastewater management through nitrogen-cycling microorganisms". In: *Nature Water* 2 (10), pp. 936–952. DOI: 10.1038/s44221-024-00307-5	Springer Nature	Mar 21, 2025	yes	Written permission obtained via Copyright Clearance Centre's RightsLink service
62	Figure 20 Denitrification and methanotrophic genes present in *Methylomirabilis oxyfera*	Katharina F. Ettwig et al. (2010). "Nitrite-driven anaerobic methane oxidation by oxygenic bacteria". In: *Nature* 464 (7288), pp. 543–548. DOI: 10.1038/nature08883	Springer Nature	Mar 21, 2025	yes	Written permission obtained via Copyright Clearance Centre's RightsLink service
64	Figure 21 Phylogeny of putative nitric oxide dismutase and selected nitric oxide reductase gene sequences	Baoli Zhu et al. (2017). "Unexpected diversity and high abundance of putative nitric oxide dismutase (Nod) genes in contaminated aquifers and wastewater treatment systems". In: *Applied and Environmental Microbiology* 83 (4). DOI: 10.1128/AEM.02750-16	American Society for Microbiology	Mar 21, 2025	yes	Written permission obtained via Copyright Clearance Centre's Marketplace service
67	Figure 23 Pathways and enzymes of dissimilatory nitrate reduction to ammonia	Xiaoguang Wang et al. (2019b). "The role of the NADH-dependent nitrite reductase, Nir, from Escherichia coli in fermentative ammonification". In: *Archives of Microbiology* 201 (4), pp. 519–530. DOI: 10.1007/S00203-018-1590-3	Springer Nature	Mar 21, 2025	yes	Written permission obtained via Copyright Clearance Centre's RightsLink service
69	Figure 24 Nitrate removal rates in denitrifying communities with and without *Geobacter*	Yuxuan Wan et al. (2018). "Syntrophic growth of Geobacter sulfurreducens accelerates anaerobic denitrification". In: *Frontiers in Microbiology* 9. DOI: 10.3389/fmicb.2018.01572	Wan et al. 2018	N/A	yes	Article distributed under the terms of the Creative Commons Attribution License (CC BY)

Continued...

Table 40 Continued.

Page no.	Name of work	Source of work	Copyright holder	Permission request date	Permission obtained, yes/no	Permission note
71	Figure 25 Concentration changes of ammonium, nitrite, and nitrate in microbial electrolysis cells and biotic controls in two cycles	Qinmao Zhou et al. (2021). "Electrode-dependent ammonium oxidation with different low C/N ratios in single-chambered microbial electrolysis cells". In: *Bioelectrochemistry* 142. DOI: 10.1016/j.bioelechem.2021.107889	Elsevier	Mar 21, 2025	yes	Written permission obtained via Copyright Clearance Centre's RightsLink service
72	Figure 26 Possible mechanism of biochar-mediated DNRA pathway of anammox bacteria	Weigang Wang et al. (2022a). "Biochar-mediated DNRA pathway of anammox bacteria under varying COD/N ratios". In: *Water Research* 212. DOI: 10.1016/j.watres.2022.118100	Elsevier	Mar 21, 2025	yes	Written permission obtained via Copyright Clearance Centre's RightsLink service
100	Figure 32 Methane yields from anaerobic fluidised-bed membrane bioreactors using coated and uncoated PVDF beads	Daeeun Kwon et al. (2022). "Polyaniline-coated conductive media promotes direct interspecies electrons transfer (DIET) and kinetics enhancement of low-strength wastewater treatment in anaerobic fluidized bed membrane bioreactor (AFMBR)". in: *Chemical Engineering Journal* 446 (2). DOI: 10.1016/j.cej.2022.136711	Elsevier	N/A	yes	I co-authored this paper, hence permission not required